N to Delta Transition Amplitudes from QCD Sum Rules

by **Lai Wang**

B.S. in Physics, July 2003, Nanjing University, China
M.S. in Physics, May 2005, Washington State University

A Dissertation submitted to

The Faculty of
Columbian College of Arts and Sciences
of The George Washington University
in partial fulfillment of the requirements
for the degree of Doctor of Philosophy

January 31, 2011

Dissertation directed by

Frank X. Lee
Professor of Physics

The Columbian College of Arts and Sciences of The George Washington University certifies that Lai Wang has passed the Final Examination for the degree of Doctor of Philosophy as of 15th of July, 2010. This is the final and approved form of the dissertation.

N to Delta Transition Amplitudes from QCD Sum Rules

Lai Wang

Dissertation Research Committee:

Frank X. Lee, Professor of Physics, Dissertation Director
William Parke, Professor of Physics, Committee Member
Andrei Alexandru, Assistant Professor of Physics, Committee Member

Acknowledgments

First and foremost I would like to express my sincere gratitude to my supervisor Dr. Frank X. Lee. It has been an honor to be his Ph.D. student. He provided me with many helpful suggestions, important advice and constant encouragement during the course of this work. He taught me how to write academic papers, made me a better programmer, gave me confidence when I doubted myself, and brought out the good ideas. Without his encouragement and constant guidance, I would have been lost. With his patience, his inspiration, and his great efforts to explain things clearly and simply, he helped me to develop and understanding of QCD theories and related computation knowledge. I appreciate all his contributions of time, ideas, and funding to make my Ph.D. experience productive and stimulating.

My time at GWU was enjoyable in large part due to the friendly environment in the physics department. I am also thankful for Dr. Andrei Alexandru, who has been set as an excellent example of a successful physicist and professor. I am grateful for time spent with the folks at the physics department for interesting discussions and being fun to be with.

I would also gratefully acknowledge the funding sources that made my Ph.D. work possible. I was funded by Teaching Assistantships from the Physics Department and Research Fellowship from the U.S. Department of Energy via grant to the Physics Department.

Last, but not least, I thank my family: my parents for giving me life in the first place, for unconditional support and encouragement to pursue my interest, even when

the interests went beyond boundaries of language, field and geography. I feel very sorry that I am unable to be with my mum especially when she's sick these years. I would also like to thank my husband Xinyu Huang, for sharing his knowledge with me, for listening to my complaints and frustrations, and for believing in me. A special thanks to our newborn son Joshua Huang. He is a powerful source of happiness and energy. To them I dedicate this thesis.

Abstract of Dissertation

N to Delta Transition Amplitudes from QCD Sum Rules

A calculation of the N to Δ electromagnetic transition amplitudes using the method of QCD sum rules is presented. First, the method is demonstrated using the computation of the proton mass as an example. Next the magnetic moments of octet baryons are re-examined in the external field method. Then the same methodology is applied to the entire family of transitions from the baryon octet to decuplet. The complete set of QCD sum rules derived for the process are analyzed in conjunction with the corresponding mass sum rules using a Monte-Carlo-based analysis procedure. The performance of each of the sum rules is examined using the criteria of OPE convergence and ground-state dominance, along with the role of the transitions in intermediate states. Individual contributions from the u, d and s quarks are isolated and their implications in the underlying dynamics are explored. Valid sum rules are identified and their predictions are obtained. The results are compared with experiment and other calculations. Finally, a Mathematica package developed in the project to carry out the construction and analysis is presented.

Contents

Acknowledgments **iii**

Abstract **v**

Table of Contents **vi**

List of Figures **x**

List of Tables **xv**

1 Introduction **1**

1.1 Strong Interaction and QCD 1

1.2 QCD Sum Rules and N to Δ Transition Amplitudes 3

2 Physics of N to Δ Transitions **6**

2.1 Definition of the Form Factors 6

2.2 Experimental Information 11

3 The QCD Sum Rules Method **14**

3.1 Baryon Interpolating Fields (Baryon Currents) 15

3.2 Operator Product Expansion (OPE) 16
3.3 Phenomenological Representation (RHS) 26
3.4 Fourier Transform 28
3.5 Borel Transformation 34
3.6 Excited State Approximation 37
3.7 Sum Rules for Octet Baryon Masses 39
3.8 Sum Rule Analysis for Proton Masses 45

4 Baryon Magnetic Moments from QCD Sum Rules 48

4.1 Introduction 48
4.2 Method 50
4.2.1 Phenomenological Representation 52
4.2.2 Calculation of the QCD Side 57
4.3 QCD Sum Rules 62
4.4 Monte Carlo Sum Rule Analysis 72
4.5 Result and Discussion 75
4.5.1 The Sum Rule at WE_1 77
4.5.2 The Sum Rule at WO_1 80
4.5.3 The Sum Rule at WO_2 81
4.5.4 Some Physics Discussions 85
4.5.5 Individual Quark Contributions 88
4.5.6 Correlations 94

5 N to Δ Transitions Amplitudes from QCD Sum Rules 96

5.1 Phenomenological Representation (RHS) 97
5.2 QCD Side 103
5.2.1 Interpolating Fields 103
5.3 Sum Rules 106
5.4 Monte-Carlo Analysis 114
5.5 Results and Discussion 116
5.5.1 The Sum Rules at WE_1 117
5.5.2 The Sum Rule at WO_2 122
5.5.3 The Sum Rule at WE_6 122
5.5.4 Individual Quark Contributions 123
5.5.5 Comparison with other Theoretical Calculations 124

6 MathQCDSR: a Mathematica Package for QCD Sum Rules Calculations 129

6.1 Example 1: Mass of Octet Baryons 130
6.1.1 Sum Rule Construction 131
6.1.2 Sum Rule Analysis 133
6.2 Example 2: Magnetic Moments of Octet Baryons. 141
6.2.1 Sum Rules Construction 141
6.2.2 Sum Rule Analysis 142

7 Summary and Conclusion 143

7.1 Masses and Magnetic Moments 143
7.2 Transition Amplitudes 145

7.3 MathQCDSR 147

7.4 Final Remarks 148

References **150**

A QCD Sum Rules for $N\gamma \to \Delta$ Transitions **155**

B Mathematica Source Code **170**

List of Figures

3.1 Skeleton diagrams considered in the calculation of the QCD side for a baryon 18

3.2 Skeleton diagrams linear in the quark mass, denoted by the cross symbol . 19

3.3 Model the excited states by a pole and a continuum function. 37

4.1 The three kinds of contributions to the spectral function in the presence of an external field: ground state, transitions between ground state and excited states, and pure excited states 56

4.2 Non-mass diagrams considered for the octet baryon magnetic moments. . . 60

4.3 Diagrams considered for the strange quark mass corrections to the octet baryon magnetic moments. 61

4.4 Histogram for the proton magnetic moment (top) and transition amplitude (bottom) obtained from Monte-Carlo fits of Eq. (4.28) at WE_1 for 2000 QCD parameter sets. They are based on 10% uncertainty given to all the QCD input parameters. 77

4.5 Analysis of the QCD sum rule in Eq. (4.28) (structure WE_1) for the proton at $\beta = -0.4$ according to Eq. (4.45). In the top, the pole plus transition terms (solid lines) are compared against the OPE minus the excited-state contributions (dashed lines) as a function of $1/M^2$ (the two should match for an ideal sum rule). Also plotted are the individual contributions from u (long-dashed lines) and d (dot-dashed lines) quarks. In the middle, the total in the OPE side and its various terms are plotted as a function of M^2. In the bottom, the 3 terms in the phenomenological side: pole (solid), transition (long-dashed), and excited (dot-dashed) are plotted as a function of M^2. 79

4.6 Similar to Fig. 4.5, but at structure WO_1 and $\beta = -1.2$. 82

4.7 Similar to Fig. 4.5, but at structure WO_2 and $\beta = -1.2$. 84

4.8 Similar to Fig. 4.5, But for the neutron at all three structures: WE_1 (left panel), WO_1 (middle panel), WO_2 (right panel). 85

4.9 Similar to Fig. 4.8, but for Σ^0. 86

4.10 Scatter plots showing correlations between the magnetic moment and the QCD parameters for the proton at structure WE_1. They are obtained from 2000 Monte-Carlo samples with 10% uncertainty on all the QCD parameters. 94

4.11 Similar to Fig. 4.10, but for the Σ^0 and a different set of QCD parameters. 95

5.1 The four contributions to the spectral function in the presence of an external field: transition between ground state N to ground state Δ, transitions between ground state N and excited states Δ^*, transition between excited state N^* and ground state Δ and pure excited states $N^* \to \Delta^*$. 102

5.2 Histogram for the G_1 transition amplitude (top) and transition amplitude (bottom) obtained from Monte-Carlo fits of Eq.(5.19) at WE_1 for 2000 QCD parameter sets. They are based on 10% uncertainty given to all the QCD input parameters. 119

5.3 Analysis of the QCD sum rule in Eq. (5.19) (structure WE_1) for the proton at $\beta = -0.2$ according to Eq. (5.34). Top figure, the pole plus transition terms (solid lines) are compared against the OPE minus the excited-state contributions (dashed lines) as a function of $1/M^2$ (the two should match for an ideal sum rule). Also plotted are the individual contributions from u (long-dashed lines) and d (dot-dashed lines) quarks. Middle figure, the total in the OPE side and its various terms are plotted as a function of M^2. Bottom figure, the 3 terms in the phenomenological side: pole (solid), transition (long-dashed), and excited (dot-dashed) are plotted as a function of M^2. 120

5.4 A scatter plot showing correlations between the transition amplitude G_1 and one of the QCD parameters χ for the $p\gamma \to \Delta^+$ at structure WE_1. It is obtained from 2000 Monte-Carlo samples with 10% uncertainty on all the QCD parameters. 121

5.5 A comparison of the magnetic dipole transition amplitude G_{M1} in units of nucleon magnetons in the $p\gamma \to \Delta^+$ transition from different approaches. See text for discussions. 126

5.6 A comparison of the R_{EM} ratio in the $p\gamma \to \Delta^+$ transition. See text for discussions. 126

6.1 Outline of *qcdsr2pt-construction* program for constructing of octet baryon mass sum rules. All the codes are hidden in the outline. 131

6.2 Outline of $qcdsr2pt-analysis$ program for analyzing the octet baryon mass sum rules. 134

6.3 The matching of the chiral-odd QCD sum rule in Eq. (3.87) for the nucleon. A three-parameter search was performed, with $\beta = 1.2$ and about 2800 QCD parameter sets. 135

6.4 Individual terms in the spectral representation for the chiral-odd QCD sum rule in Eq. (3.87) for the nucleon. 136

6.5 Individual terms in the OPE for the chiral-odd QCD sum rule in Eq. Eq.(3.87) for the nucleon. 136

6.6 Histogram for the nucleon mass at $\beta = -1.2$ for chiral-odd sum rule Eq.(3.87) after making section for physical continuum threshold. 137

6.7 The correlation between the nucleon mass and the quant condensate, gluon condensate and mix condensate for chiral-odd sum rule(Eq.3.87) at the optimal $\beta = -1.2$. 138

6.8 The correlation between the nucleon mass and the residue of the pole for chiral-odd sum rule(Eq.3.87) at the optimal $\beta = -1.2$. 140

6.9 The correlation between the nucleon mass and the continuum threshold for chiral-odd sum rule(Eq.3.87) at the optimal $\beta = -1.2$. 140

List of Tables

2.1 A summary of experimental results for the G_{E2}/G_{M1} ratio R_{EM} in the $\gamma p \to \Delta^+$ transition. 12

3.1 Logarithmic Fourier transforms 32

3.2 Fourier transforms 32

4.1 Results for the magnetic moment of octet baryons from the QCD sum rule in Eq. (4.28) (structure WE_1). The seven columns correspond to, from left to right: particle, β value, Borel region in which the two sides of the QCD sum rule are matched, continuum threshold, transition strength, extracted magnetic moment in unit of nuclear magnetons, and experimental value. The errors are derived from 2000 samples in the Monte-Carlo analysis with 10% uncertainty on all QCD input parameters. 76

4.2 Similar to Table 4.1, but for the QCD sum rule in Eq. (4.34) (structure WO_1). 80

4.3 Similar to Table 4.1, but for the QCD sum rule in Eq. (4.38) (structure WO_2). 83

4.4 A comparison of selected ratios of magnetic moments. 87

4.5 Individual quark contributions and total magnetic moments in unit of nuclear magnetons extracted from the QCD sum rules at WE_1 (denoted by the subscript SR) are compared with those from a lattice QCD calculation (denoted by the subscript LAT) [43, 49]. 89

4.6 The result for s s' and s'' quark effective moments from QCD sum rule, experiment and lattice calculation. 93

5.1 Results for G_1 in $N \to \Delta$ transitions from the QCD sum rule at structure WE_1 in Eq. (5.19). The columns correspond to, from left to right: transition channel, β value, Borel window, continuum threshold, transition strength A, amplitude G_1. The errors in the results are derived from 2000 samples in the Monte-Carlo analysis with 10% uncertainty on all the QCD input parameters. 118

5.2 Similar to Table 5.1, but for the QCD sum rule in Eq. (5.27) (structure WO_2). 122

5.3 Similar to Table 5.3, but for the G_2 amplitude from the QCD sum rule in Eq. (5.23) (structure WE_6). 123

5.4 Individual quark contributions to the transition amplitude G_1 in units of GeV^{-1} extracted from the QCD sum rules in Eq. (5.19) (structure WE_1). 124

5.5 Individual quark contributions to the transition amplitude G_2 in units of GeV^{-2} extracted from the QCD sum rules in Eq. (5.23) (structure WE_6). 124

5.6 A comparison of N to Δ transition amplitudes from various approaches: this work (QCDSR) in three different conventions; lattice QCD [5] and quark model [53]. The experiment [11] gives $3.02\text{GeV}^{-\frac{1}{2}}$ for G_{M1} and $-2.5(5)\%$ for R_{EM} in $p\gamma \to \Delta^+$ transition channel. 125

Chapter 1

Introduction

1.1 Strong Interaction and QCD

Quantum chromodynamics (abbreviated as QCD) is the theory of the strong interaction (color force), a fundamental force describing the interactions of the quarks and gluons found in hadrons (such as the proton, neutron or pion) [1, 2]. It is generally accepted as the underlying theory of the strong interaction. At high energy limit, QCD is perturbative, described by asymptotic freedom. However, QCD is highly non-perturbative at the energy scale of low-lying hadrons, described as confinement and it is hard to solve.

In the hadronic QCD theory, it is assumed that the fundamental constituents of hadrons are three-colored quarks,

$$u^\alpha,\ d^\alpha,\ s^\alpha,\ c^\alpha,\ b^\alpha,\ t^\alpha, \quad \alpha = 1, 2, 3 \tag{1.1}$$

and gluons. Their interaction is described by the QCD Lagrangian,

$$\mathcal{L} = -\frac{1}{4}G^a_{\mu\nu}G^a_{\mu\nu} + \sum_{q=u,d,...} \bar{q}(i\not{D} - m_q)q, \tag{1.2}$$

where m_q is quark mass and q is quark field. $G^a_{\mu\nu}$ is the gluon field strength tensor,

$$G^a_{\mu\nu} = \partial_\mu A^a_\nu - \partial_\nu A^a_\mu + g f^{abc} A^b_\mu A^c_\nu. \tag{1.3}$$

Numbers f^{abc} $(a, b, c = 1, ..., 8)$ are structure constants of the SU(3) colour group.

$\not{D}_\alpha$ is the covariant derivative,

$$i\not{D}_\alpha \;=\; i\partial_\alpha \;+\; g A^a_\alpha T^a, \tag{1.4}$$

where g is gauge constant that determines the coupling between the quark fields and gluon field A^a_α as well as the self-interactions of the gluon fields. T^a stands for the generator of the SU(3) color group in the fundamental representation.

The QCD vacuum is densely populated by violent, non-perturbative fluctuations of quark and gluon fields. The strength of the fluctuations is characterized on average by the vacuum condensates (also known as vacuum expectation values of QCD local operators); the most dominant ones are the quark condensates, gluon condensates, and mixed condensates. A very important feature of QCD is that all hadronic properties are determined by the very peculiar structure of the QCD vacuum. These condensates allow people to predict quantitatively hadron properties not yet measured experimentally. Various methods based on the vacuum and hadronic structure

have been developed to explore the properties of hadrons. Among them the most effective ones are the QCD sum rules and the lattice QCD computer simulations. The focus of this thesis is on the QCD sum rules.

1.2 QCD Sum Rules and N to Δ Transition Amplitudes

The QCD sum rules method [3] was introduced in 1979. It is a nonperturbative analytic formalism firmly entrenched in QCD with minimal modeling. As such, it continues to be a highly active field. The influence of the field is reflected in over 3000 references to the seminar paper of Shifman, Vainshtein and Zakharov (it's currently no.10 on the all-time top cites according to spires) [4]. The approach has been successfully applied to almost every aspect of strong-interaction physics. The success of this approach in predicting hadron properties has historically given us a unique perspective on hadron structure, compared to other conventional views, like the phenomenologically successful constituent quark model. As an analytical method, it reveals a direct link between hadron phenomenology and QCD vacuum structure via the QCD vacuum condensate parameters. The strength of the vacuum fluctuations is characterized on average by the vacuum condensates (which are vacuum expectation values of QCD local operators); the most dominant ones are the quark condensates, gluon condensates, and mixed condensates.

The determination of low-energy electromagnetic properties of baryons, such as

charge radii, magnetic and quadrupole moments, has long been a subject of interest in nucleon structure studies. For example, the G_{E2}/G_{M1} ratio of the transition amplitudes in the process $\gamma N \to \Delta$ is a signature of the deviation of the nucleon from spherical symmetry.

The first serious attempt to determine the G_{E2}/G_{M1} ratio from quantum chromodynamics (QCD), the fundamental theory of the strong interaction, was the lattice calculation of Leinweber *et al.* [5]. The calculation has been updated recently by Alexandrou *et al.* [6, 7] with better technology and statistics. In this work, we present a calculation of the transition amplitudes using the method of QCD sum rules [3]. The only previous attempt using this method on the N to Δ transition that we know of by Ioffe [8] over 25 years ago. It was a limited study conducted in the context of the magnetic moments of the nucleon, and the results were inconclusive due to large contamination from the excited-state contributions.

Our goal is to carry out a comprehensive study of the N to Δ transition in the QCD sum rule method with a number of features. First, we employ generalized interpolating fields which allow us to use the optimal mixing of interpolating fields to achieve the best match in the QCD sum rules. The interpolating field used previously is a special case. Second, we derive the complete Dirac structure and construct a new set of QCD sum rules. The previous study was quite limited in its Dirac structure. Third, we study all transitions from the octet to the decuplet, not just the proton channel. Fourth, we perform a Monte-Carlo uncertainty analysis which has become the standard for evaluating errors in the QCD sum rule approach. The advantage of such an analysis is explained later. Fifth, we use a different procedure to

extract the transition amplitudes and to treat the transition terms in the intermediate states. Our results show that these transitions cannot be simply ignored. Sixth, we isolate the individual quark contributions to the transition amplitudes and discuss their implications in the underlying quark-gluon dynamics. A similar study has been performed for the magnetic moments of octet baryons [9].

The work is organized as follows. In Chap. 2, the physics of N to Δ transition is reviewed. In Chap. 3, the QCD sum rule method is introduced using proton mass as an example. Interpolating fields, master formula are calculated, followed by the derivation of the phenomenological representation. In Chap. 4, the external field method is applied. The magnetic moments are extracted from the linear response to the field. In Chap. 5, the same external field method is used to develop a complete set of QCD sum rules for the entire family of transitions from the octet to the decuplet. The results are summarized and a comparison of our results with experiment and other calculations is given. In Chap. 6, a Mathematica package developed to carry out both construction and analysis is described. The calculation is presented to compute the magnetic moments of octet baryons. The summary and conclusion are given in Chap. 7.

Chapter 2

Physics of N to Δ Transitions

2.1 Definition of the Form Factors

The concept of form factors plays an important role in the study of internal structure of composite particles. The non-trivial dependence of form factors on the momentum transfer (*i.e.*, its deviation from the constant behavior) is a signal of the non-elementary nature of the investigated particle.

In the literature, there are several different definitions of the form factors. For completeness, we will relate our definitions to other definitions of the form factors which have been used in the past. In theoretical papers, form factors are usually decomposed in terms of what we may call perturbative covariants, in analogy with the Dirac-Pauli decomposition of the nucleon form factor. While experimental papers are more often concerned with the determination of the multipole amplitudes, defined in terms of helicity amplitudes, or operationally from the cross-section formula.

The current matrix element for the $\gamma N \to \Delta$ transition can be written as

$$< \Delta(k', s')|j_\mu|N(k, s) >= \bar{u}^\rho(k', s')\Gamma_{\rho\mu}u(k, s), \tag{2.1}$$

where k, s and k', s' denote initial and final momenta and spins, j_μ the electromagnetic current, u the spin-1/2 nucleon spinor, and u^ρ the Rarita-Schwinger spinor for the spin-3/2 Δ. This matrix element is the most general form required for describing on-shell nucleon and Δ states with both real and virtual photons. There exist different definitions in the literature for the form factors describing the vertex function $\Gamma_{\rho\mu}$. One is in terms of G_1, G_2, and G_3 by Jones and Scadron [10]:

$$\Gamma_{\rho\mu} = G_1(q^2)\mathrm{H}^1_{\rho\mu} + G_2(q^2)\mathrm{H}^2_{\rho\mu} + G_3(q^2)\mathrm{H}^3_{\rho\mu}, \tag{2.2}$$

where the covariant structures are

$$\begin{aligned} H^1_{\rho\mu} &= q_\rho\gamma_\mu - q\cdot\gamma g_{\rho\mu}; \\ H^2_{\rho\mu} &= q_\rho P_\mu - q\cdot P g_{\rho\mu}; \\ H^3_{\rho\mu} &= q_\rho q_\mu - q^2 g_{\rho\mu}. \end{aligned} \tag{2.3}$$

Here $P = (k' + k)/2$, and $q = k' - k$ is the four-momentum transfer. For real photons ($q^2 = 0$), only $G_1(0)$ and $G_2(0)$ play a role. Note that the form factors defined this way are dimensional: G_1 in GeV^{-1}, G_2 in GeV^{-2}, and G_3 in GeV^{-3}.

This set of form factors is analogous to the Dirac-Pauli decomposition of the nucleon form factors F_1 and F_2, is useful as a standard reference, but has the disad-

vantage of not diagonalizing the cross-section formula. For this purpose it is useful to have a covariant multiple decomposition analogous to the Sachs choice of nucleon form factors which is Jones and Scadron form factors.

This definition is commonly used in lattice QCD calculations [5, 6]

$$< \Delta(k',s')|j^{\mu}|N(k,s) >= i\sqrt{\tfrac{2}{3}}\left(\tfrac{m_{\Delta}m_N}{E_{\Delta}E_N}\right)^{1/2}\bar{u}_{\rho}(k',s')\Gamma^{\rho\mu}u(k,s), \tag{2.4}$$

where

$$\Gamma^{\rho\mu} = G_{M1}(q^2)K^{\rho\mu}_{M1} + G_{E2}(q^2)K^{\rho\mu}_{E2} + G_{C2}(q^2)K^{\rho\mu}_{C2}, \tag{2.5}$$

in terms of the magnetic dipole G_{M1}, electric quadrupole G_{E2}, and Coulomb quadrupole G_{C2} form factors. They are analogous to the Sachs form factors G_E and G_M for the nucleon. The invariant functions involve the masses of the particles explicitly,

$$\begin{aligned} K^{\rho\mu}_{M1} &= -\tfrac{3}{(m_{\Delta}+m_N)^2+q^2}\tfrac{(m_{\Delta}+m_N)}{2m_N}\varepsilon^{\rho\mu\alpha\beta}P_{\alpha}q_{\beta}; \\ K^{\rho\mu}_{E2} &= -K^{\rho\mu}_{M1} - 6\Omega^{-1}(q^2)\varepsilon^{\rho\lambda\alpha\beta}P_{\alpha}q_{\beta}\varepsilon^{\mu}\lambda^{\gamma\delta}(2P_{\gamma}+q_{\gamma}) \\ &\quad \times q_{\delta}i\gamma_5\tfrac{(m_{\Delta}+m_N)}{2m_N}; \\ K^{\rho\mu}_{C2} &= -6\Omega^{-1}(q^2)q^{\rho}(q^2P^{\mu} - q\cdot Pq^{\mu})i\gamma_5\tfrac{(m_{\Delta}+m_N)}{2m_N}, \end{aligned} \tag{2.6}$$

where $\Omega(q^2) = [(m_{\Delta}+m_N)^2 - q^2][(m_{\Delta}-m_N)^2 - q^2]$.

We stress that the two sets of form factors are equivalent in describing the physics

of N to Δ transitions. They are related by

$$\begin{aligned}
G_{M1}(Q^2) &= \tfrac{m_N}{3(m_N+m_\Delta)}[((3m_\Delta+m_N)(m_\Delta+m_N)+Q^2)\tfrac{G_1(Q^2)}{m_\Delta} \\
&\quad +(m_\Delta^2-m_N^2)G_2(Q^2)-2Q^2G_3(Q^2)]; \\
G_{E2}(Q^2) &= \tfrac{m_N}{3(m_N+m_\Delta)}[(m_\Delta^2-m_N^2-Q^2)\tfrac{G_1(Q^2)}{m_\Delta}+(m_\Delta^2-m_N^2)G_2(Q^2)-2Q^2G_3(Q^2)]; \\
G_{C2}(Q^2) &= \tfrac{2m_N}{3(m_\Delta+m_N)}[2m_\Delta G_1(Q^2)+\tfrac{1}{2}(3m_\Delta^2+m_N^2+Q^2)G_2(Q^2) \\
&\quad +(m_\Delta^2-m_N^2-Q^2)G_3(Q^2)].
\end{aligned} \tag{2.7}$$

Here we have switched to the notation of $Q^2=-q^2$ since most experimental studies of form factors are for space-like momentum transfers ($q^2<0$ or $Q^2>0$). The inverse form, omitting the explicit Q^2 dependence in the G's, is given as:

$$\begin{aligned}
G_1 &= -3(G_{E2}-G_{M1})[m_\Delta(m_\Delta+m_N)]/[2m_N((m_\Delta+m_N)^2+Q^2)]; \\
G_2 &= -3(m_\Delta+m_N)[(-2G_{C2}Q^2+G_{M1}(m_\Delta^2-2m_\Delta m_N+m_N^2+Q^2) \\
&\quad +G_{E2}(-3m_\Delta^2+2m_\Delta m_N+m_N^2+Q^2))]/[2m_N((m_\Delta^2-m_N^2-Q^2)^2+4m_N^2Q^2)]; \\
G_3 &= -3(m_\Delta+m_N)[(-2G_{C2}(m_\Delta^2-m_N^2)+G_{M1}(m_\Delta^2-2m_\Delta m_N+m_N^2+Q^2) \\
&\quad +G_{E2}(5m_\Delta^2+2m_\Delta m_N+m_N^2+Q^2))]/[4m_N((m_\Delta^2-m_N^2-Q^2)^2+4m_N^2Q^2)].
\end{aligned} \tag{2.8}$$

From these relations, we see that G_{M1} is on the same order as G_1, G_{E2} is proportional to $G_1/m_\Delta+G_2$ at $Q^2=0$. Because of cancellation between G_1 and G_2, the G_{E2} is small and then make it quite difficult to measure accurately.

The Particle Data Group (PDG) [11] uses the transition amplitudes f_{M1} and f_{E2}

which are re-scaled versions of the Sachs form factors [12]

$$\begin{aligned} f_{M1} &= \frac{e}{2m_N}\left(\frac{|\vec{q}|m_\Delta}{m_N}\right)^{1/2} G_{M1}, \\ f_{E2} &= -\frac{e}{2m_N}\left(\frac{|\vec{q}|m_\Delta}{m_N}\right)^{1/2} \frac{2|\vec{q}|m_\Delta}{m_\Delta^2 - m_N^2} G_{E2}, \end{aligned} \tag{2.9}$$

where $e = \sqrt{4\pi\alpha}$. In the rest frame of the Δ at $q^2 = 0$, energy-momentum conservation sets $2|\vec{q}|m_\Delta = m_\Delta^2 - m_N^2$ so the relations simplify to

$$\begin{aligned} f_{M1} &= \frac{e}{2m_N}\left(\frac{m_\Delta^2 - m_N^2}{2m_N}\right)^{1/2} G_{M1}; \\ f_{E2} &= -\frac{e}{2m_N}\left(\frac{m_\Delta^2 - m_N^2}{2m_N}\right)^{1/2} G_{E2}. \end{aligned} \tag{2.10}$$

They are related to the well-known helicity amplitudes by

$$\begin{aligned} f_{M1} &= \frac{-1}{2\sqrt{3}}(3A_{3/2} + \sqrt{3}A_{1/2}); \\ f_{E2} &= \frac{1}{2\sqrt{3}}(A_{3/2} - \sqrt{3}A_{1/2}). \end{aligned} \tag{2.11}$$

A commonly quoted quantity is the ratio

$$R_{EM} = \frac{f_{E2}}{f_{M1}} = -\frac{G_{E2}}{G_{M1}}. \tag{2.12}$$

Partial photonuclear decay widths may also be related to the Sachs form factors assuming continuum dispersion relations,

$$\begin{aligned} \Gamma_{M1} &= \frac{\alpha}{16}\frac{(m_\Delta^2 - m_N^2)^3}{m_\Delta^3 m_N^2} G_{M1}^2, \\ \Gamma_{E2} &= \frac{3\alpha}{16}\frac{(m_\Delta^2 - m_N^2)^3}{m_\Delta^3 m_N^2} G_{E2}^2. \end{aligned} \tag{2.13}$$

2.2 Experimental Information

Throughout this work, we use the generic term N to Δ transition to refer to the eight transitions from the baryon octet to the decuplet:

$$\begin{aligned}
\gamma p &\rightarrow \Delta^{+}, \\
\gamma n &\rightarrow \Delta^{0}, \\
\gamma \Sigma^{+} &\rightarrow \Sigma^{*+}, \\
\gamma \Sigma^{0} &\rightarrow \Sigma^{*0}, \\
\gamma \Sigma^{-} &\rightarrow \Sigma^{*-}, \\
\gamma \Xi^{0} &\rightarrow \Xi^{*0}, \\
\gamma \Xi^{-} &\rightarrow \Xi^{*-}, \\
\gamma \Lambda &\rightarrow \Sigma^{*0}.
\end{aligned} \tag{2.14}$$

Experimentally, pion photo- or electro-production has been used to access the transition amplitudes G_M and G_E. The only transition measured so far is $\gamma p \rightarrow \Delta^{+}$. The Laser Electron Gamma Source (LEGS) at Brookhaven has made measurement of proton cross sections and photon asymmetries. Experiments on pion electroproduction were performed at the Mainz Microtron (MAMI) in the Δ resonance region and low momentum transfer. A program using the CEBAF Large Acceptance Spectrometer (CLAS) at Jefferson Lab has been inaugurated to improve the systematic and statistical precision by covering a wide kinematic range of four-momentum transfer Q^2. At the MIT-Bates linear accelerator, an extensive program has also been carried out.

Table 2.1 lists some of the main experimental data and analysis results at low mo-

Table 2.1: A summary of experimental results for the G_{E2}/G_{M1} ratio R_{EM} in the $\gamma p \to \Delta^+$ transition.

Experiment	Q^2 (GeV^2)	G_{M1} (μ_N)	G_{E2} (μ_N)	R_{EM} (%)
MAMI [13]	0.06	2.51	0.057(14)	-2.28(62)
MAMI [14]	0.38	3.01(1)	0.096(9)	-3.2(0.25)
LEGS [15]	0			-2.5
JLab [16]	0.4	1.16	0.040(10)	-3.4(4)(4)
Bates [17]	0.126	2.2	0.050(9)	-2.0(2)(2)
PDG [11]	0	3.02	0.050	-2.5(0.5)

mentum transfer. It is clear from the results on G_{E2}/G_{M1} ratio R_{EM} that the quadruple component in the N to Δ transition is quite small, signaling a slight deformation of the nucleon. The minus sign implies that its shape is oblate rather than prolate. The bulk of the transition is dominated by the magnetic dipole component, which results from a spin-flip in one of the quarks. The PDG results corresponding to G_{M1} and G_{E2} in other notations are $G_1 = 2.70$ GeV^{-1}, $G_2 = -1.65$ GeV^{-2}; $A_{1/2} = -0.135$ GeV$^{-1/2}$, $A_{3/2} = -0.250$ GeV$^{-1/2}$; $f_{M1} = 0.284$ GeV$^{-1/2}$, $f_{E2} = -0.0047$ GeV$^{-1/2}$;

The extraction of the small G_{E2} amplitude is very sensitive to the details of the models and the specific database used in the fit. Three commonly used are the dynamical model of Sato and Lee (SL model) [18], the unitary isobar model MAID [19], and the partial-wave analysis model SAID [20]. The SL model uses an effective Hamiltonian consisting of bare vertex interactions and energy-independent meson-exchange $N \to \Delta$ transition operators which are derived by applying a unitary transformation to a model Lagrangian describing interactions among $\gamma, \Pi, \rho, \omega, N$ and Δ fields. With appropriate phenomenological form factors and coupling constants for ρ and Δ, the model gives a good description of πN scattering phase shifts up to the Δ excitation

energy region. The MAID and SAID models are partial-wave-based models for pion photo and electroproduction. They start from the Lagrangian for the nonresonant terms, including explicit nucleon and light meson degrees of freedom coupled to the electromagnetic field. The resonance contributions are included by taking into account unitarity to provide the correct phases of the pion photoproduction multipoles. This model provides a good description for individual multipoles as well as differential cross sections and polarization observables.

Chapter 3

The QCD Sum Rules Method

To explain how the QCD sum rules method works, we take the problem of determining the mass of proton as an example. The reason we treat this case is twofold. First, the mass sum rule is the easiest example of baryon QCD sum rules and so our treatment will be partly pedagogical in that we may work out this case in detail. Second, we will need these sum rules for the analysis of the magnetic moments of the $\frac{1}{2}^+$ baryon octet and N to Δ transitions.

QCD sum rule calculations center around the time-ordered two-point correlation function in the QCD vacuum,

$$\Pi(p) = i \int d^4x \; e^{ip\cdot x} \langle 0 \,|\, T\{ \; \eta(x) \, \bar{\eta}(0) \; \} \,|\, 0 \rangle. \tag{3.1}$$

This two-point correlation function describes the process that a baryon propagates from 0 to x in the QCD vacuum. Here η is the interpolating field (or hadron current) with the quantum numbers of the hadron under consideration.

The QCD sum rule approach is to evaluate this correlation function at two different levels. On the quark level, it describes a hadron as quarks and gluons interacting in the QCD vacuum. On the phenomenological level, it is saturated by a tower of hadronic intermediate states with the same quantum numbers. This way, a connection can be established between a description in terms of hadronic degrees of freedom and one based on the underlying quark and gluon degrees of freedom governed by QCD.

In fact, both Lattice QCD and QCD sum rule method have the primary goal of solving the two-point correlation function through QCD vacuum properties and hadron phenomenology, described as duality.

3.1 Baryon Interpolating Fields (Baryon Currents)

To begin the analysis we need an interpolating field (also known as baryon current) η to describe the baryon. The expression of η is not unique under the constraint of consistent quantum numbers. It is build from products of quark field operators. For proton, we use a linear combination of two independent local interpolating field

$$\eta^N_{1/2}(x) = -2 \left[\eta^N_1(x) + \beta \, \eta^N_2(x) \right], \tag{3.2}$$

where

$$\eta^N_1(x) = \epsilon^{abc} \left(u^{aT}(x) C\gamma_5 d^b(x) \right) u^c(x), \tag{3.3}$$

and

$$\eta_2^N(x) = \epsilon^{abc} \left(u^{aT}(x) C d^b(x) \right) \gamma_5 u^c(x). \tag{3.4}$$

Here u and d are up-quark and down-quark field operators, C is the charge conjugation operator, the superscript T means transpose, and ϵ^{abc} makes it color-singlet. The real parameter β allows for the mixture of the two independent currents. The choice advocated by Ioffe [21] and often used in QCD sum rules studies corresponds to $\beta = -1$. We will take advantage of this freedom to achieve optimal matching in the sum rule analysis.

3.2 Operator Product Expansion (OPE)

The two-point correlation function (3.1) is described as the QCD vacuum expectation value of the time ordered product of baryon currents. Wick's theorem suggests that the correlation function may be expressed in the form of quark propagators, which may be further expanded into a series of QCD vacuum condensates, described as operator product expansion (OPE) [8, 22, 23]. Substituting the proton baryon currents into the two-point correlation function will generate contractions of those quark field operators. Therefore, a baryon's two-point correlation function is reduced to a master formula in the form of product of three quark propagators. The result for this spin-1/2 nucleon with uud quark content is:

$$\langle \Omega \,|\, T\{\eta_{1/2}^N(x)\, \bar{\eta}_{1/2}^N(0) \,|\, \Omega \rangle = -4\epsilon^{abc}\epsilon^{a'b'c'}\{$$

$$+S_u^{aa'}\gamma_5 C S_d^{cc'\,T} C\gamma_5 S_u^{bb'} + S_u^{aa'}\mathrm{Tr}(C S_d^{cc'\,T} C\gamma_5 S_u^{bb'}\gamma_5)$$

$$
\begin{aligned}
&+\beta\gamma_5 S_u^{aa'}\gamma_5 C S_d^{cc'T} C S_u^{bb'} + \beta\gamma_5 S_u^{aa'}\mathrm{Tr}(C S_u^{cc'T} C S_d^{bb'}\gamma_5) \\
&+\beta S_u^{aa'} C S_d^{cc'T} C\gamma_5 S_u^{bb'}\gamma_5 + \beta S_u^{aa'}\gamma_5\mathrm{Tr}(C S_u^{cc'T} C\gamma_5 S_d^{bb'}) \\
&+\beta^2\gamma_5 S_u^{aa'} C S_d^{cc'T} C S_u^{bb'}\gamma_5 + \beta^2\gamma_5 S_u^{aa'}\gamma_5\mathrm{Tr}(C S_d^{cc'T} C S_u^{bb'})\ \}. \qquad (3.5)
\end{aligned}
$$

The fully-interacting quark propagator $S(x)$ can be derived from Wick's theorem for the time-ordered product of two fermion fields under the assumption of vacuum saturation of the intermediate states of composite operators. The result, which includes operators up to dimension 8 and terms linear in the quark mass, is explicitly given by [8, 22, 23]

$$
\begin{aligned}
S_q^{ab}(x,0) \;\equiv\; & \langle\Omega \mid T\left\{q^a(x)\overline{q}^b(0)\right\} \mid \Omega\rangle = \\
& \frac{i}{2\pi^2 x^4}\,\gamma\cdot x\,\delta^{ab} - \frac{m_q}{2^2\pi^2 x^2}\delta^{ab} - \frac{1}{2^2\,3}\langle\overline{q}q\rangle\delta^{ab} + \frac{i}{2^4\,3}m_q\langle\overline{q}q\rangle\,\gamma\cdot x\,\delta^{ab} \\
& +\frac{x^2}{2^6\,3}\langle\overline{q}g_c\sigma\cdot Gq\rangle\delta^{ab} - \frac{ix^2}{2^7\,3^2}m_q\langle\overline{q}g_c\sigma\cdot Gq\rangle\,\gamma\cdot x\,\delta^{ab} \\
& -\frac{x^4}{2^{10}\,3^3}\langle\overline{q}q\rangle\langle g_c^2G^2\rangle\delta^{ab} + \frac{i}{2^5\pi^2 x^2}(g_cG^n_{\alpha\beta})(\gamma\cdot x\,\sigma^{\alpha\beta} + \sigma^{\alpha\beta}\,\gamma\cdot x)\frac{\lambda^n_{ab}}{2} \\
& +\frac{1}{2^5\pi^2}m_q\left[\ln\left(\frac{-x^2\Lambda^2}{4}\right) + 2\gamma_{EM}\right](g_cG^n_{\alpha\beta})\sigma^{\alpha\beta}\frac{\lambda^n_{ab}}{2} \\
& +\frac{i}{2^8\,3}m_q\langle\overline{q}g_c\sigma\cdot Gq\rangle(\gamma\cdot x\,\sigma_{\alpha\beta} + \sigma_{\alpha\beta}\,\gamma\cdot x)\frac{\lambda^n_{ab}}{2} \\
& -\frac{1}{2^6\,3}\langle\overline{q}g_c\sigma\cdot Gq\rangle\sigma_{\alpha\beta}\frac{\lambda^n_{ab}}{2} + \frac{x^2}{2^{10}\,3^2}\langle g_c^2G^2\rangle\langle\overline{q}q\rangle\sigma_{\alpha\beta}\frac{\lambda^n_{ab}}{2} + \text{higher order terms.}
\end{aligned} \qquad (3.6)
$$

In this expression, the various vacuum expectation values $\langle O\rangle$ are called QCD vacuum condensates and m_q is the quark mass. Their values will be specified later. The next step is to substitute the quark propagator into the master formula and expand to the

desired order. In the end, one obtains the correlation function in the form

$$\langle 0|T\eta(x)\bar{\eta}(0)|0\rangle = \sum_i C_i(x)\langle O_i\rangle, \tag{3.7}$$

where $C_i(x)$ are the Wilson coefficients in coordinate space and $\langle O_i\rangle$ are the QCD vacuum condensates. The calculation is very tedious. Each term is a product of three copies of the quark propagator $S(x)S(x)S(x)$ with the associated gamma-matrix multiplication and trace operations. There are hundreds of such terms to evaluate, counting all possible color permutations.

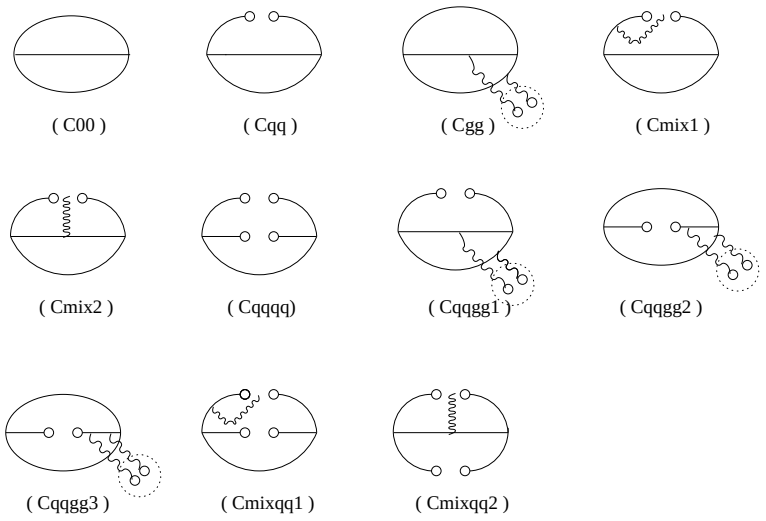

Figure 3.1: Skeleton diagrams considered in the calculation of the QCD side for a baryon

We organize the Wilson coefficients by a graphic representation (similar to Feynmann diagrams) shown in Fig. 3.1 and Fig. 3.2. Each diagram represents a class of terms in the expansion and is named intuitively. For example, *C00* represents the pure perturbative contribution where 3 massless quarks propagate freely, *Cqq* the nonperturbative contribution where one of the quarks picks up the quark conden-

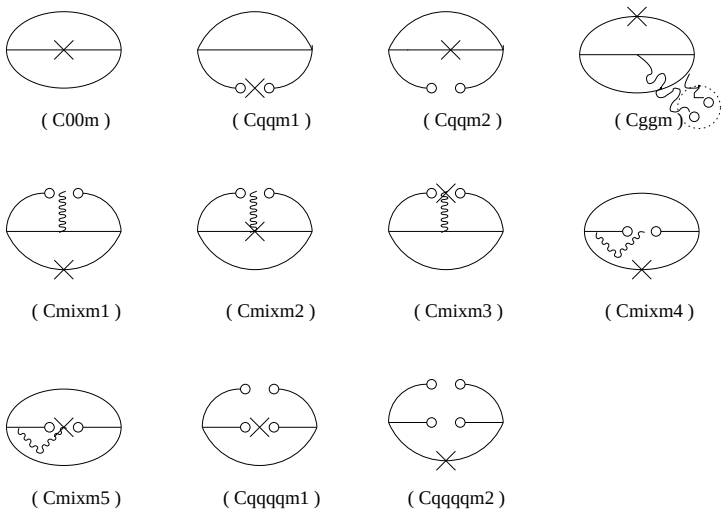

Figure 3.2: Skeleton diagrams linear in the quark mass, denoted by the cross symbol

sate, *Cgg* the gluon condensate contribution where the dangling gluon lines are to be contracted, *Cmix* the mixed condensate contribution, and so on.

We can see that each term except the first two terms is associated with some QCD vacuum condensates, the vacuum expectation values of the operator. m_q is the quark mass correction. For our computation, we only take account of strange quark mass and $m_s = 0.15\text{GeV}$. u quark and d quark masses are taken to be zero.

The minimum independent set of condensate values includes quark condensate $\langle\bar{q}q\rangle$, gluon condensate $\langle\frac{\alpha_s}{\pi}G^a_{\mu\nu}G^{a\mu\nu}\rangle$, and mixed condensate $\langle\bar{q}g_c\sigma\cdot Gq\rangle = -m_0^2\langle\bar{q}q\rangle$. Other condensates may be expressed as a product of the condensates.

We developed a Mathematica package to handle the tedious algebraic computations which will be explained later in Chap. 6. Here we will show how to calculate three diagrams in proton calculation by hand as an example. We take the first term in master formula Eq. (3.5) as a start.

First, we explicitly calculate the contribution of the identity operator. This is

represented diagrammatically by *C00* in Fig. 3.1. The solid lines denote the ordinary coordinate space propagator for a massless quark. This correlator, which is the first term in the quark propagator in Eq.(3.6), can be written as:

$$S_u^{aa\prime}(x) = \delta^{aa\prime}\frac{i}{2\pi^2 x^4}\hat{x}. \tag{3.8}$$

$\hat{x}$ is the contraction of x^μ and γ_μ, that is

$$\hat{x} = x^\mu \gamma_\mu. \tag{3.9}$$

Then we calculate the correlation function Π in Eq. (3.1) using the master formula in Eq. (3.5):

$$\begin{aligned}\Pi(x) = -4\varepsilon^{abc}\varepsilon^{a\prime b\prime c\prime}\{&[\delta^{aa\prime}\frac{i}{2\pi^2 x^4}\hat{x}\gamma_5 C[\delta^{cc\prime}\frac{i}{2\pi^2 x^4}\hat{x}]^T C\gamma_5(\delta^{bb\prime}\frac{i}{2\pi^2 x^4}\hat{x})] \\ &+[\delta^{aa\prime}\frac{i}{2\pi^2 x^4}\hat{x}\ [C(\delta^{cc\prime}\frac{i}{2\pi^2 x^4}\hat{x})^T C\gamma_5(\delta^{bb\prime}\frac{i}{2\pi^2 x^4}\hat{x})\gamma_5]]\}\end{aligned} \tag{3.10}$$

Using gamma matrix identities, we have:

$$\begin{aligned}\Pi(x) &= -4\cdot 6\cdot(\frac{i}{2\pi^2 x^4})^3\{\hat{x}\gamma_5 C\hat{x}^T C\gamma_5\hat{x} + \hat{x}\ [C\hat{x}^T C\gamma_5\hat{x}\gamma_5]\} \\ &= \frac{3i}{\pi^6 x^{12}}\{\hat{x}\gamma_5\hat{x}\gamma_5\hat{x} + \hat{x}\ [\hat{x}\gamma_5\hat{x}\gamma_5]\} \\ &= \frac{3i}{\pi^6 x^{12}}(-x^2\hat{x} + \hat{x}\ [-x^2]) \\ &= \frac{-15i}{\pi^6 x^{10}}\hat{x}\end{aligned} \tag{3.11}$$

The procedure just outlined is how we will calculate the Wilson coefficients of the various operators in an Operator Product Expansion (OPE) for the correction function $\Pi(p)$. We present two more examples calculated by hand. Next, we calculate the Wilson coefficient of the quark condensate $\langle\bar{q}q\rangle$ in the diagrams Cqq. In this diagram, there are two solid lines and one quark line. The correlator for Cqq comes from the 3rd term in the quark propagator in Eq.(3.6). Then, the correlators for these three quarks are:

$$\begin{aligned} S_u^{aa\prime}(x) &= -\delta^{aa\prime}\frac{1}{12}\langle\bar{u}u\rangle \\ S_u^{bb\prime}(x) &= \delta^{bb\prime}\frac{i}{2\pi^2x^4}\hat{x} \\ S_d^{cc\prime}(x) &= \delta^{cc\prime}\frac{i}{2\pi^2x^4}\hat{x}. \end{aligned} \tag{3.12}$$

We need to consider all possible permutations of where the quark line is. The contribution to the correlation function Π from the first situation, denoted as $\Pi(x)_{\rm A}$ is:

$$\begin{aligned} \Pi(x)_{\rm A} &= -4\varepsilon^{abc}\varepsilon^{a\prime b\prime c\prime}[S_u^{aa\prime}\gamma_5 C S_d^{cc\prime {\rm T}} C\gamma_5 S_u^{bb\prime} + S_u^{aa\prime}Tr(cS_d^{cc\prime T}C\gamma_5 S_u^{bb\prime}\gamma_5)] \\ &= -4\cdot 6[-\frac{1}{12}\langle\bar{u}u\rangle\gamma_5 C(\frac{i}{2\pi^2x^4}\hat{x})^T C\gamma_5(\frac{i}{2\pi^2x^4}\hat{x}) \\ &\quad -\frac{1}{12}\langle\bar{u}u\rangle Tr(C(\frac{i}{2\pi^2x^4}\hat{x})^T C\gamma_5(\frac{i}{2\pi^2x^4}\hat{x})\gamma_5)] \\ &= \frac{24}{12}\cdot(\frac{i}{2\pi^2x^4})^2\langle\bar{u}u\rangle[\gamma_5 C\hat{x}^T C\gamma_5\hat{x} + Tr(c\hat{x}^T C\gamma_5\hat{x}\gamma_5)] \\ &= \frac{\langle\bar{u}u\rangle}{2\pi^4x^8}[-x^2 + Tr(-x^2)] \\ &= \frac{5\langle\bar{u}u\rangle}{2\pi^4x^6} \end{aligned} \tag{3.13}$$

Now, we consider another permutation

$$\begin{aligned} S_u^{aa\prime} &= \delta^{aa\prime}\frac{i}{2\pi^2 x^4}\hat{x} \\ S_u^{bb\prime} &= -\delta^{bb\prime}\frac{1}{12}\langle\bar{u}u\rangle \\ S_d^{cc\prime} &= \delta^{cc\prime}\frac{i}{2\pi^2 x^4}\hat{x} \end{aligned} \tag{3.14}$$

We have:

$$\begin{aligned} \Pi(x)_B &= -4\cdot 6\cdot(\frac{-1}{12})(\frac{i}{2\pi^2 x^4})^2[\hat{x}\gamma_5 C\hat{x}^T C\gamma_5\langle\bar{u}u\rangle + \hat{x}\ (c\hat{x}^T C\gamma_5\langle\bar{u}u\rangle\gamma_5)] \\ &= \frac{-\langle\bar{u}u\rangle}{2\pi^4 x^8}[-\hat{x}^2 + \hat{x}\ (+\hat{x})] \\ &= \frac{\langle\bar{u}u\rangle}{2\pi^4 x^6} \end{aligned} \tag{3.15}$$

Similarly, the third diagram is:

$$\begin{aligned} S_u^{aa\prime} &= \delta^{aa\prime}\frac{i}{2\pi^2 x^4}\hat{x} \\ S_u^{bb\prime} &= \delta^{bb\prime}\frac{i}{2\pi^2 x^4}\hat{x} \\ S_d^{cc\prime} &= +\delta^{cc\prime}(-\frac{1}{12})\langle\bar{d}d\rangle \end{aligned} \tag{3.16}$$

$$\begin{aligned} \Pi(x)_C &= -4\cdot 6\cdot(-\frac{1}{12})\cdot(\frac{i}{2\pi^2 x^4})^2\cdot\langle\bar{d}d\rangle[\hat{x}\gamma_5 C\cdot 1^T\cdot C\gamma_5\hat{x} + \hat{x}\ (C\cdot 1^T\cdot C\gamma_5\cdot\hat{x}\cdot\gamma_5)] \\ &= \frac{-\langle\bar{d}d\rangle}{2\pi^4 x^8}[-x^2 + \hat{x}\ \hat{x}] \end{aligned} \tag{3.17}$$

The final answer for the correlation function is:

$$\Pi(x) = \Pi(x)_A + \Pi(x)_B + \Pi(x)_C = \frac{6 < \bar{\mu}\mu > + \langle \bar{d}d \rangle}{2\pi^4 x^6}. \tag{3.18}$$

Now, let us calculate the third example of the Wilson coefficient of the gluon condensate $\langle G^n_{\mu\nu} G^{n\mu\nu} \rangle$ (diagram Cgg). The down quark is the lowest line and the first up quark in the trace is the top line and the second up quark in the trace. They are represented by term 8th and 10th in the quark propagator.

$$\begin{aligned} S_u^{aa\prime} &= \delta^{aa\prime} \frac{i}{2\pi^2 x^4} \hat{x} \\ S_u^{bb\prime} &= (\frac{\lambda^n}{2})^{bb\prime} (\hat{x}\sigma^{\alpha\beta} + \sigma^{\alpha\beta}\hat{x}) \frac{i}{32\pi^2 x^2} \\ S_d^{cc\prime} &= (\frac{\lambda^n}{2})^{cc\prime} \frac{1}{3 \cdot 2^4} < g_s^2 G^2 > (\hat{x}\sigma_{\rho\sigma} + \sigma_{\rho\sigma}\hat{x}) \frac{i}{32\pi^2 x^2} \end{aligned} \tag{3.19}$$

$$\begin{aligned} \Pi(x)_{\rm A} &= -4\varepsilon^{abc}\varepsilon^{a\prime b\prime c\prime} [S_u^{aa\prime} \gamma_5 C S_d^{cc\prime \rm T} C \gamma_5 S_u^{bb\prime} + S_u^{aa\prime} Tr(c S_d^{cc\prime T} C \gamma_5 S_u^{bb\prime} \gamma_5)] \\ &= -4\varepsilon^{abc}\varepsilon^{a\prime b\prime c\prime} \cdot \delta^{aa\prime} \frac{i}{2\pi^2 x^4} \cdot (\frac{\lambda^n}{2})^{bb\prime} (\frac{i}{32\pi^2 x^2})^2 \cdot (\frac{\lambda^n}{2})^{cc\prime} \frac{1}{3 \cdot 2^4} \cdot < g_s^2 G^2 > \cdot \\ &\quad (\hat{x}\gamma_5 C (\hat{x}\sigma_{\rho\sigma} + \sigma_{\rho\sigma}\hat{x})^T C \gamma_5 (\hat{x}\sigma^{\alpha\beta} + \sigma^{\alpha\beta}\hat{x}) \\ &\quad + \hat{x}\, [C (\hat{x}\sigma_{\rho\sigma} + \sigma_{\rho\sigma}\hat{x})^T C \gamma_5 (\hat{x}\sigma^{\alpha\beta} + \sigma^{\alpha\beta}\hat{x}) \gamma_5]) \end{aligned} \tag{3.20}$$

Using identities:

$$\begin{aligned} \varepsilon^{abc}\varepsilon^{a\prime b\prime c\prime} \delta^{aa\prime} (\frac{\lambda^n}{2})^{bb\prime} (\frac{\lambda^n}{2})^{cc\prime} &= -4 \\ C(\hat{x}\sigma^{\alpha\beta} + \sigma^{\alpha\beta}\hat{x})^T C &= -(\hat{x}\sigma^{\alpha\beta} + \sigma^{\alpha\beta}\hat{x}) \end{aligned}$$

$$\begin{aligned}
\hat{x}\sigma_{\rho\sigma} + \sigma_{\rho\sigma}\hat{x} &= -2\varepsilon^{\mu\nu}_{\rho\sigma} x_\mu \gamma_\nu \gamma_5 \\
\hat{x}\sigma^{\alpha\beta} + \sigma^{\alpha\beta}\hat{x} &= -2\varepsilon^{\alpha\beta\mu\nu} x_\mu \gamma_\nu \gamma_5
\end{aligned} \tag{3.21}$$

$$\begin{aligned}
\Pi(x)_{\rm A} &= (-4)(-4)\cdot \frac{(-i<g_s^2G^2>)}{3\cdot 2^{15}\cdot \pi^6 x^8}(-\hat{x}\gamma_5(\hat{x}\sigma_{\rho\sigma}+\sigma_{\rho\sigma}\hat{x})\gamma_5(\hat{x}\sigma^{\alpha\beta}+\sigma^{\alpha\beta}\hat{x}) \\
&\quad +\hat{x}\,[-(\hat{x}\sigma_{\rho\sigma}+\sigma_{\rho\sigma}\hat{x})\gamma_5(\hat{x}\sigma^{\alpha\beta}+\sigma^{\alpha\beta}\hat{x})\gamma_5]) \\
&= \frac{+i<g_s^2G^2>}{3\cdot 2^{11}\pi^6 x^8}[\hat{x}\gamma_5 2\varepsilon^{\mu\nu}_{\rho\sigma} x_\mu\gamma_\nu\gamma_5\gamma_5 2\varepsilon^{\alpha\beta\mu\nu}x_\mu\gamma_\nu\gamma_5 \\
&\quad +\hat{x}\,(2\varepsilon^{\mu\nu}_{\rho\sigma}x_\mu\gamma_\nu\gamma_5\gamma_5 2\varepsilon^{\alpha\beta\mu\nu}x_\mu\gamma_\nu\gamma_5\gamma_5)]
\end{aligned} \tag{3.22}$$

We have $\varepsilon^{\mu\nu}_{\rho\sigma}\varepsilon^{\alpha\beta\mu\nu} = -\varepsilon^{\rho\sigma}_{\mu\nu}\varepsilon^{\mu\nu\alpha\beta} = 2(g_{\alpha\rho}g_{\beta\rho} - g_{\alpha\sigma}g_{\rho\beta})$.

$$\begin{aligned}
\Pi(x)_{\rm A} &= \frac{i<g_s^2G^2>}{3\cdot 2^{10}\pi^6 x^8}(g_{\alpha\rho}g_{\beta\rho}-g_{\alpha\sigma}g_{\rho\beta})[4\hat{x}\gamma_5 x_\mu\gamma_\nu x_\mu\gamma_\nu\gamma_5 + \hat{x}\,(4x_\mu\gamma_\nu x_\mu\gamma_\nu\gamma_5\gamma_5)] \\
&= \frac{i<g_s^2G^2>}{3\cdot 2^{8}\pi^6 x^8}(g_{\alpha\rho}g_{\beta\rho}-g_{\alpha\sigma}g_{\rho\beta})[\hat{x}x^2 + \hat{x}\,(x^2)] \\
&= \frac{5i<g_s^2G^2>}{2^8\pi^6 x^6}\hat{x}
\end{aligned} \tag{3.23}$$

Similarly, consider all the possible permutations of attaching the gluon lines to the quark lines. We have already done the case where one gluon is attached to the down quark and the other to one of the up quarks and the factor of two we included took care of both possibilities. One should also do the case where the two gluons are attached to the two up quarks.This contribution is actually zero when one does the computation. One should also consider the case when one quark line emits two gluons. Thus we have actually got the complete Wilson coefficient for the gluon condensate

operator.

$$
\begin{aligned}
S_u^{aa\prime} &= (\frac{\lambda^n}{2})^{aa\prime}(\hat{x}\sigma^{\alpha\beta}+\sigma^{\alpha\beta}\hat{x})\frac{i}{32\pi^2x^2} \\
S_u^{bb\prime} &= \delta^{bb\prime}\frac{i}{2\pi^2x^4}\hat{x} \\
S_d^{cc\prime} &= (\frac{\lambda^n}{2})^{cc\prime}\frac{1}{3\cdot 2^4}<g_s^2G^2>(\hat{x}\sigma_{\rho\sigma}+\sigma_{\rho\sigma}\hat{x})\frac{i}{32\pi^2x^2}
\end{aligned}
\tag{3.24}
$$

$$
\begin{aligned}
\Pi(x)_{\mathbf{B}} &= -4\varepsilon^{abc}\varepsilon^{a\prime b\prime c\prime}[S_u^{aa\prime}\gamma_5 C S_d^{cc\prime \mathrm{T}} C\gamma_5 S_u^{bb\prime}+S_u^{aa\prime}Tr(cS_d^{cc\prime T}C\gamma_5 S_u^{bb\prime}\gamma_5)] \\
&= (-4)(-4)\cdot\frac{-i<g_s^2G^2>}{3\cdot 2^{15}\pi^6x^8}(-(\hat{x}\sigma^{\alpha\beta}+\sigma^{\alpha\beta}\hat{x})\gamma_5(\hat{x}\sigma_{\rho\sigma}+\sigma_{\rho\sigma}\hat{x})\gamma_5\hat{x} \\
&\quad +(\hat{x}\sigma^{\alpha\beta}+\sigma^{\alpha\beta}\hat{x})Tr(-(\hat{x}\sigma_{\rho\sigma}+\sigma_{\rho\sigma}\hat{x})\gamma_5\hat{x}\gamma_5)) \\
&= \frac{i<g_s^2G^2>}{3\cdot 2^8\pi^6x^8}(g_{\alpha\rho}g_{\rho\sigma}-g_{\alpha\sigma}g_{\rho\beta})[x_\mu\gamma_\nu\gamma_5\gamma_5 x_\mu\gamma_\nu\gamma_5\gamma_5\hat{x}+x_\mu\gamma_\nu\gamma_5 Tr(x_\mu\gamma_\nu\gamma_5\gamma_5\hat{x}\gamma_5)] \\
&= \frac{i<g_s^2G^2>}{3\cdot 2^8\pi^6x^8}[-x^2\hat{x}+x_\mu\gamma_\nu\gamma_5 Tr(x^2\gamma_\nu\gamma_\mu\gamma_5)] \\
&= \frac{-i<g_s^2G^2>}{3\cdot 2^8\pi^6x^8}\cdot\hat{x}
\end{aligned}
\tag{3.25}
$$

Consider another permutation, we get:

$$
\begin{aligned}
S_u^{aa\prime} &= (\frac{\lambda^n}{2})^{aa\prime}(\hat{x}\sigma^{\alpha\beta}+\sigma^{\alpha\beta}\hat{x})\frac{i}{32\pi^2x^2} \\
S_u^{bb\prime} &= (\frac{\lambda^n}{2})^{bb\prime}\frac{1}{3\cdot 2^4}<g_s^2G^2>(\hat{x}\sigma_{\rho\sigma}+\sigma_{\rho\sigma}\hat{x})\frac{i}{32\pi^2x^2} \\
S_d^{cc\prime} &= \delta^{cc\prime}\frac{i}{2\pi^2x^4}\hat{x}
\end{aligned}
\tag{3.26}
$$

$$
\begin{aligned}
\Pi(x)_C &= \frac{i<g_s^2G^2>}{3\cdot 2^8\pi^6x^8}(g_{\alpha\rho}g_{\beta\sigma}-g_{\alpha\sigma}g_{\rho\beta})[x_\mu\gamma_\nu\gamma_5\gamma_5\cdot\hat{x}\gamma_5 x_\mu\gamma_\nu\gamma_5 \\
&\quad +x_\mu\gamma_\nu\gamma_5 Tr(\hat{x}\gamma_5 x_\mu\gamma_\nu\gamma_5\gamma_5)]
\end{aligned}
$$

$$= \frac{i < g_s^2 G^2 >}{3 \cdot 2^8 \pi^6 x^8} [x^2 \gamma_\nu \hat{x} \gamma_5 \gamma_\nu \gamma_5 + x_\mu \gamma_\nu \gamma_5 Tr(\hat{x} \gamma_5 x_\mu \gamma_\nu)]$$
$$= \frac{i < g_s^2 G^2 >}{3 \cdot 2^8 \pi^6 x^6} \hat{x}. \tag{3.27}$$

Add them up, we have:

$$\Pi(x) = \frac{5i < g_s^2 G^2 >}{2^8 \pi^6 x^6} \hat{x}. \tag{3.28}$$

As one can see, while we evaluated these diagrams by hand, it becomes necessary in later calculation to use symbolic manipulators owing to the complexities of the allowed diagrams. We subsequently came back to check the mass sum rule diagrams using Mathematica code. The use of such symbolic manipulators greatly eases the computation. The QCD calculation is traditionally referred to as the LHS of a QCD sum rule.

3.3 Phenomenological Representation (RHS)

In this section, we want to evaluate the same correlation function in Eq. (3.1) at the phenomenological level. Conventionally, it is defined as the right hand side (RHS) of a QCD sum rule. This is done by inserting a complete set of eigenstates with the quantum numbers of the correlation function (3.1). The complete set has the following form

$$1 = \int \frac{d^4 p}{(2\pi)^4} \sum_{B,\sigma} \frac{-i}{p^2 - M_N^2} |pB\sigma >< pB\sigma|, \tag{3.29}$$

where q is the momentum of the baryon; B denotes the summation over all baryons (nucleon resonances) having the same quantum numbers as the proton; σ represents

the spin sum. The rest is for normalization. This leads to a set of terms in the form of $\langle 0|\eta|q\sigma\rangle$, which represent the transition of a baryon of momentum q and spin σ to the QCD vacuum.

Use translation invariance on $< 0|\eta|pB\sigma >$. The ability to do so is described by a phenomenological parameter λ_B (called current coupling or pole residue), defined by the overlap with the ground state

$$< 0|\eta|pB\sigma >= \lambda_B u(p,\sigma), \tag{3.30}$$

where u is a Dirac spinor.

Considering $q^2 = {M_N}^2$ for real particles, and the famous spin sum becomes:

$$\sum_\sigma u(p,\sigma)\bar{u}(p,\sigma) = \hat{p} + M_N. \tag{3.31}$$

Now, we have

$$\begin{aligned} \Pi(p) &= \sum_{B\sigma} \frac{< \Omega|\eta|pB\sigma >< pB\sigma|\bar{\eta}|\Omega >}{p^2 - M_N^2} \\ &= \sum_{B\sigma} \frac{\lambda_N^2 u(p,\sigma)\bar{u}(p,\sigma)}{p^2 - M_N^2} \\ &= \sum_{B} \frac{\lambda_N^2(\hat{p} \pm M_N)}{p^2 - M_N^2} \end{aligned} \tag{3.32}$$

where $+/-$ corresponds to positive/negative parity baryons. The sum is over the entire spectrum with both parities.

As one can see, there are two distinct Dirac structures $\hat{p}$ and the identity 1 in

this correlation function from which two independent sum rules can be constructed.

3.4 Fourier Transform

Remember we have a Fourier transform in the definition of 2-point correlation function.

Let D be the dimensionality of space-time. Define the quantity $\epsilon \equiv \frac{4-D}{2}$. Then the following identity holds:

$$\int d^D x e^{ipx} \frac{1}{[x^2]^\beta} = -i \frac{\Gamma(2+\epsilon-\beta)}{\Gamma(\beta)} (4\pi)^{2+\epsilon} \frac{1}{4^\beta} \frac{1}{[p^2]^{2+\epsilon-\beta}}; \tag{3.33}$$

with inverse

$$\int \frac{d^D p}{(2\pi)^D} e^{-ipx} \frac{1}{[p^2]^\beta} = +i \frac{\Gamma(2+\epsilon-\beta)}{\Gamma(\beta)} (\pi)^{-(2+\epsilon)} \frac{1}{4^\beta} \frac{1}{[x^2]^{2+\epsilon-\beta}}. \tag{3.34}$$

This first equation is the basic formula; all else in this section will be derived from it. We define the following bracket symbol

$$[f]_\beta \equiv \int d^D x e^{ipx} f(x) \frac{1}{[x^2]^\beta}. \tag{3.35}$$

So, for instance,

$$[1]_\beta \equiv \int d^D x e^{ipx} f(x) \frac{1}{[x^2]^\beta} = -i \frac{\Gamma(2+\epsilon-\beta)}{\Gamma(\beta)} (4\pi)^{2+\epsilon} \frac{1}{4^\beta} \frac{1}{[p^2]^{2+\epsilon-\beta}}, \tag{3.36}$$

which is our basic formula. Terms where $f(x) = x_{\mu_1} \cdots x_{\mu_n}$ are obtained by differentiating with $(-i)^n(\partial_{\mu_1} \cdots \partial_{\mu_n})$, where $\partial_\mu \equiv \frac{\partial}{\partial p^\mu}$, viz.

$$[x_{\mu_1} \cdots x_{\mu_n}]_\beta = (-i)^n(\partial_{\mu_1} \cdots \partial_{\mu_n})[1]_\beta. \tag{3.37}$$

Terms involving $\ln x^2$ can be obtained by differentiating

$$\frac{\partial}{\partial\beta}(x^2)^{-\beta} = -\ln x^2(x^2)^{-\beta} \tag{3.38}$$

$$[\ln x^2]_\beta = -\frac{\partial}{\partial\beta}[1]_\beta \tag{3.39}$$

$$[x_{\mu_1} \cdots x_{\mu_n} \ln x^2]_\beta = -\frac{\partial}{\partial\beta}(-i)^n(\partial_{\mu_1} \cdots \partial_{\mu_n})[1]_\beta. \tag{3.40}$$

As mentioned above, we are only interested in terms which survive in transforming. These are terms having inverse powers of p^2 or terms in $\ln p^2$, that is, non-polynomial terms. Let's dispose of the simple cases first emanating $[1]_\beta$. For $\beta = 1$, Eq.(3.36) reduces to:

$$[1]_1 = -i\frac{4\pi^2}{p^2}, \tag{3.41}$$

for $\beta \geq 2$, Eq.(3.36) will have divergences coming from the poles of the gamma. But as mentioned above we need only consider the $\ln p^2$ part.

$$[1]_\beta = -i(4\pi)^2(p^2)^{\beta-2}\frac{\Gamma(2+\epsilon-\beta)}{\Gamma(\beta)4^\beta}(\frac{4\pi}{p^2})^\epsilon, \tag{3.42}$$

when $\beta \geq \alpha$ we have the following:

$$\frac{\Gamma(\alpha+\epsilon-\beta)}{\Gamma(\epsilon)} = (-1)^{\beta-\alpha}\frac{1}{(\beta-\alpha)!}[1+\mathrm{O}(\epsilon)]. \tag{3.43}$$

Expanding to order ϵ we have:

$$[1]_\beta = -i(4\pi)^2(p^2)^{\beta-2}\frac{1}{\Gamma(\beta)4^\beta}(\frac{1}{\varepsilon}\gamma_{\mathrm{EM}})(1+\epsilon\ln(\frac{4\pi}{p^2}))(-1)^{\beta-2}\frac{1}{(\beta-2)!}(1+\mathrm{O}(\epsilon)). \tag{3.44}$$

where γ_{EM} is Euler constant.

Considering only the $\ln p^2$ part we have:

$$[1]_\beta = +i\pi^2(-1)^\beta\frac{1}{(\beta-1)!(\beta-2)!}(\frac{p^2}{4})^{\beta-2}\ln p^2 + z.b.t., \tag{3.45}$$

where *z.b.t.* means "zero on Borel transforming". The Borel transform will be explained in the next section. We can now simply obtain the transforms $[x_\mu]_\beta$ and $[x_\mu x_\nu]$.

$$[x_\mu]_1 = 8\pi^2\frac{p_\mu}{p^4} \tag{3.46}$$

$$[x_\mu]_2 = 2\pi^2\frac{p_\mu}{p^2} \tag{3.47}$$

$$[x_\mu]_\beta = \pi^2(-1)^\beta\frac{1}{(\beta-1)!(\beta-3)!}\frac{1}{2}p_\mu(\frac{p^2}{4})^{\beta-3}\ln p^2 \tag{3.48}$$

$$[x_\mu x_\nu]_1 = -8i\pi^2[\frac{g_{\mu\nu}}{p^4} - 4\frac{p_\mu p_v}{p^6}] \tag{3.49}$$

$$[x_\mu x_\nu]_2 = -2i\pi^2[\frac{g_{\mu\nu}}{p^2} - 2\frac{p_\mu p_v}{p^4}] \tag{3.50}$$

$$[x_\mu x_\nu]_3 = \frac{1}{4} i\pi^2 [g_{\mu\nu} \ln p^2 + 2\frac{p_\mu p_v}{p^2}] \tag{3.51}$$

$$[x_\mu x_\nu]_\beta = -i\pi^2 (-1)^\beta \frac{1}{(\beta-1)!(\beta-3)!} \frac{1}{2} \frac{1}{4^{\beta-3}} [g_{\mu\nu}(p^2)^{\beta-3} + (\beta-3) p_\mu p_v (p^2)^{\beta-4}] \ln p^2 \tag{3.52}$$

Now we turn to the logarithmic transforms. Examining (3.36) and (3.39) we need the derivative:

$$-\frac{\partial}{\partial\beta}\{(\frac{p^2}{4})^\beta \frac{\Gamma(\alpha+\epsilon+\beta)}{\Gamma(\beta)}\} = \{\frac{\Gamma(\alpha+\epsilon+\beta)}{\Gamma(\beta)}\}[-\ln\frac{p^2}{4} + \psi(\alpha+\epsilon-\beta) + \psi(\beta)] \tag{3.53}$$

where $\psi(x) = \frac{d}{d_x} \ln\Gamma(x)$. Then

$$[\ln x^2]_\beta = -i(4\pi)^{2+\epsilon} \frac{\Gamma(2+\epsilon-\beta)}{\Gamma(\beta) 4^\beta} (p^2)^{\beta-(2+\epsilon)} [-\ln\frac{p^2}{4} + \psi(2+\epsilon-\beta)] + \psi(\beta)] \tag{3.54}$$

For $\beta = 1$ we have

$$[\ln x^2]_1 = 4i\pi^2 \frac{1}{p^2} [\ln\frac{p^2}{4} + 2\gamma_{\rm EM}] \tag{3.55}$$

where we have used $\psi(1) = -\gamma_{\rm EM}$ and $\gamma_{\rm EM} = 0.5777...$ is the Euler-Mascheroni constant. For $\beta = 2$ we have:

$$[\ln x^2]_2 = -i\pi^2 (\frac{4\pi}{p^2})^\epsilon \Gamma(\epsilon)[-\ln\frac{p^2}{4} + \psi(\epsilon) + \psi(2)] \tag{3.56}$$

which, after some expansion and algebra, gives:

$$[\ln x^2]_2 = i\pi^2 \ln p^2 [-\frac{1}{2}\ln p^2 + \ln 4 + 1 - 2\gamma_{\rm EM}] + z.b.t. \tag{3.57}$$

For $\beta > 2$ Eq.(3.36) becomes very messy and since we only need these transforms in this thesis up to $\beta = 2$ we will stop here. One can get the transforms $[x_\mu \ln x^2]_{1,2}$ and $[x_u x_\nu \ln x^2]_{1,2}$. In Table 3.1 and Table 3.2, we have tabulated the logarithmic and non-logarithmic transforms we have used in this thesis.

Table 3.1: Logarithmic Fourier transforms

$[\ln x^2]_1 = 4i\pi^2 \frac{1}{p^2}[\ln \frac{p^2}{4} + 2\gamma_{\rm EM}]$
$[x_\alpha \ln x^2]_1 = -8\pi^2 \frac{p_\mu}{p^4}[\ln \frac{p^2}{4} + 2\gamma_{\rm EM} - 1]$
$[x_\alpha x_\beta \ln x^2]_1 = 8i\pi^2[\frac{g_{\mu\nu}}{p^4}(\ln \frac{p^2}{4} + 2\gamma_{\rm EM} - 1) - \frac{4p_\mu p_\nu}{p^6}(\ln \frac{p^2}{4} + 2\gamma_{\rm EM} - \frac{3}{2})]$
$[\ln x^2]_2 = i\pi^2 \ln p^2[\frac{1}{2}\ln p^2 - \ln 4 + 1 - 2\gamma_{\rm EM}]$
$[x_\alpha \ln x^2]_2 = -2\pi^2 \frac{p_\mu}{p^2}[\ln \frac{p^2}{4} + 2\gamma_{\rm EM} - 1]$
$[x_\alpha x_\beta \ln x^2]_2 = 2i\pi^2[\frac{g_{\alpha\beta}}{p^2}(\ln \frac{p^2}{4} + 2\gamma_{\rm EM} - 1) - \frac{2p_\alpha p_\beta}{p^2}(\ln \frac{p^2}{4} + 2\gamma_{\rm EM} - 2)]$

Table 3.2: Fourier transforms

$[1]_1 = -4i\pi^2[\frac{1}{p^2}]$
$[x_\alpha]_1 = 8\pi^2[\frac{p_\alpha}{p^4}]$
$[x_\alpha x_\beta]_1 = -8i\pi^2[\frac{g_{\alpha\beta}}{p^4} - 4\frac{p_\alpha p_\beta}{p^6}]$
$[1]_2 = i\pi^2 \ln \lvert p^2 \rvert$
$[x_\alpha]_2 = 2\pi^2[\frac{p_\alpha}{p^2}]$
$[x_\alpha x_\beta]_2 = -2i\pi^2[\frac{g_{\alpha\beta}}{p^2} - 2\frac{p_\alpha p_\beta}{p^4}]$
$[1]_3 = \frac{-i\pi^2}{8} p^2 \ln \lvert p^2 \rvert$
$[x_\alpha]_3 = -\frac{\pi^2}{4} p_\alpha \ln \lvert p^2 \rvert$
$[x_\alpha x_\beta]_3 = \frac{i\pi^2}{4}[g_{\alpha\beta} \ln \lvert p^2 \rvert + 2\frac{p_\alpha p_\beta}{p^2}]$
$[1]_4 = \frac{i\pi^2}{3\cdot 2^6} p^4 \ln \lvert p^2 \rvert$
$[x_\alpha]_4 = \frac{\pi^2}{3\cdot 2^4} p_\alpha p^2 \ln \lvert p^2 \rvert$
$[x_\alpha x_\beta]_4 = \frac{-i\pi^2}{3\cdot 2^4}[g_{\alpha\beta} p^2 + 2p_\alpha p_\beta] \ln \lvert p^2 \rvert$
$[1]_5 = \frac{-i\pi^2}{3^2 \cdot 2^{10}} p^6 \ln \lvert p^2 \rvert$
$[x_\alpha]_5 = \frac{-\pi^2}{3\cdot 2^9} p^4 p_\alpha \ln \lvert p^2 \rvert$
$[x_\alpha x_\beta]_5 = \frac{i\pi^2}{3\cdot 2^9}[g_{\alpha\beta} p^4 + 4p_\alpha p_\beta p^2] \ln \lvert p^2 \rvert$

Using the table above, we can Fourier transform from x space to momentum space. Take three diagrams we have done for example, Fourier transforming Eq.

(3.11) for *C00* gives:

$$\Pi(p) = \frac{-15i}{\pi^6} \cdot \frac{-\pi^2}{3 \cdot 2^a} p^4 \ln(p^2)\hat{p} = \frac{5i}{2^8 \cdot (2\pi)^4} p^4 \ln(p^2)\hat{p}; \tag{3.58}$$

Fourier transforming the Eq. (3.18) for diagram *Cqq* gives:

$$\begin{aligned} \Pi(p) &= \frac{6\langle\bar{u}u\rangle + \langle\bar{d}d\rangle}{2\pi^4}[1]_3 \\ &= \frac{6\langle\bar{u}u\rangle + \langle\bar{d}d\rangle}{2\pi^4} \cdot \frac{-i\pi^2}{8} \cdot p^2 \ln|p^2| \\ &= -i\frac{6\langle\bar{u}u\rangle + \langle\bar{d}d\rangle}{4(2\pi)^2} p^2 \ln(-p^2); \end{aligned} \tag{3.59}$$

and Fourier transforming the Eq. (3.28)) for diagram *Cgg* gives

$$\Pi(p) = \frac{5i < g_s^2 G^2 >}{2^8\pi^6}[\hat{x}]_3 = \frac{5i < g_s^2 G^2 >}{2^{10}\pi^4} \ln|p^2|. \tag{3.60}$$

After the Fourier transform of the OPE side and matching with the phenomenological side, the QCD sum rule from either structure takes the following generic form,

$$\begin{aligned} \cdots + c_4 p^4 ln(-p^2) + c_2 p^2 ln(-p^2) + c_0 ln(-p^2) + c_{-2}\frac{1}{p^2} + c_{-4}\frac{1}{p^4} + \cdots \\ = \frac{\lambda_N^2}{p^2 - M_N^2} + \sum_{N^*} \frac{\lambda_{N^*}^2}{p^2 - M_{N^*}^2} \end{aligned} \tag{3.61}$$

The LHS comes from OPE results, while the RHS is the Phenomenological results. The OPE side is a power series in p^2. In the meantime, the RHS is composed of a ground state term plus a sum over all excited state contributions.

In fact, all the sum rules associated with various Dirac structures share the same

structure as Eq.(3.61). In principle, this equation can be solved for the ground state $(\lambda^2, \mathrm{M_N})$. But there is a problem: excited states are not suppressed.

3.5 Borel Transformation

While there is some suppression of excited state contributions to the two-point correlation function, it seems there is little hope of isolating ground state properties from excited states contributions. Hence the well-known Borel Transform is introduced to achieve a better convergence. This transformation helps to improve the convergence on both sides of the equation Eq. (3.61). The result is an exponential suppression of excited state contributions on the phenomenological side, and a $n!$ factorial suppression on the OPE side of the sum rules for the terms of order n. The Borel transform is defined by the following limit:

$$\hat{B}[f(p^2)] = \lim_{-p^2,n\to\infty;-p^2/n=M^2} \frac{1}{n!}(-p^2)^{n+1}(\frac{d}{dp^2})^n f(p^2). \tag{3.62}$$

An important feature of the Borel transform is that it removes all polynomial terms in $f(p^2)$. Because of this feature it is not necessary to carry polynomial terms arising in either RHS or LHS of the two-point correlation function.

Now, consider a simple case,

$$\begin{aligned}\hat{B}(\frac{1}{p^2-M_B^2}) &= \lim_{-p^2,n\to\infty;-p^2/n=M^2} \frac{1}{n!}(-p^2)^{n+1}\, n!\, (\frac{1}{p^2-M_B^2})^{n+1} \\ &= \lim_{n\to\infty}(1+\frac{M_B^2}{M^2 n})^{-(n+1)},\end{aligned}$$

$$= \quad -e^{-M_B^2/M^2} \tag{3.63}$$

Moreover, the OPE side simply follows the patterns depicted in Eq. (3.63). We may easily obtain a general formula applicable to the OPE side,

$$\hat{B}[(p^2 - M_B^2)^{-k}] = (-1)^k \frac{1}{(k-1)!} \frac{1}{(M^2)^{k-1}} \; e^{-M_B^2/M^2}. \tag{3.64}$$

In the limit of $M_B^2 \to 0$, we have the following Borel transform pattern,

$$\hat{B}[(p^2)^{-k}] = (-1)^k \frac{1}{(k-1)!} \frac{1}{(M^2)^{k-1}}. \tag{3.65}$$

We can extend to:

$$\hat{B}[(-p^2)^{-k}] = \frac{1}{\Gamma(k)} \frac{1}{(M^2)^{k-1}}. \tag{3.66}$$

where Γ is the Gamma function.

Now,

$$\frac{d}{dk}(-p^2)^{-k} = -ln(-p^2)(-p^2)^{-k}. \tag{3.67}$$

So we get the Borel transform for this frequently encountered pattern,

$$\begin{aligned} \hat{B}[ln(-p^2)(-p^2)^{-k}] &= -\frac{d}{dk} \frac{1}{\Gamma(k)} \frac{1}{(M^2)^{k-1}} \\ &= \frac{1}{\Gamma(k)} (M^2)^{1-k} \{\psi(k) + lnM^2\}. \end{aligned} \tag{3.68}$$

where $\psi(k) = -\gamma_{EM} + \sum_{s=1}^{k-1} \frac{1}{s}$

So we have the form

$$\hat{B}[ln(\frac{-p^2}{\Lambda^2})(p^2)^{-k}] = (-1)^k \frac{1}{(k-1)!}(M^2)^{1-k}\{\psi(k) + ln\frac{M^2}{\Lambda^2}\}. \tag{3.69}$$

Another form we may encounter is: $(p^2)^k ln(-p^2)$

$$\begin{aligned}
\hat{B}[(p^2)^k ln(-p^2)] &= \lim_{-p^2,n\to\infty;\frac{-p^2}{n}=M^2} \frac{1}{n!}(-p^2)^{n+1}\,(\frac{d}{d\,p^2})^n\,(p^2)^k ln(-p^2) \\
&= \lim_{-p^2,n\to\infty;\frac{-p^2}{n}=M^2} \frac{1}{n!}(-p^2)^{n+1}\,(\frac{d}{d\,p^2})^{n-k}\,\{k!\,ln(-p^2) + polynomial\} \\
&= \lim_{n\to\infty;\frac{-p^2}{n}=M^2} -\frac{k!(n-k-1)!}{n!}(-p^2)^{k+1} \\
&= \lim_{n\to\infty} -k!\frac{n^{k+1}(n-k-1)!}{n!}(M^2)^{k+1} \\
&= -k!(M^2)^{k+1}
\end{aligned} \tag{3.70}$$

Now, we can apply the Borel transform on Eq.(3.29), we have

$$\begin{aligned}
\cdots + c'_4 2! M^6 \; + c'_2 M^4 \; + c'_0 M^2 \; + c'_{-2} \; + c'_{-4}\frac{1}{M^2} \; + c'_{-6}\frac{1}{2!}\frac{1}{M^4} \; + \cdots \\
= \; \tilde{\lambda}^2_N \, e^{-M^2_N/M^2} \; + \sum_{N^*} \tilde{\lambda}^2_{N^*} \, e^{-M^2_{N^*}/M^2}
\end{aligned} \tag{3.71}$$

This indeed carries a "one stone two birds" effect by giving us a factorial suppression of higher order terms on the OPE side, and an exponential suppression of excited states on the phenomenological side of the sum rules.

3.6 Excited State Approximation

After the Borel transform, the contributions from the excited baryon states is exponential suppressed. However, the excited state effects in QCD sum rules still can not be ignored. We must take account of the low-lying excited states, which enclose a great number of unknown parameters and make our calculation meaningless. At this point, we need to introduce a "pole+continuum ansatz" for excited state contributions, so that all the discrete excited states above the ground state under consideration are modeled by a continuous function started from a single continuum threshold w. Figure 3.3 shows how to estimate the excited state contributions. We replace the

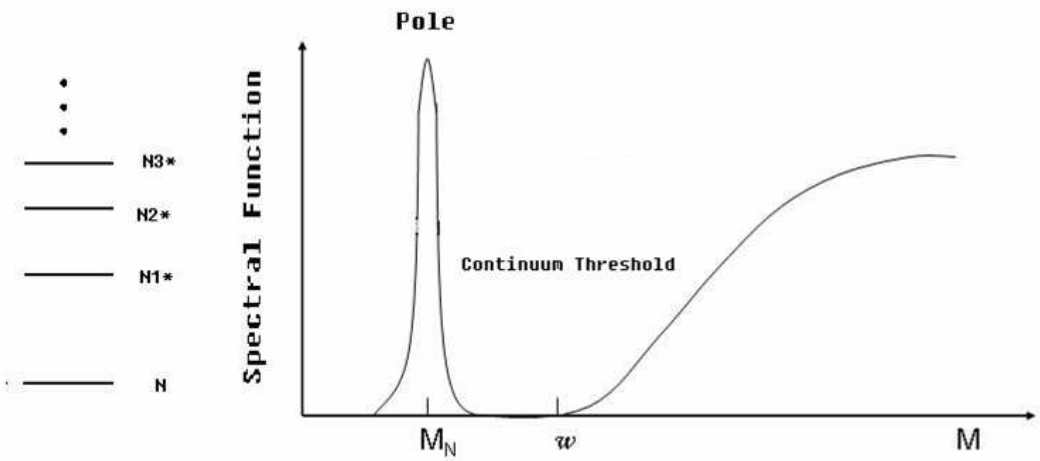

Figure 3.3: Model the excited states by a pole and a continuum function.

poles with $\delta(s - M_N)$, and all excited state with a smoother function $f(s)$. Therefore, the RHS now takes the form of a pole of the ground state plus a continuum function. The continuum function for the excited states is given by,

$$\Pi(M) = \int h(s)\, e^{-s^2/M^2}\, d\, s. \tag{3.72}$$

where

$$h(s) = \delta(s - M_N) + f(s). \tag{3.73}$$

w is introduced as a threshold describing the low bound of the continuum function. For example, we may estimate for the nucleon $w \sim 1.44$GeV, which is the Roper $N^+_{\frac{1}{2}}(1440)$ mass. Here we leave the threshold w as a free parameter to get optimized fitting in calculations of the sum rules.

In order to determine $f(s)$ we will exploit the large M behavior of the OPE side of the sum rules, which is in the non-perturbative limit. Eq. (3.71) gives that the OPE after Borel transform takes the form which is proportional to terms including M^2, M^4, and M^6 at large M. We now rewrite the continuum contributions into the following form, such that the RHS and OPE share the same form under the perturbative limit.

$$\int_0^\infty ds\, e^{-s^2/M^2}\, f(s) = A_6 M^6 + A_4 M^4 + A_2 M^2. \tag{3.74}$$

This is a Laplace transform of $f(s)$. Therefore, $f(s)$ must take the following form

$$f(s) = \frac{1}{2} A_6 s^2 + A_4 s + A_2, \tag{3.75}$$

Continuum model contributions associated with M^4 and M^2 terms are calculated in a similar manner. Usually we move the continuum contributions from the RHS to the OPE side of the sum rules, as they share the same form. Hence, the OPE side

terms surviving in the limit $M \to \infty$ have the following factors associated with them:

$$\begin{aligned} M^6 \quad &: \left[1 - e^{-w^2/M^2} \left(\frac{w^4}{2M^4} + \frac{w^2}{M^2} + 1\right)\right], \\ M^4 \quad &: \left[1 - e^{-w^2/M^2} \left(\frac{w^2}{M^2} + 1\right)\right], \\ M^2 \quad &: \left[1 - e^{-w^2/M^2}\right]. \end{aligned} \tag{3.76}$$

They are represented by the E_n factors

$$E_n(w) = 1 - e^{-w^2/M^2} \sum_n \frac{(w^2/M^2)^n}{n!}, \tag{3.77}$$

The contributions of this excited state model relative to the ground state, whose properties are to be determined, are not small. They are typically 10 to 50% [24]. The validity of this model relies upon the removal of the excited state contaminations.

3.7 Sum Rules for Octet Baryon Masses

The phenomenological side of the correlation function can be written as

$$\Pi(p) = \frac{\lambda_{1/2}^2}{p^2 - M_N^2} \left(\hat{p} \pm M_N\right) + \cdots, \tag{3.78}$$

where the dots denote excited state contributions.

The correlation function has two Dirac structures, $\hat{p}$ and 1, from which two independent QCD sum rules can be constructed for each member of the octet family. It turns out that the QCD sum rules from the structure $\hat{p}$ contain dimension-even

condensates only, so we will refer to the QCD sum rules from the structure $\hat{p}$ as chiral-even. Similarly, we refer to those from the structure 1 as chiral-odd, because they involve dimension-odd condensates only. This classification scheme will be used throughout this work.

The QCD side are calculated by the Mathematica program: *qcdsr2pt-construction .nb*, which will be discussed later in Chap. 6 and Appendix A. We need the mass sum rules for octet baryon in the analysis of magnetic moment and N to Δ transition in later chapters, so here we list the sum rule for N, Σ, Ξ and Λ. The chiral-even sum rules coupling to spin-1/2 octet states at structure $\hat{p}$ are:

$$\begin{aligned}
& p_1\, L^{-4/9}\, E_2\, M^6 + p_2\, b\, L^{-4/9}\, E_0\, M^2 + p_3\, m_s\, a\, L^{-4/9}\, E_0\, M^2 \\
& + p_4\, m_s\, m_0^2 a\, L^{-26/27} + p_5\, \kappa_v a^2\, L^{4/9} + p_6\, m_0^2 a^2\, L^{-2/27}\, \frac{1}{M^2} \\
& = \tilde{\lambda}_N^2 e^{-M_N^2/M^2},
\end{aligned} \tag{3.79}$$

In the sum rule, the condensates and couplings are re-scaled to remove all factors of π. The basic parameter set includes re-scaled quark condensate a, gluon condensate b, mix condensate m_0^2 and re-scaled coupling constant $\tilde{\lambda}$. They are defined as:

$$\begin{aligned}
a &= -(2\pi)^2 \langle \bar{q} q \rangle, \\
b &= \langle g_c^2\, G^2 \rangle, \\
\langle \bar{q} g_c \sigma \cdot G q \rangle &= -m_0^2 \langle \bar{q} q \rangle, \\
\tilde{\lambda} &= (2\pi)^2 \lambda
\end{aligned} \tag{3.80}$$

The four-quark condensate is not well-known and we use the factorization approximation $\langle\bar{u}u\bar{u}u\rangle = \kappa_v\langle\bar{u}u\rangle^2$ and investigate the possible violation via the parameter κ_v.

We have included the normalization factor L raised to various anomalous dimensions to take into account the scaling behavior of the various operators. The anomalous dimension corrections of the interpolating fields and the various operators are taken into account in the leading logarithmic approximation via the factor

$$L^\gamma = \left[\frac{\alpha_s(\mu^2)}{\alpha_s(M^2)}\right]^\gamma = \left[\frac{\ln(M^2/\Lambda^2_{QCD})}{\ln(\mu^2/\Lambda^2_{QCD})}\right]^\gamma, \tag{3.81}$$

where $\mu = 500$ MeV is the renormalization scale and Λ_{QCD} is the QCD scale parameter. The function $t(M^2) \equiv \ln\frac{M^2}{\mu^2} - \gamma_{EM}$ with $\gamma_{EM} \approx 0.577$ the Euler-Mascheroni constant.

The Wilson coefficients for N are:

$$\begin{aligned}
p_1 &= \frac{1}{64}(5 + 2\beta + 5\beta^2),\\
p_2 &= \frac{1}{256}(5 + 2\beta + 5\beta^2),\\
p_3 &= 0,\\
p_4 &= 0,\\
p_5 &= \frac{1}{24}[7 - 2\beta - 5\beta^2],\\
p_6 &= -\frac{1}{96}[13 - 2\beta - 11\beta^2],
\end{aligned} \tag{3.82}$$

for Σ:

$$
\begin{aligned}
p_1 &= \frac{1}{64}(5+2\beta+5\beta^2),\\
p_2 &= \frac{1}{256}(5+2\beta+5\beta^2),\\
p_3 &= \frac{1}{32}[(12-5f_s)-2f_s\beta-(12+5f_s)\beta^2],\\
p_4 &= -\frac{1}{96}[(4f_s+21+18t(M^2))+4f_s\beta+(4f_s-21-18t(M^2))\beta^2],\\
p_5 &= \frac{1}{24}[(6f_s+1)-2\beta-(6f_s-1)\beta^2],\\
p_6 &= -\frac{1}{96}[(12f_s+1)-2\beta-(12f_s-1)\beta^2],
\end{aligned}
\tag{3.83}
$$

The parameter f_s account for the flavor-symmetry breaking of the strange quark in the condensates and susceptibilities:

$$
f_s = \frac{\langle \bar{s}s\rangle}{\langle \bar{u}u\rangle} = \frac{\langle \bar{s}g_c\sigma\cdot Gs\rangle}{\langle \bar{u}g_c\sigma\cdot Gu\rangle}. \tag{3.84}
$$

The Wilson coefficients for Ξ are:

$$
\begin{aligned}
p_1 &= \frac{1}{64}(5+2\beta+5\beta^2),\\
p_2 &= \frac{1}{256}(5+2\beta+5\beta^2),\\
p_3 &= \frac{3}{16}[(2-f_s)-2f_s\beta-(2+f_s)\beta^2],\\
p_4 &= -\frac{1}{96}[(15-f_s+18t(M^2))-10f_s\beta-(15+f_s+18t(M^2))\beta^2],\\
p_5 &= \frac{f_s}{24}[(f_s+6)-2f_s\beta+(f_s-6)\beta^2],\\
p_6 &= -\frac{f_s}{96}[(f_s+12)-2f_s\beta+(f_s-12)\beta^2],
\end{aligned}
\tag{3.85}
$$

for Λ

$$
\begin{aligned}
p_1 &= \frac{1}{64}(5+2\beta+5\beta^2), \\
p_2 &= \frac{1}{256}(5+2\beta+5\beta^2), \\
p_3 &= \frac{1}{96}[(20-15f_s)-(16+6f_s)\beta-(4+15f_s)\beta^2], \\
p_4 &= \frac{1}{96}[(4f_s-5-6t(M^2))+(4+4f_s)\beta+(4f_s+1+6t(M^2))\beta^2], \\
p_5 &= \frac{1}{72}[(10f_s+11)+(2-8f_s)\beta-(2f_s+13)\beta^2], \\
p_6 &= \frac{1}{288}[(-16f_s-23)+(8f_s-2)\beta+(8f_s+25)\beta^2],
\end{aligned}
\tag{3.86}
$$

A trivial check of the calculation is provided by the fact that the QCD sum rules for Σ should reduce to those for the nucleon by replacing the d-quark with the s-quark, which is equivalent to setting $m_s = 0$ and $f_s = 1$. This check is performed throughout the work.

The chiral-odd sum rules coupling to spin-1/2 states at structure 1 are

$$
\begin{aligned}
& p_1\, m_s\, L^{-8/9}\, E_2\, M^6 + p_2\, a\, E_1\, M^4 + p_3\, m_0^2 a\, L^{-14/27}\, E_0\, M^2 \\
& + p_4\, m_s\, b\, L^{-8/9}\, E_0\, M^2 + p_5\, a\, b + p_6\, m_s\, \kappa_v a^2 \\
& = \tilde{\lambda}_N^2 M_N e^{-M_N^2/M^2},
\end{aligned}
\tag{3.87}
$$

where the Wilson coefficients for N are:

$$p_1 = 0,$$

$$
\begin{aligned}
p_2 &= \frac{1}{16}[7 - 2\beta - 5\beta^2)], \\
p_3 &= -\frac{3}{16}(1 - \beta^2), \\
p_4 &= 0, \\
p_5 &= \frac{1}{1152}[19 + 10\beta - 29\beta^2],\ p_6 = 0,
\end{aligned} \tag{3.88}
$$

for Σ

$$
\begin{aligned}
p_1 &= \frac{1}{16}(1 - \beta)^2, \\
p_2 &= \frac{1}{16}[(6 + f_s) - 2f_s\beta - (6 - f_s)\beta^2)], \\
p_3 &= -\frac{3}{16}(1 - \beta^2), \\
p_4 &= -\frac{1}{128}(1 - \beta)^2, \\
p_5 &= \frac{1}{1152}[(24 - 5f_s) + 10f_s\beta - (24 + 5f_s)\beta^2], \\
p_6 &= \frac{1}{24}[(5 - 3f_s) + 2\beta + (5 + 3f_s)\beta^2],
\end{aligned} \tag{3.89}
$$

for Ξ:

$$
\begin{aligned}
p_1 &= \frac{3}{8}(1 - \beta^2), \\
p_2 &= \frac{1}{16}[(6f_s + 1) - 2\beta - (6f_s - 1)\beta^2)], \\
p_3 &= -\frac{3f_s}{16}(1 - \beta^2), \\
p_4 &= \frac{3}{64}(1 - \beta^2), \\
p_5 &= \frac{1}{1152}[(24f_s - 5) + 10\beta - (24f_s + 5)\beta^2], \\
p_6 &= \frac{f_s}{8}[(3 - f_s) + 2\beta + (3 + f_s)\beta^2],
\end{aligned} \tag{3.90}
$$

for Λ

$$
\begin{aligned}
p_1 &= \frac{1}{48}(11 + 2\beta - 13\beta^2), \\
p_2 &= \frac{1}{48}[(10 + 11f_s) + (-8 + 2f_s)\beta - (2 + 13f_s)\beta^2)], \\
p_3 &= \frac{1}{16}((-1 - 2f_s) + (1 + 2f_s)\beta^2), \\
p_4 &= \frac{1}{384}(13 - 2\beta - 11\beta^2), \\
p_5 &= \frac{1}{3456}[(4 + 53f_s) + (40 - 10f_s)\beta - (44 + 43f_s)\beta^2], \\
p_6 &= \frac{1}{72}[(15 - 5f_s) + (6 + 4f_s)\beta + (15 + f_s)\beta^2], \qquad (3.91)
\end{aligned}
$$

3.8 Sum Rule Analysis for Proton Masses

Perhaps the crudest analysis on can perform is to simply take the first term from each sum rule, then take the ratio:

$$\frac{M^2}{2a} = \frac{1}{M_N}, \qquad (3.92)$$

This is the famous Ioffe formula [21]:

$$M_N = \frac{2a}{M^2} = -\frac{8\pi^2}{M^2}\langle\bar{q}q\rangle. \qquad (3.93)$$

Using the value $a = 0.52\ \mathrm{GeV}^3$ [21] and setting $M = M_N$, the proton mass is estimated as:

$$M_N \approx 1.01 GeV \qquad (3.94)$$

which is not too far from the physical value of 0.94 GeV.

Maybe the result is a little coincidental, but it makes a direct link between the proton mass and the quark condensate.

To do full analysis, we need go back to the original sum rules equations. The method of analysis is to fit the sum rules in a region of the Borel parameter M^2. We call it Borel window. The Borel window is chosen so that:

1. Contributions to the left hand side form higher dimensional operators(which have more powers of M^2 in the denominator) are small. This naturally fixes the small M^2

2. The ground state pole dominates. By this we mean excited states contribute less than 50% to the sum rules. This will set the upper limit on M^2.

Use these two criteria, we can determine the two cut-offs to get our Borel window. Within this Borel window, using the least squares criterion, we can extract the mass of proton and other parameters through best matching of both sides.

The QCD input parameters are given as follows. The quark condensate in standard notation is taken as $a = 0.52$ GeV^3, corresponding to a central value of $\langle \bar{u}u \rangle = -(236)^3$ MeV^3. For the gluon condensate, early estimates from charmonium [3] place it at $b = 0.47$ GeV^4, a value commonly used in QCD sum rule analysis. But more recent investigations support much larger values [25, 26, 27]. Here we adopt $b = 1.2$ GeV^4. The mixed condensate parameter is placed at $m_0^2 = 0.72$ GeV^2. For the four-quark condensate, there are claims of significant violation of the factorization hypothesis [25, 26, 27]. Here we use $\kappa_v = 2$. The QCD scale parameter is restricted to $\Lambda_{QCD} = 0.15$ GeV. The strange quark mass is taken as $m_s = 0.15$ GeV. The value of f_s flavor symmetry breaking has been determined in [28, 29] and is given by

$f_s = 0.83$. We apply Monte-Carlo method to do the analysis. It allow us to do the most realistic estimation of the uncertainties. We apply 10% uniform uncertainty in all the QCD input parameters. Of course, the uncertainties in the QCD parameters can be non-uniform. While some may argue that some values are better known, others may find that the errors are underestimated. In any event, one will learn how the uncertainties in the QCD parameters are mapped into the uncertainties in the phenomenological results representing baryon properties. The detailed analysis and result will be in Chap. 6.

Chapter 4

Baryon Magnetic Moments from QCD Sum Rules

4.1 Introduction

Before we go into the N to Δ transitions calculation in the next chapter, we will revisit the magnetic moments of baryons using the QCD sum rule method. This is instructive because the same method is used in both calculations. The only difference is the initial and final states. One is N to N and the other is N to Δ, which gives different Dirac structures. By comparing with the published sum rules [30, 22, 23, 31], we have an independent check and gain confidence in our way of deriving the sum rules. Calculations of the magnetic moment were carried out soon after the QCD sum rule method was introduced for the proton, neutron [32, 8] and hyperons [33] in the external field method. In this method, a static magnetic field is introduced that couples to the quarks and polarizes the QCD vacuum. Magnetic moments can be

extracted from the linear response to this field. The results of the studies validated the external field method as a way of probing hadron properties other than the mass, such as magnetic moments, form factors, axial charge and isospin-breakings. Later, a more systematic study was made for the magnetic moments of octet baryons [30, 22, 23, 31]. Calculations were also carried out for decuplet baryons [34, 35, 36, 37] and the rho meson [38].

In this work, we carry out a comprehensive, independent calculation of the magnetic moments of the octet baryons in the external field method. It can be considered as an update over the previous calculations [30, 22, 23] which were done more than 20 years ago. There are a number of things we do differently. First, we employ generalized interpolating fields which allow us to use the optimal mixing of interpolating fields to achieve the best match. Second, we derive a new, complete set of QCD sum rules for all three Dirac structures and analyze all of them. The previous sum rules, which were mostly limited to one of the Dirac structures, correspond to a special case of the mixing in our sum rules. In this way, we provide an independent check of the previous sum rules. Third, we perform a Monte-Carlo analysis which has become standard nowadays [39]. The advantage of such an analysis is explained later. Fourth, we use a different procedure to extract the magnetic moments and to treat the transition terms in the intermediate states. Our results show that these transitions cannot be simply ignored. Fifth, we isolate the individual quark contributions to the magnetic moments and discuss their implications in the underlying quark-gluon dynamics in the baryons.

This chapter is organized as follows. In Section 4.2, the method of QCD sum rules

is introduced. Using the interpolating fields for the octet baryons, master formulae are calculated. Then both the phenomenological representation and QCD side are derived. Section 4.3 will list the sum rules we derived for the octet baryon family, followed by the analysis to extract the magnetic moments in Section 4.4. Section 4.5 summarizes the results and gives a comparison of our results with experiment and previous calculation, followed by an in-depth discussion of our findings.

4.2 Method

The starting point is still the time-ordered correlation function in the QCD vacuum, but in the presence of a *constant* background electromagnetic field $F_{\mu\nu}$:

$$\Pi(p) = i \int d^4x \; e^{ip\cdot x} \langle 0 \,|\, T\{ \; \eta(x) \, \bar{\eta}(0) \; \} \,|\, 0 \rangle_F. \tag{4.1}$$

The subscript F means that the correlation function is to be evaluated with an electromagnetic interaction term added to the QCD Lagrangian:

$$\mathcal{L}_I = -A_\mu J^\mu, \tag{4.2}$$

where A_μ is the external electromagnetic potential and $J^\mu = e_q \bar{q} \gamma^\mu q$ is the quark electromagnetic current.

Since the external field can be made arbitrarily small, one can expand the correlation function

$$\Pi(p) = \Pi^{(0)}(p) + \Pi^{(1)}(p) + \cdots, \tag{4.3}$$

where $\Pi^{(0)}(p)$ is the correlation function in the absence of the field, and gives rise to the mass sum rules of the baryons. The magnetic moments will be extracted from the QCD sum rules obtained from the linear response function $\Pi^{(1)}(p)$.

The action of the external electromagnetic field is two-fold: it couples directly to the quarks in the baryon interpolating fields, and it also polarizes the QCD vacuum. The latter can be described by introducing new parameters called vacuum susceptibilities.

The interpolating field for the baryon octet family are:

$$\begin{aligned}
\eta^{p}(uud) &= -2\epsilon^{abc}[(u^{aT}C\gamma_5 d^b)u^c + \beta(u^{aT}Cd^b)\gamma_5 u^c], \\
\eta^{n}(ddu) &= -2\epsilon^{abc}[(d^{aT}C\gamma_5 u^b)d^c + \beta(d^{aT}Cu^b)\gamma_5 d^c], \\
\eta^{\Lambda}(uds) &= -2\sqrt{\frac{1}{6}}\epsilon^{abc}[2(u^{aT}C\gamma_5 d^b)s^c + (u^{aT}C\gamma_5 s^b)d^c - (d^{aT}C\gamma_5 s^b)u^c \\
&\quad +\beta(2(u^{aT}Cd^b)\gamma_5 s^c + (u^{aT}Cs^b)\gamma_5 d^c - (d^{aT}Cs^b)\gamma_5 u^c)], \\
\eta^{\Sigma^-}(dds) &= -2\epsilon^{abc}[(d^{aT}C\gamma_5 s^b)d^c + \beta(d^{aT}Cs^b)\gamma_5 d^c], \\
\eta^{\Sigma^0}(uds) &= -\sqrt{2}\epsilon^{abc}[(u^{aT}C\gamma_5 s^b)d^c + (d^{aT}C\gamma_5 s^b)u^c \\
&\quad +\beta((u^{aT}Cs^b)\gamma_5 d^c + (d^{aT}Cs^b)\gamma_5 u^c)], \\
\eta^{\Sigma^+}(uus) &= -2\epsilon^{abc}[(u^{aT}C\gamma_5 s^b)u^c + \beta(u^{aT}Cs^b)\gamma_5 u^c], \\
\eta^{\Xi^-}(ssd) &= -2\epsilon^{abc}[(s^{aT}C\gamma_5 d^b)s^c + \beta(s^{aT}Cd^b)\gamma_5 s^c], \\
\eta^{\Xi^0}(ssu) &= -2\epsilon^{abc}[(s^{aT}C\gamma_5 u^b)s^c + \beta(s^{aT}Cu^b)\gamma_5 s^c].
\end{aligned} \tag{4.4}$$

The normalization factors are chosen so that correlation functions of these interpolating fields coincide with each other under SU(3)-flavor symmetry.

4.2.1 Phenomenological Representation

We start with the structure of the two-point correlation function in the presence of the electromagnetic vertex to first order

$$\Pi(p) = i \int d^4x e^{ipx} < 0|\eta(x)[-i \int d^4y A_\mu(y) J^\mu(y)]\bar{\eta}(0)|0 > . \tag{4.5}$$

Inserting two complete sets of physical intermediate states, we restrict our attention only to the positive energy ones and write

$$\begin{aligned} &\Pi(p) = \int d^4x d^4y \frac{d^4k'}{(2\pi)^4} \frac{d^4k}{(2\pi)^4} \sum_{N'N} \sum_{s's} \frac{-i}{k'^2 - M^2_{N'} - i\varepsilon} \frac{-i}{k^2 - M^2_N - i\varepsilon} \\ &e^{ipx} A_\mu(y) < 0|\eta(x)|N'k's' >< N'k's'|J^\mu(y)|Nks >< Nks|\bar{\eta}(0)|0 > . \end{aligned} \tag{4.6}$$

We can use translation invariance to express $\eta(x)$ in terms of $\eta(0)$

$$< 0|\eta(x)|N'k's' >=< 0|\eta(0)|N'k's' > e^{-ik'x}. \tag{4.7}$$

The interpolating field excites (or annihilates) the ground state as well as the excited states of the baryon from the QCD vacuum. We have $< 0|\eta(0)|Nks >= \lambda_N u(k,s)$ from Eq. (3.30).

Translation invariance on $J^\mu(y)$ gives

$$< N'k's'|J^\mu(y)|Nks >= e^{iqy} < N'k's'|J^\mu(0)|Nks >, \tag{4.8}$$

where $q = k' - k$ is the momentum transfer and we will use $Q^2 = -q^2$.

The matrix element of the electromagnetic current has the general form

$$< k's'|J^{\mu}(0)|ks >= \bar{u}(k',s')[F_1(Q^2)\gamma_{\mu} + F_2(Q^2)i\sigma^{\mu\nu}\frac{q^{\nu}}{2M_N}]u(k,s), \tag{4.9}$$

where the Dirac form factors F_1 and F_2 are related to the Sachs form factors by

$$\begin{aligned} G_E(Q^2) &= F_1(Q^2) - \frac{Q^2}{(2M_N)^2}F_2(Q^2) \\ G_M(Q^2) &= F_1(Q^2) + F_2(Q^2). \end{aligned} \tag{4.10}$$

At $Q^2 = 0$, $F_1(0) = 1$, $F_2(0) = \mu^a$ which is the anomalous magnetic moment, and $G_M(0) = F_1(0) + F_2(0) = \mu$ which is the total magnetic moment.

Writing out explicitly only the contribution of the ground-state nucleon and denoting the excited state contribution by ESC, we have

$$\begin{aligned} &\Pi(p) = -\lambda_N^2 \int d^4x d^4y \frac{d^4k'}{(2\pi)^4}\frac{d^4k}{(2\pi)^4}[k'^2 - M_N^2 - i\varepsilon]^{-1}[k^2 - M_N^2 - i\varepsilon]^{-1}A_{\mu}(y)e^{i(p-k')x} \\ &e^{iqy}\sum_{s'} u(k',s')\bar{u}(k',s')[F_1(Q^2)\gamma^{\mu} + F_2(Q^2)i\sigma^{\mu\nu}\frac{q^{\nu}}{2M_N}]\sum_{s} u(k,s)\bar{u}(k,s) + ESC. \end{aligned} \tag{4.11}$$

The spin sums are of the form in Eq. (3.31)

QCD sum rule calculations are most conveniently done in the fixed-point gauge. For electromagnetic field, fixed-point gauge is defined by $x^{\mu}A_{\mu}(x) = 0$. In this gauge, the electromagnetic potential is given by

$$A_{\mu}(y) = -\frac{1}{2}F_{\mu\nu}y^{\nu}. \tag{4.12}$$

Changing integration variables from k to $q = k' - k$, then $d^4k = -d^4q$, we have

$$\Pi(p) = \frac{-\lambda_N^2}{2} F_{\mu\nu} \int d^4x d^4y \frac{d^4k'}{(2\pi)^4} \frac{d^4q}{(2\pi)^4} [k'^2 - M_N^2 - i\varepsilon]^{-1} [(q-k')^2 - M_N^2 - i\varepsilon]^{-1}$$
$$\times e^{i(p-k')x} (-i\frac{\partial}{\partial q_\nu} e^{iq\cdot y})(\hat{p} + M_N)[F_1(Q^2)\gamma_\mu + F_2(Q^2) i\sigma^{\mu\nu} \frac{q^\nu}{2M_N}](\hat{k'} - \hat{q} + M_N) + ESC. \tag{4.13}$$

Integrating over x, we get a delta function

$$\int d^4x \frac{1}{(2\pi)^4} e^{i(p-k')x} = \delta^4(p - k'). \tag{4.14}$$

Integrating $\partial/\partial q_\nu$ by parts, then doing $\int d^4y$, we get another delta function $\delta(q)$. Since we have a $\delta(q)$, when doing $\partial/\partial q_\nu$ only terms linear in q_ν contribute. We have $F_1(Q^2)|_{q=0} = 1, F_2(Q^2)|_{q=0} = \mu^a = \mu - 1$, and $\partial/\partial q_\nu F_{1,2}(Q^2)|_{q=0} = 0$, so derivatives of the structure functions do not enter. Finally, we arrive at

$$\Pi(p) = \frac{i}{2}\lambda_N^2 F_{\mu\nu} [p^2 - M_N^2 - i\varepsilon]^{-2} (\hat{p} + M_N) \{ \frac{i(\mu_N - 1)}{2M_N} \sigma^{\mu\nu} (\hat{p} + M_N) + i\sigma^{\mu\nu}$$
$$-(p^\mu \gamma^\nu - p^\nu \gamma^\mu)(\hat{p} + M_N)[p^2 - M_N^2 - i\varepsilon]^{-1} \} + ESC. \tag{4.15}$$

Examination of its Dirac structure reveals that its has 3 independent combinations: $F^{\mu\nu}(\hat{p}\sigma_{\mu\nu} + \sigma_{\mu\nu}\hat{p})$, $F^{\mu\nu} i(p_\mu \gamma_\nu - p_\nu \gamma_\mu)\hat{p}$ and $F^{\mu\nu}\sigma_{\mu\nu}$. The momentum-space correlation function in the above equation can be written in terms of these three structures

$$\Pi(p) = -\frac{1}{4} \frac{\lambda_N^2 F_{\mu\nu}}{[p^2 - M_N^2 - i\varepsilon]^2} \{ [\sigma^{\mu\nu}](2M_N\mu_N) + \frac{\mu_N - 1}{M_N}(p^2 - M_N^2) + \mu_N [\hat{p}\sigma^{\mu\nu} + \sigma^{\mu\nu}\hat{p}]$$
$$+ \frac{2(\mu_N - 1)}{M_N} [i(p^\mu \gamma^\nu - p^\nu \gamma^\mu)]\hat{p} \} + ESC, \tag{4.16}$$

where we have used the following identities

$$
\begin{aligned}
&(\hat{p}+M_N)\sigma^{\mu\nu} = M_N\sigma^{\mu\nu} + \tfrac{1}{2}(\hat{p}\sigma^{\mu\nu} + \sigma^{\mu\nu}\hat{p}) + i(p^\mu\gamma^\nu - p^\nu\gamma^\mu),\\
&(\hat{p}+M_N)\sigma^{\mu\nu}(\hat{p}+M_N) = \sigma^{\mu\nu}(p^2+M_N^2) + M_N(\hat{p}\sigma^{\mu\nu} + \sigma^{\mu\nu}\hat{p}) + 2i(p^\mu\gamma^\nu - p^\nu\gamma^\mu)\hat{p},\\
&(\hat{p}+M_N)(p^\mu\gamma^\nu - p^\nu\gamma^\mu)(\hat{p}+M_N) = -(p^2-M_N^2)(p^\mu\gamma^\nu - p^\nu\gamma^\mu).
\end{aligned}
\tag{4.17}
$$

The result in Eq. (4.16) was checked by our mathematica code in *qcdsr2pt-construction .nb*. Upon Borel transform the ground state takes the form

$$
\begin{aligned}
&\hat{B}[\Pi(p)] = -\tfrac{\lambda_N^2}{4M^2}e^{-M_N^2/M^2}\{\tfrac{1}{M_N}(2M_N^2\mu_N - M^2(\mu_N-1))[F_{\mu\nu}\sigma^{\mu\nu}] +\\
&\mu_N[F_{\mu\nu}(\hat{p}\sigma^{\mu\nu} + \sigma^{\mu\nu}\hat{p})] + \tfrac{2(\mu_N-1)}{M_N}[F_{\mu\nu}i(p^\mu\gamma^\nu - p^\nu\gamma^\mu)\hat{p}]\},
\end{aligned}
\tag{4.18}
$$

where M is the Borel mass, not to be confused with the nucleon mass M_N.

Here we must treat the excited states with care. For a generic invariant function, the pole structure can be written as

$$
\tfrac{C_{N\leftrightarrow N}^2}{(p^2-M_N^2)^2} + \sum_{N^*}\tfrac{C_{N\leftrightarrow N^*}^2}{(p^2-M_N^2)(p^2-M_{N^*}^2)} + \sum_{N^*}\tfrac{C_{N^*\leftrightarrow N^*}^2}{(p^2-M_{N^*}^2)^2},
\tag{4.19}
$$

where $C_{N\leftrightarrow N}$, $C_{N\leftrightarrow N^*}$ and $C_{N^*\leftrightarrow N^*}$ are constants. The first term is the ground state pole which contains the desired magnetic moment μ_N. The second term represents the non-diagonal transitions between the ground state and the excited states caused by the external field. The third term is pure excited state contributions. These different contributions can be represented by the diagrams in Fig. 4.1. Upon Borel transform,

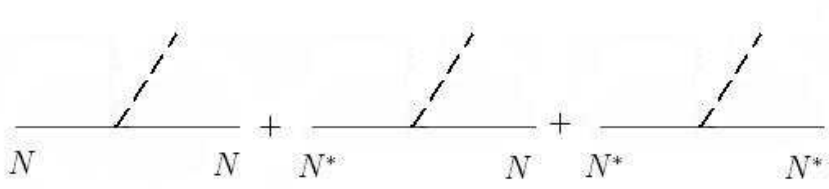

Figure 4.1: The three kinds of contributions to the spectral function in the presence of an external field: ground state, transitions between ground state and excited states, and pure excited states

the ground state takes the form

$$\frac{\lambda_N^2 \mu_N}{M^2} e^{-M_N^2/M^2} + e^{-M_N^2/M^2} \left[\sum_{N^*} \frac{C^2_{N \leftrightarrow N^*}}{M^2_{N^*} - M^2_N} \left(1 - e^{-\left(M^2_{N^*} - M^2_N\right)/M^2} \right) \right] + \sum_{N^*} \frac{C^2_{N^* \leftrightarrow N^*}}{M^2} e^{-M^2_{N^*}/M^2}. \tag{4.20}$$

The important point is that the transitions give rise to a contribution that is not exponentially suppressed relative to the ground state. This is a general feature of the external-field technique. The strength of such transitions at each structure is a *priori* unknown and is an additional source of contamination in the determination of the magnetic moment μ_N. The standard treatment of the transitions is to approximate the quantity in the square brackets by a constant, which is to be extracted from the sum rule along with the ground state property of interest. Inclusion of such contributions is necessary for the correct extraction of the magnetic moments. The pure excited state contributions are exponentially suppressed relative to the ground state and can be modeled in the usual way by introducing a continuum model and threshold parameter.

4.2.2 Calculation of the QCD Side

Similarly, we start by contracting out the quark pairs in Eq. (4.1) using Wick's theorem, resulting in the so-called *master formula* in terms of quark propagators. The master formula for the proton (with uud quark content) is same as Eq. (3.5). The master formula for neutron (with ddu quark content) can be obtained by exchanging the d quark with a u quark from. By replacing the d quark with a s quark, one can get the master formula for Σ^+ (with uus quark content). While the master formula for Σ^- (with uus quark content) can be obtained by replacing the u quark with a d quark from Σ^+ master formula. By exchanging the u quarks and s quarks in Σ^+ master formula, the master formula for Ξ^0 (with ssu quark content) can be obtained. Likewise, by replacing the u quark with a d quark, one can get the master formula for Ξ^+ (with ssd quark content).

The master formulae for Σ^0 and Λ (uds quark content) have a more complicated structure. They can be written in a combined way as

$$
\begin{aligned}
&\langle\Omega\,|\,T\{\,\eta(x)\,\bar{\eta}(0)\,\}\,|\,\Omega\rangle = -f\epsilon^{abc}\epsilon^{a'b'c'}\{ \\
&f_1 f_2 S_s^{aa'}\gamma_5 C S_u^{cc'\,T} C\gamma_5 S_d^{bb'} - f_1 f_3 S_s^{aa'}\gamma_5 C S_d^{cc'\,T} C\gamma_5 S_u^{bb'} + f_1 f_1 S_s^{aa'}\mathrm{Tr}(C S_u^{cc'\,T} C\gamma_5 S_d^{bb'}\gamma_5) \\
&+ f_2 f_1 S_d^{aa'}\gamma_5 C S_u^{cc'\,T} C\gamma_5 S_s^{bb'} + f_2 f_3 S_d^{aa'}\gamma_5 C S_s^{cc'\,T} C\gamma_5 S_u^{bb'} + f_2 f_2 S_d^{aa'}\mathrm{Tr}(C S_s^{cc'\,T} C\gamma_5 S_u^{bb'}\gamma_5) \\
&- f_3 f_1 S_u^{aa'}\gamma_5 C S_d^{cc'\,T} C\gamma_5 S_s^{bb'} + f_3 f_2 S_u^{aa'}\gamma_5 C S_s^{cc'\,T} C\gamma_5 S_d^{bb'} + f_3 f_3 S_u^{aa'}\mathrm{Tr}(C S_s^{cc'\,T} C\gamma_5 S_d^{bb'}\gamma_5) \\
&+ \beta[f_1 f_5 S_s^{aa'} C S_u^{cc'\,T} C\gamma_5 S_d^{bb'}\gamma_5 - f_1 f_6 S_s^{aa'} C S_d^{cc'\,T} C\gamma_5 S_u^{bb'}\gamma_5 + f_1 f_4 S_s^{aa'}\gamma_5\mathrm{Tr}(C S_d^{cc'\,T} C\gamma_5 S_u^{bb'}) \\
&+ f_2 f_4 S_d^{aa'} C S_u^{cc'\,T} C\gamma_5 S_s^{bb'}\gamma_5 + f_2 f_6 S_d^{aa'} C S_s^{cc'\,T} C\gamma_5 S_u^{bb'}\gamma_5 + f_2 f_5 S_d^{aa'}\gamma_5\mathrm{Tr}(C S_s^{cc'\,T} C\gamma_5 S_u^{bb'}) \\
&- f_3 f_4 S_u^{aa'} C S_d^{cc'\,T} C\gamma_5 S_s^{bb'}\gamma_5 + f_3 f_5 S_u^{aa'} C S_s^{cc'\,T} C\gamma_5 S_d^{bb'}\gamma_5 + f_3 f_6 S_u^{aa'}\gamma_5\mathrm{Tr}(C S_s^{cc'\,T} C\gamma_5 S_d^{bb'})
\end{aligned}
$$

$$+f_4f_2\gamma_5 S_s^{aa'}\gamma_5 C S_u^{cc'T} C S_d^{bb'} - f_4f_3\gamma_5 S_s^{aa'}\gamma_5 C S_d^{cc'T} C S_u^{bb'} + f_4f_1\gamma_5 S_s^{aa'}\mathrm{Tr}(C S_d^{cc'T} C S_u^{bb'}\gamma_5)$$

$$+f_5f_1\gamma_5 S_d^{aa'}\gamma_5 C S_u^{cc'T} C S_s^{bb'} + f_5f_3\gamma_5 S_d^{aa'}\gamma_5 C S_s^{cc'T} C S_u^{bb'} + f_5f_2\gamma_5 S_d^{aa'}\mathrm{Tr}(C S_s^{cc'T} C S_u^{bb'}\gamma_5)$$

$$-f_6f_1\gamma_5 S_u^{aa'}\gamma_5 C S_d^{cc'T} C S_s^{bb'} + f_6f_2\gamma_5 S_u^{aa'}\gamma_5 C S_s^{cc'T} C S_d^{bb'} + f_6f_3\gamma_5 S_u^{aa'}\mathrm{Tr}(C S_s^{cc'T} C S_d^{bb'}\gamma_5)]$$

$$+\beta^2[f_4f_5\gamma_5 S_s^{aa'} C S_u^{cc'T} C S_d^{bb'}\gamma_5 - f_4f_6\gamma_5 S_s^{aa'} C S_d^{cc'T} C S_u^{bb'}\gamma_5 + f_4f_4\gamma_5 S_s^{aa'}\gamma_5\mathrm{Tr}(C S_u^{cc'T} C S_d^{bb'})$$

$$+f_5f_4\gamma_5 S_d^{aa'} C S_u^{cc'T} C S_s^{bb'}\gamma_5 + f_5f_6\gamma_5 S_d^{aa'} C S_s^{cc'T} C S_u^{bb'}\gamma_5 + f_5f_5\gamma_5 S_d^{aa'}\gamma_5\mathrm{Tr}(C S_s^{cc'T} C S_u^{bb'})$$

$$-f_6f_4\gamma_5 S_u^{aa'} C S_d^{cc'T} C S_s^{bb'}\gamma_5 + f_6f_5\gamma_5 S_u^{aa'} C S_s^{cc'T} C S_d^{bb'}\gamma_5 + 4f_6f_6\gamma_5 S_u^{aa'}\gamma_5\mathrm{Tr}(C S_s^{cc'T} C S_d^{bb'})]\},$$

where the various factors are: for Σ^0, $f = 2/3, f_1 = 0, f_2 = 1, f_3 = 1, f_4 = 0, f_5 = 1, f_6 = 1$; and for Λ, $f = 2, f_1 = 2, f_2 = 1, f_3 = -1, f_4 = 2, f_5 = 1, f_6 = -1$.

In the above equations,

$$S_q^{ab}(x,0;F) \equiv \langle 0\,|\,T\{\,q^a(x)\,\bar{q}^b(0)\,\}\,|\,0\rangle_F, \quad q = u,d,s, \tag{4.22}$$

is the fully interacting quark propagator in the presence of the electromagnetic field. To first order in $F_{\mu\nu}$ and m_q (assume $m_u = m_d = 0, m_s \neq 0$), and order x^4, the propagator is given by the operator product expansion (OPE) [8, 22, 23]:

$$\begin{aligned}
S_q^{ab}(x,0;F) \equiv{}& \frac{i}{2\pi^2}\frac{\hat{x}}{x^4}\delta^{ab} - \frac{m_q}{4\pi^2x^2}\delta^{ab} - \frac{1}{12}\langle\bar{q}q\rangle\delta^{ab} + \frac{im_q}{48}\langle\bar{q}q\rangle\hat{x}\delta^{ab} \\
&+\frac{1}{192}\langle\bar{q}g_c\sigma\cdot Gq\rangle x^2\delta^{ab} - \frac{im_q}{1152}\langle\bar{q}g_c\sigma\cdot Gq\rangle\hat{x}x^2\delta^{ab} - \frac{1}{3^32^{10}}\langle\bar{q}q\rangle\langle g_c^2G^2\rangle x^4\delta^{ab} \\
&+\frac{i}{32\pi^2}(g_cG^n_{\alpha\beta})\frac{\hat{x}\sigma^{\alpha\beta}+\sigma^{\alpha\beta}\hat{x}}{x^2}\left(\frac{\lambda^n}{2}\right)^{ab} + \frac{1}{48}\frac{i}{32\pi^2}\langle g_c^2G^2\rangle\frac{\hat{x}\sigma^{\alpha\beta}+\sigma^{\alpha\beta}\hat{x}}{x^2}\left(\frac{\lambda^n}{2}\right)^{ab} \\
&+\frac{1}{3^22^{10}}\langle\bar{q}q\rangle\langle g_c^2G^2\rangle x^2\sigma^{\alpha\beta}\left(\frac{\lambda^n}{2}\right)^{ab} - \frac{1}{192}\langle\bar{q}g_c\sigma\cdot Gq\rangle\sigma^{\alpha\beta}\left(\frac{\lambda^n}{2}\right)^{ab} \\
&+\frac{im_q}{768}\langle\bar{q}g_c\sigma\cdot Gq\rangle\left(\hat{x}\sigma^{\alpha\beta}+\sigma^{\alpha\beta}\hat{x}\right)\left(\frac{\lambda^n}{2}\right)^{ab} + \frac{ie_q}{32\pi^2}F_{\alpha\beta}\frac{\hat{x}\sigma^{\alpha\beta}+\sigma^{\alpha\beta}\hat{x}}{x^2}\delta^{ab}
\end{aligned}$$

$$
\begin{aligned}
&-\frac{e_q}{24}\chi\langle\bar{q}q\rangle F_{\alpha\beta}\sigma^{\alpha\beta}\delta^{ab}+\frac{ie_q m_q}{96}\chi\langle\bar{q}q\rangle F_{\alpha\beta}\left(\hat{x}\sigma^{\alpha\beta}+\sigma^{\alpha\beta}\hat{x}\right)\delta^{ab}\\
&+\frac{e_q}{288}\langle\bar{q}q\rangle F_{\alpha\beta}\left(x^2\sigma^{\alpha\beta}-2x_\rho x^\beta\sigma^{\beta\alpha}\right)\delta^{ab}\\
&+\frac{e_q}{576}\langle\bar{q}q\rangle F_{\alpha\beta}\left[x^2(\kappa+\xi)\sigma^{\alpha\beta}-x_\rho x^\beta(2\kappa-\xi)\sigma^{\beta\alpha}\right]\delta^{ab}\\
&-\frac{e_q}{16}\langle\bar{q}q\rangle\left(\kappa F_{\alpha\beta}-\frac{i}{4}\xi\epsilon_{\alpha\beta\mu\nu}F^{\mu\nu}\right)\left(\frac{\lambda^n}{2}\right)^{ab}+\text{higher order terms.}
\end{aligned}
\tag{4.23}
$$

We use the convention $\epsilon^{0123}=+1$ and $\epsilon_{0123}=-1$ in this work.

In addition to the standard vacuum condensates, the vacuum susceptibilities induced by the external field are defined by

$$
\begin{aligned}
\langle\bar{q}\sigma_{\mu\nu}q\rangle_F &\equiv e_q\chi\langle\bar{q}q\rangle F_{\mu\nu},\\
\langle\bar{q}g_c G_{\mu\nu}q\rangle_F &\equiv e_q\kappa\langle\bar{q}q\rangle F_{\mu\nu},\\
\langle\bar{q}g_c\epsilon_{\mu\nu\rho\lambda}G^{\rho\lambda}\gamma_5 q\rangle_F &\equiv ie_q\xi\langle\bar{q}q\rangle F_{\mu\nu}.
\end{aligned}
\tag{4.24}
$$

Note that χ has the dimension of GeV^{-2}, while κ and ξ are dimensionless.

With the above elements in hand, it is straightforward to evaluate the correlation function by substituting the quark propagator into the various master formulae. The calculation can be organized by diagrams in Fig. 4.2 and Fig. 4.3. We developed a Mathematica notebook *qcdsr3pt-construction.nb* to perform the algebraic calculations. The QCD side has the same Dirac structure as the phenomenological side and the results can be organized according to the same 3 independent structures.

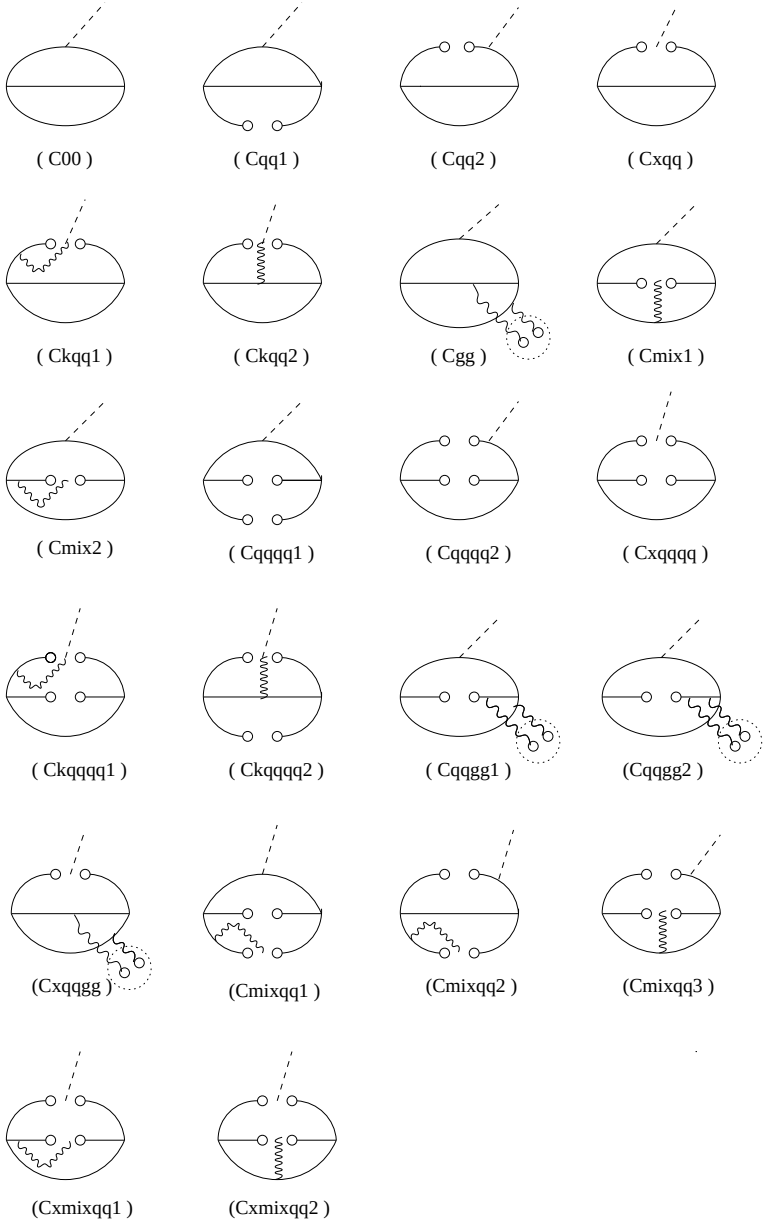

Figure 4.2: Non-mass diagrams considered for the octet baryon magnetic moments.

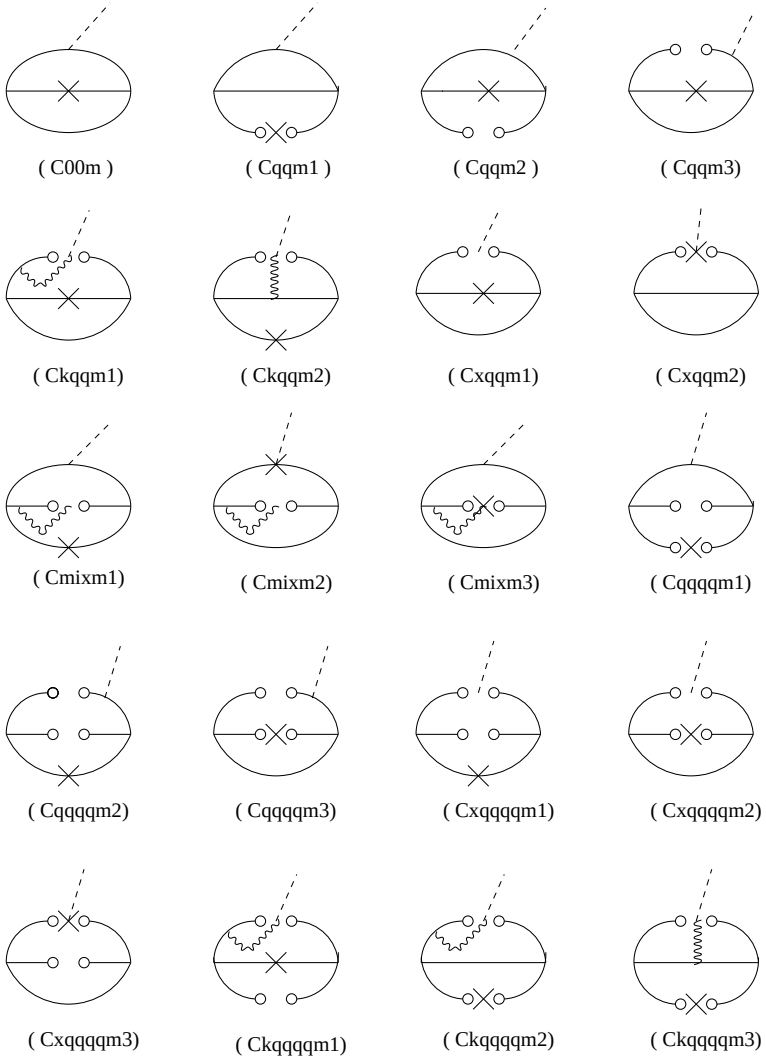

Figure 4.3: Diagrams considered for the strange quark mass corrections to the octet baryon magnetic moments.

4.3 QCD Sum Rules

Once we have both the QCD side (LHS) and the phenomenological side (RHS), we can derive sum rules by matching both sides. Since there are three independent Dirac structures, three sum rules can be constructed. We denote these Dirac structures by the following short-hand notation

$$\mathrm{WE}_1 = F^{\mu\nu}(\hat{p}\sigma_{\mu\nu} + \sigma_{\mu\nu}\hat{p}), \tag{4.25}$$

$$\mathrm{WO}_1 = F^{\mu\nu}\sigma_{\mu\nu}, \tag{4.26}$$

$$\mathrm{WO}_2 = F^{\mu\nu}i(p_\mu\gamma_\nu - p_\nu\gamma_\mu)\hat{p} \tag{4.27}$$

The sum rule from WE_1 involves only dimension-even condensates, so we call this sum rule chiral-even. The sum rule from both WO_1 and WO_2 involves only dimension-odd condensates, so we call them chiral-odd. Note that in previous works [8, 30] the dimension of the Dirac structures, rather than the dimension of the condensates, was used to refer to the sum rules.

Now we are ready to collect all of the QCD sum rules. At the structure WE_1, all of the sum rules can be expressed in the following form

$$\begin{aligned}
&\mathrm{c}_1 L^{-4/9} E_2(w) M^4 + \mathrm{c}_2 m_s \chi a L^{-26/27} E_1(w) M^2 + \mathrm{c}_3 \chi a^2 L^{-4/27} E_0(w) + \mathrm{c}_4 b L^{-4/9} E_0(w) \\
&+(\mathrm{c}_5 + \mathrm{c}_6) m_s a L^{-4/9} E_0(w) + (\mathrm{c}_7 + \mathrm{c}_8) a^2 L^{4/9} \tfrac{1}{M^2} + \mathrm{c}_9 \chi m_0^2 a^2 L^{-18/27} \tfrac{1}{M^2} \\
&+\mathrm{c}_{10} m_s m_0^2 a L^{-26/27} \tfrac{1}{M^2} = -\tilde{\lambda}_N^2 [\tfrac{\mu_N}{M^2} + A] e^{-M_N^2/M^2},
\end{aligned} \tag{4.28}$$

The quark charge factors e_q are given in units of electric charge

$$e_u = 2/3, \quad e_d = -1/3, \quad e_s = -1/3. \tag{4.29}$$

Note that we choose to keep the quark charge factors explicit in the sum rules. The advantage is that it can facilitate the study of individual quark contribution to the magnetic moments. The parameters ϕ also account for the flavor-symmetry breaking of the strange quark in the condensates and susceptibilities:

$$\phi = \frac{\chi_s}{\chi} = \frac{\kappa_s}{\kappa} = \frac{\xi_s}{\xi}. \tag{4.30}$$

We only need to carry out four separate calculations for Σ^+(uus), Σ^0(uds), Ξ^+(ssd) and Λ(uds). The QCD sum rules for other members can be obtained from them by making appropriate substitutions specified below.

For Σ^+ at WE_1:

$$\begin{aligned}
c_1 &= \frac{1}{16}[(1+\beta)^2 e_s - 2(3+2\beta+3\beta^2)e_u]; \\
c_2 &= \frac{1}{16}(1+\beta)[(-1+3\beta)e_s f_s \phi - 2(1+3\beta)e_u]; \\
c_3 &= \frac{1}{12}(-1+\beta)[(1+\beta)e_s f_s \phi - 2e_u(1-\beta+f_s+\beta f_s)]; \\
c_4 &= -\frac{1}{384}[(3-2\beta+3\beta^2)e_s + 2(11+6\beta+11\beta^2)e_u]; \\
c_5 &= \frac{1}{24}[(3-18\beta+3\beta^2-2f_s+2\beta^2 f_s)e_s + (-5+2\beta \\
&\quad +27\beta^2 - 9f_s + 6\beta f_s + 27\beta^2 f_s)e_u]; \\
c_6 &= -\frac{1}{24}(-1+\beta)[(1+\beta)e_s f_s \phi(8\kappa-\xi) + 2e_u(4\kappa+6\beta\kappa+\xi)];
\end{aligned}$$

$$c_7 = \frac{1}{72}(-1+\beta)[e_s(-3+3\beta+2f_s+2\beta f_s)+2e_u(-1+\beta+8f_s+8\beta f_s)];$$

$$c_8 = -\frac{1}{72}(-1+\beta)[(1+\beta)e_s f_s\phi(8\kappa-\xi)$$

$$+e_u(-2\kappa+2\beta\kappa+10f_s\kappa+10\beta f_s\kappa+\xi-\beta\xi+f_s\xi+\beta f_s\xi)];$$

$$c_9 = -\frac{1}{288}[(7(1+\beta)e_s f_s\phi - e_u(3-3\beta+f_s+\beta f_s)];$$

$$c_{10} = -\frac{1}{96}[(1-14\beta+\beta^2)e_s+(-23-2\beta+13\beta^2)e_u(1+f_s)]. \tag{4.31}$$

For Ξ^0 at WE_1:

$$c_1 = \frac{1}{16}[(1+\beta)^2 e_u - 2(3+2\beta+3\beta^2)e_s];$$

$$c_2 = \frac{1}{16}(1+\beta)[(-1+3\beta)e_u - 2(1+3\beta)e_s f_s\phi];$$

$$c_3 = \frac{1}{12}(-1+\beta)[(1+\beta)e_u f_s - 2e_s f_s\phi(f_s-\beta f_s+1+\beta)];$$

$$c_4 = -\frac{1}{384}[(3-2\beta+3\beta^2)e_u+2(11+6\beta+11\beta^2)e_s];$$

$$c_5 = \frac{1}{24}[((3-18\beta+3\beta^2)f_s-2+2\beta^2)e_s$$

$$+((-5+2\beta+27\beta^2)f_s-9+6\beta+27\beta^2)e_s];$$

$$c_6 = -\frac{1}{24}(-1+\beta)[(1+\beta)e_u(8\kappa-\xi)+2e_s f_s\phi(4\kappa+6\beta\kappa+\xi)];$$

$$c_7 = \frac{1}{72}(-1+\beta)[e_u f_s((-3+3\beta)f_s+2+2\beta)+2e_s f_s((-1+\beta)f_s+8+8\beta)];$$

$$c_8 = -\frac{1}{72}(-1+\beta)[(1+\beta)e_u f_s(8\kappa-\xi)$$

$$+e_s f_s\phi(-2\kappa f_s+2\beta\kappa f_s+10\kappa+10\beta\kappa+\xi-\beta f_s\xi+f_s\xi+\beta\xi)];$$

$$c_9 = -\frac{1}{288}[(7(1+\beta)e_u f_s - e_s f_s\phi((3-3\beta)f_s+1+\beta)];$$

$$c_{10} = -\frac{1}{96}[(1-14\beta+\beta^2)e_u+(-23-2\beta+13\beta^2)e_s(1+f_s)]. \tag{4.32}$$

For Λ at WE_1:

$$
\begin{aligned}
c_1 &= -\frac{1}{48}((-1+\beta)^2(e_d+e_u)+(13+10\beta+13\beta^2)e_s);\\
c_2 &= \frac{1}{16}(1+\beta)((-1+\beta)(e_d+e_u)-(1+5\beta)e_s f_s\phi);\\
c_3 &= \frac{1}{72}(-1+\beta)((e_d+e_u)(1-\beta+f_s+5\beta f_s)-2(5+\beta)e_s f_s\phi);\\
c_4 &= -\frac{1}{1152}((17+2\beta+17\beta^2)(e_d+e_u)+(41+26\beta+41\beta^2)e_s);\\
c_5 &= \frac{1}{144}(e_s(-78+\beta(84-16f_s)+\beta^2(210-4f_s)+20f_s)\\
&\quad +(-1+\beta)(e_d+e_u)(7+3f_s+\beta(41+33f_s)));\\
c_6 &= -\frac{1}{72}(-1+\beta)(e_s f_s\phi(8(1+2\beta)\kappa+(5+\beta)\xi)\\
&\quad +(e_d+e_u)((20+22\beta)\kappa-(1+2\beta)\xi));\\
c_7 &= \frac{1}{216}(-1+\beta)(e_s(39+33\beta-10f_s-2\beta f_s)+(e_d+e_u)(1-\beta+4f_s+20\beta f_s));\\
c_8 &= -\frac{1}{432}(-1+\beta)(2e_s f_s\phi(8(1+2\beta)\kappa+(5+\beta)\xi)\\
&\quad +(e_d+e_u)(2(19+17\beta+f_s+5\beta f_s)\kappa-(1-\beta+f_s+5\beta f_s)\xi));\\
c_9 &= -\frac{1}{576}(-1+\beta)((e_d+e_u)(5+3\beta+3f_s+7\beta f_s)-2(5+\beta)e_s f_s\phi);\\
c_{10} &= \frac{1}{192}((62-4\beta-34\beta^2)e_s-(-7-10\beta+5\beta^2)(e_d+e_u)(1+f_s)).
\end{aligned}
\tag{4.33}
$$

At the structure WO_1, the sum rules can be expressed in the following form

$$
\begin{aligned}
&\mathrm{c}_1 m_s L^{-8/9}E_2(w)M^4+\mathrm{c}_2\chi a L^{-16/27}E_2(w)M^4+(\mathrm{c}_3{+}\mathrm{c}_4)aE_1(w)M^2\\
&+\mathrm{c}_5 m_s\chi a^2L^{-16/27}E_0(w)+\mathrm{c}_6\chi abL^{-16/27}E_0(w)+(\mathrm{c}_7+\mathrm{c}_8)m_s a^2\tfrac{1}{M^2}+\mathrm{c}_9 ab\tfrac{1}{M^2}\\
&=-\tilde{\lambda}_N^2 M_N\left[\tfrac{2\mu_N}{M^2}+\tfrac{\mu_N-1}{M_N^2}+A\right]e^{-M_N^2/M^2}.
\end{aligned}
\tag{4.34}
$$

For Σ^+ at WO_1:

$$
\begin{aligned}
c_1 &= -\frac{1}{2}(-1+\beta)((1+\beta)e_s - 2e_u);\\
c_2 &= -\frac{1}{24}(-1+\beta)[(-1+\beta)e_s f_s\phi + 18(1+\beta)e_u];\\
c_3 &= \frac{1}{24}(-1+\beta)[e_s(-6-6\beta-f_s+\beta f_s) - 6e_u(2+2\beta-f_s+\beta f_s)];\\
c_4 &= \frac{1}{96}(-1+\beta)[(-1+\beta)e_s f_s\phi(14\kappa-13\xi) - 18(1+\beta)e_u(2\kappa+\xi)];\\
c_5 &= -\frac{1}{12}[(3+2\beta+3\beta^2)e_s f_s\phi - (3+4\beta+9\beta^2)e_u(1+f_s)];\\
c_6 &= \frac{1}{576}(-1+\beta)[(-1+\beta)e_s f_s\phi - 18(1+\beta)e_u];\\
c_7 &= -\frac{1}{36}[e_s(-3+3\beta^2+5f_s-2\beta f_s+5\beta^2 f_s)\\
&\quad -e_u(3+4\beta+9\beta^2-3f_s+10\beta f_s+9\beta^2 f_s)];\\
c_8 &= -\frac{1}{144}[e_s f_s\phi(4\kappa+8\beta\kappa+4\beta^2\kappa+\xi-10\beta\xi+\beta^2\xi)\\
&\quad -e_u(-(3+4\beta+9\beta^2)(1+f_s)\xi + 4(2\beta+6\beta^2+3f_s+2\beta f_s+3\beta^2 f_s)\kappa)];\\
c_9 &= -\frac{1}{576}[3e_s - e_u(-3+3\beta^2-f_s+2\beta f_s)].
\end{aligned}
\tag{4.35}
$$

For Ξ^0 at WO_1:

$$
\begin{aligned}
c_1 &= -\frac{1}{2}(-1+\beta)((1+\beta)e_u - 2e_s);\\
c_2 &= -\frac{1}{24}(-1+\beta)[(-1+\beta)e_u + 18(1+\beta)e_s f_s\phi];\\
c_3 &= \frac{1}{24}(-1+\beta)[e_u((-6-6\beta)f_s - 1+\beta) - 6e_s((2+2\beta)f_s - 1+\beta)];\\
c_4 &= \frac{1}{96}(-1+\beta)[(-1+\beta)e_u(14\kappa-13\xi) - 18(1+\beta)e_s f_s\phi(2\kappa+\xi)];\\
c_5 &= -\frac{1}{12}[(3+2\beta+3\beta^2)e_u - (3+4\beta+9\beta^2)e_s f_s\phi(1+f_s)];
\end{aligned}
$$

$$c_6 = \frac{1}{576}(-1+\beta)[(-1+\beta)e_u - 18(1+\beta)e_s f_s \phi];$$

$$c_7 = -\frac{1}{36}[e_u f_s((-3+3\beta^2)f_s + 5 - 2\beta + 5\beta^2)$$

$$-e_s f_s((3+4\beta+9\beta^2)f_s - 3 + 10\beta + 9\beta^2)];$$

$$c_8 = -\frac{1}{144}[e_u f_s(4\kappa + 8\beta\kappa + 4\beta^2\kappa + \xi - 10\beta\xi + \beta^2\xi)$$

$$-e_s f_s \phi(-(3+4\beta+9\beta^2)(1+f_s)\xi + 4((2\beta+6\beta^2)f_s + 3 + 2\beta + 3\beta^2)\kappa)];$$

$$c_9 = -\frac{1}{576}[3e_u - e_s((-3+3\beta^2)f_s - 1 + 2\beta)]. \tag{4.36}$$

For Λ at WO_1:

$$c_1 = -\frac{1}{6}(-1+\beta)((e_d+e_u)(1+2\beta) - (5+\beta)e_s);$$

$$c_2 = -\frac{1}{72}(-1+\beta)((7+11\beta)(e_d+e_u) + (37+35\beta)e_s f_s \phi);$$

$$c_3 = -\frac{1}{72}(-1+\beta)((e_d+e_u)(14+\beta(22-3f_s)+3f_s)$$

$$+e_s(-30-6\beta+35f_s+37\beta f_s));$$

$$c_4 = \frac{1}{288}(-1+\beta)((e_d+e_u)(2(-23+5\beta)\kappa + (17-35\beta)\xi)$$

$$-e_s f_s \phi(58\kappa + 86\beta\kappa + 49\xi + 23\beta\xi));$$

$$c_5 = \frac{1}{24}((-1+\beta^2)(e_d+e_u)(1+f_s) + 2(5+6\beta+13\beta^2)e_s f_s \phi);$$

$$c_6 = -\frac{1}{1728}((-1+\beta)((11+7\beta)(e_d+e_u) + (35+37\beta)e_s f_s \phi));$$

$$c_7 = \frac{1}{216}(-(-1+\beta)(e_d+e_u)(-7+\beta-f_s+13\beta f_s)$$

$$+e_s(-30+34f_s+4\beta(6+7f_s)+\beta^2(6+82f_s)));$$

$$c_8 = \frac{1}{864}(2e_s f_s \phi(4(7+10\beta+19\beta^2)\kappa - (11+26\beta+35\beta^2)\xi)$$

$$+(-1+\beta)(e_d+e_u)(4(-4-2\beta+5f_s+7\beta f_s)\kappa - (-5+11\beta)(1+f_s)\xi));$$

$$c_9 = \frac{1}{3456}((-1+\beta)(2(5+\beta)e_s + (e_d+e_u)(5+\beta+11f_s+13\beta f_s))). \qquad (4.37)$$

At the structure WO_2, the sum rules can be expressed in the following form

$$\begin{aligned}
&\mathrm{c}_1 m_s L^{-8/9} E_1(w) M^2 + \mathrm{c}_2 \chi a L^{-16/27} E_1(w) M^2 + (\mathrm{c}_3{+}\mathrm{c}_4) a E_0(w) + \mathrm{c}_5 m_s \chi a^2 L^{-16/27} E_0(w) \\
&+\mathrm{c}_6 m_0^2 a L^{-4/9} \tfrac{1}{M^2} + c_7 \chi a b L^{-16/27} \tfrac{1}{M^2} + (\mathrm{c}_8 + \mathrm{c}_9) m_s a^2 \tfrac{1}{M^4} + \mathrm{c}_{10} a b \tfrac{1}{M^4} \\
&= -\tfrac{\tilde{\lambda}_N^2}{M_N} [\tfrac{2(\mu_N - 1)}{M^2} + A] e^{-M_N^2/M^2}.
\end{aligned} \qquad (4.38)$$

For Σ^+ at WO_2:

$$\begin{aligned}
c_1 &= -\frac{1}{2}(-1+\beta)[(1+\beta)e_s - 2e_u]; \\
c_2 &= -\frac{1}{6}(-1+\beta)^2 e_s f_s \phi; \\
c_3 &= -\frac{1}{4}(-1+\beta)[e_s(2+2\beta - f_s + \beta f_s) + 2e_u(-2-2\beta - f_s + \beta f_s)]; \\
c_4 &= \frac{1}{16}(-1+\beta)[e_s f_s \phi + 2(1+\beta)e_u](2\kappa - \xi); \\
c_5 &= -\frac{1}{3}(-1+\beta)[2e_s f_s \phi + e_u(-1-\beta - f_s + \beta f_s)]; \\
c_6 &= \frac{1}{24}(-1+\beta)[7(1+\beta)e_s + e_u(-1-\beta - 3f_s + 3\beta f_s)]; \\
c_7 &= -\frac{1}{144}(-1+\beta)^2 e_s f_s \phi; \\
c_8 &= \frac{1}{18}[e_s(-3+3\beta^2 + 5f_s - 2\beta f_s + 5\beta^2 f_s) \\
&\quad -e_u(3+4\beta+9\beta^2 - 3f_s + 10\beta f_s + 9\beta^2 f_s)]; \\
c_9 &= \frac{1}{72}[e_s f_s \phi((1-10\beta+\beta^2)\xi + 4(1+\beta)^2\kappa) \\
&\quad -e_u(4(2\beta+6\beta^2+3f_s+2\beta f_s+3\beta^2 f_s)\kappa - (3+4\beta+9\beta^2)(1+f_s)\xi)]; \\
c_{10} &= -\frac{1}{288}(-1+\beta)((1+\beta)e_s - e_u(-3-3\beta - f_s + \beta f_s)].
\end{aligned} \qquad (4.39)$$

For Ξ^0 at WO_2:

$$
\begin{aligned}
c_1 &= -\frac{1}{2}(-1+\beta)[(1+\beta)e_u - 2e_s];\\
c_2 &= -\frac{1}{6}(-1+\beta)^2 e_u;\\
c_3 &= -\frac{1}{4}(-1+\beta)[e_u f_s((2+2\beta)f_s - 1 + \beta) + 2e_s f_s(-(2+2\beta)f_s - 1 + \beta)];\\
c_4 &= \frac{1}{16}(-1+\beta)[e_s f_s \phi + 2(1+\beta)e_u](2\kappa - \xi);\\
c_5 &= -\frac{1}{3}(-1+\beta)[2e_u f_s + e_s f_s \phi(-(1+\beta)f_s - 1 + \beta)];\\
c_6 &= \frac{1}{24}(-1+\beta)[7(1+\beta)e_u f_s + e_s(-(1+\beta)f_s - 3 + 3\beta)];\\
c_7 &= -\frac{1}{144}(-1+\beta)^2 e_u;\\
c_8 &= \frac{1}{18}[e_u f_s((-3+3\beta^2)f_s + 5 - 2\beta + 5\beta^2)\\
&\quad -e_s f_s((3+4\beta+9\beta^2)f_s - 3 + 10\beta + 9\beta^2)];\\
c_9 &= \frac{1}{72}[e_u f_s((1-10\beta+\beta^2)\xi + 4(1+\beta)^2\kappa)\\
&\quad -e_s f_s(4((2\beta+6\beta^2)f_s + 3 + 2\beta + 3\beta^2)\kappa - (3+4\beta+9\beta^2)(1+f_s)\xi)];\\
c_{10} &= -\frac{1}{288}(-1+\beta)((1+\beta)e_u - e_s(-(3+3\beta)f_s - 1 + \beta)].
\end{aligned}
\tag{4.40}
$$

For Λ at WO_2:

$$
\begin{aligned}
c_1 &= -\frac{1}{12}(-1+\beta)((e_d+e_u)(1+2\beta) - (5+\beta)e_s);\\
c_2 &= -\frac{1}{36}(-1+\beta)^2(2(e_d+e_u) - e_s f_s \phi);\\
c_3 &= \frac{1}{24}(-1+\beta)((e_d+e_u)(2+\beta(-6+f_s) - f_s) + +e_s(10+3f_s+\beta(2+5f_s)));\\
c_4 &= \frac{1}{96}(-1+\beta)((-1+3\beta)(e_d+e_u) + (5+3\beta)e_s f_s \phi)(2\kappa - \xi);
\end{aligned}
$$

$$
\begin{aligned}
c_5 &= \frac{1}{12}(-1+\beta)((e_d+e_u)(-1+\beta(-1+f_s)-f_s)+4e_sf_s\phi);\\
c_6 &= \frac{1}{96}(-1+\beta)(-2(5+\beta)e_s+(e_d+e_u)(3+7\beta+5f_s+3\beta f_s));\\
c_7 &= -\frac{1}{864}(-1+\beta)^2(2(e_d+e_u)-e_sf_s\phi);\\
c_8 &= \frac{1}{216}((-1+\beta)(e_d+e_u)(-7+\beta-f_s+13\beta f_s)\\
&\quad -2e_s(-15+17f_s+2\beta(6+7f_s)+\beta^2(3+41f_s)));\\
c_9 &= \frac{1}{864}(2e_sf_s\phi(-4(7+10\beta+19\beta^2)\kappa+(11+26\beta+35\beta^2)\xi)\\
&\quad -(-1+\beta)(e_d+e_u)(4(-4-2\beta+5f_s+7\beta f_s)\kappa-(-5+11\beta)(1+f_s)\xi));\\
c_{10} &= -\frac{1}{3456}((-1+\beta)(2(5+\beta)e_s+(e_d+e_u)(5+\beta+11f_s+13\beta f_s)).
\end{aligned}
\tag{4.41}
$$

It is not necessary to list all the coefficients for all 8 members since the coefficients for other members of the octet family can be obtained by appropriate replacements of quark contents in the following way:

- for proton p, replace s quark by d quark in Σ^+.
- for neutron n, exchange d quark with u quark in proton p,
- for Σ^-, replace u quark by d quark in Σ^+,
- for Ξ^-, replace u quark by d quark in Ξ^0,
- for Σ^0, change corresponding factors in Ξ^0.

Here the conversions between u and d quarks are achieved by simply switching their charge factors e_u and e_d. Moreover, The conversions from s quark to u or d quarks involve setting $m_s = 0$, $f_s = \phi = 1$, in addition to the switching of charge factors.

This way, they can also provide additional checks for our calculations.

At this point, we can make some comparisons with previous calculations in Ref. [22, 30, 23]. First, we use general interpolating fields where we can vary β to achieve the best match in sum rules. The previous calculations correspond to a fixed value of β=-1. This effect was studied in detail in Ref. [39], and it was found that $\beta = -1.2$ is the optimal value. Most of our results are at $\beta = -1.2$. Second, we have checked that our sum rules agree with those in the previous calculations for the most part. For example, for the proton at WE_1, we completely agree except for the $\kappa - 2\xi$ term in Eq. (2.16) in Ref. [30]. In all of our sum rules, we have the combination $2\kappa - \xi$ instead of $\kappa - 2\xi$. For the strange members (Σ, Ξ, Λ), they have 8 terms in the OPE, while we have 10 terms. For the sum rules at structure WO_1, they have only 3 terms, while we have 9 terms. For the sum rules at structure WO_2, they have only 4 terms, while we have 10 terms. Third, they only analyzed the sum rules at structure WE_1, while we will examine all the structures. Fourth, we use a completely different analysis method.

Before going into the analysis, we would like to point out some relations among the correlation functions (or OPE) follow from symmetries, which lead to the same relations in the magnetic moments. In exact SU(3)-flavor symmetry, it is known that

the magnetic moments of the octet family are related by (see, for example, Ref. [40])

$$\begin{aligned}
\mu_{\Sigma^+} &= \mu_p, \\
2\mu_\Lambda &= \mu_n, \\
\mu_{\Sigma^-} + \mu_n &= -\mu_p, \\
\mu_{\Xi^-} &= \mu_{\Sigma^-}, \\
\mu_{\Xi^0} &= \mu_n.
\end{aligned} \tag{4.42}$$

These relations are borne out in the OPE of our sum rules if SU(3)-flavor symmetry is enforced. They are approximately true since SU(3)-flavor symmetry is broken by the strange quark mass difference. Here we have the advantage of studying the symmetry-breaking effects since the terms are explicit in our QCD sum rules.

4.4 Monte Carlo Sum Rule Analysis

The sum rules for magnetic moments have the generic form of OPE - ESC = Pole + Transition, where OPE, ESC and Pole represent QCD side from OPE, ESC contribution and pole contribution respectively. Or the sum rule can be in the form

$$\Pi_{mag}(QCD, \beta, w, M^2) = \tilde{\lambda}_N^2 \left(\frac{\mu_N}{M^2} + A \right) e^{-M_N^2/M^2}, \tag{4.43}$$

where QCD represents all the QCD input parameters. The task then becomes: given the function Π_{mag} with known QCD input parameters and the ability to vary β, find the phenomenological parameters (magnetic moment μ_N, transition strength A,

coupling strength $\tilde{\lambda}_N^2$, and continuum threshold w) by matching the two sides over some region in the Borel mass M. A χ^2 minimization is best suited for this purpose. It turns out that there are too many fit parameters for this procedure to be successful in general. To alleviate the situation, we employ the corresponding mass sum rules which have a similar generic form of OPE - ESC = Pole, or

$$\Pi_{mass}(QCD, \beta, w_1, M^2) = \tilde{\lambda}_N^2 e^{-M_N^2/M^2}, \tag{4.44}$$

which shares some of the common parameters. Note that the continuum threshold may not be the same in the two sum rules. By taking the ratio of the two equations, we are left with

$$\frac{\Pi_{mag}(QCD, \beta, w, M^2)}{\Pi_{mass}(QCD, \beta, w_1, M^2)} = \frac{\mu_N}{M^2} + A. \tag{4.45}$$

This is the form we are going to implement. By plotting the two sides as a function of $1/M^2$, the slope will be the magnetic moment and the intercept the transition strength. The linearity (or deviation from it) of the left-hand side gives an indication of OPE convergence and the role of excited states. The two sides are expected to match for a good sum rule. This way of matching the sum rules has two advantages. First, the slope, which is the magnetic moment of interest, is usually better determined than the intercept. Second, by allowing the possibility of different continuum thresholds, we ensure that both sum rules stay in their valid regimes.

For the mass sum rule in the dominator, we use the chiral-even mass sum rules developed by *qcdsr2pt-construction.nb* which are listed in Eq. (3.79), with corre-

sponding coefficients in Eq.(3.82) to Eq.(3.86).

We use the Monte-Carlo procedure first introduced in Ref. [39] to carry out the search which allows a rigorous error analysis. In this method, the entire phase-space of the input QCD parameters is explored simultaneously, and is mapped into uncertainties in the phenomenological parameters. This lead to more realistic uncertainty estimates than traditional approaches.

First, a set of randomly-selected, Gaussianly-distributed condensates are generated with assigned uncertainties. Here we give 10% for the uncertainties of input parameters, and this number can be adjusted to test the sensitivity of the QCD parameters. Then the OPE is constructed in the Borel window with evenly distributed points M_j. Note that the uncertainties in the OPE are not uniform throughout the Borel window. They are larger at the lower end where uncertainties in the higher-dimensional condensates dominate. Thus, it is crucial that the appropriate weight is used in the calculation of χ^2. For the OPE obtained from the k'th set of QCD parameters, the χ^2 per degree of freedom is

$$\frac{\chi^2_k}{N_{DF}} = \sum_{j=1}^{n_B} \frac{[\Pi^{OPE}_k(M_j^2, \beta, w, w_1) - \Pi^{Phen}_k(M_j^2, \mu, A)]^2}{(n_B - n_p)\, \sigma^2_{OPE}(M_j)}, \tag{4.46}$$

where Π^{OPE} refers to the LHS of Eq. (4.45) and Π^{Phen} its RHS. The integer n_p is the number of phenomenological search parameters. In this work, n_B=51 points were used along the Borel axis. The procedure is repeated for many QCD parameter sets, resulting in distributions for phenomenological fit parameters, from which errors are derived. In practice, 200 configurations are sufficient for getting stable uncertainties.

We used about 2000 sets to resolve more subtle correlations among the QCD parameters and the phenomenological fit parameters. This means that each sum rule is fitted 2000 times to arrive at the final results. We developed a Mathematica program *qcdsr3pt-analysis.nb* to carry out the analysis.

The values for the basic QCD input parameters are given in previous chapter. In the presence of external fields, additional condensates called vacuum susceptibilities are introduced. These parameters are less well-known. They have been estimated in studies of nucleon magnetic moments [8, 30, 9, 37] where the availability of precise experimental data has put strict constraints on these parameters. In particular, the magnetic susceptibility χ is the subject of two recent studies [41, 42]. We use the values $\chi = -6.0\ GeV^{-2}$ and $\kappa = 0.75$, $\xi = -1.5$. Note that χ is almost an order of magnitude larger than κ and ξ, and is the most important of the three. The strange quark parameters are placed at $\phi = 0.60$ [22, 34]. These input parameters are just central values. We will explore sensitivity to these parameters by assigning uncertainties to them in the Monte-Carlo analysis.

4.5 Result and Discussion

We have 24 sum rules in total to analyze: 3 for each member of the octet. For each sum rule, we have in principle 5 parameters to determine: magnetic moment μ, transition A, continuum threshold for magnetic moment sum rule w, continuum threshold for mass sum rule w_1 and the real parameter in interpolating fields β. But a search treating all five parameters as free does not work because there is not

Table 4.1: Results for the magnetic moment of octet baryons from the QCD sum rule in Eq. (4.28) (structure WE_1). The seven columns correspond to, from left to right: particle, β value, Borel region in which the two sides of the QCD sum rule are matched, continuum threshold, transition strength, extracted magnetic moment in unit of nuclear magnetons, and experimental value. The errors are derived from 2000 samples in the Monte-Carlo analysis with 10% uncertainty on all QCD input parameters.

	β	Region (GeV)	w (GeV)	A (GeV^{-2})	μ_B (μ_N)	Exp. (μ_N)
p	-1.2	0.7 to 0.9	1.40	1.46 ± 0.34	3.01 ± 0.24	2.79
	-0.4	0.8 to 1.2	1.60	0.74 ± 0.13	2.82 ± 0.26	2.79
n	-1.2	0.7 to 1.1	1.40	-0.19 ± 0.09	-1.97 ± 0.15	-1.91
Λ	-1.2	1.1 to 1.2	1.60	-0.45 ± 0.05	-0.56 ± 0.15	-0.61
Σ^+	-1.2	1.1 to 1.3	1.85	0.56 ± 0.06	2.31 ± 0.25	2.45
Σ^0	-1.2	1.0 to 1.6	1.80	0.07 ± 0.02	0.69 ± 0.07	0.65
Σ^-	-1.2	1.3 to 1.8	1.80	-0.08 ± 0.01	-1.16 ± 0.10	-1.16
Ξ^0	-1.2	1.6 to 1.9	2.15	-0.16 ± 0.01	-1.15 ± 0.05	-1.25
Ξ^-	-1.2	1.1 to 1.4	2.00	-0.34 ± 0.02	-0.64 ± 0.06	-0.65

enough information in the OPE. In fact, the freedom to vary β can be used as an advantage to yield the optimal match. We find that $\beta = -1.2$ gives the best match in most cases. This agrees with the value suggested in Ref. [39]. One exception is the proton: we found a better solution at $\beta = -0.4$ than at $\beta = -1.2$. Another parameter that can be used to our advantage is the continuum threshold w_1 for the corresponding mass sum rule. We fix it to the value that gives the best solution to the mass sum rule independently. The following values for w_1 are used: for the nucleon, $w_1 = 1.44$ GeV; for Λ, $w_1 = 1.60$ GeV; for Σ, $w_1 = 1.66$ GeV; for Ξ, $w_1 = 1.82$ GeV. In this way the magnetic moment sum rule and the mass sum rule can stay in their respective valid Borel regimes. This leaves us with three parameters: μ, A, w. Unfortunately, a three-parameter search is either unstable or returns values for w smaller than the particle mass, an unphysical situation. Again we think this is a symptom of insufficient information in the OPE. So we are forced to fix the continuum

threshold w that corresponds to the best match for the central values of the QCD parameters.

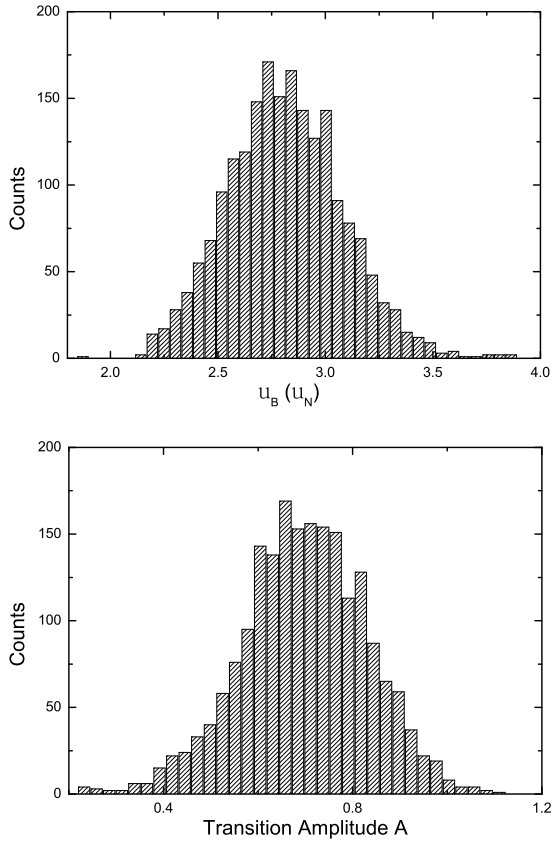

Figure 4.4: Histogram for the proton magnetic moment (top) and transition amplitude (bottom) obtained from Monte-Carlo fits of Eq. (4.28) at WE_1 for 2000 QCD parameter sets. They are based on 10% uncertainty given to all the QCD input parameters.

4.5.1 The Sum Rule at WE_1

The results determined this way at the WE_1 structure are displayed in Table 4.1. The Borel window is determined by the following two criteria: OPE convergence which gives the lower bound, and ground-state dominance which gives the upper bound. It is done iteratively. For each value of β, we adjust the Borel window until the best solution is found. We see that our calculated magnetic moments agree with

experiment fairly well within error bars.

We stress that the errors are derived from Monte-Carlo distributions which give the most realistic estimation of the uncertainties. An example of such distributions is given in Fig. 4.4. We see that they are roughly Gaussian distributions. The central value is taken as the average, and the error is one standard deviation of the distribution. We found about 10% accuracy for the magnetic moments in our Monte-Carlo analysis, resulting from 10% uniform uncertainty in all the QCD input parameters. Of course, the uncertainties in the QCD parameters can be non-uniform. For example, we tried the uncertainty assignments (which are quite conservative) in Ref. [39], and found about 30% uncertainties in our output.

To gain a better appreciation on how the QCD sum rules produce the results, we show Fig. 4.5, using the proton as an example. There are three graphs in this figure to give three different aspects of the analysis. The first graph shows how the two sides of Eq. (4.45) match over the Borel window, which should be linear as a function of $1/M^2$ according to the right-hand side of this equation. Indeed, we observe excellent linear behavior from the OPE side (LHS). The match is almost perfect (barely distinguishable between the solid and dotted lines). The slope gives the magnetic moment μ, and the intercept give the transition contribution A. We find that the inclusion of A is important in producing the best match. Also plotted are the individual contributions from u and d quarks. We see that for the proton, the u-quark contribution is the dominant one, which is expected because it is doubled-represented in the proton (uud). We define the slope from an individual quark contribution as the effective magnetic moment of that quark in the particle.

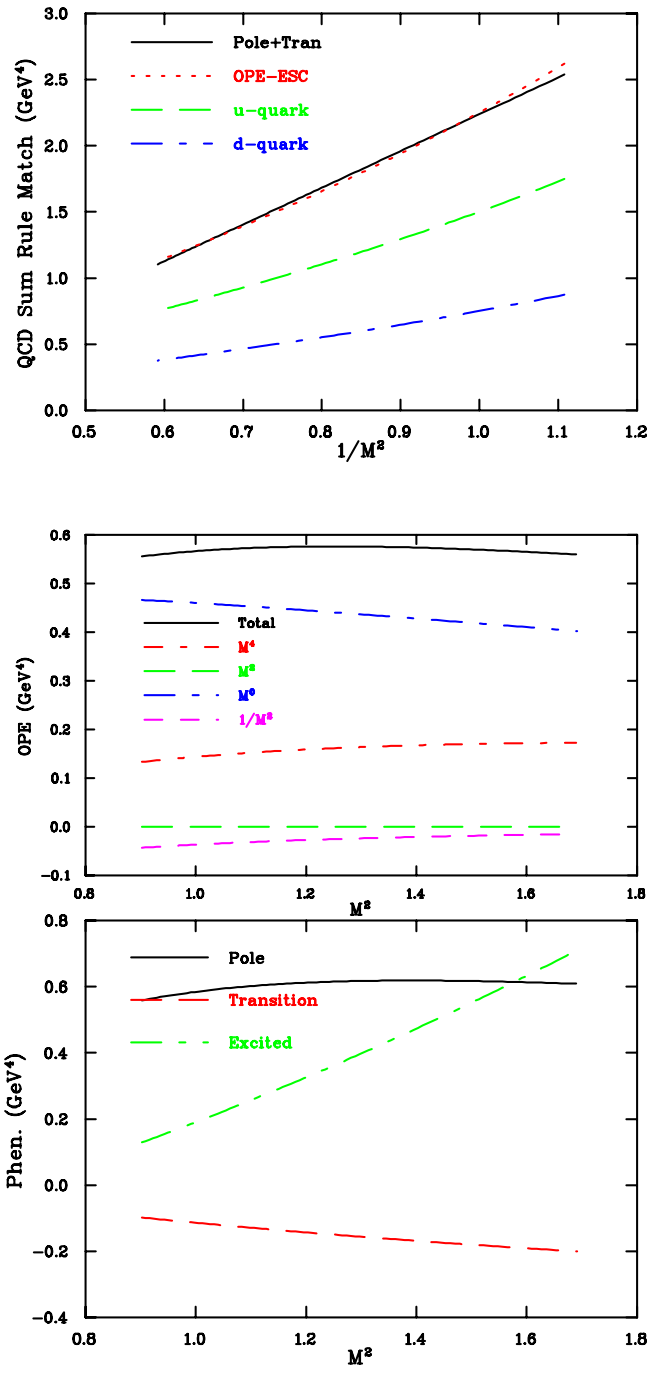

Figure 4.5: Analysis of the QCD sum rule in Eq. (4.28) (structure WE_1) for the proton at $\beta = -0.4$ according to Eq. (4.45). In the top, the pole plus transition terms (solid lines) are compared against the OPE minus the excited-state contributions (dashed lines) as a function of $1/M^2$ (the two should match for an ideal sum rule). Also plotted are the individual contributions from u (long-dashed lines) and d (dot-dashed lines) quarks. In the middle, the total in the OPE side and its various terms are plotted as a function of M^2. In the bottom, the 3 terms in the phenomenological side: pole (solid), transition (long-dashed), and excited (dot-dashed) are plotted as a function of M^2.

The second graph in Fig. 4.5 shows how the various terms in the OPE contribute to determination of magnetic moments. The M^0 term, which contains the contributions from the condensates χa^2 and b, plays an important role. It is the leading contribution in the region below $M^2 < 1.2$ GeV^2. For this reason, the sum rule at WE_1 is expected to have good spectral properties. Indeed this is confirmed in the third graph where we plot the three terms in the phenomenological side (pole, transition, and excited) as a function of M^2. The ground-state pole is dominant (over 70% of the RHS at the low end of the Borel window). The excited-state contribution starts small, then grows with M^2, as expected from the continuum model. The transition contribution is small in this sum rule. It is consistently smaller than the excited-state contribution and has a weak dependence on the Borel mass.

4.5.2 The Sum Rule at WO_1

Table 4.2: Similar to Table 4.1, but for the QCD sum rule in Eq. (4.34) (structure WO_1).

	β	Region (GeV)	w (GeV)	A (GeV^{-1})	μ_B (μ_N)	Exp. (μ_N)
p	-0.8	1.4 to 1.6	1.50	1.03±0.16	2.67 ±0.16	2.79
n	-1.2	1.2 to 1.4	1.40	-0.54 ±0.11	-1.70 ±0.11	-1.91
Λ	-1.2	1.0 to 1.3	1.60	-2.3 ±0.31	-0.62 ±0.17	-0.61
Σ^+	-0.6	1.5 to 1.7	1.60	1.60 ±0.50	2.46 ±0.40	2.45
Σ^0	-1.0	1.4 to 1.6	1.70	0.23 ±0.11	0.58 ±0.09	0.65
Σ^-	-0.6	1.2 to 1.5	1.60	-2.04 ±0.34	-0.57 ±0.26	-1.16
Ξ^0	-1.2	1.2 to 1.4	2.10	-1.52 ±0.21	-1.27 ±0.15	-1.25
Ξ^-	-0.2	1.7 to 1.8	1.90	-0.4 ±0.41	-0.49 ±0.29	-0.65

Next, we analyze the sum rule in Eq. (4.34) at the structure WO_1, using the same procedure. Table 4.2 displays the results extracted from this sum rule. The

magnetic moments have larger errors than those from WE_1: about 15% as opposed to 10%. The agreement with experiment is reasonable (with the exception of Σ^-), but not as good as those from WE_1. We had to search a wider region in β to find the best match. The transition contribution (A) are larger for the strange particles, as well as their errors.

Fig. 4.6 shows the details of the analysis in the case of the proton. The matching is very good, as indicated in the top graph. The middle graphs shows that the leading contribution in the OPE (M^4 term) is χa, followed by the quark condensate a (M^2 term). The condensate χab (M^0 term) and ab (M^{-2} term) are very small in this sum rule. The bottom graph reveals a surprising result: the excited-state contribution dominates over the pole and the transition contributions. As a result, this sum rule is less reliable. This is the reason why the results from this sum rule are not as good as those from WE_1. This sum rule also shows the importance of checking the individual terms in the phenomenological side, in addition to looking at the best match of the two sides. In this case, there is no pole dominance, even though the leading terms is non-perturbative and the match is almost perfect.

4.5.3 The Sum Rule at WO_2

Finally, we present the results from the sum rule in Eq. (4.38) at the structure WO_2 in Table 4.2. The agreement with experiment is not as good as the other two sum rules. For example, Σ^- and Ξ^- have the wrong sign. Fig. 4.7 shows the details of the analysis for the proton. The matching is very good, as indicated in the top graph. The

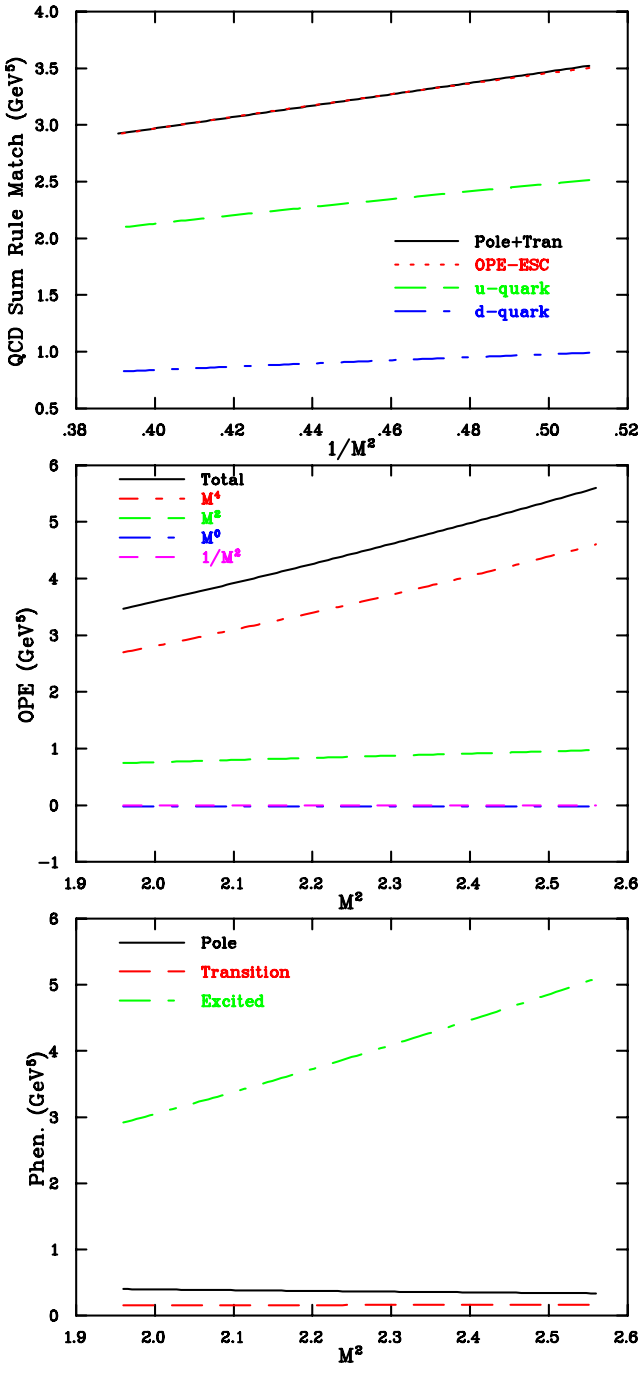

Figure 4.6: Similar to Fig. 4.5, but at structure WO_1 and $\beta = -1.2$.

middle graph shows that the leading contribution in the OPE is M^2 with a coefficient of χa, followed by the M^0 term. The $1/M^2$ term is slightly negative, while the $1/M^4$ term is very small. The bottom graph shows that the excited-state dominates over the pole and the transition, like the sum rule from WO_1, but the relative size of the pole is much larger. Since the WO_2 sum rule has power corrections up to $1/M^4$, it is expected to be more reliable than the WO_1 sum rule. But our analysis shows that this advantage is offset by the smallness of the $1/M^2$ and $1/M^4$ terms. As a result, the reliability of the WO_2 sum rule is about the same as the WO_1 sum rule.

Table 4.3: Similar to Table 4.1, but for the QCD sum rule in Eq. (4.38) (structure WO_2).

	β	Region (GeV)	w (GeV)	A (GeV^{-2})	μ_B (μ_N)	Exp. (μ_N)
p	-1.2	1.3 to 1.4	1.60	0.42 $\pm$0.07	2.53 $\pm$0.13	2.79
n	-1.2	1.7 to 1.9	1.60	0.26 $\pm$0.03	-1.73 $\pm$0.28	-1.91
Λ	-1.2	1.3 to 1.4	1.90	-0.85 $\pm$0.22	-0.53 $\pm$0.17	-0.61
Σ^+	-1.0	1.2 to 1.4	1.70	0.21 $\pm$0.05	1.50 $\pm$0.11	2.45
Σ^0	-1.2	1.0 to 1.6	1.60	-0.02 $\pm$0.02	1.04 $\pm$0.07	0.65
Σ^-	-1.2	1.4 to 1.6	1.65	0.0 $\pm$0.01	0.61 $\pm$0.06	-1.16
Ξ^0	-1.2	1.6 to 2.0	2.1	-0.08 $\pm$0.03	-1.20 $\pm$0.23	-1.25
Ξ^-	-1.2	1.4 to 1.5	2.2	0.22 $\pm$0.09	0.80 $\pm$0.21	-0.65

We have performed the same analysis for all the members and all three structures. Fig. 4.8 shows the graphs for the neutron. In this case, the slope is negative. Again, the sum rule at WE_1 has excellent convergence properties. The WO_1 sum rule has a good match, but the pole contribution is less than the excited-state contribution. The WO_2 sum rule does not have a good match. Fig. 4.9 shows the case for the Σ^0, which has all three quark contributions (u, d and s).

Overall, based on the quality of the match, the broadness of the Borel window and its reach into the lower end, the size of the continuum contribution, and the OPE

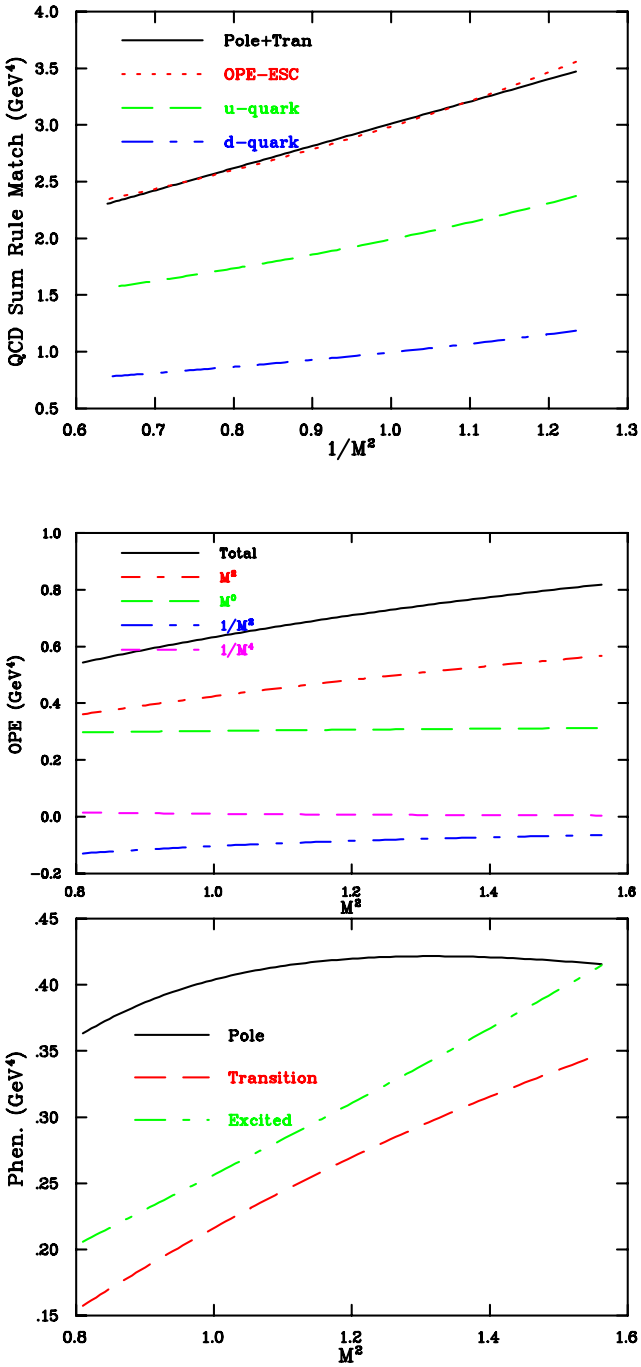

Figure 4.7: Similar to Fig. 4.5, but at structure WO_2 and $\beta = -1.2$.

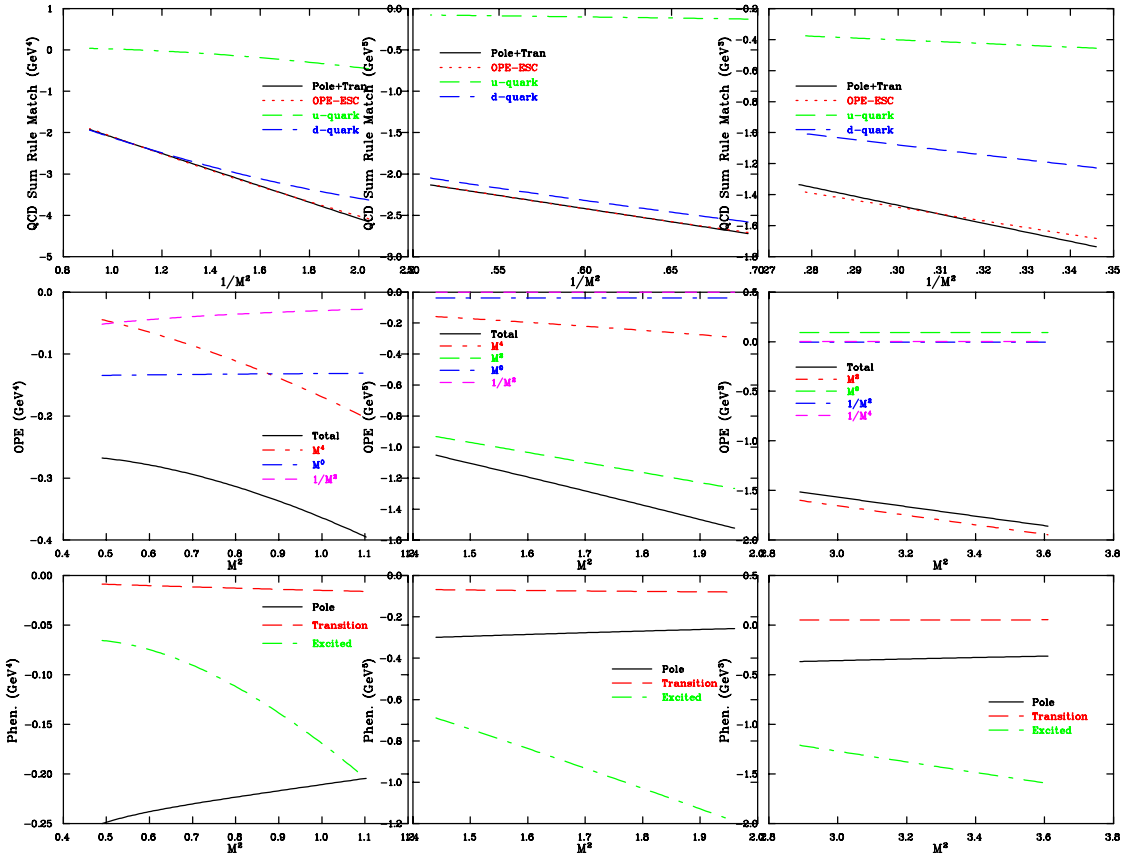

Figure 4.8: Similar to Fig. 4.5, But for the neutron at all three structures: WE_1 (left panel), WO_1 (middle panel), WO_2 (right panel).

convergence, we find that the sum rule at WE_1 is the most reliable of the three sum rules.

4.5.4 Some Physics Discussions

Based on the results of our comprehensive analysis, we conclude that the QCD sum rules at WE_1 in Eq. (4.5) are the most reliable. Here we discuss some physics implications of the results extracted from them (Table 4.1). First we look at some ratios of magnetic moments listed in Table 4.4. Here we compare our results with those from the SU(6) symmetry, lattice calculations [43] and experiment. From the table, we see that the QCD sum rule results compare well against other approaches and

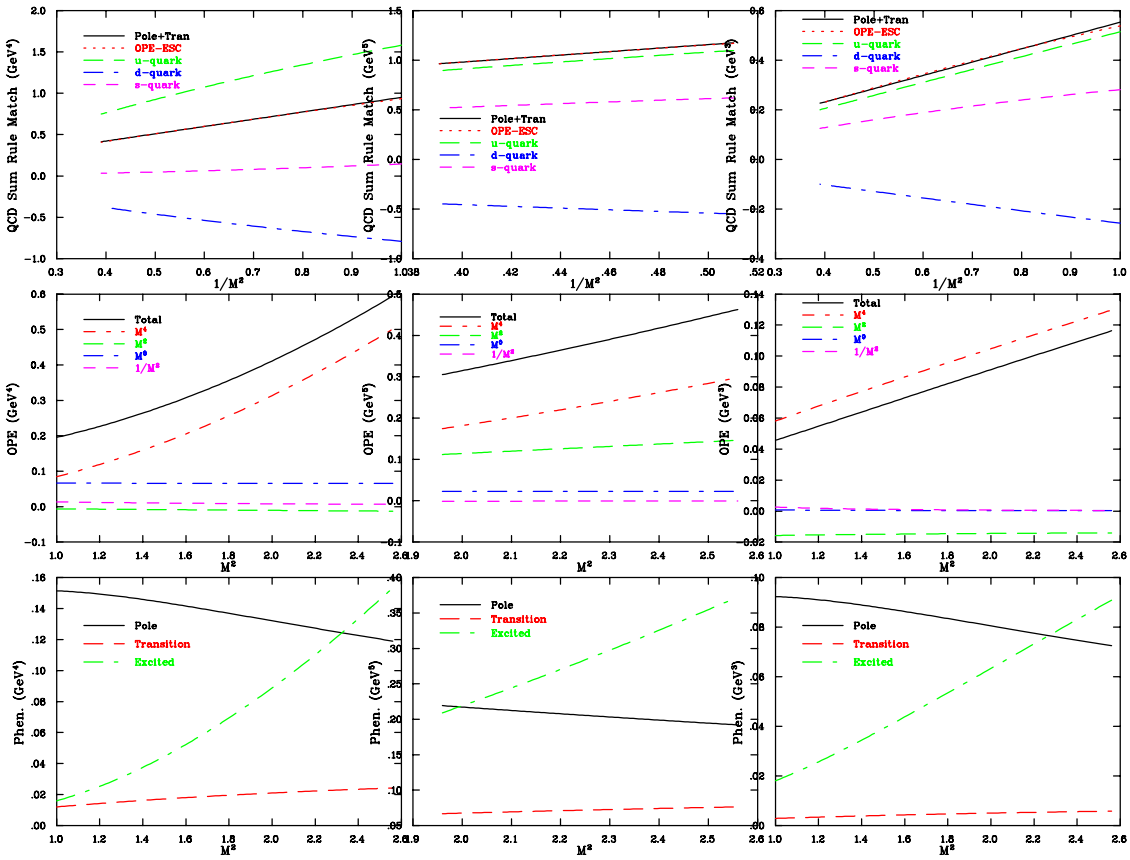

Figure 4.9: Similar to Fig. 4.8, but for Σ^0.

experiment. They agree a little better with experiment than the lattice results. Furthermore, our QCD rum rule results are an improvement over the ratios from previous QCD sum rule calculations in Ref. [30].

Next, we consider a few sum rules among magnetic moments that have been discussed in literature. They reveal interesting quark dynamics in the baryons. They are mostly based on SU(6)-symmetry considerations in the quark model. We begin with the sum rule [44]

$$\frac{3(p-\Sigma^+)}{\Xi^- - \Xi^0} = \frac{(p+3\Lambda)}{p}. \tag{4.47}$$

It assumed 'baryon independence' of quark moments: the independence of which baryon the same quark is in, a concept first mentioned by Franklin [45]. In other

Table 4.4: A comparison of selected ratios of magnetic moments.

Ratio	Sum Rule result	SU(6) symmetry	Lattice results	Exp.
n/p	-0.70(9)	$-2/3$	-0.63(5)	-0.68
Σ^-/Σ^+	-0.50(7)	$-1/3$	-0.37(3)	-0.47
Ξ^-/Ξ^0	0.56(6)	$1/2$	0.58(5)	0.52
Ξ^0/Λ	2.05(56)	2	2.4(5)	2.04
Ξ^-/Λ	1.14(32)	1	1.0(2)	1.13

words, each quark is not sensitive to the environment it resides in and quarks in different spin states had the same effective moments. In this sum rule, it also assumed that the s quark moment in the Λ is the same as in the Σ and Ξ, even though the spin states are different. This rum rule is violated the most (by a factor of 5) using present values of magnetic moments. This large violation is mostly due to the small difference in the denominator $\Xi^- - \Xi^0$ which magnifies the apparent discrepancy. So this is not a good way of testing baryon independence. Our determination of the ratio of the left hand side over the right hand side (LHS/RHS) is 7.4(1.0), compared to the experiment value of 5.7(4) and the lattice calculation of 4.1(1.5). The error are added in quadrature in forming these ratios.

One interesting sum rule for magnetic moment [46] which is fairly accurately satisfied is

$$p + n = 3\Lambda + \frac{1}{2}(\Sigma^+ + \Sigma^-) - (\Xi^0 + \Xi^-). \tag{4.48}$$

It is derived using SU(3)-flavor symmetry to characterize the Λ wave function. Our determination of the LHS/RHS ratio is 1.24(79), compared to the experimental values of 1.22(5) and the lattice calculation of 1.45(27).

Another sum rule for magnetic moment, first derived by Franklin [45],

$$p - n = \Sigma^+ - \Sigma^- + \Xi^- - \Xi^0, \tag{4.49}$$

is another test of baryon independence of the quark moments. The contribution of the strange quarks approximately cancel, leaving only u and d quarks. We give the ratio of 1.20(0.68), while the experiment measurements gives 1.133(10) and lattice results is 1.07(8) for this ratio.

Finally, the Sachs sum rule [47]

$$3(p + n) = \Sigma^+ - \Sigma^- - \Xi^- + \Xi^0 \tag{4.50}$$

is satisfied by the more general extension of SU(6) symmetry and is another test of baryon independence of quark moments. This sum rule is just the sum of the two separate sum rules proposed earlier by Franklin [48]. Our result gives the ratio of 0.86(35) which is in agreement with the experiment measurements of 0.881(11). Whereas it yields an opposite violation with a ratio of 1.29(20) from lattice moments. This contradiction is possibly because the Sachs sum rule may be sensitive to dynamics not included in the lattice calculation.

4.5.5 Individual Quark Contributions

To gain a deeper understanding of the dynamics, it is useful to consider the individual quark sector contributions to the magnetic moment. In our approach, we can easily

calculate individual quark contributions to the QCD sum rules. For example, to turn off all u-quark contributions, we set the charge factor $e_u = 0$. To turn off all s-quark contributions, we set $e_s = 0$, $m_s = 0$, $f_s = 1$, and $\phi = 1$. We can extract a number corresponding to each quark contribution from the slope of Eq. (4.45) as a function of $1/M^2$. We call this the raw individual quark contributions to the magnetic moments.

Table 4.5: Individual quark contributions and total magnetic moments in unit of nuclear magnetons extracted from the QCD sum rules at WE_1 (denoted by the subscript SR) are compared with those from a lattice QCD calculation (denoted by the subscript LAT) [43, 49].

	$\mu^u_{\mathtt{SR}}$	$\mu^u_{\mathtt{LAT}}$	$\mu^d_{\mathtt{SR}}$	$\mu^d_{\mathtt{LAT}}$	$\mu^s_{\mathtt{SR}}$	$\mu^s_{\mathtt{LAT}}$	μ^{Total}_{SR}	$\mu^{Total}_{\mathtt{LAT}}$
p	2.46(25)	2.59(24)	0.38(4)	0.15(9)	0	0	2.82(26)	2.79
n	-0.42(9)	-0.31(20)	-1.53(13)	-1.32(14)	0	0	-1.97(15)	-1.60(21)
Λ	0.18(7)	0.09(6)	-0.09(4)	-0.03(2)	-0.63(15)	-0.54(7)	-0.56(15)	-0.50(7)
Σ^+	2.06(25)	2.33(29)	0	0	0.15(2)	0.08(5)	2.31(25)	2.37(18)
Σ^0	1.09(12)	0.87(9)	-0.54(6)	-0.29(3)	0.14(2)	0.08(5)	0.69(7)	0.65(6)
Σ^-	0	0	-1.25(10)	-1.14(14)	0.10(2)	0.08(5)	-1.16(10)	-1.08(10)
Ξ^0	0.02(2)	-0.44(6)	0	0	-1.08(7)	-0.73(6)	-1.15(5)	-1.17(9)
Ξ^-	0	0	0.03(2)	0.22(3)	-0.67(6)	-0.73(6)	-0.64(6)	-0.51(7)

Table 4.5 gives the result of raw individual u, d and s quark sector contributions to the magnetic moments from the QCD sum rules at WE_1. It is compared with the lattice QCD result in [43]. The lattice results were re-scaled later in [49] and we use the re-scaled results for the comparison. Our results agree with the lattice results reasonably well. The biggest discrepancy is that our light quark moments in Ξ^0 and Ξ^- are small. In Σ^0, and Λ the total of u and d quark moments agree very well with lattice data for light quark moments. Note that only a combined number for light quark ($\mu_l = \mu_u + \mu_d$) was given on the lattice [43]. To compare with our separated u and d quark numbers, we break up the lattice number by using the SU2 relation

$\mu_u = -2\mu_d$.

In the simple quark model [50], the magnetic moment of the proton is given by $p = \frac{4}{3}\mu_u - \frac{1}{3}\mu_d$. In the SU(2) limit, there is the relation $\mu_u = -2\mu_d$. Our results for Σ^0 and Λ, the two *uds* structure baryons, agree with this very well. This relation also suggests that the ratio of the u quark and d quark contributions in proton is $\frac{4}{3}\mu_u/(-\frac{3}{4}\mu_d) = 8$. Our QCD sum rule ratio is 10.6 for $\beta = -1.2$, which agrees with the lattice ratio of 10.3(7) at κ_1. For the neutron, the quark model ratio is $\frac{4}{3}\mu_d/(-\frac{1}{3}\mu_u) = 2$, and our result is 3.64(40) for this ratio, which differs from the SU(6) spin-flavor symmetry prediction. The lattice ratio is 2.6. The bigger ratio represents an enhancement of the doubly represented quark contribution. These results suggest that although the total magnetic moments ratios agree with SU(6) ratios (see Table 4.4), the underlying quark dynamics are really quite different for different individual quark contributions.

To include the possible nonstatic effect, Franklin [46] proposed a generalization

of SU(6) results so that nonstatic components are the same for each octet baryon:

$$
\begin{aligned}
p &= \tfrac{4}{3}\mu_u - \tfrac{1}{3}\mu'_d, \\
n &= \tfrac{4}{3}\mu_d - \tfrac{1}{3}\mu'_u, \\
\Sigma^+ &= \tfrac{4}{3}\mu_u - \tfrac{1}{3}\mu'_s, \\
\Sigma^- &= \tfrac{4}{3}\mu_d - \tfrac{1}{3}\mu'_s, \\
\Xi^0 &= \tfrac{4}{3}\mu_s - \tfrac{1}{3}\mu'_u, \\
\Xi^- &= \tfrac{4}{3}\mu_s - \tfrac{1}{3}\mu'_d, \\
\Sigma^0 &= \tfrac{2}{3}\mu_u + \tfrac{2}{3}\mu_d - \tfrac{1}{3}\mu'_s, \\
\Lambda &= \mu''_s
\end{aligned}
\tag{4.51}
$$

where quark symbols refer to quark moment contributions including nonstatic effect. The magnetic moment contribution of the unlike quark in the baryon is primed.

In order to compare with the effective quark moments defined in the quark model, we convert our raw quark moments in Table quark in a similar fashion. Take the proton for example, we define effective quark moments μ_u and μ'_d from QCD sum rules by $u_{SR} = \frac{4}{3}\mu_u$, $d_{SR} = \frac{1}{3}\mu'_d$. One can define effective moments for quarks in other baryons in a similar manner.

In the proton, μ_u is 1.84(18) while in Σ^+ 1.54(18) and in Σ^0 is 1.63(18). In the neutron, μ'_u is 1.25(27), which is smaller than μ_u. This is an example that effective quark magnetic moment is sensitive to the environment the quark resides in. We find the following relation from our results

$$
\mu_u^p < \mu_u^{\Sigma^0} < \mu_u^{\Sigma^+}. \tag{4.52}
$$

For μ_d, in n it is $-1.15(11)$ while for Σ^0 is $-0.82(8)$ and for Σ^- is $-0.93(8)$. From p we can get $\mu'_d = -1.15(12)$. μ_d has a similar relation for the absolute value

$$\mu_d^n < \mu_d^{\Sigma^0} < \mu_d^{\Sigma^-}. \tag{4.53}$$

For μ_s, it is $-0.81(6)$ in Ξ^0 and $-0.50(5)$ in Ξ^-. For μ'_s, it is $-0.45(5)$, $-0.42(5)$ and $-0.30(5)$ in Σ^+, Σ^0 and Σ^-, respectively. From Λ we can get μ''_s about $-0.63(15)$.

For these individual quark effective moments, we notice that in general we have the following relation

$$\mu_s < \mu_d < \mu_u. \tag{4.54}$$

This is expected because of the quark mass effects, which is analogous to those seen in the electric properties.

Another way of looking at the individual effective quark moments is by expressing them in terms of baryon magnetic moments using Eq.(4.51) and isospin symmetry. For example, the d-quark effective moment can be expressed as

$$\mu_d = -\frac{1}{4}(2p + n) = \frac{1}{4}(\Sigma^- - \Sigma^+). \tag{4.55}$$

Our result indicates $\mu_d = -0.92(14) < -0.86(7)$ using the baryon moments in Table 4.5 or in Table 4.1. This agrees well with the experimental moments $\mu_d = -0.918 < -0.894(7)$ and the lattice result of $\mu_d = -1.00(5) < -0.86(6)$.

Similarly the d' quark effective moment is

$$\mu'_d = p + 2n = \Xi^0 - \Xi^-. \tag{4.56}$$

We have $\mu'_d = -1.12(39) < -0.51(8)$. This also agree very well with the experimental moments $\mu'_d = -1.003 < -0.578(26)$ although the two sides of this sum don't agree well.

The strange quark can be isolated as

$$\begin{aligned} \mu_s &= \tfrac{1}{4}(\Xi^0 + 2\Xi^-), \\ \mu'_s &= -\Sigma^+ - 2\Sigma^-, \\ \mu''_s &= \Lambda - \delta. \end{aligned} \tag{4.57}$$

Our results are compared with experiment and lattice calculation in Table 4.6. Not only do the results agree with the experiment and lattice calculation, they also roughly agree with the strange quark moments from individual quark moments.

Table 4.6: The result for s s' and s'' quark effective moments from QCD sum rule, experiment and lattice calculation.

	μ_s		μ''_s		μ'_s
SR	-0.61(3)	$<$	-0.60(15)	$<$	0.01(32)
Exp.	-0.651(12)	$<$	-0.57(4)	$<$	-0.107(36)
LAT.	-0.55(4)	$\approx$	-0.54(4)	$<$	-0.24(17)

Now, we can look at the quark moment difference such as $\mu'_s - \mu'_d$ and $\mu_s - \mu_d$. According to simple quark model, the difference should be the same and approximately as 0.36. In fact, from

$$\mu'_s - \mu'_d = 3(p - \Sigma^+), \tag{4.58}$$

$$\mu_s - \mu_d = \frac{3}{4}(\Xi^0 - n), \tag{4.59}$$

QCD sum rules give 1.53(8) and 0.61(12). The experiment gives 1.12(7) and 0.495(11), while lattice calculation gives 1.3(5) and 0.32(17) respectively. The large result of $\mu'_s - \mu'_d$ is difficult to reconcile with any simple model. And Eq. (4.58) is a poor way to measure the difference of s and d quark contribution.

4.5.6 Correlations

Our Monte-Carlo analysis affords the opportunity to study the correlations between any two parameters since the entire QCD input phase space is mapped into the phenomenological output space. This correlation can be explored by a scatter plot of the two parameters of interest.

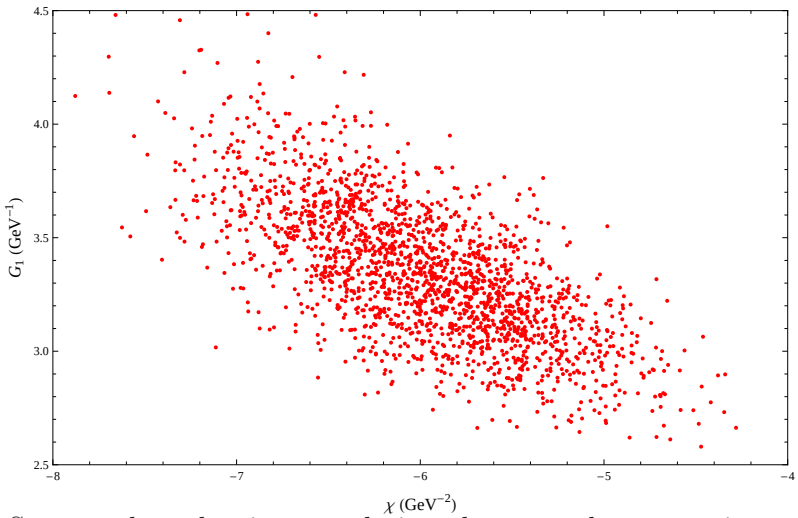

Figure 4.10: Scatter plots showing correlations between the magnetic moment and the QCD parameters for the proton at structure WE_1. They are obtained from 2000 Monte-Carlo samples with 10% uncertainty on all the QCD parameters.

Fig. 4.10 shows the scatter plots for the proton magnetic moment at structure WE_1. We see that the magnetic moment has a strong correlation with the vacuum

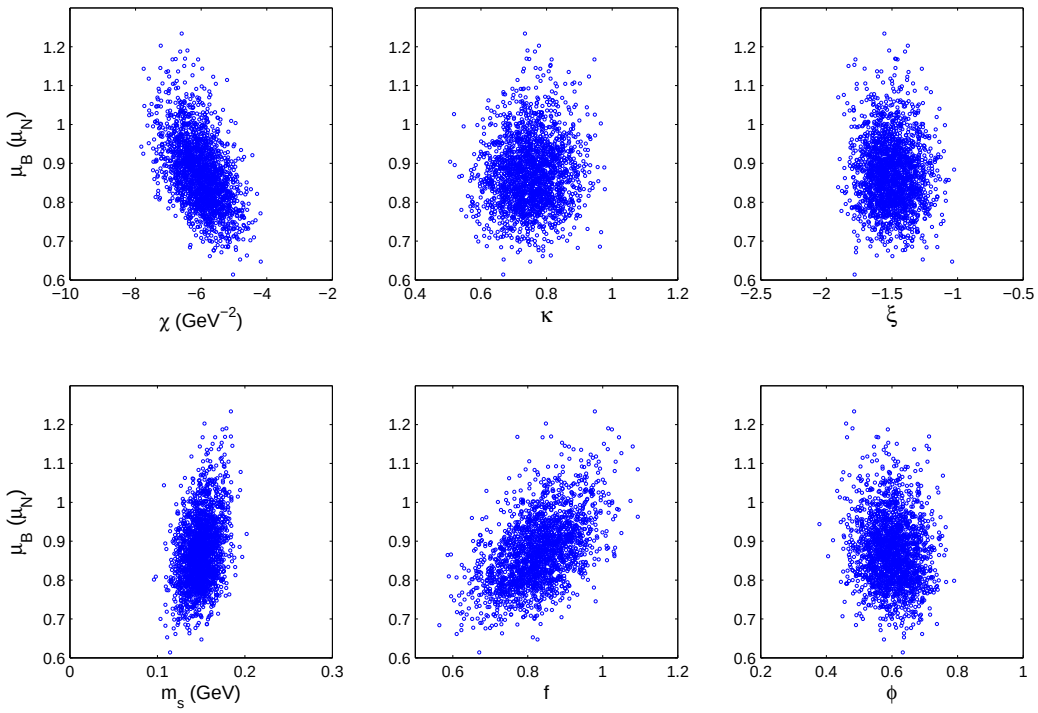

Figure 4.11: Similar to Fig. 4.10, but for the Σ^0 and a different set of QCD parameters.

susceptibility χ. It is a negative correlation, meaning larger χ (in absolute terms since χ is negative) leads to smaller μ_B. A slightly negative correlation with the mixed condensate and a slightly positive correlation with another vacuum susceptibility κ are also observed. Precise determination of the QCD parameters, especially for those that have strong correlations to the output parameters, is crucial for keeping the uncertainties in the spectral parameters under control.

Fig. 4.11 shows a similar plot for the Σ^0 at structure WE_1. Here we focus on the three vacuum susceptibilities and the three parameters that define the strange quark (m_s, f_s and ϕ). The correlations with the other condensates are similar to the proton and are not shown. A negative correlation with χ exists, but not as strong as that for the proton. A slightly positive correlation with m_s and f_s is also observed.

Chapter 5

N to Δ Transitions Amplitudes from QCD Sum Rules

The calculation proceeds in the same way as for the magnetic moment in Chap. 4. The only complication is that the different vertex function is more complicated because the final state is a spin-$\frac{3}{2}$ particle.

The starting point is still the time-ordered correlation function between a nucleon state and a Δ state in the QCD vacuum in the presence of a *static* background electromagnetic field $F_{\mu\nu}$:

$$\Pi_\alpha(p) = i \int d^4x \; e^{ip\cdot x} \langle 0 \,|\, T\{ \; \eta^\Delta_\alpha(x) \, \bar{\eta}^N(0) \; \} \,|\, 0 \rangle_F, \tag{5.1}$$

where η^Δ_α (α Lorentz index) and η^N are interpolating field operators carrying the quantum numbers of the baryons under consideration.

5.1 Phenomenological Representation (RHS)

We insert two complete sets of physical intermediate states to the correlation function Eq.(5.1), it becomes

$$\begin{aligned}\Pi_\alpha(p) &= \int d^4x d^4y \frac{d^4k'}{(2\pi)^4}\frac{d^4k}{(2\pi)^4}\sum_{\Delta N}\sum_{s's}\frac{-i}{k'^2-m_\Delta^2-i\varepsilon}\frac{-i}{k^2-m_N^2-i\varepsilon}e^{ipx} \\ &\times A_\mu(y) < 0|\eta_\alpha^\Delta(x)|\Delta k's' >< \Delta k's'|j^\mu(y)|Nks >< Nks|\bar{\eta}(0)|0 > .\end{aligned} \tag{5.2}$$

Using the translation invariance on $\eta_\alpha^\Delta(x)$ and $j^\mu(y)$, and the overlap strengths (λ_Δ and λ_N) of the interpolating fields with the states: $< 0|\eta_\alpha(0)|\Delta k', s' >= \lambda_\Delta u_\alpha(k', s')$.

The current matrix element for $N\gamma - \Delta$ transition is defined in previous chapter. Here we adopt the Jones and Scadron's definition.

$$< \Delta(k', s')|J^\mu(0)|N(k, s) >= \bar{u}_\rho(k', s')\Gamma_{\rho u}u(k, s) \tag{5.3}$$

The operator $\Gamma_{\rho\mu}$ is

$$\Gamma_{\rho\mu} = G_1(q^2)\mathrm{H}^1_{\rho\mu} + G_2(q^2)\mathrm{H}^2_{\rho\mu} + G_3(q^2)\mathrm{H}^3_{\rho\mu} \tag{5.4}$$

with $H^1_{\rho\mu}, H^2_{\rho\mu}$ defined earlier in Eq. (2.3).

We can write out explicitly the contribution of the lowest lying state and designate ESC for the excited state contributions:

$$\begin{aligned}\Pi_\alpha(p) &= -\lambda_\Delta\lambda_N^* \int d^4x d^4y \frac{d^4k'}{(2\pi)^4}\frac{d^4k}{(2\pi)^4}[k'^2 - m_\Delta^2 - i\varepsilon]^{-1}[k^2 - m_N^2 - i\varepsilon]^{-1} \\ &A_\mu(y)e^{i(p-k')x}e^{iqy}\sum_{s'}u_\alpha(k', s')\bar{u}_\rho(k', s')\Gamma^{\rho\mu}\sum_s u(k, s)\bar{u}(k, s) + ESC.\end{aligned} \tag{5.5}$$

The spin sums for N is the same as before and the Rarita-Schwinger spinsor sum for Δ is:

$$\sum_{s'} \bar{u}_\alpha(k',s')u_\rho(k',s') = -(\hat{k}' + m_\Delta)\{g_{\alpha\rho} - \frac{1}{3}\gamma_\alpha\gamma_\rho - \frac{2k'_\alpha k'_\rho}{3m_\Delta^2} + \frac{k'_\alpha\gamma_\rho - k'_\rho\gamma_\alpha}{3m_\Delta}\}. \quad (5.6)$$

We work in the fixed-point gauge in which $A_\mu(y) = -\frac{1}{2}F_{\mu\nu}y^\nu$. After changing variables from k to $q = k' - k$, which leads to $d^4k = -d^4q$, we have

$$\Pi_\alpha(p) = -\lambda_N^*\lambda_\Delta F_{\mu\nu}\int d^4x d^4y \frac{d^4k'}{(2\pi)^4}\frac{d^4q}{(2\pi)^4}[k'^2 - m_\Delta^2][(q-k')^2 - m_N^2]^{-1} \times e^{i(p-k')x}$$
$$(-\frac{i}{2}\frac{\partial}{\partial q_\nu}e^{iqy})(\hat{k}' + m_\Delta)\{g_{\alpha\rho} - \frac{1}{3}\gamma_\alpha\gamma_\rho - \frac{2k'_\alpha k'_\rho}{3m_\Delta^2} + \frac{k'_\alpha\gamma_\rho - k'_\rho\gamma_\alpha}{3m_\Delta}\} \times \Gamma^{\rho\mu} \times (\hat{k}' - \hat{q} + m_N). \quad (5.7)$$

Integrating by parts and using properties of δ functions, the expression collapses to

$$\begin{aligned}\Pi_\alpha(p) &= \frac{i\lambda_N^*\lambda_\Delta}{2}F_{\mu\nu}[p^2 - m_\Delta^2]^{-1}[p^2 - m_N^2]^{-1}(\hat{p} + m_\Delta) \\ &\quad \times\{g_{\alpha\rho} - \tfrac{1}{3}\gamma_\alpha\gamma_\rho - \tfrac{2p_\alpha p_\rho}{3m_\Delta^2} - \tfrac{p_\alpha\gamma_\rho - p_\rho\gamma_\alpha}{3m_\Delta}\} \\ &\quad \times[G_1(g_{\rho\nu}\gamma_\mu - \gamma_\nu g_{\rho\mu})\gamma_5 + G_2(g_{\rho\nu}p_\mu - p_\nu g_{\rho\mu})\gamma_5](\hat{p} + m_N),\end{aligned} \quad (5.8)$$

where we have chosen to work with the transition amplitudes G_1 and G_2 as defined in Eq. (2.2) and Eq. (2.3), rather than G_{M1} and G_{E2}. They are readily converted back and forth by Eq. (2.7) and Eq. (2.8).

A straightforward evaluation of this expression leads to numerous Dirac structures, but not all of them are independent of each other. The dependencies can be removed by ordering the gamma matrices in a specific order. After a lengthy calculation we identified 12 independent Dirac structures. They can be organized (aside

from an overall factor of i that also appears on the QCD side) as:

$$\Pi_\alpha(p) = \frac{\lambda_N^* \lambda_\Delta}{2}[p^2 - m_\Delta^2]^{-1}[p^2 - m_N^2]^{-1}$$
$$[\mathrm{WE}_1(\frac{2}{3}G_1 m_\Delta + \frac{2}{3}G_1 m_N)$$
$$+\mathrm{WE}_2(\frac{2}{3}p^2 G_1 m_\Delta^{-1} - 4/3\mathrm{G}_1 m_\Delta - \frac{2}{3}G_1 m_N)$$
$$+\mathrm{WE}_3(\frac{2}{3}G_1 m_\Delta + \frac{2}{3}G_1 m_N)$$
$$+\mathrm{WE}_4(-\frac{2}{3}p^2 G_1 m_\Delta^{-1} + \frac{2}{3}p^2 G_2 + \frac{8}{3}G_1 m_\Delta + \frac{2}{3}G_1 m_N - \frac{2}{3}G_2 m_\Delta m_N)$$
$$+\mathrm{WE}_5(-\frac{4}{3}G_1 m_\Delta^{-2} m_N - \frac{2}{3}G_2 m_\Delta^{-1} m_N + \frac{2}{3}G_2)$$
$$+\mathrm{WE}_6(2\mathrm{p}^2 G_2 - 2\mathrm{G}_2 m_\Delta m_N)$$
$$+\mathrm{WO}_1(-\frac{2}{3}p^2 G_1 - \frac{2}{3}G_1 m_\Delta m_N)$$
$$+\mathrm{WO}_2(\frac{2}{3}G_1 m_\Delta^{-1} m_N + \frac{2}{3}G_1)$$
$$+\mathrm{WO}_3(-\frac{2}{3}p^2 G_1 - \frac{2}{3}G_1 m_\Delta m_N)$$
$$+\mathrm{WO}_4(\frac{4}{3}p^2 G_1 m_\Delta^{-2} + \frac{2}{3}p^2 G_2 m_\Delta^{-1} + \frac{4}{3}G_1 m_\Delta^{-1} m_N - \frac{4}{3}G_1 - \frac{4}{3}G_2 m_\Delta + \frac{2}{3}G_2 m_N)$$
$$+\mathrm{WO}_5(-\frac{2}{3}G_1 m_\Delta^{-1} m_N - 2\mathrm{G}_1 - \frac{2}{3}G_2 m_\Delta + \frac{2}{3}G_2 m_N)$$
$$+\mathrm{WO}_6(\frac{4}{3}G_1 m_\Delta^{-1} m_N - \frac{2}{3}G_2 m_\Delta + \frac{2}{3}G_2 m_N)]. \tag{5.9}$$

The Dirac structures associated with WE_i and WO_i are listed as follows:

$$\begin{aligned}
WE_1 &= F_{\mu\nu}\gamma_5\hat{p}\gamma_\mu\gamma_\nu\gamma_\alpha & WO_1 &= F_{\mu\nu}\gamma_5\gamma_\mu\gamma_\nu\gamma_\alpha \\
WE_2 &= F_{\mu\nu}\gamma_5\gamma_\mu\gamma_\nu p_\alpha & WO_2 &= F_{\mu\nu}\gamma_5\hat{p}\gamma_\mu\gamma_\nu p_\alpha \\
WE_3 &= F_{\mu\nu}\gamma_5\hat{p}(\gamma_\nu g_{\alpha\mu} - \gamma_\mu g_{\alpha\nu}) & WO_3 &= F_{\mu\nu}\gamma_5(\gamma_\nu g_{\alpha\mu} - \gamma_\mu g_{\alpha\nu}) \\
WE_4 &= F_{\mu\nu}\gamma_5(\gamma_\mu\gamma_\alpha p_\nu - \gamma_\nu\gamma_\alpha p_\mu) & WO_4 &= F_{\mu\nu}\gamma_5(\gamma_\mu p_\nu - \gamma_\nu p_\mu)p_\alpha \\
WE_5 &= F_{\mu\nu}\gamma_5\hat{p}(\gamma_\mu p_\nu p_\alpha - \gamma_\nu p_\mu p_\alpha) & WO_5 &= F_{\mu\nu}\gamma_5\hat{p}(\gamma_\mu\gamma_\alpha p_\nu - \gamma_\nu\gamma_\alpha p_\mu) \\
WE_6 &= F_{\mu\nu}\gamma_5(g_{\alpha\mu}p_\nu - g_{\alpha\nu}p_\mu) & WO_6 &= F_{\mu\nu}\gamma_5\hat{p}(g_{\alpha\mu}p_\nu - g_{\alpha\nu}p_\mu)
\end{aligned} \tag{5.10}$$

Same as magnetic moment sum rules, the naming convention of WE_i and WO_i refers to even-odd dimension vacuum condensates. Coincidentally, the WE_i structures themselves contain odd number of gamma matrices, while WO_i even number.

The next step is to perform the standard Borel transform, which turns a function of p^2 to a function of M^2 (M is the Borel mass). Unlike the N to N transition in the calculation of magnetic moments [9], the double-pole structure in the N to Δ transition in Eq. (5.9) has unequal masses m_Δ and m_N. The existence of an equal-mass double pole in the ground state was crucial in isolating the magnetic moments from the excited states because it gives a different functional dependence on the Borel mass ($e^{-m^2/M^2}/M^2$) than the single poles (e^{-m^2/M^2}). Here for N to Δ transitions, we shall approximate the unequal-mass double pole by an equal-mass double pole,

$$\frac{1}{p^2 - m_N}\frac{1}{p^2 - m_\Delta} \approx (\frac{1}{p^2 - \bar{m}^2})^2, \tag{5.11}$$

where $\bar{m}^2 = (m_N^2 + m_\Delta^2)/2$ can be considered as an averaged square mass. For the

physical masses involved in the N to Δ transitions, this approximation is good to within 3% in the Borel region of interest we are going to explore. Because of this approximation, the determination of the N to Δ transition amplitudes will not be as accurate as the magnetic moments in the QCD sum rule approach. With the introduction of the pure double pole, the Borel transform of the ground state in Eq. (5.9) is given by

$$
\begin{aligned}
&\Pi_\alpha(p) = \frac{\lambda_N^* \lambda_\Delta}{2M^2} e^{-\bar{m}^2/M^2} \\
&[\mathrm{WE_1}\frac{2}{3}\mathrm{G_1(m_\Delta + m_N)} \\
&+WE_2\frac{2}{3}G_1\frac{1}{m_\Delta}(-M^2+\bar{m}^2-2m_\Delta^2-m_N m_\Delta) \\
&+WE_3\frac{2}{3}G_1(m_\Delta+m_N) \\
&-WE_4(\frac{2}{3}G_1\frac{1}{m_\Delta}(-M^2+\bar{m}^2-4m_\Delta^2-m_N m_\Delta)+\frac{2}{3}G_2(-M^2+\bar{m}^2-m_\Delta m_N)) \\
&-WE_5(\frac{4}{3}G_1\frac{1}{m_\Delta^2}m_N+\frac{2}{3}G_2\frac{1}{m_\Delta}(-m_N+m_\Delta)) \\
&+WE_6 2G_2(-M^2+\bar{m}^2-m_\Delta m_N) \\
&-WO_1\frac{2}{3}G_1(-M^2+\bar{m}^2+m_\Delta m_N) \\
&+WO_2\frac{2}{3}G_1\frac{1}{m_\Delta}(m_N+m_\Delta) \\
&-WO_3\frac{2}{3}G_1(-M^2+\bar{m}^2+m_\Delta m_N) \\
&+WO_4(\frac{4}{3}G_1\frac{1}{m_\Delta^2}(-M^2+\bar{m}^2+m_N m_\Delta-m_\Delta^2) \\
&+\frac{2}{3}G_2\frac{1}{m_\Delta}(-M^2+\bar{m}^2-2m_\Delta^2+m_N m_\Delta)) \\
&-WO_5(\frac{2}{3}G_1\frac{1}{m_\Delta}(m_N+m_\Delta)-\frac{2}{3}G_2(m_\Delta-m_N)) \\
&+WO_6(\frac{4}{3}G_1\frac{1}{m_\Delta}m_N-\frac{2}{3}G_2(m_\Delta-m_N))], \qquad (5.12)
\end{aligned}
$$

where M is the Borel mass parameter, not to be confused with the particle masses m_N, m_Δ, or $\bar{m}$.

The excited states must be treated with care. The pole structure can be written in the generic form

$$\frac{C_1}{(p^2-m_N^2)(p^2-m_\Delta^2)} + \sum_{N^*} \frac{C_2}{(p^2-m_{N^*}^2)(p^2-m_\Delta^2)} + \sum_{\Delta^*} \frac{C_3}{(p^2-m_N^2)(p^2-m_{\Delta^*}^2)} + \sum_{N^*,\Delta^*} \frac{C_4}{(p^2-m_{N^*}^2)(p^2-m_{\Delta^*}^2)}, \tag{5.13}$$

where C_i are constants. The first term is the ground state pole which contains the desired amplitudes G_1 and G_2. The second and third terms represent the non-diagonal transitions between the ground state and the excited states caused by the external field. The forth term is pure excited-state to excited-state transitions. These different contributions can be represented by the diagrams in Fig. 5.1. Upon Borel transform,

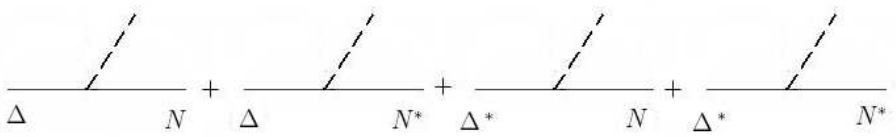

Figure 5.1: The four contributions to the spectral function in the presence of an external field: transition between ground state N to ground state Δ, transitions between ground state N and excited states Δ^*, transition between excited state N^* and ground state Δ and pure excited states $N^* \to \Delta^*$.

the ground state takes the form

$$\frac{C_1}{M^2} e^{-\bar{m}^2/M^2} + \sum_{N^*,\Delta^*} \frac{C_4}{M^2} e^{-\bar{m}^{*2}/M^2}$$
$$+ e^{-\bar{m}^2/M^2} \left[e^{(\bar{m}^2-m_\Delta^2)/M^2} \sum_{N^*} \frac{C_2(1-e^{-(m_\Delta^2-m_{N^*}^2)/M^2})}{m_\Delta^2-m_{N^*}^2} + e^{(\bar{m}^2-m_N^2)/M^2} \sum_{\Delta^*} \frac{C_3(1-e^{-(m_{\Delta^*}^2-m_N^2)/M^2})}{m_{\Delta^*}^2-m_N^2}. \right] \tag{5.14}$$

The important point is that the non-diagonal transitions (N^* to Δ and N to Δ^*)

give rise to a contribution that is not exponentially suppressed relative to the ground state. This is a general feature of the external-field technique. The strength of such transitions at each structure is *a priori* unknown and is a potential source of contamination in the determination of the amplitudes. The standard treatment of the off-diagonal transitions is to approximate the quantities in the square brackets by a parameter A, which is to be extracted from the sum rule along with the ground state property of interest. Inclusion of such contributions is necessary for the correct extraction of the amplitudes. The pure excited state transitions (N^* to Δ^*) are exponentially suppressed relative to the ground state and can be modeled in the usual way by introducing a continuum model and threshold parameter w.

5.2 QCD Side

5.2.1 Interpolating Fields

We need interpolating fields for the baryons in N to Δ transitions in Eq. (2.14). We consider a linear combination of the two standard local interpolating fields for the baryon octet are listed in Eq.(4.4).

For the spin-3/2 baryon decuplet, we use

$$\begin{aligned}
\eta_\alpha^{\Delta^+}(uud) &= \frac{1}{\sqrt{3}}\epsilon^{abc}[2(u^{aT}C\gamma_\alpha d^b)u^c + (u^{aT}C\gamma_\alpha u^b)d^c], \\
\eta_\alpha^{\Delta^0}(ddu) &= \frac{1}{\sqrt{3}}\epsilon^{abc}[2(d^{aT}C\gamma_\alpha u^b)d^c + (d^{aT}C\gamma_\alpha d^b)u^c], \\
\eta_\alpha^{\Sigma^{*+}}(uus) &= \frac{1}{\sqrt{3}}\epsilon^{abc}[2(u^{aT}C\gamma_\alpha s^b)u^c + (u^{aT}C\gamma_\alpha u^b)s^c],
\end{aligned}$$

$$
\begin{aligned}
\eta_\alpha^{\Sigma^{*0}}(uds) &= \frac{2}{\sqrt{3}}\epsilon^{abc}[(u^{aT}C\gamma_\alpha d^b)s^c + (d^{aT}C\gamma_\alpha s^b)u^c + (s^{aT}C\gamma_\alpha u^b)d^c], \\
\eta_\alpha^{\Sigma^{*-}}(dds) &= \frac{1}{\sqrt{3}}\epsilon^{abc}[2(d^{aT}C\gamma_\alpha s^b)d^c + (d^{aT}C\gamma_\alpha d^b)s^c], \\
\eta_\alpha^{\Xi^{*0}}(ssu) &= \frac{1}{\sqrt{3}}\epsilon^{abc}[2(s^{aT}C\gamma_\alpha u^b)s^c + (s^{aT}C\gamma_\alpha s^b)u^c], \\
\eta_\alpha^{\Xi^{*-}}(ssd) &= \frac{1}{\sqrt{3}}\epsilon^{abc}[2(s^{aT}C\gamma_\alpha d^b)s^c + (s^{aT}C\gamma_\alpha s^b)d^c]. \qquad (5.15)
\end{aligned}
$$

Then, we start by writing down the master formulas used in the calculation of the QCD side, which are functions of the quark propagators, obtained by contracting out pairs of time-ordered quark-field operators in the two-point correlation function in Eq. (5.1) using the interpolating fields in Eq. (4.4) and Eq. (5.15). We note that the same master formulas enter lattice QCD calculations where the fully-interacting quark propagators are generated numerically, instead of the analytical ones used here. The master formula for the transition $\gamma p \to \Delta^+$ (with uud quark content) is:

$$
\begin{aligned}
&< 0|T\{\eta_\alpha^{\Delta^+}(x)\bar{\eta}^p(0)\}|0 >= -\tfrac{4}{\sqrt{3}}\varepsilon^{abc}\varepsilon^{a'b'c'}\{ \\
&S_u^{aa'}\gamma_5 C S_d^{bb'^T} C\gamma_\alpha S_u^{cc'} + S_u^{aa'}Tr(\gamma_5 C S_u^{Tbb'} C\gamma_\alpha S_d^{cc'}) \\
&-S_d^{aa'}\gamma_5 C S_u^{Tbb'} C\gamma_\alpha S_u^{cc'} + \beta[S_u^{aa'} C S_d^{Tbb'} C\gamma_\alpha S_u^{cc'}\gamma_5 \\
&+S_u^{aa'}\gamma_5 Tr(C S_u^{Tbb'} C\gamma_\alpha S_d^{cc'}) - S_d^{aa'} C S_u^{Tbb'} C\gamma_\alpha S_u^{cc'}]\}.
\end{aligned} \qquad (5.16)
$$

It is not necessary to list all the master formulas for the other transitions separately. Only three are distinct; others can be obtained by making appropriate substitutions in the above expression as specified below:

- for $n\gamma \to \Delta^0$ (ddu quark content), interchange d quark and u quark in $p\gamma \to \Delta^+$,
- for $\Sigma^+\gamma \to \Sigma^{*+}$ (uus quark content), replace d quark by s quark in $p\gamma \to \Delta^+$,

- for $\Sigma^-\gamma \to \Sigma^{*-}$ (dds quark content), replace u quark by d quark in $\Sigma^+\gamma \to \Sigma^{*+}$,
- for $\Xi^0\gamma \to \Xi^{*0}$ (ssu quark content), interchange u quark and s quark in $\Sigma^+\gamma \to \Sigma^{*+}$,
- for $\Xi^-\gamma \to \Xi^{*-}$ (ssd quark content), replace u quark by d quark in $\Xi^0\gamma \to \Xi^{*0}$.

Here the interchange of two quarks is achieved by simply switching the corresponding propagators.

The master formula for $\Sigma^0\gamma \to \Sigma^{*0}$ (uds quark content) is:

$$
\begin{aligned}
&< 0|T\{\eta_\alpha^{\Sigma^{*0}}(x)\bar{\eta}^{\Sigma^0}(0)\}|0 >= \frac{2}{\sqrt{3}}\varepsilon^{abc}\varepsilon^{a'b'c'}\{ \\
&S_s^{aa'}\gamma_5 C S_u^{Tbb'} C\gamma_\alpha S_d^{cc'} - S_u^{aa}\gamma_5 C S_s^{Tbb'} C\gamma_\alpha S_d^{cc'} \\
&-S_d^{aa'} Tr(\gamma_5 C S_s^{Tbb'} C\gamma_\alpha S_u^{cc'}) + S_s^{aa'}\gamma_5 C S_d^{Tbb'} C\gamma_\alpha S_u^{cc'} \\
&-S_d^{aa}\gamma_5 C S_s^{Tbb'} C\gamma_\alpha S_u^{cc'} - S_u^{aa'} Tr(\gamma_5 C S_s^{Tbb'} C\gamma_\alpha S_d^{cc'}) \\
&+\beta[S_s^{aa'} C S_u^{Tbb'} C\gamma_\alpha S_d^{cc'}\gamma_5 - S_u^{aa'} C S_s^{Tbb'} C\gamma_\alpha S_d^{cc'}\gamma_5 \\
&-S_d^{aa'}\gamma_5 Tr(C S_s^{Tbb'} C\gamma_\alpha S_u^{cc'}) + S_s^{aa'} C S_d^{Tbb'} C\gamma_\alpha S_u^{cc'}\gamma_5 \\
&-S_d^{aa'} C S_s^{Tbb'} C\gamma_\alpha S_u^{cc'}\gamma_5 - S_u^{aa'}\gamma_5 Tr(C S_s^{Tbb'} C\gamma_\alpha S_d^{cc'})]. \qquad (5.17)
\end{aligned}
$$

The master formula for $\Lambda\gamma \to \Sigma^{*0}$ (uds quark content) is:

$$
\begin{aligned}
&< 0|T\{\eta_\alpha^{\Sigma^{*0}}(x)\bar{\eta}^{\Lambda}\}|0 >= \frac{2}{3}\varepsilon^{abc}\varepsilon^{a'b'c'}\{ \\
&2S_d^{aa'}\gamma_5 C S_u^{Tbb'} C\gamma_\alpha S_s^{cc'} - 2S_u^{aa}\gamma_5 C S_d^{Tbb'} C\gamma_\alpha S_s^{cc'} \\
&-2S_s^{aa'} Tr(\gamma_5 C S_u^{Tbb'} C\gamma_\alpha S_d^{cc'}) + S_s^{aa'}\gamma_5 C S_u^{Tbb'} C\gamma_\alpha S_d^{cc'}
\end{aligned}
$$

$$
\begin{aligned}
&-S_u^{aa}\gamma_5 C S_s^{Tbb'} C\gamma_\alpha S_d^{cc'} - S_d^{aa'} Tr(\gamma_5 C S_s^{Tbb'} C\gamma_\alpha S_u^{cc'}) \\
&-S_s^{aa'}\gamma_5 C S_d^{Tbb'} C\gamma_\alpha S_u^{cc'} + S_d^{aa}\gamma_5 C S_s^{Tbb'} C\gamma_\alpha S_u^{cc'} \\
&+S_u^{aa'} Tr(\gamma_5 C S_s^{Tbb'} C\gamma_\alpha S_d^{cc'}) + \beta[-2S_d^{aa'} C S_u^{Tbb'} C\gamma_\alpha S_s^{cc'}\gamma_5 \\
&+2S_u^{aa} C S_d^{Tbb'} C\gamma_\alpha S_s^{cc'}\gamma_5 - 2S_s^{aa'} Tr(C S_u^{Tbb'} C\gamma_\alpha S_d^{cc'})\gamma_5 \\
&+S_s^{aa'} C S_u^{Tbb'} C\gamma_\alpha S_d^{cc'}\gamma_5 - S_u^{aa} C S_s^{Tbb'} C\gamma_\alpha S_d^{cc'}\gamma_5 \\
&-S_d^{aa'} Tr(C S_s^{Tbb'} C\gamma_\alpha S_u^{cc'})\gamma_5 - S_s^{aa'} C S_d^{Tbb'} C\gamma_\alpha S_u^{cc'}\gamma_5 \\
&+S_d^{aa} C S_s^{Tbb'} C\gamma_\alpha S_u^{cc'}\gamma_5 + S_u^{aa'} Tr(C S_s^{Tbb'} C\gamma_\alpha S_d^{cc'})\gamma_5]\}. \qquad (5.18)
\end{aligned}
$$

The QCD side has the same Dirac structure as the phenomenological side and the results can be collected according to the same 12 independent Dirac structures in Eq. (5.10).

5.3 Sum Rules

Once we have both the QCD side (commonly referred as LHS) and the phenomenological side (RHS), we can isolate the sum rules by matching the two sides. Since there are 12 independent Dirac structures, 12 sum rules can be constructed for each transition. For the 8 transitions, the total number of sum rules is 96. We divide the sum rules into four groups according to their dependence on the amplitudes and performance. The first group consists of the sum rules at structures WE_1, WO_2 and WE_3 which only contain the amplitude G_1, and at WE_6 which only contains G_2. These sum rules are expected to perform better than other sum rules for other structures because they involve fewer parameters. The second group consists of the sum rules

at structures WE_5, WO_5 and WO_6 which have both G_1 and G_2. It is difficult to extract both amplitudes at the same time. One way out is to fix one of them and treat the other as free parameter. This reduces the predictive ability of the QCD sum rules. Our numerical analysis suggests that it can serve as a consistence check at best. Another way is to take appropriate combinations of sum rules to eliminate one of the amplitudes. We tried but found the sum rules obtained this way perform worse than the un-manipulated ones. We advocate against the practice of manipulating the original sum rules like algebraic equations (such as taking derivatives or linear combinations) to obtain new sum rules. The third group consists of the sum rules at structures WE_2, WO_1 and WO_3 which have one of the amplitudes and additional dependence on the averaged square mass $\bar{m}^2$, aside from the common factor $e^{-\bar{m}^2/M^2}$. We found these sum rules perform consistently worse than those in groups 1 and 2, possibly because of the approximation introduced by $\bar{m}^2$. The fourth group consists of the sum rules at WE_4 and WO_4 which contain both G_1 and G_2, *and* additional $\bar{m}^2$ dependence. They perform consistently the worst. In the following, we are going to give detailed analysis of the sum rules in group 1, but first let us present the sum rules in this group.

At the structure WE_1, the sum rules can be expressed in the following form:

$$\begin{aligned}
&c_1 L^{-4/27} E_2(w) M^4 + c_2 \chi a m_s L^{-20/27} E_1(w) M^2 + c_3 a m_s L^{-4/27} E_0(w) + c_4 \chi a^2 L^{4/27} E_0(w) \\
&+ c_5 b L^{-4/27} E_0(w) + c_6 m_0^2 a m_s L^{-18/27} \tfrac{1}{M^2} + c_7 a^2 L^{20/27} \tfrac{1}{M^2} + c_8 \chi m_0^2 a^2 L^{-10/27} \tfrac{1}{M^2} \\
&= \tilde{\lambda}_N \tilde{\lambda}_\Delta e^{-\bar{m}^2/M^2} [\tfrac{1}{3M^2} G_1 (m_\Delta + m_N) + A].
\end{aligned} \tag{5.19}$$

Here $\tilde{\lambda}_N$ and $\tilde{\lambda}_\Delta$ are the re-scaled current coupling $\tilde{\lambda}^2 \equiv (2\pi)^4\lambda^2$.

The c_i coefficients differ from transition to transition. It is not necessary to list the coefficients separately for all 8 transition channels. We only need to carry out three separate calculations for $\Sigma^+\gamma \to \Sigma^{*+}$, $\Xi^0\gamma \to \Xi^{*0}$ and $\Lambda\gamma \to \Sigma^{*0}$. Other channels can be obtained from them by making appropriate substitutions as specified below:

- for $p\gamma \to \Delta^+$, replace s quark by d quark in $\Sigma^+\gamma \to \Sigma^{*+}$,
- for $n\gamma \to \Delta^0$, interchange d quark and u quark in proton $p\gamma \to \Delta^+$,
- for $\Sigma^-\gamma \to \Sigma^{*-}$, replace u quark by d quark in $\Sigma^+\gamma \to \Sigma^{*+}$,
- for $\Sigma^0\gamma \to \Sigma^{*0}$, add corresponding coefficients of $\Sigma^+\gamma \to \Sigma^{*+}$ and $\Sigma^-\gamma \to \Sigma^{*-}$, then divide by 2,
- for $\Xi^-\gamma \to \Xi^{*0}$, replace u quark by d quark in $\Xi^0\gamma \to \Xi^{*0}$.

All sum rules for 12 structures and 8 channel are listed in Appendix A.

The coefficients appearing in Eq.(5.19) are given by, in the transition channel $\Sigma^+\gamma \to \Sigma^{*+}$,

$$
\begin{aligned}
c_1 &= \frac{1}{4}(-1+\beta)(e_s - e_u), \\
c_2 &= -\frac{1}{4}(1+2\beta)(e_u - e_s f_s \phi), \\
c_3 &= \frac{1}{12}(e_u(-1+\beta+3f_s+3\beta f_s+\kappa-\beta\kappa-(2+\beta)\xi) \\
&\quad +e_s(-6+f_s(4-\kappa\phi+2\phi\xi)+\beta(-6+f_s(2+\phi(\kappa+\xi))))), \\
c_4 &= \frac{1}{6}(-e_u(1+\beta+f_s)+(2+\beta)e_s f_s \phi),
\end{aligned}
$$

$$
\begin{aligned}
c_5 &= -\frac{1}{48}(-1+\beta)(e_s-e_u),\\
c_6 &= \frac{1}{24}(1+2\beta)(2e_s-e_u(1+f_s)),\\
c_7 &= \frac{1}{36}(-e_u(2-5\kappa+\xi+\beta(2+\kappa+\xi)+f_s(-4+4\kappa+\xi))\\
&\quad +e_s(-6+f_s(4+2\beta-\kappa\phi+\beta\kappa\phi+(2+\beta)\phi\xi))),\\
c_8 &= \frac{1}{144}(e_u(8+2\beta+8f_s+5\beta f_s)-(16+7\beta)e_s f_s\phi);
\end{aligned}
\tag{5.20}
$$

in the transition channel $\Xi^0\gamma \to \Xi^{*0}$,

$$
\begin{aligned}
c_1 &= -\frac{1}{8}(-1+\beta)(e_s-e_u),\\
c_2 &= \frac{1}{8}(1+3\beta)(e_u-e_s f_s\phi),\\
c_3 &= \frac{1}{12}(e_s f_s - e_s f_s\phi(\kappa+\xi)+e_u(2-3f_s+\kappa+\xi)\\
&\quad +\beta(e_u(8-3f_s+\kappa+\xi)-e_s(6+f_s(-1+\phi(\kappa+\xi))))),\\
c_4 &= \frac{1}{6}(1+\beta)f_s(e_u-e_s f_s\phi),\\
c_5 &= \frac{1}{192}(-1+\beta)(e_s-e_u),\\
c_6 &= \frac{1}{48}(e_s(2-\beta(-4+f_s)-5f_s)+e_u(1+2f_s+\beta(-7+4f_s))),\\
c_7 &= \frac{1}{36}(e_u(-3(1+\beta)f_s^2+3(1+\beta)\kappa+f_s(2-2\kappa+\xi+\beta(8-2\kappa+\xi)))+e_s(-3\\
&\quad +f_s(6-3\kappa\phi+f_s(-2+2\kappa\phi-\phi\xi))+\beta(-3-3f_s\kappa\phi+f_s^2(-2+2\kappa\phi-\phi\xi)))),\\
c_8 &= -\frac{1}{144}(1+\beta)(e_u(-1+8f_s)-e_s f_s(2+5f_s)\phi);
\end{aligned}
\tag{5.21}
$$

and in the transition channel $\Lambda\gamma \to \Sigma^{*0}$,

$$
c_1 = \frac{1}{8}(-(2+\beta)e_d+e_s+(2+\beta)e_u),
$$

$$
\begin{aligned}
c_2 &= \frac{1}{8}((3-2\beta)e_d + 2(-1+\beta)e_u),\\
c_3 &= \frac{1}{24}(e_d(-2-12f_s-\kappa+\beta(1+3f_s-\kappa-\xi)+5\xi)+e_u(-2+6f_s+5\kappa\\
&\quad -4\xi+\beta(-1-3f_s+\kappa+\xi))+e_s(-6+f_s(-2+2\kappa\phi-\phi\xi))),\\
c_4 &= \frac{1}{12}(-e_u(2-3\beta+2(1+\beta)f_s)+e_d(3+2f_s+\beta(-3+2f_s))-e_sf_s\phi),\\
c_5 &= \frac{1}{192}((5+2\beta)e_d+3e_s-(3+2\beta)e_u),\\
c_6 &= \frac{1}{96}(-2e_s-(-9+4\beta)e_d(1+f_s)+(-5+4\beta)e_u(1+f_s)),\\
c_7 &= \frac{1}{72}(e_sf_s(-2+2\kappa\phi-\phi\xi)+e_d(2f_s(-7-2\kappa+\xi)\\
&\quad +3(2+\kappa+\xi)+\beta(-3+2f_s)(2+\kappa+\xi))-e_u(2(2+\kappa+\xi)\\
&\quad +\beta(-3+2f_s)(2+\kappa+\xi)+f_s(-8-7\kappa+2\xi))),\\
c_8 &= \frac{1}{288}(-e_d(23+17f_s+\beta(-20+13f_s))+e_u(15(1+f_s)+\beta(-20+13f_s))).
\end{aligned}
\tag{5.22}
$$

At structure WE_6, the sum rule is:

$$
\begin{aligned}
&c_1\chi am_sL^{-20/27}E_1(w)M^2+c_2am_sL^{-4/27}E_0(w)+c_3\chi a^2L^{4/27}E_0(w)\\
&+c_4a^2L^{20/27}\tfrac{1}{M^2}+c_5\chi m_0^2a^2L^{-10/27}\tfrac{1}{M^2}\\
&=\tilde{\lambda}_N\tilde{\lambda}_\Delta e^{-\bar{m}^2/M^2}[\tfrac{1}{M^2}G_2(m_N^2-m_\Delta m_N)+A].
\end{aligned}
\tag{5.23}
$$

The coefficients appearing in Eq.(5.23) are given by, in the transition channel $\Sigma^+\gamma \rightarrow \Sigma^{*+}$,

$$
c_1 = \beta(-e_u+e_sf_s\phi),
$$

$$
\begin{aligned}
c_2 &= \frac{1}{3}\beta(e_u(-4-2\kappa+\xi)+e_s f_s(4+2\kappa\phi-\phi\xi)),\\
c_3 &= -\frac{2}{3}\beta(e_u-e_s f_s\phi),\\
c_4 &= \frac{1}{18}(-3e_u(-1+f_s)\xi+2\beta(e_u(-4-2\kappa+\xi)+e_s f_s(4+2\kappa\phi-\phi\xi))),\\
c_5 &= \frac{1}{6}\beta(e_u-e_s f_s\phi);
\end{aligned}
\tag{5.24}
$$

in the transition channel $\Xi^0\gamma \to \Xi^{*0}$,

$$
\begin{aligned}
c_1 &= \beta(e_u-e_s f_s\phi),\\
c_2 &= \frac{1}{3}\beta(e_u(4+2\kappa-\xi)+e_s f_s(-4-2\kappa\phi+\phi\xi)),\\
c_3 &= \frac{2}{3}\beta f_s(e_u-e_s f_s\phi),\\
c_4 &= \frac{1}{18}f_s(3e_s(-1+f_s)\phi\xi+2\beta(e_u(4+2\kappa-\xi)+e_s f_s(-4-2\kappa\phi+\phi\xi))),\\
c_5 &= \frac{1}{6}\beta f_s(-e_u+e_s f_s\phi);
\end{aligned}
\tag{5.25}
$$

and in the transition channel $\Lambda\gamma \to \Sigma^{*0}$,

$$
\begin{aligned}
c_1 &= \frac{1}{2}\beta(e_d-e_u),\\
c_2 &= \frac{1}{6}\beta(e_d-e_u)(4+2\kappa-\xi),\\
c_3 &= \frac{1}{3}\beta(e_d-e_u),\\
c_4 &= \frac{1}{36}(e_d-e_u)(\beta(8+4\kappa-2\xi)-3(-1+f_s)\xi),\\
c_5 &= \frac{1}{12}\beta(-e_d+e_u).
\end{aligned}
\tag{5.26}
$$

At structure WO_2, the sum rule is:

$$c_1 m_s L^{-16/27} E_1(w) M^2 + c_2 \chi a L^{-8/27} E_1(w) M^2 + c_3 a L^{8/27} E_0(w) + c_4 m_0^2 a L^{-6/27} \frac{1}{M^2}$$
$$+ c_5 \chi a^2 m_s L^{-8/27} \frac{1}{M^2} + c_6 \chi a b L^{-8/27} \frac{1}{M^2} + c_7 a^2 m_s L^{8/27} \frac{1}{M^4} + c_8 a b L^{8/27} \frac{1}{M^4}$$
$$= \tilde{\lambda}_N \tilde{\lambda}_\Delta e^{-\bar{m}^2/M^2} [\frac{1}{3M^2} G_1 \frac{1}{m_\Delta} (m_N + m_\Delta) + A]. \tag{5.27}$$

The coefficients appearing in Eq.(5.27) are given by, in the transition channel $\Sigma^+ \gamma \to \Sigma^{*+}$,

$$\begin{aligned}
c_1 &= \frac{1}{2}(-e_s + e_u), \\
c_2 &= \frac{1}{6}(-e_u + e_s f_s \phi), \\
c_3 &= \frac{1}{12}(e_u(-2 + 6f_s + 2\kappa + 6\beta(-2 + 2f_s + \kappa) - \xi) \\
&\quad + e_s(-6 + f_s(2 - 2(1 + 3\beta)\kappa\phi + \phi\xi))), \\
c_4 &= \frac{1}{12}(4e_s - e_u(1 + 2\beta(-1 + f_s) + 3f_s)), \\
c_5 &= \frac{1}{6}(e_u(1 + 4\beta(-1 + f_s) + 3f_s) - 4e_s f_s \phi), \\
c_6 &= \frac{1}{72}\beta(e_u - e_s f_s \phi), \\
c_7 &= \frac{1}{36}(e_s(6 + f_s(-4 + \phi(\kappa + 6\beta\kappa - 2\xi))) \\
&\quad + e_u(2 - 2\kappa + \xi + f_s(-4 + \kappa - 6\beta\kappa + \xi))), \\
c_8 &= \frac{1}{144}(-2e_s + e_u(1 - 2\beta(-1 + f_s) + f_s));
\end{aligned} \tag{5.28}$$

in the transition channel $\Xi^0 \gamma \to \Xi^{*0}$,

$$c_1 = \frac{1}{4}(1 + \beta)(e_s - e_u),$$

$$c_2 = -\frac{1}{12}(-1+\beta)(e_u - e_s f_s \phi),$$

$$c_3 = \frac{1}{24}(e_u(2-6f_s+\kappa+\xi) - e_s f_s(-4+\phi(\kappa+\xi)) + \beta(e_u(-14+6f_s-7\kappa-\xi)$$

$$+e_s(24+f_s(-16+7\kappa\phi+\phi\xi)))),$$

$$c_4 = \frac{1}{48}(-2(e_s+6\beta e_s+e_u-6\beta e_u) + ((-5+7\beta)e_s + (9-7\beta)e_u)f_s),$$

$$c_5 = \frac{1}{12}(\beta(-1+f_s)(2e_u - 7e_s f_s \phi) + f_s(-4e_u + e_s(1+3f_s)\phi)),$$

$$c_6 = -\frac{1}{288}(-1+3\beta)(e_u - e_s f_s \phi),$$

$$c_7 = \frac{1}{72}(e_s(12+2f_s(-8-5\beta+f_s+(2+\beta(-5+f_s)-f_s)\kappa\phi) - (-1+\beta)f_s$$

$$(1+f_s)\phi\xi) + 2e_u(-3\kappa + f_s(-2+3f_s+2\kappa-\xi) + \beta(2+\kappa+3f_s(1+\kappa)+\xi))),$$

$$c_8 = \frac{1}{576}(-2(-1+2\beta)(e_s+e_u) + (e_s+5\beta e_s + (-5+3\beta)e_u)f_s); \tag{5.29}$$

and in the transition channel $\Lambda\gamma \to \Sigma^{*0}$,

$$c_1 = \frac{1}{4}(-3e_d + e_s + 2e_u),$$

$$c_2 = \frac{1}{6}(e_d - e_u),$$

$$c_3 = \frac{1}{24}(6e_s + e_u(2+6f_s+7\kappa - 6\beta(-2+2f_s+\kappa) - 2\xi)$$

$$+e_d(-8-6f_s-7\kappa+6\beta(-2+2f_s+\kappa)+2\xi)),$$

$$c_4 = \frac{1}{96}(e_d(30+\beta(23-22f_s)+16f_s) + e_u(-2(7+8f_s)+\beta(-23+26f_s))),$$

$$c_5 = \frac{1}{6}(e_d(-3+2\beta(-1+f_s)-2f_s) + 2e_u(1+\beta+f_s-\beta f_s) + e_s f_s \phi),$$

$$c_6 = \frac{1}{288}((-1+2\beta)e_d - (1+2\beta)e_u),$$

$$c_7 = \frac{1}{72}(-6e_s - e_u(\kappa - 12\beta\kappa + f_s(8+(4+6\beta)\kappa - 2\xi) - 2(2+\xi))$$

$$+e_d(f_s(14+\kappa+6\beta\kappa-2\xi) - 2(2+(-2+6\beta)\kappa+\xi))),$$

$$c_8 = \frac{1}{1152}(1 - 8e_s + e_u(6 + \beta(7 - 10f_s) + 8f_s) + e_d(-14 - 7\beta - 8f_s + 6\beta f_s)). \tag{5.30}$$

This concludes the presentation of the QCD sum rules that will be used in the numerical analysis. The sum rules for N to Δ transition for other structures are listed in Appendix A.

5.4 Monte-Carlo Analysis

The sum rules for N to Δ transition have the generic form of OPE - ESC = Pole + Transition, or

$$\Pi_{tran}(QCD, \beta, w, M^2) = \tilde{\lambda}_N \tilde{\lambda}_\Delta \left(\frac{f(G_1, G_2)}{M^2} + A \right) e^{-\bar{m}^2/M^2}, \tag{5.31}$$

where QCD represents all the QCD input parameters. $f(G_1, G_2)$ is a function of transition amplitudes G_1 and G_2. The basic mathematical task is: given the function Π_{tran} with known QCD input parameters, find the phenomenological parameters (G_1, G_2, transition strength A, coupling strength $\tilde{\lambda}$, and continuum threshold w) by matching the two sides over some region in the Borel mass M. A χ^2 minimization is best suited for this purpose. Similarly, to alleviate the situation, we employ the corresponding mass sum rules which have a generic form of OPE - ESC = Pole, or

$$\Pi_{mass,N}(QCD, \beta, w_1, M^2) = \tilde{\lambda}_N^2 e^{-m_N^2/M^2}; \tag{5.32}$$

$$\Pi_{mass,\Delta}(QCD,\beta,w_2,M^2) = \tilde{\lambda}_{\Delta}^2 e^{-m_{\Delta}^2/M^2}. \tag{5.33}$$

They share some of the common parameters and factors with the transition sum rules. Note that the continuum thresholds may not be the same in different sum rules. By taking the following combination of the transition and mass sum rules,

$$\frac{\Pi_{tran}(QCD,\beta,w,M^2)}{\sqrt{\Pi_{mass,N}(QCD,\beta,w_1,M^2)\Pi_{mass,\Delta}(QCD,\beta,w_2,M^2)}} = \frac{f(G_1,G_2)}{M^2} + A, \tag{5.34}$$

the couplings λ and the exponential factors are cancelled out. This is another advantage for introducing the $\bar{m}^2$ prescription. The form in Eq. (5.34) is what we are going to implement. By plotting the two sides as a function of $1/M^2$, the slope will be related to the transition amplitudes G_1 or G_2 and the intercept the transition strength A. The linearity (or deviation from it) of the left-hand side gives an indication of OPE convergence and the role of excited states. The two sides are expected to match for a good sum rule over a certain window. This way of matching the sum rules has two advantages. First, the slope, which is proportional to the transition amplitudes, is usually better determined than the intercept. Second, by allowing the possibility of different continuum thresholds, we ensure that both sum rules stay in their valid regimes.

For the octet baryons, we use the chiral-even mass sum rules in in Eq. (3.79) which are reproduced here in the same notation used in this work.

For the decuplet baryons, we use the chiral-odd sum rules [51] at the structure

$g_{\mu\nu}$, which are reproduced here, for Δ:

$$\tfrac{4}{3}\,a\;E_1\,L^{16/27}\;M^4 - \tfrac{2}{3}\,m_0^2 a\;E_0\,L^{2/27}\;M^2 - \tfrac{1}{18}\,a\,b\;L^{16/27} = \tilde{\lambda}_\Delta^2\;M_\Delta\;e^{-M_\Delta^2/M^2}; \qquad (5.35)$$

for Σ^*:

$$\begin{aligned}&\tfrac{4}{9}\,(f_s+2)\,a\;E_1\,L^{16/27}\;M^4 - \tfrac{2}{9}\,(f_s+2)\,m_0^2 a\;E_0\,L^{2/27}\;M^2 - \tfrac{1}{54}\,(f_s+2)\,a\,b\;L^{16/27}\\ &+\tfrac{1}{2}\,m_s\;E_2\,L^{-8/27}\;M^6 + \tfrac{2}{3}\,m_s\,\kappa_v a^2\;L^{16/27} = \tilde{\lambda}_{\Sigma^*}^2\;M_{\Sigma^*}\;e^{-M_{\Sigma^*}^2/M^2};\end{aligned} \qquad (5.36)$$

for Ξ^*:

$$\begin{aligned}&\tfrac{4}{9}\,(2f_s+1)\,a\;E_1\,L^{16/27}\;M^4 - \tfrac{2}{9}\,(2f_s+1)\,m_0^2 a\;E_0\,L^{2/27}\;M^2 - \tfrac{1}{54}\,(2f_s+1)\,a\,b\;L^{16/27}\\ &+m_s\;E_2\,L^{-8/27}\;M^6 + \tfrac{4}{3}\,m_s\,f_s\,\kappa_v a^2\;L^{16/27} = \tilde{\lambda}_{\Xi^*}^2\;M_{\Xi^*}\;e^{-M_{\Xi^*}^2/M^2}.\end{aligned} \qquad (5.37)$$

All the details about monte-carlo analysis and QCD input parameters are given in Sec. 4.4.

5.5 Results and Discussion

We did a wide survey of the 96 sum rules at the 12 structures and the 8 transitions. Overall, based on the quality of the match, the broadness of the Borel window and its reach into the lower end, the size of the continuum and non-diagonal contributions, and OPE convergence, we found that most of the sum rules do not perform well in terms of their ability to predict stable values for the amplitudes. They can be roughly divided into four groups using our naming convention of WE_i and WO_i, as

alluded to earlier. Group one consistently produces the most reliable results, except the structure at WE_3. In the following, we focus on the sum rules at WE_1 and WO_2, which only contain the amplitude G_1, and at WE_6 which only contains G_2.

5.5.1 The Sum Rules at WE_1

The sum rules are found in Eq. (5.19). Ideally, we would like to extract 6 parameters: G_1, A, w, w_1,w_2 and β. But a search treating all six parameters as free does not work because there is not enough information in the OPE. In fact, the freedom to vary β can be used as an advantage to yield the optimal match. One choice is $\beta = -0.2$ which minimizes the perturbative term in the mass sum rule (the first term in Eq. (3)) [52]. Another parameter that can be used to our advantage is the continuum thresholds w_1 and w_2 for the corresponding mass sum rules. We fix them to the values that give the best solution to the mass sum rules independently. The following values are used: for the nucleon, $w_1 = 1.44$ GeV; for Λ, $w_1 = 1.60$ GeV; for Σ, $w_1 = 1.66$ GeV; for Ξ, $w_1 = 1.82$ GeV; for the Δ, $w_2 = 1.65$ GeV; for Σ^*, $w_2 = 1.80$ GeV; for Ξ^*, $w_2 = 2.0$ GeV. In this way the transition and the mass sum rules can stay in their respective valid Borel regimes. This leaves us with three parameters: G_1, A, w. Unfortunately, a three-parameter search is either unstable or returns values for w smaller than the particle masses, a clearly unphysical situation. Again we think this is a symptom of insufficient information in the OPE to resolve the parameters. So we are forced to fix the continuum threshold w to the value that corresponds to the best match for the central values of the QCD parameters, and extract two parameters: G_1 and A.

Table 5.1: Results for G_1 in $N \to \Delta$ transitions from the QCD sum rule at structure WE_1 in Eq. (5.19). The columns correspond to, from left to right: transition channel, β value, Borel window, continuum threshold, transition strength A, amplitude G_1. The errors in the results are derived from 2000 samples in the Monte-Carlo analysis with 10% uncertainty on all the QCD input parameters.

Transition	β	Window (GeV)	w (GeV)	A (GeV^{-2})	G_1 (GeV^{-1})
$p\gamma \to \Delta^+$	-0.2	0.9 to 1.2	1.5	0.76(7)	3.16 (37)
$n\gamma \to \Delta^0$	-0.2	0.9 to 1.2	1.5	-0.76(7)	-3.16 (37)
$\Sigma^+\gamma \to \Sigma^{*+}$	-0.2	0.85 to 1.3	1.6	1.06(10)	2.05 (24)
$\Sigma^0\gamma \to \Sigma^{*0}$	-0.2	0.85 to 1.3	1.5	0.42(4)	0.92 (10)
$\Sigma^-\gamma \to \Sigma^{*-}$	-0.2	0.8 to 1.4	1.8	-0.04(3)	-0.33 (6)
$\Xi^0\gamma \to \Xi^{*0}$	-0.2	0.8 to 1.4	1.6	-0.27(4)	-0.75(8)
$\Xi^-\gamma \to \Xi^{*-}$	-0.2	0.8 to 1.4	2.0	0(1)	0.12 (2)
$\Lambda\gamma \to \Sigma^{*0}$	-0.2	0.8 to 1.3	1.45	0.62(8)	2.60(24)

The results of such an analysis are given in Table 5.1. We also checked that the results are not sensitive to small changes in β and the Borel window. Our result on the $\Lambda\gamma \to \Sigma^{*0}$ transition is a prediction: we know of no other calculations of this transition channel. The results on the parameter A indicate that the non-diagonal transitions are not significant in this sum rule, perhaps due to cancellations in the excited states, but they are not negligible in the proton and neutron channels. Ignoring them will alter the slope of the RHS and lead to different results for G_1. In fact, we found that one of the main symptoms of a sum rule performing poorly is the relatively large contribution of the non-diagonal transitions represented by A. The effects of such contributions are not known until a numerical analysis is carried out.

We look at details of the analysis in Fig. 4.5, using the transition $p\gamma \to \Delta^+$ as an example. The first graph shows how the two sides of Eq. (5.34) for this sum rule match over the Borel window, which should be linear as a function of $1/M^2$ according to the right-hand side of this equation. Indeed, we observe good linear behavior from

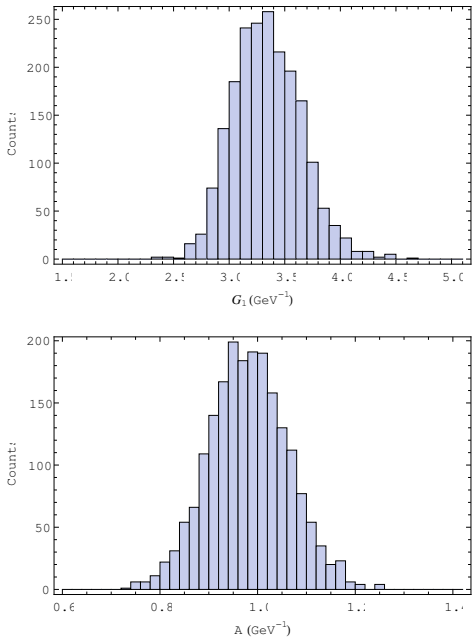

Figure 5.2: Histogram for the G_1 transition amplitude (top) and transition amplitude (bottom) obtained from Monte-Carlo fits of Eq.(5.19) at WE_1 for 2000 QCD parameter sets. They are based on 10% uncertainty given to all the QCD input parameters.

the LHS (which is OPE-ESC). The slope is directly proportional to the transition amplitude G_1, and the intercept give the non-diagonal transition contribution A. We also plot the individual contributions from u and d quarks. We see that in this transition, the u-quark contribution is the dominant one, which is expected because it is doubled-represented in the proton (uud). In the next two graphs, we give details on the individual terms in the sum rule in Eq. (5.19), remembering that the sum rule is in the generic form of OPE-ESC=Pole+Transition. The second graph in Fig. 4.5 shows how the various terms contribute to the OPE as a function of M^2. The M^0 terms, which contain the contributions from the condensates χa^2 and b, play an important role. It is followed by the M^4 term which is the perturbative contribution. The M^2 term is zero in this channel because it is proportional to the strange quark mass. The M^{-2} term gives a negative contribution and its contribution as a percentage of the

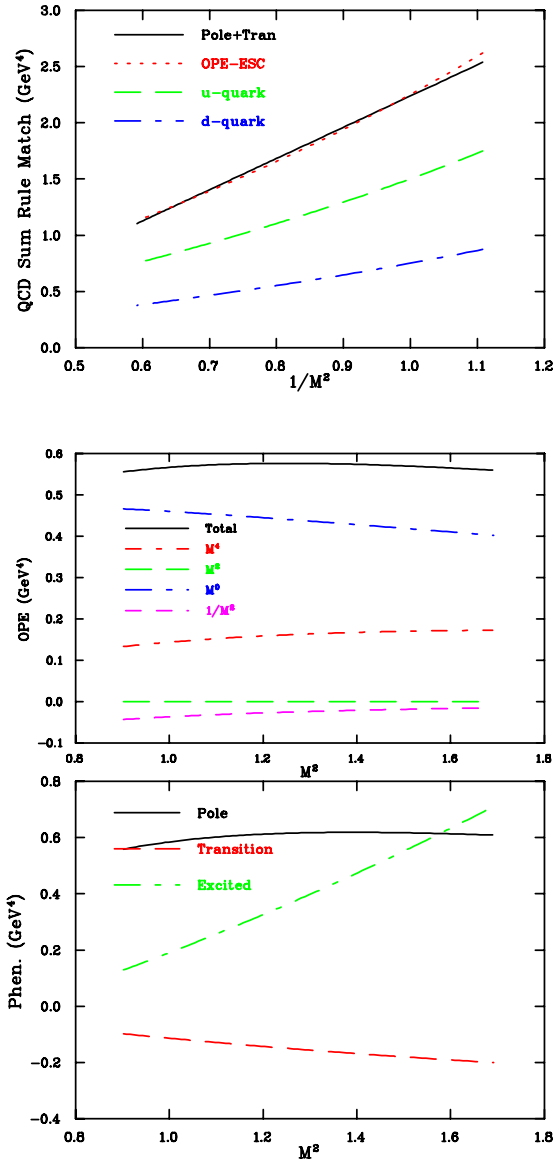

Figure 5.3: Analysis of the QCD sum rule in Eq. (5.19) (structure WE_1) for the proton at $\beta = -0.2$ according to Eq. (5.34). Top figure, the pole plus transition terms (solid lines) are compared against the OPE minus the excited-state contributions (dashed lines) as a function of $1/M^2$ (the two should match for an ideal sum rule). Also plotted are the individual contributions from u (long-dashed lines) and d (dot-dashed lines) quarks. Middle figure, the total in the OPE side and its various terms are plotted as a function of M^2. Bottom figure, the 3 terms in the phenomenological side: pole (solid), transition (long-dashed), and excited (dot-dashed) are plotted as a function of M^2.

entire OPE is about 10% at the lower end of the Borel window. In the third graph we show the three terms that comprise the phenomenological side (Pole, Transition, and ESC) as a function of M^2. The ground-state pole is dominant at the low end of the Borel window. The excited-state contribution starts small, then grows with M^2, as expected from the continuum model. The transition contribution is small in this sum rule. It is consistently smaller than the excited-state contribution and has a weak dependence on the Borel mass.

We also looked into look into correlations between any two parameters by way of scatter plots of the two parameters of interest. Fig. 5.4 shoes that the transition amplitude G_1 has a strong negative correlation with the vacuum susceptibility χ. Larger χ (in absolute terms since χ is negative) leads to smaller G_1. We found similar strong correlations with in other transition channels. It is similar to magnetic moment case. So precise determination of χ is crucial for keeping the uncertainties in the spectral parameters under control.

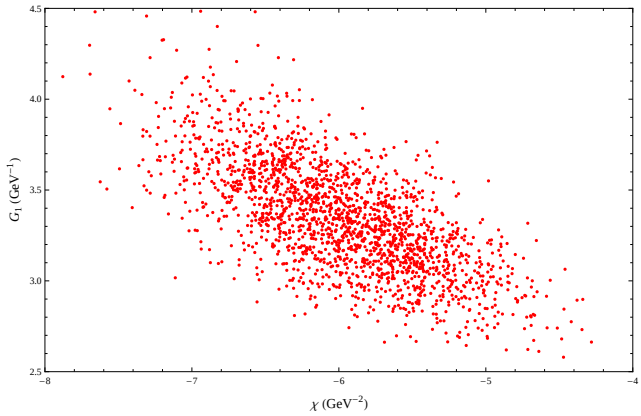

Figure 5.4: A scatter plot showing correlations between the transition amplitude G_1 and one of the QCD parameters χ for the $p\gamma \to \Delta^+$ at structure WE_1. It is obtained from 2000 Monte-Carlo samples with 10% uncertainty on all the QCD parameters.

5.5.2 The Sum Rule at WO_2

The sum rule at this structure is found in Eq. (5.27). We use the same procedure to analyze it. Since OPE expansion in this sum rule goes deeper than others (from M^2 to $1/M^4$), it is expected to be more reliable than the WO_1 sum rule. But our analysis shows that this advantage is offset by the smallness of the $1/M^2$ and $1/M^4$ terms. As a result, its performance is about the same as the sum rule at WE_1. Table 5.2 displays the results extracted from this sum rule.

Table 5.2: Similar to Table 5.1, but for the QCD sum rule in Eq. (5.27) (structure WO_2).

Transition	β	Window (GeV)	w (GeV)	A (GeV^{-3})	G_1 (GeV^{-1})
$p\gamma \to \Delta^+$	-0.2	0.9 to 1.25	1.5	1.05(9)	3.34(31)
$n\gamma \to \Delta^0$	-0.2	0.9 to 1.25	1.5	-1.05(9)	-3.34(31)
$\Sigma^+\gamma \to \Sigma^{*+}$	-0.2	0.9 to 1.4	1.6	1.65(24)	0.75(41)
$\Sigma^0\gamma \to \Sigma^{*0}$	-0.2	0.9 to 1.4	1.6	0.65(9)	0.40(17)
$\Sigma^-\gamma \to \Sigma^{*-}$	-0.2	0.9 to 1.3	1.4	-0.19(5)	-0.08(7)
$\Xi^0\gamma \to \Xi^{*0}$	-0.2	0.9 to 1.4	1.8	-0.54(8)	-0.35(15)
$\Xi^-\gamma \to \Xi^{*-}$	-0.2	0.9 to 1.4	1.7	0.08(2)	0.10(4)
$\Lambda\gamma \to \Sigma^{*0}$	-0.2	0.9 to 1.4	1.55	1.55(13)	1.13(32)

5.5.3 The Sum Rule at WE_6

The sum rule is found in Eq. (5.23). This is the only sum rule that depends on G_2 alone. The results of our analysis are given in Table 5.3. The off-diagonal contributions (A) in the $p \to \Delta^+$ and $n \to \Delta^0$ are smaller by half than those for G_1, but the uncertainties are larger. They are small in the other channels, just like those for G_1. But others are not good. The reason of this is because he transition contribution (A) are as larger as the G_2 term, so the two terms can't distinguish and get contaminated.

Table 5.3: Similar to Table 5.3, but for the G_2 amplitude from the QCD sum rule in Eq. (5.23) (structure WE_6).

Transition	β	Window (GeV)	w (GeV)	A (GeV^{-2})	G_2 (GeV^{-2})
$p\gamma \to \Delta^+$	-0.2	1.05 to 1.3	1.5	-0.25(4)	-2.26(43)
$n\gamma \to \Delta^0$	-0.2	1.05 to 1.3	1.5	0.25(4)	2.26(43)
$\Sigma^+\gamma \to \Sigma^{*+}$	-0.2	1.2 to 1.6	1.6	-0.19(6)	-0.99(32)
$\Sigma^0\gamma \to \Sigma^{*0}$	-0.2	1.0 to 1.3	1.4	-0.11(1)	-0.92(19)
$\Sigma^-\gamma \to \Sigma^{*-}$	-0.2	0.9 to 1.4	1.7	0.05(1)	-0.17(9)
$\Xi^0\gamma \to \Xi^{*0}$	-0.2	1.0 to 1.3	1.6	0.22(2)	1.50(33)
$\Xi^-\gamma \to \Xi^{*-}$	-0.2	1.0 to 1.5	1.75	-0.03(1)	0.05(7)
$\Lambda\gamma \to \Sigma^{*0}$	-0.2	1.0 to 1.3	1.45	0.09(3)	0.63(13)

5.5.4 Individual Quark Contributions

We extract a number corresponding to each quark contribution from the slope of Eq. (5.34) as a function of $1/M^2$, while keeping other factors the same (β, Borel window, w). We call this the raw individual quark contributions to the transition amplitudes. Table 5.4 gives the results for the G_1 amplitude from such a study. We see that the u-quark contribution in the transition $p\gamma \to \Delta^+$ is twice the d-quark contribution as expected, and both contributions are positive. It is the opposite in the transition $n\gamma \to \Delta^0$. The s-quark contribution is positive in the Σ transitions, and negative in the Ξ and Λ transitions. In the $\Sigma^0\gamma \to \Sigma^{*0}$ channel, the d-quark and s-quark contributions largely cancel.

Table 5.4 gives the results for the G_2 amplitude. Similar pattern is observed in the proton and neutron channels, albeit the signs are opposite for G_1 and G_2. The s-quark contribution is opposite to that in G_1: negative in the Σ channels and positive in the Ξ channels. It dominates in the Σ channels over the u-quark and d-quark contributions. Interestingly, s-quark contribution is exactly zero in the Λ channel.

Table 5.4: Individual quark contributions to the transition amplitude G_1 in units of GeV^{-1} extracted from the QCD sum rules in Eq. (5.19) (structure WE_1).

	G_1^u	G_1^d	G_1^s	G_1^{tot}
$p\gamma \to \Delta^+$	2.10(24)	1.06(12)	0	3.16(46)
$n\gamma \to \Delta^0$	-1.05(12)	-2.10(24)	0	-3.16(46)
$\Sigma^+\gamma \to \Sigma^{*+}$	1.58(18)	0	0.47(7)	2.05(24)
$\Sigma^0\gamma \to \Sigma^{*0}$	0.84(8)	-0.42(4)	0.50(7)	0.92(10)
$\Sigma^-\gamma \to \Sigma^{*-}$	0	-1.04(8)	0.71(6)	-0.33(6)
$\Xi^0\gamma \to \Xi^{*0}$	-0.58(6)	0	-0.17(3)	-0.75(8)
$\Xi^-\gamma \to \Xi^{*-}$	0	0.38(3)	-0.26(2)	0.12(2)
$\Lambda\gamma \to \Sigma^{*0}$	1.68(16)	1.02(10)	-0.12(2)	2.60(24)

Table 5.5: Individual quark contributions to the transition amplitude G_2 in units of GeV^{-2} extracted from the QCD sum rules in Eq. (5.23) (structure WE_6).

	G_2^u	G_2^d	G_2^s	G_2^{tot}
$p\gamma \to \Delta^+$	-1.57(28)	-0.79(14)	0	-2.26(43)
$n\gamma \to \Delta^0$	0.79(14)	1.57(28)	0	2.26(43)
$\Sigma^+\gamma \to \Sigma^{*+}$	-0.56(22)	0	-0.42(6)	-0.99(32)
$\Sigma^0\gamma \to \Sigma^{*0}$	-0.50(15)	0.25(8)	-0.66(9)	-0.92(19)
$\Sigma^-\gamma \to \Sigma^{*-}$	0	0.33(12)	-0.50(7)	-0.17(9)
$\Xi^0\gamma \to \Xi^{*0}$	0.96(26)	0	0.53(7)	1.50(37)
$\Xi^-\gamma \to \Xi^{*-}$	0	-0.46(13)	0.51(7)	0.05(7)
$\Lambda\gamma \to \Sigma^{*0}$	0.42(8)	0.21(4)	0	0.63(13)

5.5.5 Comparison with other Theoretical Calculations

The determination of N to Δ transition amplitudes has been made in a number of other theoretical approaches. In the following we briefly discuss each of these approaches in order to put our results from QCD sum rules in context. The discussion is by no means exhaustive, but indicative of the breadth of interest in these transition amplitudes. First, we present our results in Table 5.6 after converting from G_1 from structure WE_1 and G_2 from WE_6 into the various conventions discussed earlier, and compare them with those from a lattice QCD calculation [5], a quark model calculation [53], and experiment [11]. For G_{M1}, we see that our results are

Table 5.6: A comparison of N to Δ transition amplitudes from various approaches: this work (QCDSR) in three different conventions; lattice QCD [5] and quark model [53]. The experiment [11] gives $3.02\text{GeV}^{-\frac{1}{2}}$ for G_{M1} and $-2.5(5)\%$ for R_{EM} in $p\gamma \to \Delta^+$ transition channel.

Transition	QCDSR					Lattice QCD		Quark Model	
	G_{M1}	R_{EM}	f_{M1}	$A_{\frac{1}{2}}$	$A_{\frac{3}{2}}$	G_{M1}	R_{EM}	G_{M1}	R_{EM}
	μ_B	%	$\text{GeV}^{-\frac{1}{2}}$	$\text{GeV}^{-\frac{1}{2}}$	$\text{GeV}^{-\frac{1}{2}}$	μ_B	%	μ_B	%
$p\gamma \to \Delta^+$	3.51(35)	-0.80(8)	0.33	-0.16	-0.29	2.46(43)	3(8)	2.15	-0.009
$n\gamma \to \Delta^0$	-3.51(35)	-0.80(8)	-0.33	0.16	0.29	-2.46(43)	3(8)	-2.15	-0.009
$\Sigma^+\gamma \to \Sigma^{*+}$	3.07(31)	-1.21(12)	0.18	-0.09	-0.16	2.61(35)	5(6)	2.61	-0.210
$\Sigma^0\gamma \to \Sigma^{*0}$	1.34 (14)	1.44 (15)	0.08	-0.04	-0.07	1.07(13)	4(6)	1.1	0.192
$\Sigma^-\gamma \to \Sigma^{*-}$	-0.52 (5)	-5.95 (6)	-0.03	0.01	0.03	-0.47(9)	8(4)	-0.4	0.985
$\Xi^0\gamma \to \Xi^{*0}$	-1.13(12)	8.45(85)	-0.06	0.04	0.05	-2.77(31)	2.4(2.7)	-2.86	0.031
$\Xi^-\gamma \to \Xi^{*-}$	0.21 (2)	-5.82(60)	0.01	-0.01	-0.01	0.47(8)	7.4(3.0)	0.44	-0.259
$\Lambda\gamma \to \Sigma^{*0}$	4.04(40)	-4.72(48)	0.23	-0.10	-0.21				

slightly higher than those from lattice QCD and quark model calculations, but the overall pattern (in terms of magnitude and sign) is consistent among the three very different calculations. For the ratio R_{EM}, the results are very different. We predict negative values for all transitions at the level of 10% uncertainty. The lattice QCD results have too large errors to resolve the sign, although a more recent calculation in the $p\gamma \to \Delta^+$ channel gives a negative value [7]. The quark model results have varying signs. It demonstrates the difficulty of quantifying the small deformation from spherical symmetry in these transitions.

Since $p\gamma \to \Delta^+$ is the channel most widely studied and the only one measured in experiments, we give a more detailed comparison including more theoretical determinations. Fig. 5.5 summarizes the calculations of the magnetic dipole transition amplitude G_{M1} in units of nucleon magneton. The calculations are grouped into six categories: lattice QCD (Latt.), QCD sum rules results from this work (QCDSR), light-cone QCD sum rules (LCSR), hedgehog models including Skyrme and hybrid

models (Skyrme), quark model calculations (Q.M), and bag models (Bag). The experimental result from the PDG is also displayed (Expt.). Fig. 5.6 summarizes the calculations of the ratio R_{EM} in the same channel.

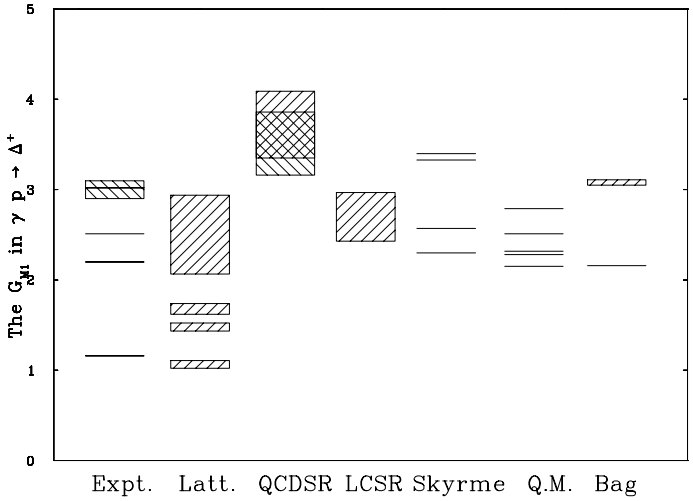

Figure 5.5: A comparison of the magnetic dipole transition amplitude G_{M1} in units of nucleon magnetons in the $p\gamma \to \Delta^+$ transition from different approaches. See text for discussions.

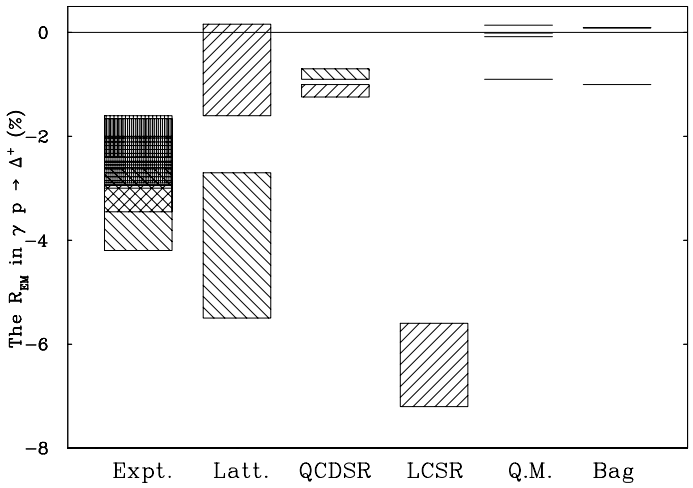

Figure 5.6: A comparison of the R_{EM} ratio in the $p\gamma \to \Delta^+$ transition. See text for discussions.

There are only a few lattice QCD calculations. The original one by Leinweber *et. al.* [5] obtained good signals for G_{M1}, but barely a signal for R_{EM} ($+3 \pm 8$ %),

and no signal for G_{C2}. Shown here are the more recent calculations by Alexandrou *et. al.* which obtained reasonable signals for all three form factors. For G_{M1}, from top down, in units of nucleon magneton (μ_N), the results are 2.5 ± 0.4 [5] with a quenched Wilson action; 1.68 ± 0.06 with a hybrid action, 1.48 ± 0.04 with a quenched Wilson action, and 1.07 ± 0.04 with a 2-flavor Wilson action [7]. Strictly speaking, we should compare results at the chiral limit and $Q^2 = 0$. The lattice results quoted are at pion mass of around 400 MeV and non-zero momentum transfer. For the ratio R_{EM}, the results are $-4.1 \pm 1.4\%$ [6] at $Q^2 = 0.13$ GeV^2 extrapolated to the chiral limit in quenched QCD; and $-0.77 \pm 0.88\%$ [7] at $Q^2 = 0.04$ GeV^2 and $m_\pi = 360$ MeV in full QCD with a hybrid action. The lattice signals for the transition form factors are by now well established. With increasing computing power and better lattice technology, lattice calculations offer the best promise for precision determination of the transitions from QCD.

The two numbers for QCDSR are from different sum rules: the top one corresponds to G_1 from WE_1 and G_2 from WE_6, the bottom one corresponds to G_1 from WO_2 and G_2 from WE_6. They are converted to G_{M1} and R_{EM} for comparison. Our results gives around 10% uncertainties. For G_{M1}, the number are a little bit higher than other models and experiments. The R_{EM} ratio is a small number, and our results agree with other models and experiment measurements.

The light-cone QCD results come from Ref. [54] which involve photon distribution amplitudes (light-cone wavefunctions).

The hedgehog models from top down include the holographic QCD calculation by Grigoryan, Lee and Yee [55] which can be considered as a 5D version of the

Skyrme model; the SU(3) Skyrme model calculation by Chemtob [56]; the SU(2) Skyrme model calculations by Kunz and Mulders [57]; and the SU(2) Skyrme model calculation by Adkins, Nappi and Witten [58]. The semiclassical hedgehog calculation of Cohen and Broniowski [59] gives a negative value (-2.8) for M1 moment so it is not shown in Fig. 5.5. Skyrme models produce reasonable results for the M1 amplitude, but vanishing ones for eletric quadrupole E2 transition matrix elements so they are left out in Fig. 5.6.

The quark model results include (from top down): a calculation by Franklin [60] (It has been correlated with G_A and provides arguably the best constraint on G_{M1} in quark-model calculations); a Bethe-Salpeter determination from Mitra and Mittal [61]; a calculation by Guiasu and Koniuk [62] in which mesonic dressings of the nucleon are explicitly included; a calculation by Capstick [63] in which configuration mixing in the baryon SU(6) wave functions is accounted for; and a calculation by Darewych *et. al.* [53] based on the simple quark model. Quark model calculations generally give small values for R_{EM}.

The bag models include a chiral bag calculation (top) by Kalbermann and Eisenberg [64], and an old MIT bag calculation (bottom) by Donoghue *et. al.* [65].

Chapter 6

MathQCDSR: a Mathematica Package for QCD Sum Rules Calculations

In this Chapter, we present a computer software package to perform almost all of the analytic derivations and numerical analysis in a QCD sum rule calculation. We decided to write the program in Mathematica because of its powerful symbolic capability, built-in numerical functions, in-line graphical features, user-friendly interface, and wide usage in the research community. To our knowledge, there have been no published software packages that perform QCDSR calculations in any language. We want to provide the framework and some standard tools so that users can focus on developing projects and trying out ideas quickly and efficiently, rather than getting buried under a mountain of algebra and fitting. To cover the wide range of QCDSR

calculations done in the field, we provide two examples in the package. One is a standard calculation of baryon masses which involves a two-point correlation function. The other is a calculation of the magnetic moments of octet baryons which involves three-point correlation function with coupling to an external electromagnetic field. The free package FeynCalc is used to handle the gamma-matrix algebra. In addition to two notebooks for the construction of the QCD sum rules, two corresponding notebooks are provided for a Monte-Carlo-based numerical analysis, complete with in-line graphical display of sum rule matching, error distributions, and scatter plots for correlations. Some sample code for this package is given in Appendix B.

This chapter is organized as follows. In Sec. 6.1, we describe how to calculate octet baryon masses using our mathematica code. It offers an example of a QCDSR calculation based on two-point correlation functions. Two Mathematica notebooks, one for construction and one for analysis of the sum rules, are introduced and their usage discussed. In Sec. 6.2, we give an example of a more complicated QCDSR calculation based on three-point correlation functions, namely, the magnetic moments of octet baryons in external electromagnetic field. Two more notebooks are provided for the task.

6.1 Example 1: Mass of Octet Baryons

Computing masses is among the simplest of QCDSR calculations. In this example, we will show how to use Mathematica to do the calculations. Furthermore, the mass sum rules derived in this section will be used as normalization in computing the magnetic

moments of baryon octet in the next example.

6.1.1 Sum Rule Construction

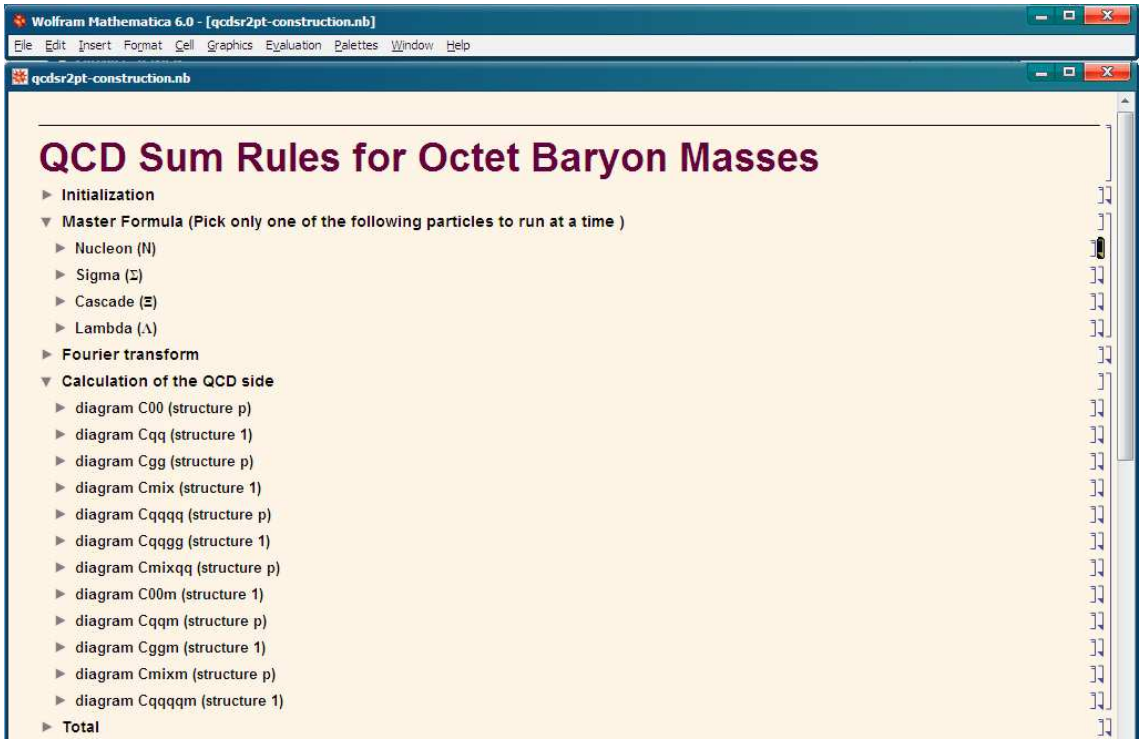

Figure 6.1: Outline of *qcdsr2pt-construction* program for constructing of octet baryon mass sum rules. All the codes are hidden in the outline.

As we mentioned in Chap. 3, Eq.(3.6) is the fully-interacting quark propagator and when putting the expression back to master formula Eq.(3.5), we will end up with hundreds of terms. This is where we introduce the Mathematica notebook *qcdsr2pt-construction.nb*. Figure 6.1 show a outline of *qcdsr2pt-construction.nb* program for constructing of octet baryon mass sum rules. All the codes are hide in the outline. We organize the Wilson coefficients by a graphic representation shown in Fig. 3.1 and Fig. 3.2. Each diagram represents a class of terms in the expansion and is named intuitively. In the Mathematica notebook, we put diagrams with common names in

one cell, and evaluate each cell individually and independently. Each cell produces a contribution to one of the two Dirac structures 1 and $\hat{p}$ (this is indicated in the cell heading). Since Mathematica does not have native functions for gamma-matrix algebra, we employ the external package FeynCalc [66] which is a freely available package for high-energy physics calculations. Here we invoke only a small portion of its capabilities, namely, gamma-matrix algebra. The installation of FeynCalc is straightforward, just like any external package to Mathematica. Since FeynCalc is written for Mathematica 6.0, our package is limited to this version. However, our package has nothing specifically tied to version 6.0: Once FeynCalc is upgraded to version 7.0, our package should work with the new version automatically.

After the calculation in coordinate space, a Fourier transform is needed into momentum space, which is incorporated into *qcdsr2pt-construction.nb*. This is achieved by defining a set of functions that correspond to the x dependence extracted from each diagram. For example, the x dependence of diagram $C00$ is $\hat{x}/x^{10}$. So we define a function called f101 where"10" denotes the power of x in the denominator, and "1" denotes x_μ from the numerator. If the x dependence is $1/x^{10}$ we name the corresponding function $f100$. If the x dependence is $x_\mu x_\nu/x^8$ we name the corresponding function $f82$, and so on. Once the x dependence is isolated, the Fourier transform can be done by a simple substitution.

The final step is a Borel transform which is incorporated by a straightforward substitution. For each diagram, we print out 4 types of intermediate results on the screen for debugging purposes. For example, for diagram $C00$, $c00x$ is the result in x space, $c00xf$ the extracted x dependence for Fourier transform, $c00p$ the result in

p space, and $c00b$ the result in Borel space. In total, there are 12 cells to evaluate. After all the diagrams are evaluated, they are added up to give the QCD side. The result falls into two groups, characterized by two distinct Dirac structures: one at $\hat{p}$ and one at 1.

In the notebook, we included master formulae for all 4 types of hadrons in the baryon octet: N, Σ, Ξ, and Λ (we assume isospin symmetry in the u and d quarks). These particles are named as *onuc*, *osig*, *oxi*, and *olam*, respectively. The user can pick a particle at the beginning of the calculation, and then just proceed to complete all the calculations for that particle. For each particle, the notebook outputs the QCD side as plain text in two files named appropriately. For example, for the nucleon channel, the two files written to disk are: *mass-onuc-1.txt* for structure 1, and *mass-onuc-p.txt* for structure $\hat{p}$. These files should not be modified since they will be read later by another Mathematica notebook for analysis. Since the construction of the sum rule needs to be done only once, this way of separating the sum rule from the analysis improves efficiency.

6.1.2 Sum Rule Analysis

The task is: given the function Eq. (3.79) or Eq. (3.87) with known QCD input parameters and the freedom to vary β, find the phenomenological parameters (mass m_N, coupling strength λ_N^2, and continuum threshold w) by matching the two sides (LHS=RHS) over some region in the Borel mass M. A χ^2 minimization is used. A crucial question in QCD sum rule analysis is how to estimate the errors in the results.

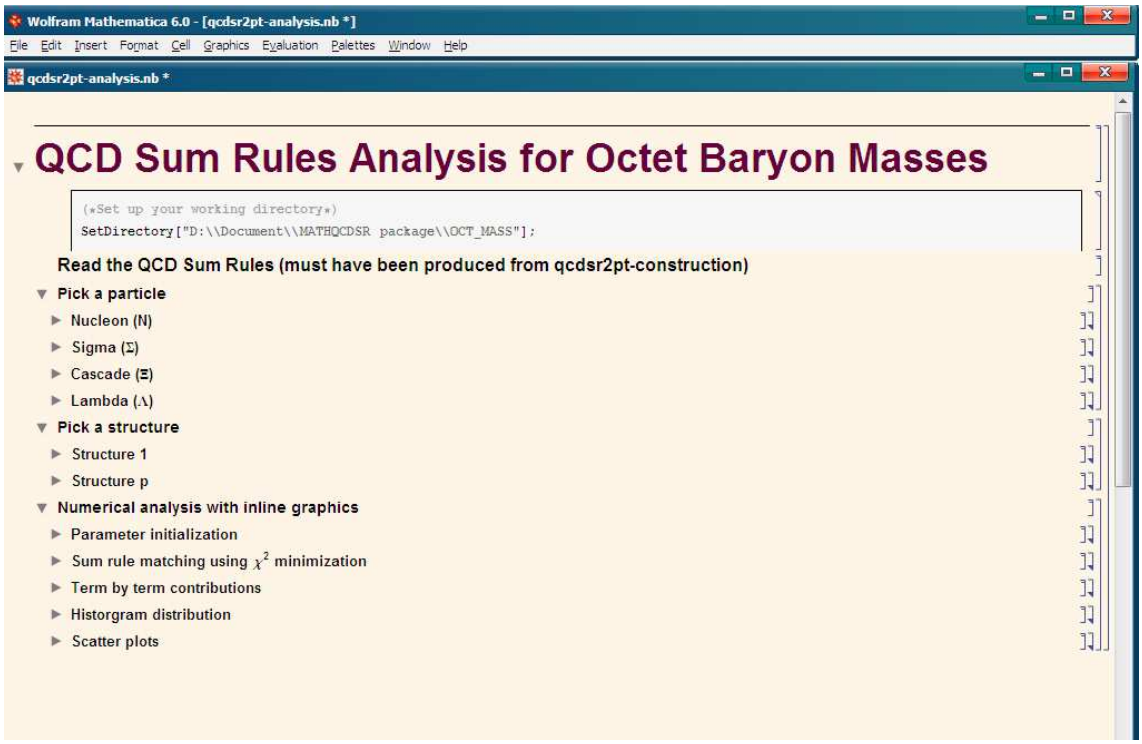

Figure 6.2: Outline of *qcdsr2pt − analysis* program for analyzing the octet baryon mass sum rules.

A related question is how to assess the reliability of a QCD sum rule, since not all QCD sum rules are created equal. Traditionally QCD sum rule analysis is regarded as the weak link in the QCDSR method: there is a general lack of rigor in the wide variety of practices.

We use the Monte-Carlo-based procedure. In this method, the entire phase-space of QCD input parameters is explored simultaneously, and is mapped into uncertainties in the phenomenological parameters. It takes as input the QCD sum rules derived in *qcdsr2pt-construction.nb* so the construction must be run before the analysis. Figure 6.2 gives a overview of *qcdsr2pt-analysis.nb* program. At the beginning of the analysis, the user has the option of picking a particle and a sum rule (at a particular structure) to analyze. Then the analysis is divided into the following steps.

Parameter initialization

The QCD input parameters are given in parameter initialization section. Once the parameters are initialized, a normal distribution can be created for each, as well as the standard deviation σ^2 for the LHS. The user can adjust the parameter Nr for a desired number of Monte-Carlo samples.

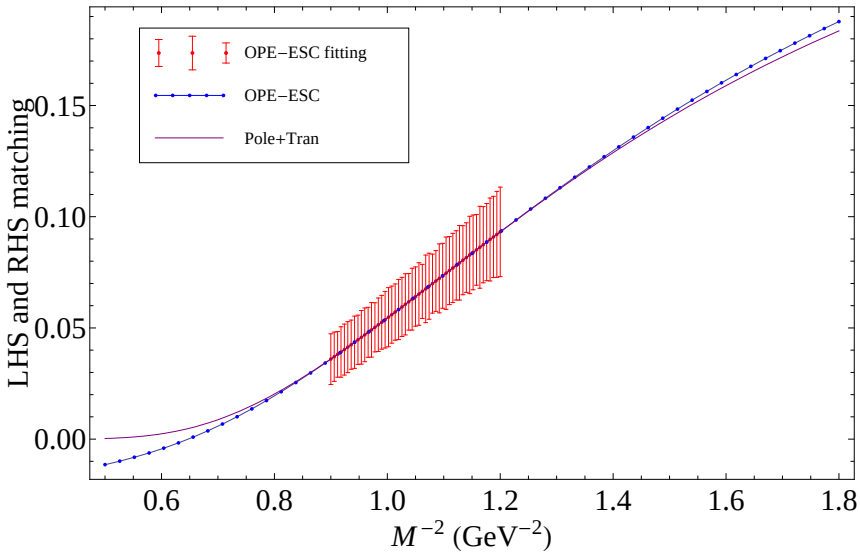

Figure 6.3: The matching of the chiral-odd QCD sum rule in Eq. (3.87) for the nucleon. A three-parameter search was performed, with $\beta = 1.2$ and about 2800 QCD parameter sets.

Sum rule matching via χ^2 minimization

The analysis does a three-parameter search, treating the mass m_N, coupling λ^2, and continuum threshold w as free parameters. Fig. 6.3 show an example of the matching. We can see that the two curves agree very well. The solution at the best match is $m_N = 1.21 \pm 0.05$GeV, $\beta = 1.2$, $w = 1.54 \pm 0.06$ GeV and $\lambda^2 = 0.20 \pm 0.03$GeV^6 over a Borel window of 0.9 to 1.2 GeV. Based on the quality of the match, the broadness of the Borel window and its reach into the lower end, the size of the continuum

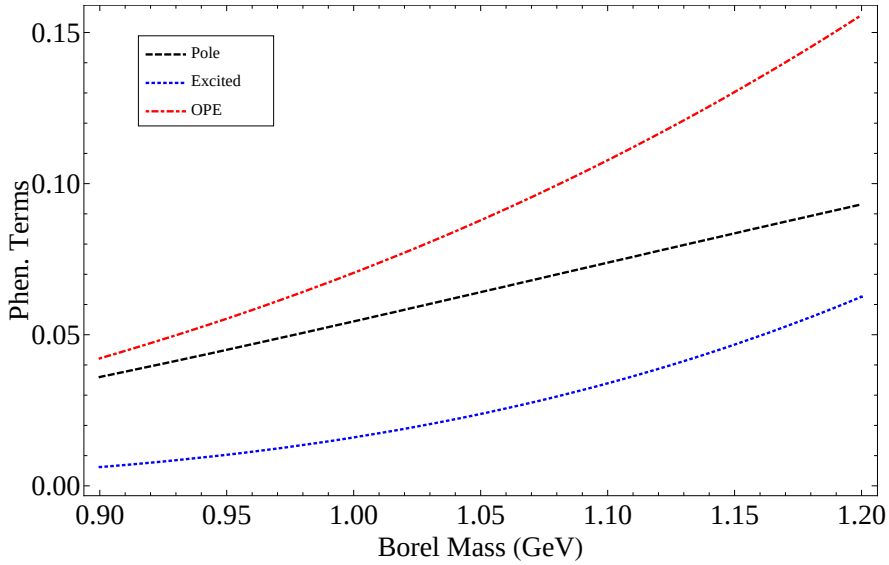

Figure 6.4: Individual terms in the spectral representation for the chiral-odd QCD sum rule in Eq. (3.87) for the nucleon.

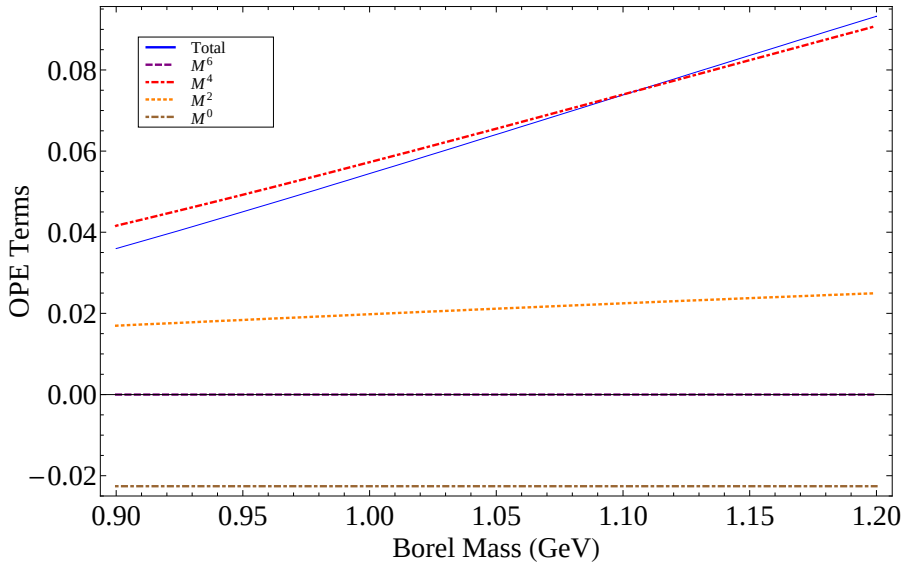

Figure 6.5: Individual terms in the OPE for the chiral-odd QCD sum rule in Eq. Eq.(3.87) for the nucleon.

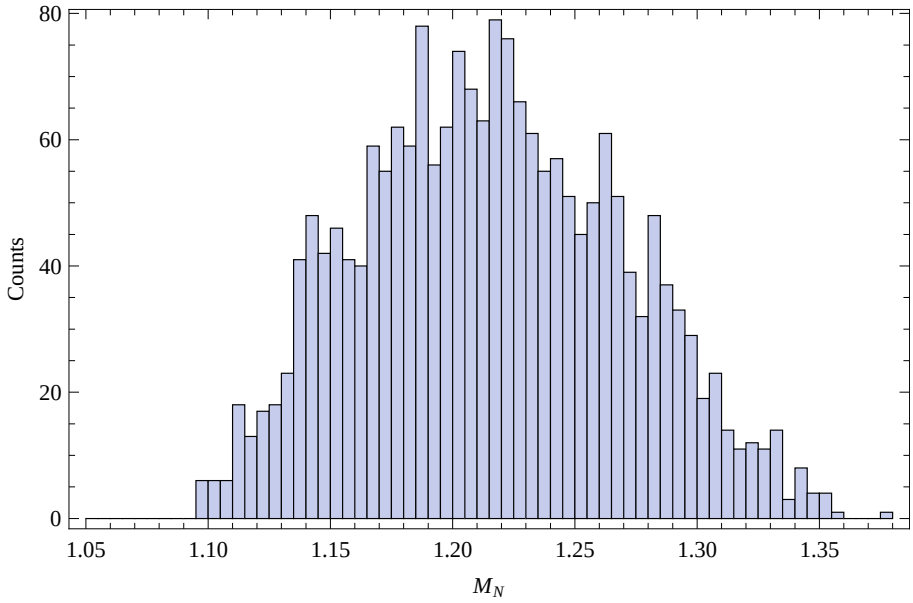

Figure 6.6: Histogram for the nucleon mass at $\beta = -1.2$ for chiral-odd sum rule Eq.(3.87) after making section for physical continuum threshold.

contribution, and the OPE convergence, we find that the chiral-odd sum rule from structure 1 is more reliable than the chiral-even sum rule at structure p. The physical reason is that the contributions of positive- and negative-parity excited states partially cancel each other in the chiral-odd sum rules whereas they add up in the chiral-even sum rules.

Term by term contributions

A more detailed understanding of how a QCD sum rule works can be achieved by monitoring individual contributions from each term. Fig. 6.4 shows the terms in the phenomenological representation. Fig. 6.5 shows the OPE terms grouped by powers of M^2.

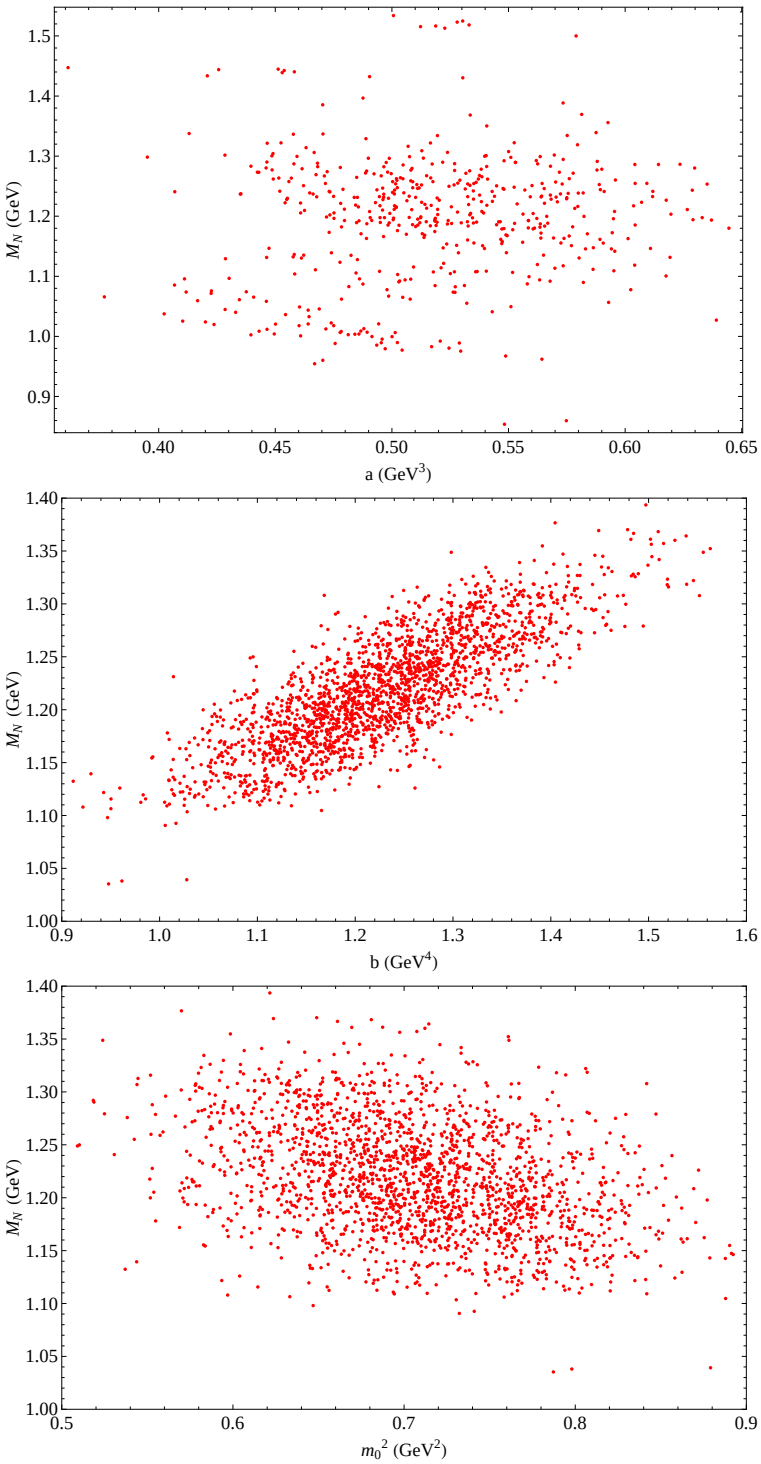

Figure 6.7: The correlation between the nucleon mass and the quant condensate, gluon condensate and mix condensate for chiral-odd sum rule(Eq.3.87) at the optimal $\beta = -1.2$.

Histograms

The search results for each Monte-Carlo sample are saved and can be displayed in histograms. It turns out for some samples, the search returns negative values for the continuum threshold w (or w smaller than the mass m_N). These solutions are clearly unphyical in the pole-plus continuum ansatz. So we impose the condition $w > m_N$ for each Monte-Carlo sample and exclude those who violate the condition. This means that to obtain a desired number of physical samples, one has to use a larger number of total samples (controlled by the parameter Nr). Histograms for all three search parameters are displayed inline, both for all samples (before) and for the physical samples (after). Fig. 6.6 shows an example for the nucleon mass using only physical samples. We see that the distribution is roughly Gaussian, whose central value is taken as the average. The error is taken as one standard deviation of the distribution. We stress that the error derived this way provides the most realistic estimate because the entire phase space has been taken into account by Monte-Carlo.

Scatter plots

Another advantage afforded by the Monte-Carlo analysis is the ability to study correlations between any two parameters in the input and output, by way of scatter plots. Fig. 6.7 shows the correlations between nucleon mass and the vacuum condensates. One can see that the nucleon mass has a relatively strong positive correlation with the gluon condensate, not so much with the quark and mixed condensates. Since the gluon condensate is the least well-known of the three, a better determination of

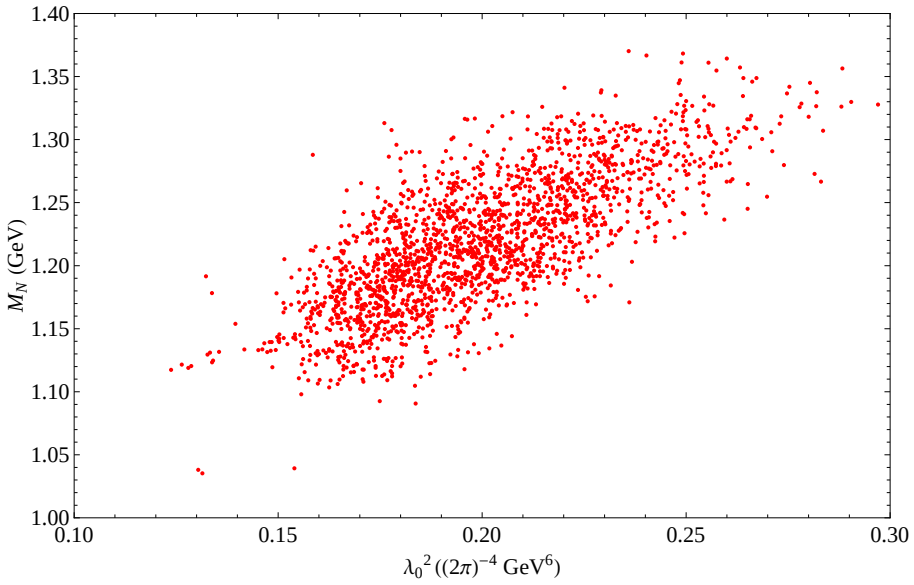

Figure 6.8: The correlation between the nucleon mass and the residue of the pole for chiral-odd sum rule(Eq.3.87) at the optimal $\beta = -1.2$.

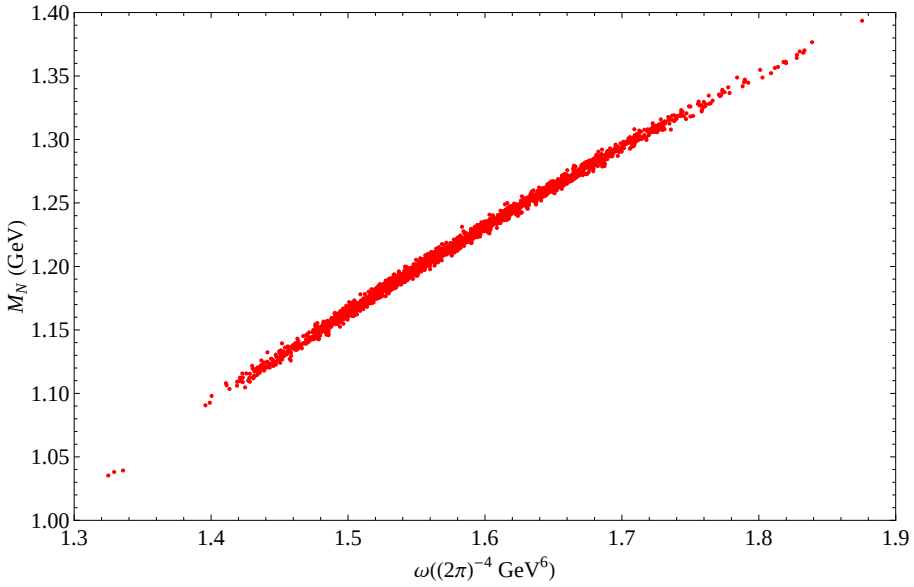

Figure 6.9: The correlation between the nucleon mass and the continuum threshold for chiral-odd sum rule(Eq.3.87) at the optimal $\beta = -1.2$.

its value would lead to improved accuracy on the calculated nucleon mass. Fig. 6.8 and Fig. 6.9 show scatter plots for m_N vs λ^2 and m_N vs w, respectively. The striking one-to-one association between the nucleon mass and the continuum threshold is found despite the underlying scatter of QCD parameter values. No output is written to disk during the analysis. However, it is very easy for a user to save a figure to disk in Mathematica: just select the figure by clicking on it, then pick a format (pdf, eps, gif, etc) under "Save Selection As" in the "File" pull-down menu.

6.2 Example 2: Magnetic Moments of Octet Baryons.

Now we move to the next example. Using the package described below, we can calculate the magnetic moments of octet baryons.

6.2.1 Sum Rules Construction

The construction program is organized in a similar fashion as in the mass example *qcdsr2pt-construction.nb*. Here we add the phenomenological side calculation because the Dirac structure of the correlation function is not as straightforward as the mass example. We use Mathematica to handle the gamma-matrix part of the calculation, which is incorporated in a new Mathematica notebook *qcdsr3pt-construction.nb*. It is reassuring that Mathematica produces the same three independent Dirac structures found in the literature, WE_1, WE_2 and WO_2 defined in Eq.(4.27).

Calculation of the QCD side contains more diagrams. The diagrams have a one-to-one correspondence in the notebook. All eight members of the octet are included.

The user can pick a member at the beginning, and then proceed to the subsequent calculations for that member. As expected, the same three Dirac structures as the phenomenological side emerge from the evaluation of the various diagrams. (Which diagram corresponds to which structure is indicated in the notebook). For each member, the notebook outputs the QCD side as plain text in three files that correspond to the three Dirac structures. For example, if the proton cell is picked, the three files written to disk are: *Mag-opro-WO1.txt*, *Mag-opro- WO2.txt*, and *Mag-opro-WE1.txt*. In all, 24 files will be produced if the notebook is run for all 8 members of the octet, one member at a time. As part of the package, we include all 24 files in a subdirectory Mag-output for reference purposes. The user should run the notebook on their own computer to produce the files, and check against the provided files to ensure everything behaves correctly. By matching the QCD side and the phenomenological side structure by structure, three QCD sum rules can be constructed for each particle. These sum rules could be found in Chap. 4.

6.2.2 Sum Rule Analysis

The analysis program for Octet baryon magnetic moment *qcdsr3pt-analysis.nb* is very similar to *qcdsr2pt-analysis.nb*, so it will not be discussed further. The result produced by this program can be found in Chap. 4.

Chapter 7

Summary and Conclusion

Here let me summarize the main findings in separate sections.

7.1 Masses and Magnetic Moments

We have calculated the proton mass as an example to get familiar with how the QCD sum rule works. Along this line, we carried out a comprehensive study of the magnetic moment of octet baryons using the method of QCD sum rules. We derived a new, complete set of QCD sum rules using generalized interpolating fields and examined them by a Monte-Carlo analysis. Here is a summary on our findings in magnetic moments.

We proposed a new way of determining the magnetic moments. We find this new 'slope' method is more robust than the normalization (intercept) method or looking for 'flatness' as a function of Borel mass. The linearity displayed from the OPE side matches almost perfectly with the phenomenological side in most cases. The method

also demonstrates clearly that the transition terms caused by the external field in the intermediate terms cannot be ignored. They are needed to make the two sides of a QCD sum rule match.

Out of the three independent structures, we find that the sum rules from chiral-even structure WE_1 are the most reliable based on OPE convergence and ground-state pole dominance. The QCD sum rules from this structure are in Eq. (4.28); its prediction are found in Table 4.1, and convergence properties are displayed in Fig. 4.5. They should be considered as the best results in this work. The extracted magnetic moments are in good agreement with experiment. These results are used to shed light on a variety of magnetic moment sum rules based on SU(6) spin-flavor symmetries in the quark model, along with experiment and lattice QCD. Reasonable results from the other two chiral-odd structures (WO_1 and WO_2) are obtained for the first time, but they are less reliable due to poor convergence properties.

We also isolated the individual quark contributions to the magnetic moments. These contributions provide insight into the rich dynamics in the baryons. By comparing them with the simple quark model and lattice QCD results, we reveal the effects of SU(3)-flavor symmetry breakings due to the strange quark mass and the environment sensitivity of quarks in different baryons.

Taken together, this work can be considered an updated and improved determination of the magnetic moments of octet baryons, bringing it to the same level of sophistication as the decuplet baryons [34].

7.2 Transition Amplitudes

We carried out a comprehensive study of the $N\gamma \to \Delta$ transition amplitudes using the method of QCD sum rules. We derived a new, complete set of QCD sum rules using generalized interpolating fields and examined them by a Monte-Carlo analysis.

We extracted the transition amplitudes as a function of $1/M^2$ in conjunction with the corresponding mass sum rules, as defined in Eq. (5.34). We find that extracting slopes is more robust than looking for 'flatness' as a function of Borel mass as before. The linearity displayed from the OPE side matches well with the phenomenological side in most cases. The method also demonstrates clearly the role of the non-diagonal transition terms in the intermediate states caused by the external field: wherever such transitions are large, the corresponding sum rules perform poorly.

Of the 96 sum rules we derived (from 12 independent structures, each for 8 transitions), we find that the sum rules from chiral-even WE_1 and chiral-odd WO_2 structures are the most reliable for the transition amplitude G_1, based on OPE convergence and ground-state pole dominance, and smallness of the non-diagonal transitions. The QCD sum rules from these structures are in Eq. (5.19) and Eq. (5.27); their predictions are found in Table 5.1 and Table 5.2. Our attempt to extract the G_2 amplitude was less successful. The only sum rules that can give stable results are in Eq. (5.23) from chiral-even WE_6 structure because WE_6 sum rule is the only sum rule contain only G_2. Their predictions are found in Table 5.3. Our final results in the various conventions are found in Table 5.6.

Our Monte-Carlo analysis revealed that there is an uncertainty on the level of

10% in the transition amplitudes if we assign 10% uncertainty in the QCD input parameters. It goes up to about 30% if we adopt the conservative assignments that have a wide range of uncertainties in Ref. [39]. The Monte-Carlo analysis also revealed some correlations between the input and output parameters. The most sensitive is the vacuum susceptibility χ. So a better determination of this parameter can help improve the accuracy on the transition amplitudes and other quantities computed from the same method. We also isolated the individual quark contributions to the transition amplitudes. +

We compared our results with a variety of theoretical calculations, and with experiment in the proton channel. Our result for transition amplitude G_{M1} is larger than the experiment and other calculations, while our result for the ratio R_{EM} is consistent with experiment. In general, we find that G_1 amplitudes are more stable than G_2 amplitudes in this approach. Our results for the $\Lambda\gamma \to \Sigma^{*0}$ transition are new.

Overall, the results for the N to Δ transition amplitudes in the QCD sum rule approach are not as robust as those for the baryon magnetic moments [9, 34, 35]. This lack of robustness is in large part due to the intrinsic un-equal mass double pole in the phenomenological representation of the spectral functions. Nonetheless, the calculations offer a physically-transparent, QCD-based perspective on the transitions in terms of quarks, gluons and vacuum condensates.

7.3 MathQCDSR

Finally, we have developed a Mathematica software package called *MathQCDSR* for standard QCD sum rules calculations. It includes 4 notebooks to carry out both the construction and analysis of QCD sum rules for two examples. One is the mass spectrum of octet baryons (based on two-point correlation functions), handled by *qcdsr2pt-constructon.nb* and *qcdsr2pt-analysis.nb*. The other is the magnetic moments of octet baryons based on the external-field method (an example of of three-point correlation functions), handled by *qcdsr3pt-constructon.nb* and *qcdsr3pt-analysis.nb*.

The construction uses an external Mathematica package called FeynCalc to perform all gamma-matrix computations, since Mathematica does not have native gamma-matrix algebra. The calculation is organized by diagrams which have a one-to-one correspondence with those in the text. For both examples, we use generalized interpolating fields with a mixing parameter β, which provides a means to study dependence on the interpolating fields. Although relations exist among the octet members by appropriate substitutions, we coded each member separately and used the relations for consistency checks. The user has the option to pick a member and carry out the rest of the calculations for that member. Intermediate results are displayed on the screen for each diagram to facilitate debugging purposes, and the final results written to disk in plain text. All of the results have been checked by using an independent computer algebra system called REDUCE.

The analysis of the QCD sum rules is an important task whose treatment has been traditionally less than rigorous. To this end, we implemented a state-of-the-art Monte-

Carlo-based procedure, taking advantage of some of Mathematica's powerful features such as build in functions, statistics, and in-line graphics. With this procedure, one can study in detail how a QCD sum rule resolves its spectral properties by monitoring each individual term, how errors in the input QCD parameters map into uncertainties in the output parameters by histograms, and how any two parameters are correlated by scatter plots. One also has the ability to monitor individual quark contributions to study the underlying quark-gluon dynamics.

The package is structured in a way that is relatively straightforward to modify for new physics projects. It is our hope that user can benefit from this package by focusing on discovering new physical insights in our understanding of strong-interaction physics from QCD, rather than getting bogged down by algebra and numerics.

7.4 Final Remarks

It has been a rewarding experience personally to work on QCD in general and QCD sum rules in particular. It is a first-principles-based method that truly works. By nature it is an analytic method, comparing to method of lattice QCD. The method is physically transparent: it can connect all hadron properties to the non-perturbative QCD vacuum structure via a few QCD vacuum condensates. One can literally trace back the contribution of each term or diagram to see how it affects the outcome.

I started with the quantum mechanical example of solving the harmonic oscillator using this method, then moved on to projects in increasing complexity and challenge in nuclear physics, namely, proton mass, magnetic moments, and the central focus

of this work: the N to Δ transitions. In addition to the physics I learned, I also learned how to carry out complicated calculations using computational tools (JAVA, REDUCE, and Mathematica, etc). I have come to appreciate the power of computers in solving physics problems, be it analytical or numerical. I also learned a lot about high-performance computing (parallel architecture and algorithms) by earning a graduate certificate in HPC from IMPACT, and by interacting with other students and professors in the QCD research group, the Physics Department, and GW at large. I hope to apply these skills in my future endeavors, be it in physics or elsewhere.

Looking to the future, I think the power of QCD sum rules is fairly unlimited. Masses, magnetic moments, and N to Δ transition amplitudes are just a few examples of what it can do. A variety of hadronic observables in both vacuum and finite density nuclear matter can be investigated, such as charge radii, strong coupling constants, and electromagnetic polarizabilities (the quadratic response in the external field method). I hope I have contributed a small step in this long journey.

Bibliography

[1] F. J. Yndurain, *The theory of quark and gluon interaction.* (Springer-Verlag,New York, 1983)

[2] A. W. Thomas *The structure of the nucleon.* (Wiley, Berlin, 2001)

[3] M.A. Shifman, A.I. Vainshtein and Z.I. Zakharov, Nucl. Phys. **B147**, 385, 448 (1979).

[4] Try a search in electronic archives such as SPIRES (http://www.slac.stanford.edu/spires/topcites/2006/alltime.shtml)

[5] D. B. Leinweber, T. Draper, R. M. Woloshyn, Phys. Rev. D **48**, 2230-2249 (1993).

[6] C. Alexandrou, Ph. de Forcrand, Th. Lippert, Phys. Rev. D **69**, 114506 (2004).

[7] C. Alexandrou *et. al.*, Phys. Rev. D **77**, 085012 (2008).

[8] B. L. Ioffe and A. V. Simlfa, Nucl. Phys. **B232**, 109, (1984).

[9] L. Wang and F.X. Lee, Phys. Rev. D **78**, 013003 (2008).

[10] H. F. Jones, M. D. Scadron, Ann. of Phys. **81**, 1 (1973).

[11] Particle Data Group: C. Amsler *et al.*, Phys. Lett. **B667**, 1 (2008).

[12] S. Nozawa, B. Blankleider, and T.H.H. Lee, Nucl. Phys.**A513**, 459 (1990).

[13] N. F. Sparveris *et al.*, Phys. Lett. B **651**, 102 (2007).

[14] R. M. Davidson, N. C. Mukhopadhyay, Phys. Rev. Lett. **79**, 4509 (1997).

[15] G. Blanpied *et al.*, Phys. Rev. Lett. **79**, 4337 (1997).

[16] K. Joo *et al.*, Phys. Rev. Lett. **88**, 122001 (2002).

[17] C. Mertz *et al.*, Phys. Rev. Lett. **86**, 2963 (2001).

[18] T. Sato and T. S. H. Lee, Phys. Rev. C **54**, 2660 (1996).

[19] D. Drechsel *et al.*, Nucl. Phys. A **645**, 145 (1999).

[20] R.A. Arndt, W.J. Briscoe, I.I. Strakovsky, R.L. Workman, Phys. Rev. C **66**, 055213 (2002).

[21] B. L. Ioffe, Nucl. Phys. **B188**, 317 (1981); Z. Phys. C **18**, 67 (1983).

[22] J. Pasupathy, J.P. Singh, S.L. Wilson, and C.B. Chiu, Phys. Rev. **D36** , 1442 (1986).

[23] S.L. Wilson, J. Pasupathy, C.B. Chiu, Phys. Rev. **D36** , 1451 (1987).

[24] D.B. Leinweber, Ann. of Phys. (N.Y.) **198**, 203 (1990).

[25] J. Marrow, J. Parker, and G. Shaw, Z. Phys. C **37**, 209 (1987).

[26] R.A. Bertlmann *et al.*, Z. Phys. C **39**, 231 (1988).

[27] S. Narison, Phys. Lett. **B361**, 121 (1995).

[28] L.J. Reinders, H. Rubinstein and S. Yazaki, Phys. Rep. **127**, 1-97 (1985).

[29] V.M. Belyaev and B.L. Ioffe, Sov. Phys. JETP **57**, 716 (1983).

[30] C.B. Chiu, J. Pasupathy, S.L. Wilson, Phys. Rev. **D33** , 1961 (1986).

[31] S. Zhu, W. Hwang and Z. Yang, Phys. Rev. **D57**, 1527 (1998).

[32] I.I. Balitsky and A.V. Yung Phys. Lett. **B129**, 328 (1983).

[33] B.L. Ioffe and A.V. Smilga, Phys. Lett. **B133**, 436 (1983);

[34] F.X. Lee, Phys. Rev. **D57**, 1801 (1998).

[35] F.X. Lee, Phys. Lett. **B419**, 14 (1998).

[36] J. Dey, M. Dey and A. Iqubal, Phys. Lett. **B477**, 125 (2000).

[37] M. Sinha, A. Iqubal, M. Dey and J. Dey, Phys. Lett. **B610**, 283 (2005).

[38] A. Samsonov, Phys. Atom. Nucl. **68**, 114 (2005).

[39] D.B. Leinweber, Ann. of Phys. (N.Y.) **254**, 328 (1997).

[40] S. Coleman and S. Glashow, Phys. Rev. Lett. **6**, 423 (1961).

[41] P. Ball, V. M. Braun and N. Kivel, Nucl. Phys. B **649**, 263 (2003).

[42] J. Rohrwild, JHEP **0709**, 073 (2007).

[43] D. B. Leinweber, Phys. Rev. **D43**, 1659, (1991).

[44] H. J. Lipkin, Phys. Rev. **D24**, 1437 (1981).

[45] J. Franklin, Phys. Rev. **182**, 1607 (1969).

[46] J. Franklin, Phys. Rev. **D29**, 2648 (1984).

[47] R. G. Sachs, Phys. Rev. **D23**, 1148 (1981).

[48] J. Franklin, Phys. Rev. **D20**, 1742 (1979).

[49] D.B.Leinweber, Phys. Rev. D **45**, 252 (1992).

[50] D. H. Perkins, *Introduction to High Energy Physics* (Cambridge, 4th ed., 2000).

[51] F. X. Lee, Phys. Rev. C **57**, 322 (1998).

[52] S. Narison Phys. Lett. **B666** 455 (2008).

[53] J.W.Darewych, M. Horbatsch, and R. Koniuk, Phys. Rev. D **28**, 1125 (1983).

[54] J. Rohrwild, Phys. Rev. D **75**, 074025 (2007).

[55] H.R. Grigoryan, T.-S.H. Lee, H.-U. Yee, arXiv:0904.3710 [hep-ph].

[56] M. Chemtob, Nucl. Phys.**B256**, 600 (1985).

[57] J.Kunz and P.J. Mulders, Phys. Rev. D **41**, 1578 (1990).

[58] G.S.Adkins, C.R.Nappi, and E.Witten, Nucl. Phys.**B288**, 552 (1983).

[59] T.D.Cohen and W.Broniowski, Phys. Rev. D **34**, 3472 (1986).

[60] J. Franklin, Phys. Rev. D **66**, 033010 (2002).

[61] A.Mitra and A.Mittal, Phys. Rev. D **29**, 1399 (1984).

[62] H.Guiasu and R.Koniuk, Phys. Rev. D **36**, 2757 (1987).

[63] S.Capstick, Phys. Rev. D **46**, 1965 (1992).

[64] G. Kalbermann and J.M. Eisenberg, Phys. Rev. D **28**, 71 (1983).

[65] J.F.Donoghue, E.Golowich, and B.R.Holstein, Phys. Rev. D **12**, 2875 (1975).

[66] FeynCalc is freely available. See details at www.feyncalc.org.

Appendix A

QCD Sum Rules for $N\gamma \to \Delta$ Transitions

In $N\gamma \to \Delta$ Transitions, we identified 12 independent Dirac structures defined in Eq.(5.10). We have listed the 3 sum rules at structures we made detail analysis: chiral-even WE_1, chiral-even WE_6 and chiral-odd WO_2 structures in Chap. 5. Here we write out the other 9 structures. We only need to list the coefficients for the in the transition channels: $\Sigma^+\gamma \to \Sigma^{*+}$, $\Xi^0\gamma \to \Xi^{*0}$ and $\Lambda\gamma \to \Sigma^{*0}$. All other coefficients can be derived from them.

At chiral-even structure WE_2, the sum rule is:

$$c_1 L^{-4/27} E_2(w) M^4 + c_2 \chi a m_s L^{-20/27} E_1(w) M^2 + c_3 a m_s L^{-4/27} E_0(w) + c_4 \chi a^2 L^{4/27} E_0(w) + c_5 b L^{-4/27} E_0(w) + c_6 m_0^2 a m_s L^{-18/27} \frac{1}{M^2} + c_7 a^2 L^{20/27} \frac{1}{M^2} + c_8 \chi m_0^2 a^2 L^{-10/27} \frac{1}{M^2} + c_9 m_0^2 a^2 L^{6/27} \frac{1}{M^4} = \tilde{\lambda}_N \tilde{\lambda}_\Delta e^{-\bar{m}^2/M^2} [\frac{1}{3M^2} G_1 \frac{1}{M_\Delta} (-\bar{m}^2 - 2M_\Delta^2 - m_N M_\Delta) + A]. \tag{A.1}$$

The coefficients are given by, in the transition channel $\Sigma^+\gamma \to \Sigma^{*+}$,

$$c_1 = -\frac{3}{8}(-1+\beta)(e_s - e_u),$$

$$
\begin{aligned}
c_2 &= \frac{1}{6}(1+5\beta)(e_u - e_s f_s \phi),\\
c_3 &= \frac{1}{8}(e_u(2(3+f_s+\kappa)+\xi+\beta(2-2f_s+2\kappa+\xi))\\
&\quad -e_s(4+f_s(4+2\kappa\phi+\phi\xi)+\beta(-4+f_s(4+2\kappa\phi+\phi\xi)))),\\
c_4 &= \frac{1}{3}(e_u(f_s+\beta(-1+2f_s))-(1+\beta)e_s f_s\phi),\\
c_5 &= \frac{1}{96}(-1+\beta)(e_s-e_u),\\
c_6 &= -\frac{1}{24}(-1+\beta)(2e_s - e_u(1+f_s)),\\
c_7 &= \frac{1}{36}(f_s(e_u(8+4\kappa+\xi)-e_s(8+4\kappa\phi+\phi\xi))\\
&\quad +\beta(2e_u(-3+5f_s)(2+\kappa)+e_u f_s\xi - e_s f_s(8+4\kappa\phi+\phi\xi))),\\
c_8 &= \frac{1}{72}(-e_u(2+6f_s+\beta(-2+9f_s))+(8+7\beta)e_s f_s\phi),\\
c_9 &= \frac{1}{216}(7(1+\beta)e_s f_s - e_u(2+5f_s+\beta(-4+11f_s))).
\end{aligned}
\tag{A.2}
$$

in the transition channel $\Xi^0\gamma \to \Xi^{*0}$,

$$
\begin{aligned}
c_1 &= \frac{3}{16}(-1+\beta)(e_s-e_u),\\
c_2 &= -\frac{1}{12}(1+5\beta)(e_u - e_s f_s\phi),\\
c_3 &= \frac{1}{16}(e_u(-4-4f_s-6\kappa+\beta(-4+4f_s-6\kappa-\xi)-\xi)\\
&\quad +e_s(6+f_s(2+6\kappa\phi+\phi\xi)+\beta(10+f_s(-10+6\kappa\phi+\phi\xi)))),\\
c_4 &= -\frac{1}{6}f_s((1+\beta)e_u+e_s(-1+\beta(-3+2f_s))\phi),\\
c_5 &= \frac{1}{192}(-1+\beta)(e_s-e_u),\\
c_6 &= \frac{1}{48}((7+5\beta)e_s - 2(-1+\beta)e_u)(-1+f_s),\\
c_7 &= \frac{1}{72}((1+\beta)e_u(-12\kappa+f_s(-8+2\kappa-\xi)+e_s(12+12f_s\kappa\phi+f_s^2(-4-2\kappa\phi\\
&\quad +\phi\xi)+\beta(12+2f_s(8+10\kappa\phi+\phi\xi)-f_s^2(20+10\kappa\phi+\phi\xi)))),\\
c_8 &= \frac{1}{144}(e_u(-2+9f_s+\beta(-2+11f_s))+e_s f_s(-5-11\beta+2(-1+\beta)f_s)\phi),\\
c_9 &= \frac{1}{432}f_s(9(1+\beta)e_u+e_s(-8-f_s+\beta(-14+5f_s))),
\end{aligned}
\tag{A.3}
$$

and in the transition channel $\Lambda\gamma \to \Sigma^{*0}$,

$$
c_1 = \frac{1}{16}(3(2+\beta)e_d - 4e_s - 3(2+\beta)e_u),
$$

$$
\begin{aligned}
c_2 &= \frac{1}{12}(5(-1+\beta)e_d + (2-5\beta)e_u - 3e_s f_s \phi),\\
c_3 &= \frac{1}{48}(3e_u(4(3+f_s+\kappa) + \beta(-2+2f_s-2\kappa-\xi)+2\xi)\\
&\quad -3e_d(16+4f_s+6\kappa+\beta(-2+2f_s-2\kappa-\xi)+3\xi) + e_s(24+f_s(-4-2\kappa\phi+\phi\xi))),\\
c_4 &= \frac{1}{6}(e_d(-2+\beta-f_s) + e_u(1-\beta+f_s)),\\
c_5 &= \frac{1}{384}(-8e_d - 3\beta e_d - 12e_s - \beta e_u),\\
c_6 &= \frac{1}{48}(2e_s + (3+\beta)e_d(1+f_s) - (1+\beta)e_u(1+f_s)),\\
c_7 &= \frac{1}{72}(-2(-2+\beta)e_u(1+f_s)(2+\kappa) + 2e_d(-4+\beta\\
&\quad +(-2+\beta)f_s)(2+\kappa) + e_u(1+\beta(-2+f_s)+f_s)\xi\\
&\quad -e_d(2+\beta(-2+f_s)+f_s)\xi + e_s f_s(-4-2\kappa\phi+\phi\xi)),\\
c_8 &= \frac{1}{288}(2(3(5-3\beta)e_d + 7(-1+\beta)e_u) + (16+3\beta)(e_d-e_u)f_s),\\
c_9 &= \frac{1}{432}(e_u(-7+2\beta+5(-1+\beta)f_s) + e_d(13+3f_s-\beta(2+5f_s))).
\end{aligned}
\tag{A.4}
$$

At chiral-even structure WE_3, the sum rule is:

$$
\begin{aligned}
&c_1 L^{-4/27}E_2(w)M^4 + c_2\chi a m_s L^{-20/27}E_1(w)M^2 + c_3 a m_s L^{-4/27}E_0(w) + c_4\chi a^2 L^{4/27}E_0(w)\\
&+c_5 b L^{-4/27}E_0(w) + c_6 m_0^2 a m_s L^{-18/27}\tfrac{1}{M^2} + c_7 a^2 L^{20/27}\tfrac{1}{M^2} + c_8\chi m_0^2 a^2 L^{-10/27}\tfrac{1}{M^2}\\
&+c_9 m_0^2 a^2 L^{6/27}\tfrac{1}{M^4} = \tilde{\lambda}_N\tilde{\lambda}_\Delta e^{-\bar{m}^2/M^2}[\tfrac{1}{3M^2}G_1(M_\Delta+m_N) + A].
\end{aligned}
\tag{A.5}
$$

The coefficients are given by, in the transition channel $\Sigma^+\gamma \to \Sigma^{*+}$,

$$
\begin{aligned}
c_1 &= \frac{1}{8}(-1+\beta)(e_s-e_u),\\
c_2 &= -\frac{1}{6}(-1+\beta)(e_u - e_s f_s\phi),\\
c_3 &= \frac{1}{24}(2e_u(-1-3f_s+\kappa+\beta(5+3f_s+\kappa))\\
&\quad -2e_s(2(-3+f_s+\beta(3+f_s)) + (1+\beta)f_s\kappa\phi) - (1+\beta)e_u\xi + (1+\beta)e_s f_s\phi\xi),\\
c_4 &= \frac{2}{3}\beta e_u(-1+f_s),\\
c_5 &= -\frac{1}{32}(-1+\beta)(e_s-e_u),\\
c_6 &= \frac{1}{8}(-1+\beta)(2e_s - e_u(1+f_s)),\\
c_7 &= \frac{1}{36}(f_s(e_u(4+2\kappa-\xi) + e_s(-4-2\kappa\phi+\phi\xi))\\
&\quad +\beta(2e_u(-4+5f_s)(2+\kappa) + e_u(-2+f_s)\xi + e_s f_s(-4-2\kappa\phi+\phi\xi))),\\
c_8 &= \frac{1}{36}(-2\beta e_u(-1+f_s) + f_s(e_u - e_s\phi)),
\end{aligned}
$$

$$c_9 = \frac{1}{216}(7(1+\beta)e_s f_s - e_u(2+5f_s+\beta(-4+11f_s))). \tag{A.6}$$

in the transition channel $\Xi^0\gamma \to \Xi^{*0}$,

$$\begin{aligned}
c_1 &= -\frac{1}{16}(-1+\beta)(e_s-e_u),\\
c_2 &= \frac{1}{12}(-1+\beta)(e_u - e_s f_s \phi),\\
c_3 &= \frac{1}{48}(e_u(-4+12f_s+22\kappa+\xi+\beta(-4-12f_s+22\kappa+\xi))\\
&\quad -e_s(30+f_s(-22+22\kappa\phi+\phi\xi)+\beta(66+f_s(-82+22\kappa\phi+\phi\xi)))),\\
c_4 &= -\frac{1}{3}(1+\beta)e_s(-1+f_s)f_s\phi,\\
c_5 &= -\frac{1}{192}(-1+\beta)(e_s-e_u),\\
c_6 &= \frac{1}{48}(e_s(15+\beta(9-11f_s)-13f_s)+2(-1+\beta)e_u(-2+3f_s)),\\
c_7 &= \frac{1}{72}(-(1+\beta)e_u(-24\kappa+f_s(4+14\kappa-\xi))\\
&\quad -e_s(24+f_s(-40+4\kappa\phi-2\phi\xi+3f_s(4+2\kappa\phi+\phi\xi))\\
&\quad +\beta(24+f_s(-48+f_s(20+10\kappa\phi+\phi\xi))))),\\
c_8 &= \frac{1}{72}(2e_u(1+\beta-\beta f_s)+e_s f_s(-3+3\beta(-1+f_s)+f_s)\phi),\\
c_9 &= \frac{1}{432}f_s(9(1+\beta)e_u+e_s(-8-f_s+\beta(-14+5f_s))),
\end{aligned} \tag{A.7}$$

and in the transition channel $\Lambda\gamma \to \Sigma^{*0}$,

$$\begin{aligned}
c_1 &= \frac{1}{16}(-(2+\beta)e_d+8e_s+(2+\beta)e_u),\\
c_2 &= -\frac{1}{12}(2+\beta)(e_d-e_u),\\
c_3 &= \frac{1}{48}(\beta(e_d-e_u)(10+6f_s+2\kappa-\xi)+3e_d(4f_s-2\kappa+\xi)\\
&\quad -2e_u(2+6f_s-2\kappa+\xi)-e_s(48+f_s(20+10\kappa\phi+7\phi\xi))),\\
c_4 &= \frac{1}{3}(\beta(e_d-e_u)(-1+f_s)-e_s f_s\phi),\\
c_5 &= \frac{1}{384}((20+7\beta)e_d+24e_s-(4+3\beta)e_u),\\
c_6 &= \frac{1}{96}(-8e_s-(16+7\beta)e_d(1+f_s)+(8+3\beta)e_u(1+f_s)),\\
c_7 &= \frac{1}{72}(2e_d(-2-f_s+\beta(-2+3f_s))(2+\kappa)+e_d(2+f_s\\
&\quad +\beta(-4+3f_s))\xi-3e_s f_s(4+2\kappa\phi+\phi\xi)+e_u((1\\
&\quad +f_s)(4+2\kappa-\xi)+\beta(4(2+\kappa+\xi)-3f_s(4+2\kappa+\xi)))),
\end{aligned}$$

$$c_8 = \frac{1}{72}(3e_u(2\beta(-1+f_s)+f_s) - e_d(2+6\beta(-1+f_s)+5f_s)),$$
$$c_9 = \frac{1}{432}(e_u(-7+2\beta+5(-1+\beta)f_s) + e_d(13+3f_s-\beta(2+5f_s))). \quad \text{(A.8)}$$

At chiral-even structure WE_4, the sum rule is:

$$\begin{aligned}
&c_1 L^{-4/27} E_2(w) M^4 + c_2 \chi a m_s L^{-20/27} E_1(w) M^2 + c_3 a m_s L^{-4/27} E_0(w) \\
&+c_4 \chi a^2 L^{4/27} E_0(w) + c_5 b L^{-4/27} E_0(w) + c_6 m_0^2 a m_s L^{-18/27} \tfrac{1}{M^2} + c_7 a^2 L^{20/27} \tfrac{1}{M^2} \\
&+c_8 \chi m_0^2 a^2 L^{-10/27} \tfrac{1}{M^2} + c_9 m_0^2 a^2 L^{6/27} \tfrac{1}{M^4} \\
&= \tilde{\lambda}_N \tilde{\lambda}_\Delta e^{-\bar{m}^2/M^2} [\tfrac{1}{3M^2}(-G_1 \tfrac{1}{M_\Delta}(-\bar{m}^2 - 4M_\Delta^2 - m_N M_\Delta) + G_2(-\bar{m}^2 - M_\Delta m_N)) + A].
\end{aligned} \quad \text{(A.9)}$$

The coefficients are given by, in the transition channel $\Sigma^+\gamma \to \Sigma^{*+}$,

$$\begin{aligned}
c_1 &= \frac{5}{8}(-1+\beta)(e_s - e_u), \\
c_2 &= -\frac{1}{6}(5+13\beta)(e_u - e_s f_s \phi), \\
c_3 &= \frac{1}{24}(e_u(6f_s - 2\kappa + 3\beta(-6+6f_s-6\kappa-\xi) - 11(2+\xi)) \\
&\quad + e_s(-12 + f_s(28 + 2\kappa\phi + 11\phi\xi) + 3\beta(-12 + f_s(12 + 6\kappa\phi + \phi\xi)))), \\
c_4 &= -\frac{1}{3}(1+\beta)(e_u + 2e_u f_s - 3e_s f_s \phi), \\
c_5 &= -\frac{1}{32}(-1+\beta)(e_s - e_u), \\
c_6 &= \frac{1}{24}(1+5\beta)(2e_s - e_u(1+f_s)), \\
c_7 &= \frac{1}{36}(-e_u(2\beta(3+f_s)(2+\kappa) + 2(-1+f_s)(-2+5\kappa) \\
&\quad + \beta(-3+5f_s)\xi + (-1+7f_s)\xi) + 2e_s(-6 + f_s(6 + 4\beta(2+\kappa\phi) + (3+\beta)\phi\xi))), \\
c_8 &= \frac{1}{72}(e_u(9 + 7\beta + 14(1+\beta)f_s) - (23+21\beta)e_s f_s \phi), \\
c_9 &= \frac{1}{216}(7(1+\beta)e_s f_s - e_u(2 + 5f_s + \beta(-4+11f_s))).
\end{aligned} \quad \text{(A.10)}$$

in the transition channel $\Xi^0\gamma \to \Xi^{*0}$,

$$\begin{aligned}
c_1 &= -\frac{5}{16}(-1+\beta)(e_s - e_u), \\
c_2 &= \frac{2}{3}(1+2\beta)(e_u - e_s f_s \phi), \\
c_3 &= \frac{1}{48}(e_u(44 - 12f_s + 22\kappa + \xi + \beta(92 - 36f_s + 22\kappa + \xi)) \\
&\quad - e_s(6 + f_s(26 + 22\kappa\phi + \phi\xi) + \beta(42 + f_s(14 + 22\kappa\phi + \phi\xi)))), \\
c_4 &= \frac{1}{3}(1+\beta)f_s(2e_u - e_s(1+f_s)\phi),
\end{aligned}$$

$$
\begin{aligned}
c_5 &= \frac{1}{192}(-1+\beta)(e_s-e_u),\\
c_6 &= \frac{1}{48}(e_s(5+7\beta-3(3+\beta)f_s)+2e_u(1+f_s+\beta(-7+5f_s))),\\
c_7 &= \frac{1}{72}(e_u(-12(1+\beta)f_s^2+6(1+\beta)(2\kappa-\xi)\\
&\quad +f_s(20-2\kappa+7\xi+\beta(44-2\kappa+7\xi)))\\
&\quad +e_s(-12+3f_s^2(-4+2\kappa\phi+\phi\xi)-4f_s(-4+4\kappa\phi+\phi\xi)\\
&\quad +\beta(-12-6f_s\phi(2\kappa+\xi)+f_s^2(-20+2\kappa\phi+5\phi\xi)))),\\
c_8 &= \frac{1}{72}f_s(-2(7+8\beta)e_u+e_s(7+7\beta+7f_s+9\beta f_s)\phi),\\
c_9 &= \frac{1}{432}f_s(9(1+\beta)e_u+e_s(-8-f_s+\beta(-14+5f_s))),
\end{aligned}
\tag{A.11}
$$

and in the transition channel $\Lambda\gamma \to \Sigma^{*0}$,

$$
\begin{aligned}
c_1 &= \frac{1}{16}(-5(2+\beta)e_d+4e_s+5(2+\beta)e_u),\\
c_2 &= \frac{1}{12}(-13(-1+\beta)(e_d-e_u)+3e_sf_s\phi),\\
c_3 &= \frac{1}{48}(3e_d(8-12f_s+2\kappa+\beta(-6+6f_s-6\kappa-\xi)+11\xi)\\
&\quad -3e_u(\beta(-6+6f_s-6\kappa-\xi)+4(5-f_s+\xi))+e_s(-24+f_s(4+14\kappa\phi+5\phi\xi))),\\
c_4 &= \frac{1}{6}(e_u(-3+3\beta-4f_s)+e_d(5-3\beta+2f_s)),\\
c_5 &= \frac{1}{384}((16+7\beta)e_d+12e_s-(8+3\beta)e_u),\\
c_6 &= \frac{1}{96}(-4e_s-(-14+11\beta)e_d(1+f_s)+(-6+7\beta)e_u(1+f_s)),\\
c_7 &= \frac{1}{72}(3e_sf_s\phi(2\kappa+\xi)-e_d(-10(2+\kappa)+2\beta(3+f_s)(2+\kappa)\\
&\quad +f_s(32+10\kappa-5\xi)-13\xi+\beta(9-7f_s)\xi)+e_u(2\beta(3+f_s)\\
&\quad (2+\kappa)+f_s(4+8\kappa-\xi)+\beta(9-7f_s)\xi-6(2+\kappa+\xi))),\\
c_8 &= \frac{1}{144}(-e_d(35+\beta(-23+f_s)+18f_s)+e_u(23+\beta(-19+f_s)+28f_s)),\\
c_9 &= \frac{1}{432}(e_u(-7+2\beta+5(-1+\beta)f_s)+e_d(13+3f_s-\beta(2+5f_s))).
\end{aligned}
\tag{A.12}
$$

At chiral-even structure WE_5, the sum rule is:

$$
\begin{aligned}
&c_1L^{-4/27}E_1(w)M^2+c_2\chi am_sL^{-20/27}E_0(w)+c_3bL^{-4/27}\tfrac{1}{M^2}+c_4am_sL^{-4/27}\tfrac{1}{M^2}\\
&+c_5a^2L^{20/27}E_2(w)\tfrac{1}{M^4}+c_6m_0^2am_sL^{-18/27}\tfrac{1}{M^4}+c_7m_0^2a^2L^{6/27}\tfrac{1}{M^6}\\
&=\tilde{\lambda}_N\tilde{\lambda}_\Delta e^{-\bar{m}^2/M^2}[\tfrac{1}{3M^2}(-2G_1\tfrac{1}{M_\Delta^2}m_N+G_2\tfrac{1}{M_\Delta}(-m_N+M_\Delta))+A].
\end{aligned}
\tag{A.13}
$$

The coefficients are given by, in the transition channel $\Sigma^+\gamma \to \Sigma^{*+}$,

$$
\begin{aligned}
c_1 &= -\frac{1}{4}(-1+\beta)(e_s - e_u),\\
c_2 &= \frac{1}{3}(-1+\beta)(e_u - e_s f_s \phi),\\
c_3 &= -\frac{1}{48}(-1+\beta)(e_s - e_u),\\
c_4 &= \frac{1}{12}(e_s(4(-3+f_s+\beta(3+f_s)) + 2(1+\beta)f_s\kappa\phi - (1+\beta)\\
&\quad f_s\phi\xi) + e_u(2+6f_s - 2\kappa + \xi + \beta(-2(5+3f_s+\kappa)+\xi))),\\
c_5 &= \frac{1}{18}(f_s(e_u(-4-2\kappa+\xi) + e_s(4+2\kappa\phi - \phi\xi))\\
&\quad +\beta(-e_u(-2+3f_s)(4+2\kappa-\xi) + e_s f_s(4+2\kappa\phi-\phi\xi))),\\
c_6 &= -\frac{1}{12}(-1+\beta)(2e_s - e_u(1+f_s)),\\
c_7 &= \frac{1}{108}(-7(1+\beta)e_s f_s + e_u(2+5f_s+\beta(-4+11f_s))).
\end{aligned}
\tag{A.14}
$$

in the transition channel $\Xi^0\gamma \to \Xi^{*0}$,

$$
\begin{aligned}
c_1 &= \frac{1}{8}(-1+\beta)(e_s - e_u),\\
c_2 &= -\frac{1}{6}(-1+\beta)(e_u - e_s f_s \phi),\\
c_3 &= \frac{1}{96}(-1+\beta)(e_s - e_u),\\
c_4 &= \frac{1}{24}(2e_u(2-6f_s+\kappa+\beta(2+6f_s+\kappa)) - (1+\beta)e_u\xi\\
&\quad +e_s(2(3+f_s) - 2(\beta(3+5f_s) + (1+\beta)f_s\kappa\phi) + (1+\beta)f_s\phi\xi)),\\
c_5 &= \frac{1}{36}f_s((1+\beta)e_u(4+2\kappa-\xi)\\
&\quad +e_s(-4+(-2+f_s)\phi(2\kappa-\xi) + \beta(-4+3f_s)(4+2\kappa\phi-\phi\xi))),\\
c_6 &= \frac{1}{24}(-1+\beta)(e_s + e_s f_s - 2e_u f_s),\\
c_7 &= \frac{1}{216}f_s(-9(1+\beta)e_u + e_s(8+\beta(14-5f_s)+f_s)),
\end{aligned}
\tag{A.15}
$$

and in the transition channel $\Lambda\gamma \to \Sigma^{*0}$,

$$
\begin{aligned}
c_1 &= \frac{1}{8}(2+\beta)(e_d - e_u),\\
c_2 &= \frac{1}{6}(2+\beta)(e_d - e_u),\\
c_3 &= \frac{1}{192}((4+\beta)e_d - (4+5\beta)e_u),
\end{aligned}
$$

$$
\begin{aligned}
c_4 &= \frac{1}{24}(-\beta(e_d-e_u)(10+6f_s+2\kappa-\xi)-3e_d(4f_s-2\kappa+\xi)\\
&\quad +2e_u(2+6f_s-2\kappa+\xi)+e_sf_s(4+2\kappa\phi-\phi\xi)),\\
c_5 &= \frac{1}{36}(-e_d(-2+(-1+\beta)f_s)(4+2\kappa-\xi)\\
&\quad +e_u(-1+(-1+\beta)f_s)(4+2\kappa-\xi)+e_sf_s(4+2\kappa\phi-\phi\xi)),\\
c_6 &= \frac{1}{48}((4+3\beta)e_d+(-4+\beta)e_u)(1+f_s),\\
c_7 &= \frac{1}{216}(e_u(7+5f_s-\beta(2+5f_s))+e_d(-13-3f_s+\beta(2+5f_s))).
\end{aligned}
\tag{A.16}
$$

At structure WO_1, the sum rule is:

$$
\begin{aligned}
&c_1m_sL^{-16/27}E_2(w)M^4+c_2\chi aL^{-8/27}E_2(w)M^4+c_3aL^{8/27}E_1(w)M^2+c_4m_0^2aL^{-6/27}\\
&E_0(w)+c_5\chi a^2m_sL^{-8/27}E_0(w)+c_6\chi abL^{-8/27}E_0(w)+c_7a^2m_sL^{8/27}\tfrac{1}{M^2}+c_8abL^{8/27}\tfrac{1}{M^2}\\
&=\tilde{\lambda}_N\tilde{\lambda}_\Delta e^{-\bar{m}^2/M^2}[-\tfrac{2}{3M^2}G_1(-\bar{m}^2+M_\Delta m_N)+A].
\end{aligned}
\tag{A.17}
$$

The coefficients are given by, in the transition channel $\Sigma^+\gamma\to\Sigma^{*+}$,

$$
\begin{aligned}
c_1 &= \frac{1}{2}(1+\beta)(e_s-e_u),\\
c_2 &= -\frac{1}{12}\beta(e_u-e_sf_s\phi),\\
c_3 &= \frac{1}{48}(4e_u(-4+3f_s+\kappa)-5e_u\xi+e_sf_s(4-4\kappa\phi+5\phi\xi)\\
&\quad +2\beta(e_u(-16+6f_s+\kappa+\xi)-e_s(-1+f_s(-4+\phi(\kappa+\xi))))),\\
c_4 &= \frac{1}{24}(7e_s-e_u(1+2\beta(-1+f_s)+6f_s)),\\
c_5 &= \frac{1}{12}(e_u(4+8f_s+\beta(-5+3f_s))+2(-6+\beta)e_sf_s\phi),\\
c_6 &= \frac{1}{288}(-1+4\beta)(e_u-e_sf_s\phi),\\
c_7 &= \frac{1}{144}(e_u(20-2(7+3\beta)\kappa-2f_s(14-8\kappa+\beta(6+6\kappa-3\xi)-5\xi)+\xi-3\beta\xi)\\
&\quad +e_s(48+3\beta(4+f_s\phi(6\kappa-\xi))-f_s(40+2\kappa\phi+11\phi\xi))),\\
c_8 &= \frac{1}{576}(-(14+3\beta)e_s+e_u(6+\beta(9-6f_s)+8f_s)).
\end{aligned}
\tag{A.18}
$$

in the transition channel $\Xi^0\gamma\to\Xi^{*0}$,

$$
\begin{aligned}
c_1 &= -\frac{1}{8}(1+3\beta)(e_s-e_u),\\
c_2 &= \frac{1}{12}\beta(e_u-e_sf_s\phi),\\
c_3 &= \frac{1}{96}(e_u(-12(f_s+\kappa)+\beta(8+12f_s-8\kappa-5\xi)+9\xi)\\
&\quad +e_s(3(8+f_s(-4+4\kappa\phi-3\phi\xi))+\beta(24+f_s(-44+8\kappa\phi+5\phi\xi)))),
\end{aligned}
$$

$$
\begin{aligned}
c_4 &= \frac{1}{96}(e_u(-2+\beta(12-7f_s)+21f_s)+e_s(-14-5f_s+\beta(-12+7f_s))),\\
c_5 &= \frac{1}{24}(2e_u(1-\beta+2(-4+\beta)f_s)+e_sf_s(7+9\beta+7f_s-11\beta f_s)\phi),\\
c_6 &= -\frac{1}{288}(-1+4\beta)(e_u-e_sf_s\phi),\\
c_7 &= \frac{1}{144}(e_u(8-8\kappa+6f_s(-4+5f_s+\kappa)+\xi-9f_s\xi+\beta(8+4\kappa\\
&\quad +3f_s(6+2\kappa-\xi)+7\xi))-2e_s(-12+f_s(24-5f_s-6\kappa\phi+5f_s\kappa\phi-(3+f_s)\phi\xi\\
&\quad +\beta(13+(4+f_s)\kappa\phi+(1+f_s)\phi\xi)))),\\
c_8 &= \frac{1}{1152}(e_u(4-17f_s+\beta(-12+5f_s))+e_s(10+3f_s+\beta(-2+9f_s))).
\end{aligned}
\tag{A.19}
$$

and in the transition channel $\Lambda\gamma \to \Sigma^{*0}$,

$$
\begin{aligned}
c_1 &= \frac{1}{8}(-2(-4+\beta)e_d-e_s+(-7+2\beta)e_u),\\
c_2 &= \frac{1}{24}(-(2+\beta)e_d+(4+\beta)e_u+3e_sf_s\phi),\\
c_3 &= \frac{1}{96}(3e_sf_s(4+2\kappa\phi+\phi\xi)+2e_u(\beta(4+6f_s-\kappa-\xi)\\
&\quad -3(4+\xi))+2e_d(20+4\kappa+\xi+\beta(-4-6f_s+\kappa+\xi))),\\
c_4 &= \frac{1}{192}(e_d(6+\beta(23-22f_s)+28f_s)+e_u(10-28f_s+\beta(-23+26f_s))),\\
c_5 &= \frac{1}{24}(e_u(2+\beta(5-3f_s)+8f_s)+e_d(-8-5\beta+3(-4+\beta)f_s)),\\
c_6 &= \frac{1}{576}(e_d+4\beta e_d-(3+4\beta)e_u+3e_sf_s\phi),\\
c_7 &= \frac{1}{288}(e_u(20+(-2+42\beta)\kappa+7\xi-3\beta\xi+4f_s(\beta(3-6\kappa)-2(5+\kappa)+\xi))\\
&\quad +e_d(-44+(2-42\beta)\kappa+(-7+3\beta)\xi+2f_s(20-8\kappa+6\beta(-1+2\kappa)+\xi))\\
&\quad -2e_s(12+f_s(4+2\kappa\phi-\phi\xi))),\\
c_8 &= \frac{1}{2304}(-16e_s+e_u(12+17\beta-26(-1+\beta)f_s)\\
&\quad +e_d(-28-30f_s+\beta(-17+22f_s))).
\end{aligned}
\tag{A.20}
$$

At structure WO_3, the sum rule is:

$$
\begin{aligned}
&c_1m_sL^{-16/27}E_2(w)M^4+c_2\chi aL^{-8/27}E_2(w)M^4+c_3aL^{8/27}E_1(w)M^2+c_4m_0^2aL^{-6/27}E_0(w)\\
&+c_5\chi a^2m_sL^{-8/27}E_0(w)+c_6\chi abL^{-8/27}E_0(w)+c_7a^2m_sL^{8/27}\tfrac{1}{M^2}+c_8abL^{8/27}\tfrac{1}{M^2}\\
&=-\tilde{\lambda}_N\tilde{\lambda}_\Delta e^{-\bar{m}^2/M^2}[\tfrac{1}{3M^2}G_1(-\bar{m}^2+M_\Delta m_N)+A].
\end{aligned}
\tag{A.21}
$$

The coefficients are given by, in the transition channel $\Sigma^+\gamma \to \Sigma^{*+}$,

$$c_1 = -e_s+e_u,$$

$$
\begin{aligned}
c_2 &= \frac{1}{3}(-e_u + e_s f_s \phi),\\
c_3 &= \frac{1}{6}(e_u(-2 + 6f_s + 2\kappa - \xi) + e_s(-6 + f_s(2 - 2\kappa\phi + \phi\xi))),\\
c_4 &= \frac{1}{12}(7e_s - e_u(1 + 2\beta(-1 + f_s) + 6f_s)),\\
c_5 &= \frac{1}{3}(e_u(1 + 2\beta(-1 + f_s) + 3f_s) - 4e_s f_s \phi),\\
c_6 &= \frac{1}{72}\beta(e_u - e_s f_s \phi),\\
c_7 &= \frac{1}{18}(e_s(6 + f_s(-4 + \phi(\kappa + 6\beta\kappa - 2\xi)))\\
&\quad + e_u(2 - 2\kappa + \xi + f_s(-4 + \kappa - 6\beta\kappa + \xi))),\\
c_8 &= \frac{1}{72}(-2e_s + e_u(1 - 2\beta(-1 + f_s) + f_s)).
\end{aligned}
\tag{A.22}
$$

in the transition channel $\Xi^0\gamma \to \Xi^{*0}$,

$$
\begin{aligned}
c_1 &= \frac{1}{4}(3 + \beta)(e_s - e_u),\\
c_2 &= -\frac{1}{6}(-1 + \beta)(e_u - e_s f_s \phi),\\
c_3 &= \frac{1}{48}(e_u(4 - 36f_s - 22\kappa + 3\beta(-12 + 4f_s - 2\kappa - \xi) + 5\xi)\\
&\quad + e_s(48 + f_s(-16 + 22\kappa\phi - 5\phi\xi) + 3\beta(8 + f_s\phi(2\kappa + \xi)))),\\
c_4 &= \frac{1}{48}(e_u(-2 + \beta(12 - 7f_s) + 21f_s) + e_s(-14 - 5f_s + \beta(-12 + 7f_s))),\\
c_5 &= \frac{1}{6}(e_u(1 - \beta + 2(-3 + \beta)f_s) + e_s f_s(2 + \beta(6 - 7f_s) + 3f_s)\phi),\\
c_6 &= -\frac{1}{144}(1 + 3\beta)(e_u - e_s f_s \phi),\\
c_7 &= \frac{1}{72}(4(2 + \beta)e_u + e_u(2(-7 + \beta)\kappa + \xi + 5\beta\xi + 2f_s(3 + 7\beta + 6\kappa + 8\beta\kappa\\
&\quad -(3 + \beta)\xi)) + e_s(36 - 3(1 + \beta)f_s^2\phi(2\kappa - \xi) - 2f_s(25 - \phi(4\kappa + \xi)\\
&\quad + 3\beta(3 + 2\kappa\phi + \phi\xi)))),\\
c_8 &= \frac{1}{576}(e_u(6 - 9f_s + \beta(-8 + 7f_s)) + e_s(4 - f_s + \beta(-6 + 7f_s))),
\end{aligned}
\tag{A.23}
$$

and in the transition channel $\Lambda\gamma \to \Sigma^{*0}$,

$$
\begin{aligned}
c_1 &= \frac{1}{4}(-2e_d - 3e_s + e_u),\\
c_2 &= \frac{1}{6}(e_d + 3e_s f_s \phi),\\
c_3 &= \frac{1}{48}(e_u(-8 + 24f_s + 14\kappa - 13\xi) + 3e_d
\end{aligned}
$$

$$
\begin{aligned}
&(4-8f_s+2\kappa+3\xi)+6e_s(-2+f_s(4+2\kappa\phi+\phi\xi))),\\
c_4 &= \frac{1}{96}(e_d(6+\beta(23-22f_s)+28f_s)+e_u(10-28f_s+\beta(-23+26f_s))),\\
c_5 &= \frac{1}{6}(e_d(-1+2\beta(-1+f_s)-3f_s)+e_u(-1-2\beta(-1+f_s)+2f_s)-e_sf_s\phi),\\
c_6 &= \frac{1}{144}((2+\beta)e_d-(1+\beta)e_u+3e_sf_s\phi),\\
c_7 &= \frac{1}{72}(-e_u(2+(7-24\beta)\kappa+f_s(8+\kappa+12\beta\kappa-2\xi)-5\xi)\\
&\quad +6e_d(-1+f_s+2\kappa-4\beta\kappa+(-1+2\beta)f_s\kappa-\xi)-2e_s(9+f_s(4+2\kappa\phi-\phi\xi))),\\
c_8 &= \frac{1}{1152}(-24e_s+e_u(10+15\beta+12f_s-18\beta f_s)\\
&\quad +e_d(-26-20f_s+\beta(-15+14f_s))).
\end{aligned}
\tag{A.24}
$$

At structure WO_4, the sum rule is:

$$
\begin{aligned}
&c_1m_sL^{-16/27}E_1(w)M^2+c_2\chi aL^{-8/27}E_1(w)M^2+c_3aL^{8/27}E_0(w)+c_4m_0^2aL^{-6/27}\tfrac{1}{M^2}\\
&+c_5\chi a^2m_sL^{-8/27}\tfrac{1}{M^2}+c_6\chi abL^{-8/27}\tfrac{1}{M^2}+c_7a^2m_sL^{8/27}\tfrac{1}{M^4}+c_8abL^{8/27}\tfrac{1}{M^4}\\
&=\tilde{\lambda}_N\tilde{\lambda}_\Delta e^{-\bar{m}^2/M^2}[\tfrac{1}{3M^2}(2G_1\tfrac{1}{M_\Delta^2}(-\bar{m}^2+m_NM_\Delta-M_\Delta^2)\\
&\quad +G_2\tfrac{1}{M_\Delta}(-\bar{m}^2-2M_\Delta^2+m_NM_\Delta))+A].
\end{aligned}
\tag{A.25}
$$

The coefficients are given by, in the transition channel $\Sigma^+\gamma\to\Sigma^{*+}$,

$$
\begin{aligned}
c_1 &= -e_s+e_u,\\
c_2 &= \frac{1}{3}(-1+\beta)(e_u-e_sf_s\phi),\\
c_3 &= \frac{1}{12}(e_u(-4+12f_s+4\kappa+2\beta(-2+6f_s+5\kappa-\xi)-5\xi)\\
&\quad +e_s(-12+f_s(4-4\kappa\phi+5\phi\xi+2\beta(-4-5\kappa\phi+\phi\xi)))),\\
c_4 &= \frac{1}{12}(7e_s-e_u(1+2\beta(-1+f_s)+6f_s)),\\
c_5 &= \frac{1}{3}(e_u(1+\beta(-3+f_s)+3f_s)+2(-2+\beta)e_sf_s\phi),\\
c_6 &= \frac{1}{72}(-1+\beta)(e_u-e_sf_s\phi),\\
c_7 &= \frac{1}{36}(e_s(12+2f_s(-4+\kappa\phi+\beta(8+7\kappa\phi))-(7+\beta)f_s\phi\xi)\\
&\quad -e_u(4\kappa+f_s(8-2\kappa-5\xi)-2(2+\xi)+\beta(8+4\kappa-2\xi+f_s(8+10\kappa+\xi)))),\\
c_8 &= \frac{1}{144}(-3e_s+e_u+2\beta e_u-2(-1+\beta)e_uf_s).
\end{aligned}
\tag{A.26}
$$

in the transition channel $\Xi^0\gamma\to\Xi^{*0}$,

$$
c_1=\frac{1}{2}(1+\beta)(e_s-e_u),
$$

$$
\begin{aligned}
c_2 &= -\frac{1}{3}(-1+\beta)(e_u - e_s f_s \phi),\\
c_3 &= \frac{1}{4}(e_u(2-2f_s+2\beta(-3+f_s-\kappa)+\xi)+e_s(2+2\beta(3+f_s(-1+\kappa\phi))\\
&\quad -f_s(2+\phi\xi))),\\
c_4 &= \frac{1}{24}(e_u(-5\beta(-2+f_s)+9f_s)+e_s(-7-2f_s+\beta(-9+4f_s))),\\
c_5 &= \frac{1}{3}(-(1+\beta)e_u+2(-1+\beta)e_u f_s+e_s f_s(2+\beta(2-3f_s)+f_s)\phi),\\
c_6 &= -\frac{1}{72}(-1+\beta)(e_u - e_s f_s \phi),\\
c_7 &= \frac{1}{72}(e_s f_s(4+8\phi(\kappa+\xi)+f_s(8-2\kappa\phi+\phi\xi)+3\beta(-12+2(-4+f_s)\kappa\phi\\
&\quad -f_s\phi\xi))+e_u(f_s(-8+12f_s+2\kappa-7\xi)-2(8+4\kappa+\xi)+\beta(-f_s(-40+12f_s\\
&\quad -14\kappa+\xi)+4(2+\kappa+\xi)))),\\
c_8 &= \frac{1}{288}(e_u(\beta(-2+f_s)-5f_s)+e_s(3+2f_s+\beta(-3+4f_s))),
\end{aligned}
\tag{A.27}
$$

and in the transition channel $\Lambda\gamma \to \Sigma^{*0}$,

$$
\begin{aligned}
c_1 &= -\frac{3e_d}{2}+e_u,\\
c_2 &= \frac{1}{6}((1+\beta)e_d-(3+\beta)e_u),\\
c_3 &= \frac{1}{24}(-2(-1+\beta)e_u(-2+6f_s+5\kappa)+(1+2\beta)e_u\xi+e_s f_s(-4-2\kappa\phi+\phi\xi)\\
&\quad +e_d(2\beta(-2+6f_s+5\kappa-\xi)+3(-4(2+f_s+\kappa)+\xi))),\\
c_4 &= \frac{1}{48}(e_d(20+11\beta+12f_s-10\beta f_s)+e_u(-8-11\beta+2(-8+7\beta)f_s)),\\
c_5 &= \frac{1}{6}(e_d(-5+\beta(-3+f_s)-3f_s)+e_u(5+3\beta+5f_s-\beta f_s)),\\
c_6 &= \frac{1}{144}((1+\beta)e_d-(3+\beta)e_u),\\
c_7 &= \frac{1}{72}(-e_u(-2(8+\kappa)+f_s(8+4\kappa-5\xi)+\xi)+3e_d(2\kappa+f_s(12+2\kappa-3\xi)+\xi)\\
&\quad +2e_s f_s(4+2\kappa\phi-\phi\xi)+\beta(e_d-e_u)(-4(2+4\kappa+\xi)+f_s(-8+2\kappa+5\xi))),\\
c_8 &= \frac{1}{576}(e_u(\beta(3-6f_s)+8f_s)+e_d(-4-3\beta+2(-2+\beta)f_s)).
\end{aligned}
\tag{A.28}
$$

At structure WO_5, the sum rule is:

$$
\begin{aligned}
&c_1 m_s L^{-16/27}E_1(w)M^2+c_2\chi a L^{-8/27}E_1(w)M^2+c_3 a L^{8/27}E_0(w)+c_4 m_0^2 a L^{-6/27}\tfrac{1}{M^2}\\
&+c_5\chi a^2 m_s L^{-8/27}\tfrac{1}{M^2}+c_6\chi ab L^{-8/27}\tfrac{1}{M^2}+c_7 a^2 m_s L^{8/27}\tfrac{1}{M^4}+c_8 ab L^{8/27}\tfrac{1}{M^4}\\
&=-\tilde{\lambda}_N\tilde{\lambda}_\Delta e^{-\bar{m}^2/M^2}[\tfrac{1}{3M^2}(G_1\tfrac{1}{M_\Delta}(m_N+M_\Delta)+G_2(M_\Delta-m_N))+A].
\end{aligned}
\tag{A.29}
$$

The coefficients are given by, in the transition channel $\Sigma^+\gamma \to \Sigma^{*+}$,

$$
\begin{aligned}
c_1 &= \frac{1}{2}(2+\beta)(e_s - e_u),\\
c_2 &= \frac{1}{6}(1+\beta)(e_u - e_s f_s \phi),\\
c_3 &= \frac{1}{24}(-e_u(8+12f_s+4\kappa-5\xi+2\beta(-4+6f_s+\kappa+\xi))\\
&\quad +e_s(24+f_s(-4+4\kappa\phi-5\phi\xi)+2\beta(6+f_s(-4+\phi(\kappa+\xi))))),\\
c_4 &= \frac{1}{24}(-(16+7\beta)e_s + e_u(8+5\beta+2(4+\beta)f_s)),\\
c_5 &= \frac{1}{6}(-e_u(3+\beta+3(1+\beta)f_s)+2(3+2\beta)e_s f_s\phi),\\
c_6 &= -\frac{1}{144}(1+3\beta)(e_u - e_s f_s\phi),\\
c_7 &= \frac{1}{24}(e_u(-4+2(1+\beta)\kappa+\xi+\beta\xi-2f_s(-2+2\kappa+\beta(-2+\xi)+\xi))\\
&\quad +e_s(-8+f_s(8+2\kappa\phi+\phi\xi)+\beta(-4+f_s\phi(-2\kappa+\xi)))),\\
c_8 &= \frac{1}{288}((8+3\beta)e_s + e_u(-4-5\beta+2(-2+\beta)f_s)).
\end{aligned}
\tag{A.30}
$$

in the transition channel $\Xi^0\gamma \to \Xi^{*0}$,

$$
\begin{aligned}
c_1 &= -\frac{1}{2}(1+\beta)(e_s - e_u),\\
c_3 &= \frac{1}{48}(e_u(4+24f_s+2\kappa-7\xi)+e_s f_s(-28-2\kappa\phi+7\phi\xi)\\
&\quad +\beta(e_u(20-2\kappa+7\xi)+e_s(-24+f_s(4+2\kappa\phi-7\phi\xi)))),\\
c_4 &= \frac{1}{24}(e_u(1+\beta(-8+f_s)-8f_s)+e_s(2+5f_s+\beta(5+2f_s))),\\
c_5 &= \frac{1}{6}(e_u(-1+\beta+(3+\beta)f_s)-2e_s f_s(\beta+f_s)\phi),\\
c_6 &= \frac{1}{72}\beta(e_u - e_s f_s\phi),\\
c_7 &= \frac{1}{72}(e_u(-8+2\kappa+\beta(-4-2\kappa+3f_s(-4+\xi)-5\xi)-\xi+3f_s(4-4f_s+\xi))\\
&\quad +e_s(-12-2(3+\beta)f_s(-4+\kappa\phi)+(-3+\beta)f_s\phi\xi\\
&\quad +f_s^2(-4+4\kappa\phi+\phi\xi+\beta(8+4\kappa\phi+\phi\xi)))),\\
c_8 &= \frac{1}{288}(e_u(-1-\beta(-4+f_s)+4f_s)-e_s(2+\beta+f_s+2\beta f_s)),
\end{aligned}
\tag{A.31}
$$

and in the transition channel $\Lambda\gamma \to \Sigma^{*0}$,

$$
\begin{aligned}
c_1 &= \frac{1}{4}(-(-5+\beta)e_d - e_s + (-4+\beta)e_u),\\
c_2 &= \frac{1}{12}((-3+\beta)e_d + e_u - \beta e_u),
\end{aligned}
$$

$$
\begin{aligned}
c_3 &= \frac{1}{48}(2e_u(-3(4+4f_s+3\kappa-2\xi)+\beta(-16+18f_s+\kappa+\xi))-2e_d(-12f_s\\
&\quad -5(2+\kappa)+4\xi+\beta(-16+18f_s+\kappa+\xi))+e_s(-12+f_s(-4-2\kappa\phi+\phi\xi))),\\
c_4 &= \frac{1}{48}(e_u(\beta(13-20f_s)+15(1+f_s))+e_d(-23-17f_s+\beta(-13+20f_s))),\\
c_5 &= \frac{1}{12}(e_d(9+\beta(3-7f_s)+7f_s)+e_u(-5(1+f_s)+\beta(-3+7f_s))-2e_sf_s\phi),\\
c_6 &= \frac{1}{288}(-3(-1+\beta)e_d+(-1+3\beta)e_u),\\
c_7 &= \frac{1}{144}(e_u(-8(2+\kappa)+2f_s(16+6\beta(-1+\kappa)+5\kappa-\xi)-5\xi+3\beta(-6\kappa+\xi))\\
&\quad +e_d(40+2(7+9\beta)\kappa+(5-3\beta)\xi-4f_s(5+3\beta(-1+\kappa)-2\kappa+\xi))\\
&\quad +2e_s(6+f_s(4+2\kappa\phi-\phi\xi))),\\
c_8 &= \frac{1}{576}(4e_s+e_d(11+\beta(5-8f_s)+9f_s)+e_u(-7(1+f_s)+\beta(-5+8f_s))).
\end{aligned}
\tag{A.32}
$$

At structure WO_6, the sum rule is:

$$
\begin{aligned}
&c_1\chi aL^{-8/27}E_1(w)M^2+c_2aL^{8/27}E_0(w)+c_3m_0^2aL^{-6/27}\tfrac{1}{M^2}+c_4\chi a^2m_sL^{-8/27}\tfrac{1}{M^2}\\
&+c_5\chi abL^{-8/27}\tfrac{1}{M^2}+c_6\tfrac{1}{M^4}a^2m_sL^{8/27}+c_7abL^{8/27}\tfrac{1}{M^4}\\
&=\tilde{\lambda}_N\tilde{\lambda}_\Delta e^{-\bar{m}^2/M^2}[\tfrac{1}{3M^2}(2G_1\tfrac{1}{M_\Delta}m_N-G_2(M_\Delta-m_N))+A].
\end{aligned}
\tag{A.33}
$$

The coefficients are given by, in the transition channel $\Sigma^+\gamma\to\Sigma^{*+}$,

$$
\begin{aligned}
c_1 &= \frac{1}{3}\beta(e_u-e_sf_s\phi),\\
c_2 &= \frac{1}{12}(-3(e_u-e_sf_s\phi)\xi-2\beta(e_u(2-6f_s-5\kappa+\xi)+e_sf_s(4+5\kappa\phi-\phi\xi))),\\
c_3 &= \frac{1}{12}(e_s+e_u(-1-2\beta(-1+f_s))),\\
c_4 &= \frac{1}{3}\beta(e_u(-3+f_s)+2e_sf_s\phi),\\
c_5 &= \frac{1}{72}(-1+\beta)(e_u-e_sf_s\phi),\\
c_6 &= \frac{1}{36}(3f_s(e_u-e_s\phi)\xi-\beta(e_sf_s(-16-14\kappa\phi+\phi\xi)\\
&\quad +e_u(8+4\kappa-2\xi+f_s(8+10\kappa+\xi)))),\\
c_7 &= \frac{1}{144}(-e_s+e_u+2\beta e_u-2\beta e_uf_s).
\end{aligned}
\tag{A.34}
$$

in the transition channel $\Xi^0\gamma\to\Xi^{*0}$,

$$
\begin{aligned}
c_1 &= -\frac{1}{3}\beta(e_u-e_sf_s\phi),\\
c_2 &= \frac{1}{24}(e_u(\beta(-16-14\kappa+\xi)+3(2\kappa+\xi))
\end{aligned}
$$

$$
\begin{aligned}
&+e_s(\beta(12+f_s(4+14\kappa\phi-\phi\xi))-3(4+f_s(-4+2\kappa\phi+\phi\xi)))),\\
c_3 &= \frac{1}{24}(-2e_u(1+\beta(-1+f_s))+e_s(5+3\beta(-1+f_s)-3f_s)),\\
c_4 &= \frac{1}{3}f_s(e_s(-1+f_s)\phi+2\beta(e_u-e_sf_s\phi)),\\
c_5 &= -\frac{1}{72}(-1+\beta)(e_u-e_sf_s\phi),\\
c_6 &= \frac{1}{72}(e_u(6(-2+f_s)\kappa-3f_s\xi+\beta(f_s(32+22\kappa-5\xi)+6\xi))\\
&+e_s(24+f_s^2(4-(-1+7\beta)\phi(2\kappa-\xi))-4f_s(7-\phi(\kappa+\xi)+2\beta(4+\phi(\kappa+\xi))))),\\
c_7 &= \frac{1}{288}(2e_u(1+\beta(-1+f_s))+e_s(-1+\beta(-1+f_s)-f_s)).
\end{aligned}
\tag{A.35}
$$

and in the transition channel $\Lambda\gamma \to \Sigma^{*0}$,

$$
\begin{aligned}
c_1 &= \frac{1}{6}\beta(e_d-e_u),\\
c_2 &= \frac{1}{24}(2\beta(e_d-e_u)(-2+6f_s+5\kappa-\xi)-6(e_d(\kappa-\xi)+e_u\xi)\\
&+e_s(12+f_s(4+2\kappa\phi-\phi\xi))),\\
c_3 &= \frac{1}{24}(-3e_u+6\beta e_u(-1+f_s)+e_d(5-6\beta(-1+f_s)+2f_s)),\\
c_4 &= \frac{1}{6}(\beta(e_d-e_u)(-3+f_s)+2e_sf_s\phi),\\
c_5 &= \frac{1}{144}(-1+\beta)(e_d-e_u),\\
c_6 &= \frac{1}{72}(6e_d\kappa+3(-e_d+e_u)(1+f_s)\xi+\beta(e_d-e_u)(-4(2+4\kappa+\xi)\\
&+f_s(-8+2\kappa+5\xi))-2e_s(6+f_s(4+2\kappa\phi-\phi\xi))),\\
c_7 &= \frac{1}{288}(-4e_s+e_u(3-2\beta(-1+f_s))+e_d(-5+2\beta(-1+f_s)-2f_s)).
\end{aligned}
\tag{A.36}
$$

Appendix B

Mathematica Source Code

MathQCDSR is a Mathematica package to do the QCD sum rule calculation. It is explained in detail in Chap. 6. There are four mathematica notebooks in the package:

- *qcdsr2pt-construction.nb*. This notebook constructs the QCD sum rules for octet baryon masses and outputs them, one particle at a time, to disk in plain text for analysis. For reference, the output files names *Mass-*.txt*, there are totaling 8 files. The user should generate the outputs on their own computer and check against the supplied ones.

- *qcdsr2pt-analysis.nb*. This notebook reads and analyzes the QCD sum rules produced by *qcdsr2pt-construction.nb*. The user can save the graphics in the analysis to disk in a variety of formats.

- *qcdsr3pt-construction.nb*. This notebook constructs the QCD sum rules for the octet baryon magnetic moments and outputs them, one particle at a time, to disk in plain text for analysis. Again, for reference, the output files (named *Mag-*.txt*), totaling 24 files. The user should generate the outputs on their own computer and check against the supplied ones.

- *qcdsr3pt-analysis.nb*. This notebook reads and analyzes the QCD sum rules produced by *qcdsr3pt-construction.nb*. The user can save the graphics in the analysis to disk in a variety of formats.

Each notebook can be run separately, apart from the simple interface between the construction and analysis programs via plain text files written to disk.

The full package is long, so only some sample code for *qcdsr2pt-construction.nb* is listed. There are 12 cells in QCD side calculation according to Fig. 3.1. We only include diagrams $C00$, Cqq, Cgg and $C00m$ here. Other cells are independent and similar. The whole analysis program *qcdsr2pt-analysis.nb* is included in this appendix. For octet magnetic moments sum rules, there are two notebook *qcdsr3pt-construction.nb* and *qcdsr3pt-analysis.nb*. They have similar structures just we need to consider more diagrams in the QCD side calculation.

All the mathematica notebooks in this package will be available in electronic version along with this thesis.

The following code is from *qcdsr2pt-construction.nb*

QCD Sum Rules for Octet Baryon Masses

Initialization

```
<<HighEnergyPhysics`FeynCalc`
```

```
(*Set up your working directory*)
SetDirectory["D:\\Document\\MATHQCDSR package"];
```

Master Formula (Pick only one of the following particles to run at a time)

Nucleon (N)

```
Clear["Global`*"]
(* Nucleon master formula *)
ms=0;fs=1;
(* In the master formula, tA,tB,tC are u and d quarks; tAA,tBB,tCC are
    s quark; tB, tBB are (C S^T C) *)
mas[col_,tA_,tB_,tC_,tAA_,tBB_,tCC_]:=4*(-i col)*(
tA*Tr[GA[5].tBB.GA[5].tC]+tA.GA[5].tBB.GA[5].tC+β*GA[5].tA*Tr[GA[5].tBB
    .tC]+β*GA[5].tA.GA[5].tBB.tC+β*tA*Tr[tBB.GA[5].tC]+β*tA.tBB.GA[5].
    tC.GA[5]+β*β*GA[5].tA.GA[5]*Tr[tBB.tC]+β*β*GA[5].tA.tBB.tC.GA[5]);
fileSR1="Mass-onuc-1.txt";
fileSRp="Mass-onuc-p.txt";
```

Sigma (σ)

```
Clear["Global`*"]
(* Sigma master formula *)
mas[col_,tA_,tB_,tC_,tAA_,tBB_,tCC_]:=4*(-i col)*(
tA*Tr[GA[5].tBB.GA[5].tC]+tA.GA[5].tBB.GA[5].tC+β*GA[5].tA*Tr[GA[5].tBB
    .tC]+β*GA[5].tA.GA[5].tBB.tC+β*tA*Tr[tBB.GA[5].tC]+β*tA.tBB.GA[5].
    tC.GA[5]+β*β*GA[5].tA.GA[5]*Tr[tBB.tC]+β*β*GA[5].tA.tBB.tC.GA[5]);
fileSR1="Mass-osig-1.txt";
fileSRp="Mass-osig-p.txt";
```

Cascade (Ξ)

```
Clear["Global`*"]
(* Cascade master formula *)
mas[col_,tA_,tB_,tC_,tAA_,tBB_,tCC_]:=(4)*(-i*col)*(+tAA*Tr[GA[5].tB.GA
    [5].tCC]+tAA.GA[5].tB.GA[5].tCC+β*GA[5].tAA*Tr[GA[5].tB.tCC]+β*GA
    [5].tAA.GA[5].tB.tCC+β*tAA*Tr[tB.GA[5].tCC]+β*tAA.tB.GA[5].tCC.GA
    [5]+β*β*GA[5].tAA.GA[5]*Tr[tB.tCC]+β*β*GA[5].tAA.tB.tCC.GA[5]);
fileSR1="Mass-oxi-1.txt";
fileSRp="Mass-oxi-p.txt";
```

Lambda (Λ)

```
Clear["Global`*"]
(* Lambda master formula *)
mas[col_,tA_,tB_,tC_,tAA_,tBB_,tCC_]:=(2/3)*(-i*col)*(+4*tAA*Tr[GA[5].
    tB.GA[5].tC]+4*tAA.GA[5].tB.GA[5].tC
+4*tA*Tr[GA[5].tBB.GA[5].tC]+4*tA.GA[5].tBB.GA[5].tC-2*tA*Tr[GA[5].tB.
    GA[5].tCC]-2*tA.GA[5].tB.GA[5].tCC+β*(+4*GA[5].tAA*Tr[GA[5].tB.tC
    ]+4*GA[5].tAA.GA[5].tB.tC+4*GA[5].tA*Tr[GA[5].tBB.tC]+4*GA[5].tA.GA
    [5].tBB.tC-2*GA[5].tA*Tr[GA[5].tB.tCC]-2*GA[5].tA.GA[5].tB.tCC)+β
    *(+4*tAA*Tr[tB.GA[5].tC]+4*tAA.tB.GA[5].tC.GA[5]+4*tA*Tr[tBB.GA[5].
    tC]+4*tA.tBB.GA[5].tC.GA[5]-2*tA*Tr[tB.GA[5].tCC]-2*tA.tB.GA[5].tCC
    .GA[5])+β*β*(+4*GA[5].tAA.GA[5]*Tr[tB.tC]+4*GA[5].tAA.tB.tC.GA
    [5]+4*GA[5].tA.GA[5]*Tr[tBB.tC]+4*GA[5].tA.tBB.tC.GA[5]-2*GA[5].tA.
    GA[5]*Tr[tB.tCC]-2*GA[5].tA.tB.tCC.GA[5]));
fileSR1="Mass-olam-1.txt";
fileSRp="Mass-olam-p.txt";
```

Fourier transform

```
(*The following functions are used for Fourier trnsform *)
f20:=-4*i*π^2/Contract[FV[p,u],FV[p,u]];
f21[u_]:=8*π^2*FV[p,u]/Contract[FV[p,u],FV[p,u]];
f22[u_,v_]:=-8*i*π^2*(MT[u,v]/Contract[FV[p,u],FV[p,u]]^2-4*FV[p,u]*FV[p,v
    ]/Contract[FV[p,u],FV[p,u]]);
f40:=i*π^2*log;
f41[u_]:=2*π^2*FV[p,u]/Contract[FV[p,u],FV[p,u]];
f42[u_,v_]:=-2*i*π^2*(MT[u,v]/Contract[FV[p,u],FV[p,u]]-2*FV[p,u]*FV[p,v
    ]/Contract[FV[p,u],FV[p,u]]^2);
f43[u_,v_,w_]:=4*π^2*((MT[u,v]*FV[p,w]+MT[v,w]*FV[p,u]+w.u*FV[p,v])/
    Contract[FV[p,u],FV[p,u]]^2-4*FV[p,u]*FV[p,v]*FV[p,w]/Contract[FV[p,u
    ],FV[p,u]]^3);
f60:=-i*π^2/8*Contract[FV[p,u],FV[p,u]]*log;
f61[u_]:=-π^2/4*FV[p,u]*log;
f62[u_,v_]:=i*π^2/4*(MT[u,v]*log+2*FV[p,u]*FV[p,v]/Contract[FV[p,u],FV[p,
    u]]);
f63[u_,v_,w_]:=π^2/2*((MT[u,v]*FV[p,w]+MT[v,w]*FV[p,u]+w.u*FV[p,v])/
    Contract[FV[p,u],FV[p,u]]-2*FV[p,u]*FV[p,v]*FV[p,w]/Contract[FV[p,u
    ],FV[p,u]]^2);
f80:=i*π^2/(2^6*3)*Contract[FV[p,u],FV[p,u]]^2*log;
f81[u_]:=π^2/(2^4*3)*FV[p,u]*Contract[FV[p,u],FV[p,u]]*log;
f82[u_,v_]:=-i*π^2/(2^4*3)*(MT[u,v]*Contract[FV[p,u],FV[p,u]]*log+2*FV[p,u
    ]*FV[p,v]*log);
f83[u_,v_,w_]:=-π^2/(2^3*3)*((MT[u,v]*FV[p,w]+MT[v,w]*FV[p,u]+w.u*FV[p,v
    ])*log+2*FV[p,u]*FV[p,v]*FV[p,w]/Contract[FV[p,u],FV[p,u]]);
f100:=-i*π^2/(2^10*3^2)*Contract[FV[p,u],FV[p,u]]^3*log;
f101[u_]:=-π^2/(2^9*3)*FV[p,u]*Contract[FV[p,u],FV[p,u]]^2*log;
f102[u_,v_]:=i*π^2/(2^9*3)*(MT[u,v]*Contract[FV[p,u],FV[p,u]]^2*log+4*FV[p,
    u]*FV[p,v]*Contract[FV[p,u],FV[p,u]]*log);
f120:=i*π^2/(2^14*3^2*5)*Contract[FV[p,u],FV[p,u]]^4*log;
f121[u_]:=π^2/(2^11*3^2*5)*FV[p,u]*Contract[FV[p,u],FV[p,u]]^3*log;
f122[u_,v_]:=-i*π^2/(2^11*3^2*5)*(MT[u,v]*Contract[FV[p,u],FV[p,u]]^3*log
    +6*FV[p,u]*FV[p,v]*Contract[FV[p,u],FV[p,u]]^2*log);
f123[u_,v_,w_]:=-π^2/(2^10*3*5)*((MT[u,v]*FV[p,w]+MT[v,w]*FV[p,u]+w.u*FV[p
    ,v])*Contract[FV[p,u],FV[p,u]]^2*log+4*FV[p,u]*FV[p,v]*FV[p,w]*
    Contract[FV[p,u],FV[p,u]]*log);
```

```
(* The following factors are used for proper scaling  of various terms
such as qq=-a/(2π)^2, mix=-m0^2*qq=m0^2*a/(2π)^2, gg=b multiply overall
    factor (2π)^4. *)
tpi2=(2*π)^2;tpi4=(2*π)^4;
xfac=1;
f00=xfac*tpi4*d00;f00m=xfac*tpi4*d00m;
fgg=xfac*tpi4*dgg;fggm=xfac*tpi4*dggm;
fmix=xfac*tpi4/tpi2*dmix;fmixm=xfac*tpi4/tpi2*dmixm;
fmixqq=xfac*(-1)*dmixqq;
fqq=xfac*(-1)*tpi4/tpi2*dqq;fqqm=xfac*(-1)*tpi4/tpi2*dqqm;
fqqqq=xfac*1*dqqqq;fqqqqm=xfac*1*dqqqqm;
fqqgg=xfac*(-1)*tpi4/tpi2*dqqgg;
```

Calculation of the QCD side

diagram C00 (structure p)

```
(* This cell is for calculating diagram "C00" *)
(* calculation in x space *)
colour:=6;
termA:=(i/(2*π^2*Contract[FV[x,μ],FV[x,μ]]^2))*GS[x];
termB:=(i/(2*π^2*Contract[FV[x,μ],FV[x,μ]]^2))*GS[x];
termC:=(i/(2*π^2*Contract[FV[x,μ],FV[x,μ]]^2))*GS[x];
termAA:=termA;
termBB:=termB;
termCC:=termC;
mas[colour,termA,termB,termC,termAA,termBB,termCC]//DiracReduce;
c00x=%;
Print["c00x=",Expand[%]]
(* Fourier transform *)
c00xf=DiracReduce[c00x*f101*Contract[FV[x,u],FV[x,u]]^5/.GS[x]-> GA[r]];
Print["c00xf=",%]
c00p=c00xf/.{f101->f101[r]}//DiracReduce//Simplify;
(* Borel transform *)
c00b=c00p/.{log->-2*M^6/Contract[FV[p,u],FV[p,u]]^2}//DiracReduce;
Print["c00p=",DiracReduce[c00p]]
c00b=c00b*f00//DiracReduce//Simplify;
Print["c00b=",c00b];
```

diagram Cqq (structure 1)

```
(* This cell is for calculating diagram "Cqq" *)
(* calculation in x space *)
colour:=6;
termA:=(-1/12);
termB:=(i/(2*π^2*Contract[FV[x,μ],FV[x,μ]]^2))*GS[x];
termC:=(i/(2*π^2*Contract[FV[x,μ],FV[x,μ]]^2))*GS[x];
termAA:=fs*termA;
termBB:=termB;
termCC:=termC;
mas[colour,termA,termB,termC,termAA,termBB,termCC]//DiracReduce;
term1=%;
termB:=-(-1/12);
termC:=(i/(2*π^2*Contract[FV[x,μ],FV[x,μ]]^2))*GS[x];
```

```
termA:=(i/(2*π^2*Contract[FV[x,μ],FV[x,μ]]^2))*GS[x];
termAA:=termA;
termBB:=fs*termB;
termCC:=termC;
mas[colour,termA,termB,termC,termAA,termBB,termCC]//DiracReduce;
term2=%;
termC:=(-1/12);
termA:=(i/(2*π^2*Contract[FV[x,μ],FV[x,μ]]^2))*GS[x];
termB:=(i/(2*π^2*Contract[FV[x,μ],FV[x,μ]]^2))*GS[x];
termAA:=termA;
termBB:=termB;
termCC:=fs*termC;
mas[colour,termA,termB,termC,termAA,termBB,termCC]//DiracReduce;
term3=%;
result=term1+term2+term3;
cqqx=%;
Print["cqqx=",Expand[%]]
(* Fourier transform *)
cqqxf=DiracReduce[cqqx*ff60*Contract[FV[x,u],FV[x,u]]^3];
Print["cqqxf=",cqqxf]
cqqp=cqqxf/.{ff60->f60}//DiracReduce//Simplify;
(* Borel transform *)
cqqb=cqqp/.{log->-M^4/Contract[FV[p,u],FV[p,u]]}//DiracReduce;
Print["cqqp=",DiracReduce[cqqp]]
cqqb=cqqb*fqq//DiracReduce//Simplify;
Print["cqqb=",cqqb]
```

diagram Cgg (structure p)

```
(* This cell is for calculating diagram "Cgg" *)
(* calculation in x space *)
colour:=-4;
termA:=(i/(2*π^2*Contract[FV[x,μ],FV[x,μ]]^2))*GS[x];
termB:=-(i/(32*π^2*Contract[FV[x,μ],FV[x,μ]])))*(GS[x].DiracSigma[GA[al],
    GA[b]]+DiracSigma[GA[al],GA[b]].GS[x]);
termC:=(i/(32*π^2*Contract[FV[x,μ],FV[x,μ]])))*(GS[x].DiracSigma[GA[al],
    GA[b]]+DiracSigma[GA[al],GA[b]].GS[x])/(2^4*3);
termAA:=termA;
termBB:=termB;
termCC:=termC;
mas[colour,termA,termB,termC,termAA,termBB,termCC]//DiracReduce;
term1=%;
termB:=(i/(2*π^2*Contract[FV[x,μ],FV[x,μ]]^2))*GS[x];
termC:=(i/(32*π^2*Contract[FV[x,μ],FV[x,μ]])))*(GS[x].DiracSigma[GA[al],
    GA[b]]+DiracSigma[GA[al],GA[b]].GS[x]);
termA:=(i/(32*π^2*Contract[FV[x,μ],FV[x,μ]])))*(GS[x].DiracSigma[GA[al],
    GA[b]]+DiracSigma[GA[al],GA[b]].GS[x])/(2^4*3);
termAA:=termA;
termBB:=termB;
termCC:=termC;
mas[colour,termA,termB,termC,termAA,termBB,termCC]//DiracReduce;
term2=%;
termC:=(i/(2*π^2*Contract[FV[x,μ],FV[x,μ]]^2))*GS[x];
```

```
termA:=(i/(32*π^2*Contract[FV[x,μ],FV[x,μ]]))*(GS[x].DiracSigma[GA[al],
    GA[b]]+DiracSigma[GA[al],GA[b]].GS[x]);
termB:=-(i/(32*π^2*Contract[FV[x,μ],FV[x,μ]]))*(GS[x].DiracSigma[GA[al],
    GA[b]]+DiracSigma[GA[al],GA[b]].GS[x])/(2^4*3);
termAA:=termA;
termBB:=termB;
termCC:=termC;
mas[colour,termA,termB,termC,termAA,termBB,termCC]//DiracReduce;
term3=%;
result=term1+term2+term3;
cggx=%;
Print["cggx=",Expand[%]]
(* Fourier transform *)
cggxf=DiracReduce[cggx*f61*Contract[FV[x,u],FV[x,u]]^3/.GS[x]->GA[r]];
Print["cggxf=",%]
cggp=cggxf/.{f61->f61[r]}//DiracReduce//Simplify;
(* Borel transform *)
cggb=cggp/.{log->-M^2}//DiracReduce;
Print["cggp=",DiracReduce[cggp]]
cggb=cggb*fgg//DiracReduce//Simplify;
Print["cggb=",cggb]
```

diagram Cmix (structure 1)

```
 \normalsize{diagram C00m (structure 1)}
\vspace*{-0.5cm}
\begin{lstlisting}
(* This cell is for calculating diagram "C00m" *)
(* calculation in x space *)
colour:=6;
termA:=0;
termB:=(i/(2*π^2*Contract[FV[x,μ],FV[x,μ]]^2))*GS[x];
termC:=(i/(2*π^2*Contract[FV[x,μ],FV[x,μ]]^2))*GS[x];
termAA:=(-ms/(4*π^2*Contract[FV[x,μ],FV[x,μ]]));
termBB:=termB;
termCC:=termC;
mas[colour,termA,termB,termC,termAA,termBB,termCC]//DiracReduce;
term1=%;
termB:=0;
termC:=(i/(2*π^2*Contract[FV[x,μ],FV[x,μ]]^2))*GS[x];
termA:=(i/(2*π^2*Contract[FV[x,μ],FV[x,μ]]^2))*GS[x];
termAA:=termA;
termBB:=-(-ms/(4*π^2*Contract[FV[x,μ],FV[x,μ]]));
termCC:=termC;
mas[colour,termA,termB,termC,termAA,termBB,termCC]//DiracReduce;
term2=%;
termC:=0;
termA:=(i/(2*π^2*Contract[FV[x,μ],FV[x,μ]]^2))*GS[x];
termB:=(i/(2*π^2*Contract[FV[x,μ],FV[x,μ]]^2))*GS[x];
termAA:=termA;
termBB:=termB;
termCC:=(-ms/(4*π^2*Contract[FV[x,μ],FV[x,μ]]));
mas[colour,termA,termB,termC,termAA,termBB,termCC]//DiracReduce;
term3=%;
```

```
result=term1+term2+term3;
c00mx=%;
Print["c00mx=",Expand[%]]
(* Fourier transform *)
c00mxf=DiracReduce[c00mx*ff80*Contract[FV[x,u],FV[x,u]]^4];
Print["c00mxf=",c00mxf]
c00mp=c00mxf/.{ff80->f80}//DiracReduce//Simplify;
(* Borel transform *)
c00mb=c00mp/.{log->-2M^6/Contract[FV[p,u],FV[p,u]]^2}//DiracReduce;
Print["c00mp=",DiracReduce[c00mp]]
c00mb=c00mb*f00m//DiracReduce//Simplify;
Print["c00mb=",c00mb]
```

Total

```
resx=d00*c00x+dqq*cqqx+dgg*cggx+dmix*cmixx+dqqqq*cqqqqx+dqqgg*cqqggx+
    dmixqq*cmixqqx+d00m*c00mx+dqqm*cqqmx+dggm*cggmx+dmixm*cmixmx+dqqqqm
    *cqqqqmx;
(*Print["resx =",resx]*)
resxf=d00*c00xf+dqq*cqqxf+dgg*cggxf+dmix*cmixxf+dqqqq*cqqqqxf+dqqgg*
    cqqggxf+dmixqq*cmixqqxf+d00m*c00mxf+dqqm*cqqmxf+dggm*cggmxf+dmixm*
    cmixmxf+dqqqqm*cqqqqmxf;
(*Print["resxf =",resxf]*)
resp=d00*c00p+dqq*cqqp+dgg*cggp+dmix*cmixp+dqqqq*cqqqqp+dqqgg*cqqggp+
    dmixqq*cmixqqp+d00m*c00mp+dqqm*cqqmp+dggm*cggmp+dmixm*cmixmp+dqqqqm
    *cqqqqmp;
(*Print["resp =",resp]*)
resb=c00b+cqqb+cggb+cmixb+cqqqqb+cqqggb+cmixqqb+c00mb+cqqmb+cggmb+
    cmixmb+cqqqqmb;
Print["resb =",resb]
resbW1=resb/.GS[p]-> 0
resbWp=(resb-resbW1)/.GS[p]-> 1
Export[fileSR1, resbW1]
Export[fileSRp, resbWp]
```

The following code is from *qcdsr2pt-analysis.nb*

QCD Sum Rules Analysis for Octet Baryon Masses

```
(*Set up your working directory*)
SetDirectory["D:\\Document\\MATHQCDSR package"];
```

Read the QCD Sum Rules (must have been produced from qcdsr2pt-construction)

Pick a particle

Nucleon (N)

```
Clear["Global`*"]
F01 =ToExpression[Import["Mass-onuc-1.txt"]]
```

```
F0p =ToExpression[Import["Mass-onuc-p.txt"]]
sflag=0; (*flag to handle strange quarks*)
(*Only for selecting and uncertainty purpose*)
MN0=0.938; w0=1.44;
```

Sigma (Σ)

```
Clear["Global`*"]
F01 =ToExpression[Import["Mass-osig-1.txt"]]
F0p =ToExpression[Import["Mass-osig-p.txt"]]
MN0=1.193;
w0=1.66;
sflag=1;
```

Cascade (Ξ)

```
Clear["Global`*"]
F01 =ToExpression[Import["Mass-oxi-1.txt"]];
F0p =ToExpression[Import["Mass-oxi-p.txt"]];
sflag=1;
MN0=1.318; w0=1.82;
```

Lambda (Λ)

```
Clear["Global`*"]
F01 =ToExpression[Import["Mass-olam-1.txt"]];
F0p =ToExpression[Import["Mass-olam-p.txt"]];
sflag=1;
MN0=1.116; w0=1.60;
```

Pick a structure
Structure 1

```
tflag=1; (*flag to handle different structures*)
Clear[a,b,m02,ms,fs,kv,β,mu,LQCD];
L[M_]:=Log[M/LQCD]/Log[mu/LQCD];

p1[β1_] :=F01/.{d00m->1,dqq-> 0,dmix->0,dggm-> 0,dqqgg-> 0,dqqqqm->0,M
    ->1,ms-> 1}/.β-> β1
p2[β1_] :=F01/.{d00m->0,dqq-> 1,dmix->0,dggm-> 0,dqqgg-> 0,dqqqqm->0,M
    ->1,ms-> 1}/.β-> β1
p3[β1_] :=F01/.{d00m->0,dqq-> 0,dmix->1,dggm-> 0,dqqgg-> 0,dqqqqm->0,M
    ->1,ms-> 1}/.β-> β1
p4[β1_] :=F01/.{d00m->0,dqq-> 0,dmix->0,dggm-> 1,dqqgg-> 0,dqqqqm->0,M
    ->1,ms-> 1}/.β-> β1
p5[β1_] :=F01/.{d00m->0,dqq-> 0,dmix->0,dggm-> 0,dqqgg-> 1,dqqqqm->0,M
    ->1,ms-> 1}/.β-> β1
p6[β1_] :=F01/.{d00m->0,dqq-> 0,dmix->0,dggm-> 0,dqqgg-> 0,dqqqqm->1,M
    ->1,ms-> 1}/.β-> β1

FONEU[β_,w_,M_]:=
1/4*( p1[β]*ms *M^6*L[M]^(-8/9)*(1-Exp[(-w^2/M^2)]*(w^4/(2*M^4)+w^2/(M^2)+1))
+p2[β]* a*M^4*(1-Exp[(-w^2/M^2)]*(w^2/(M^2)+1))+p3[β]*m02*a*M^2*L[M]^(-14/27)
    *(1-Exp[(-w^2/M^2)])+p4[β]ms *b*M^2*(1-Exp[(-w^2/M^2)])+p5[β]*a*b+p6[β] ms
    *kv*a^2)
```

```
F0d1NEU[β_,w_,M_]:=
1/4*( p1[β]*ms *M^6*L[M]^(-8/9)*(1-Exp[(-w^2/M^2)]*(w^4/(2*M^4)+w^2/(M^2)+1)))
F0d2NEU[β_,w_,M_]:=1/4*( p2[β]* a*M^4*(1-Exp[(-w^2/M^2)]*(w^2/(M^2)+1)))
F0d3NEU[β_,w_,M_]:=1/4*(p3[β]*m02*a*M^2*L[M]^(-14/27)*(1-Exp[(-w^2/M^2)])+
    p4[β]*ms *b*M^2*(1-Exp[(-w^2/M^2)])))
F0d4NEU[β_,w_,M_]:=1/4*( p5[β]*a*b+p6[β]* ms*kv*a^2)
F0NEUOPE[β_,w_,M_]:=
1/4*( p1[β]*ms *M^6*L[M]^(-8/9)+p2[β]* a*M^4+p3[β]*m02*a*M^2*L[M]^(-14/27)
    +p4[β]*ms *b+p5[β]*a*b+p6[β] *ms*kv*a^2)
F0NEUEsc[β_,w_,M_]:=F0NEUOPE[β,w,M]-F0NEU[β,w,M]

Print["The proton mass sum rule at structure 1 is"];
F0NEU[β,w,M]
F0NEUEsc[β0,w,M];
F0NEUOPE[β,w,M];
F0d4NEU[β,w,M];
```

Structure p

```
tflag=0; (*flag to handle different structures*)
Clear[a,b,m02,ms,fs,kv,β,mu,LQCD];
L[M_]:=Log[M/LQCD]/Log[mu/LQCD];
lnl=Log[M^2/mu^2]-0.577;
p1[β1_] :=F0p/.{d00->1,dgg-> 0,dqqm->0,dmixm->0,dqqqq-> 0,dmixqq->0,M
    ->1,ms-> 1}/.β-> β1
p2[β1_] :=F0p/.{d00->0,dgg-> 1,dqqm->0,dmixm->0,dqqqq->0,dmixqq->0,M
    ->1,ms-> 1}/.β-> β1
p3[β1_] :=F0p/.{d00->0,dgg-> 0,dqqm->1,dmixm->0,dqqqq->0,dmixqq->0,M
    ->1,ms-> 1}/.β-> β1
p4[β1_] :=F0p/.{d00->0,dgg-> 0,dqqm->0,dmixm->1,dqqqq->0,dmixqq->0,M
    ->1,ms-> 1}/.β-> β1
p5[β1_] :=F0p/.{d00->0,dgg-> 0,dqqm->0,dmixm->0,dqqqq->1,dmixqq->0,M
    ->1,ms-> 1}/.β-> β1
p6[β1_] :=F0p/.{d00->0,dgg-> 0,dqqm->0,dmixm->0,dqqqq->0,dmixqq->1,M
    ->1,ms-> 1}/.β-> β1

F0NEU[β_,w_,M_]:=
1/4*(p1[β]*M^6*L[M]^(-4/9)*(1-Exp[(-w^2/M^2)]*(w^4/(2*M^4)+w^2/(M^2)+1))+p2[β]*
    b*M^2*L[M]^(-4/9)*(1-Exp[(-w^2/M^2)])+p3[β]*ms*a*L[M]^(4/9)*M^2*(1-Exp
    [(-w^2/M^2)])+p4[β]*ms*m02*a*L[M]^(-26/27)+p5[β]*a^2*kv*L[M]^(4/9)+p6[β
    ]*m02*a^2/M^2*L[M]^(-2/27))

F0d1NEU[β_,w_,M_]:=
1/4*(p1[β]*M^6*L[M]^(-4/9)*(1-Exp[(-w^2/M^2)]*(w^4/(2*M^4)+w^2/(M^2)+1)));
F0d2NEU[β_,w_,M_]:=1/4*(p2[β]*b*M^2*L[M]^(-4/9)*(1-Exp[(-w^2/M^2)])+p3[β]*
    ms*a*L[M]^(4/9)*M^2*(1-Exp[(-w^2/M^2)]));
F0d3NEU[β_,w_,M_]:=1/4*(p4[β]*ms*m02*a*L[M]^(-26/27)+p5[β]*a^2*kv*L[M
    ]^(4/9));
F0d4NEU[β_,w_,M_]:=+1/4*(p6[β]*m02*a^2/M^2*L[M]^(-2/27));

F0NEUOPE[β_,w_,M_]:=
1/4*(p1[β]*M^6*L[M]^(-4/9)*(1)+p2[β]*b*M^2*L[M]^(-4/9)*(1)+p3[β]*ms*a*L[M
    ]^(4/9)*M^2*(1)+p4[β]*ms*m02*a*L[M]^(-26/27)+p5[β]*a^2*kv*L[M]^(4/9)+
```

```
    p6[β]*m02*a^2/M^2*L[M]^(-2/27))
F0NEUEsc[β_,w_,M_]:=F0NEUOPE[β,w,M]-F0NEU[β,w,M]

Print["The proton mass sum rule at structure p is"]
F0NEU[β,w,M]
F0NEUEsc[β,w0,M]//Simplify;
F0NEUOPE[β,w0,M];
```

Numerical analysis with inline graphics

Parameter initialization

```
Needs["ErrorBarPlots`"]
Needs["Histograms`"]
Needs["PlotLegends`"]
Clear[fs,a,b,m02,MN,β,ms,mu,LQCD,LAM2]
β0=-1.2; (*beta value*)
Mmin=0.9; Mmax=1.2; (*Borel window to match*)
Mmin1=0.5; Mmax1=1.8;

(* mean value for QCD input parameters*)
am=0.52;bm=1.2;m02m=0.72;  msm=0.15;fsm=0.8;
mu=0.5;LQCD=0.15;kv=2;
Nr=280;  (*# of monte carlo samples*)
uns=0.1;  (* uncertaintity of input parameters*)
Nc=200;  (*# of monte carlo samples to get stable std*)
Nb=51;    (* # of M *)

LAMLAM=MNMN=OMA=Table[0,{j,Nr}];
aa=bb=m0m0=Table[0,{j,Nr}];
MS=FS=Table[0,{i,Nr}];
LAMnew=MNnew=OMAnew=Table[0,{j,Nr}];
Anew=Bnew=M0new=Table[0,{j,Nr}];
MSnew=FSnew=Table[0,{i,Nr}];
y1=y12=y3=Table[0,{j,Nc}];
σ=σ1=σ3=Table[0,{j,Nb}];

f2=F0NEUOPE[β0,w0,M];
For[j=1, j<=Nb, j++,
x2=Mmin+(Mmax-Mmin)/Nb*j;
x3=Mmin1+(Mmax1-Mmin1)/Nb*j;
For[ii=1, ii<=Nc, ii++,
Clear[a,b,m02,ms,fs];
SeedRandom[1234];
a=RandomReal[NormalDistribution[am,Abs[uns*am]]];
b=RandomReal[NormalDistribution[bm,Abs[0.5*bm]]];
      m02=RandomReal[NormalDistribution[m02m,Abs[uns*m02m]]];
If[sflag==0,
ms=0;fs=1,
ms=RandomReal[NormalDistribution[msm,Abs[uns*msm]]];
     fs=RandomReal[NormalDistribution[fsm,Abs[uns*fsm]]]];
y1[[ii]]=f2/.M-> x2;
y3[[ii]]=f2/.M-> x3;
y12[[ii]]=Log[y1[[ii]]];
```

```
σ[[j]]=StandardDeviation[y1];
σ3[[j]]=StandardDeviation[y3];
σ1[[j]]=StandardDeviation[y12]];
σ (* std for y*)
σ1; (* std for log y*)
```

Sum rule matching using χ^2 minimization

```
For[ii=1, ii<=Nr, ii++,
Clear[a,b,m02,ms,fs];
a=RandomReal[NormalDistribution[am,Abs[uns*am]]]; aa[[ii]]=a;
b=RandomReal[NormalDistribution[bm,Abs[uns*bm]]];bb[[ii]]=b;
    m02=RandomReal[NormalDistribution[m02m,Abs[uns*m02m]]];m0m0[[ii]]=
       m02;

If[sflag==0,
ms=0;MS[[ii]]=0;fs=1;FS[[ii]]=1,
ms=RandomReal[NormalDistribution[msm,Abs[uns*msm]]];MS[[ii]]=ms;
      fs=RandomReal[NormalDistribution[fsm,Abs[uns*fsm]]];FS[[ii]]=fs;
];

 F1[M_, w_] :=FONEU[β0,w,M];
x1=Range[Mmin, Mmax,(Mmax-Mmin)/(Nb-1)];
data1=Table[{x1[[i]],0},{i,1,Length[x1]}];

If[tflag==1,
(*at structure 1, with MN*)
yf=FindFit[data1,LAM2*MN*Exp[-MN^2/M^2]-F1[M,w],{LAM2,MN,w},M,
   NormFunction->(Norm[#/σ]&)]];

If[tflag==0,
(*at structure p, no MN*)
yf=FindFit[data1,LAM2*Exp[-MN^2/M^2]-F1[M,w],{LAM2,MN,w},M,NormFunction
   ->(Norm[#/σ]&)]];

LAMLAM[[ii]]=LAM2/.yf;
MNMN[[ii]]=MN/.yf;
OMA[[ii]]=w/.yf];

Y0=Table[{OMA[[i]], MNMN[[i]],LAMLAM[[i]],aa[[i]],bb[[i]],m0m0[[i]],MS
   [[i]],FS[[i]]},{i,Length[OMA]}];

Y1=Select[Y0,#[[1]]> #[[2]]&&#[[1]]<3&]; (*set condition for w, ( w>M_N
    ) to take out non physical values*)
Print["There are ", Length[Y1]," physical w values selected from ",Nr,"
    samples."]
YY=Table[{Y1[[i,1]], Y1[[i,2]],Y1[[i,3]],Y1[[i,4]],Y1[[i,5]],Y1[[i,6]],
   Y1[[i,7]],Y1[[i,8]]},{i,Length[Y1]}];

OMAnew=YY[[All,1]];
Print["w mean= ",Mean[OMAnew], "    w std= ",StandardDeviation[OMAnew]]
MNnew=YY[[All,2]];
Print["M_N mean= ",Mean[MNnew], "; M_N std= ",StandardDeviation[MNnew]]
LAMnew=YY[[All,3]];
```

```
Print["λ^2 mean= ",Mean[LAMnew], "; λ^2 std= ",StandardDeviation[LAMnew]]

Anew=YY[[All,4]];
Bnew=YY[[All,5]];
M0new=YY[[All,6]];
MSnew=YY[[All,7]];
FSnew=YY[[All,8]];

(*matching plot*)
p=1; (*select one set of QCD input which gives physical w*)
a=Anew[[p]]; b=Bnew[[p]];m02=M0new[[p]];fs=FSnew[[p]];ms=MSnew[[p]];
Print["a= ",a,"; b= ",b,"; m0^2= ",m02,"; fs= ",fs,"; ms= ",ms]
x1=Range[Mmin, Mmax,(Mmax-Mmin)/(Nb-1)];
data1=Table[{x1[[i]],0},{i,1,Length[x1]}];
x1=Range[Mmin, Mmax,(Mmax-Mmin)/(Nb-1)];

If[tflag==1,
(*at structure 1, with MN*)
yf=FindFit[data1,LAM2*MN*Exp[-MN^2/M^2]-F1[M,w],{LAM2,MN,w},M,
    NormFunction->(Norm[#/σ]&)];
Print[yf];
Print["At structure 1"];];

If[tflag==0,
(*at structure p, no MN*)
yf=FindFit[data1,LAM2*Exp[-MN^2/M^2]-F1[M,w],{LAM2,MN,w},M,NormFunction
    ->(Norm[#/σ]&)];
Print[yf];
ym=LAM0*Exp[-MN0^2/M^2];
Print["Structure p"]];

LAM0=LAM2/.yf;
MN0=MN/.yf;
OMA0=w/.yf;

If[tflag==0,ym=LAM0*Exp[-MN0^2/M^2];,ym=LAM0*MN0*Exp[-MN0^2/M^2];]
x1=Range[Mmin, Mmax,(Mmax-Mmin)/(Nb-1)];
x3=Range[Mmin1, Mmax1,(Mmax1-Mmin1)/(Nb-1)];
yf1=F1[x1,OMA0];
yf3=F1[x3,OMA0];
y4=F1[x,OMA0];
data1=Table[{x1[[i]],yf1[[i]]},{i,1,Length[x1]}];

data3=Table[{x3[[i]],yf3[[i]]},{i,1,Length[x3]}];

makeLegend[plotMark_,sizex_,sizey_,position_]:=Module[{graphics={}},
    graphics={Graphics[#[[1]]],#[[2]]}&/@plotMark;
Return[{graphics,LegendSize->{sizex,sizey},LegendPosition->position,
    LegendShadow->None,BaseStyle->{FontSize->14,FontFamily->"Times"}}]
    ]

Errorbarplot=Graphics[{Red,PointSize[0.05],Point[{1,0}],Point[{2,0}],
    Point[{3,0}],Thin,Line[{{1,-0.4},{1,0.4}}],Line
    [{{0.9,0.4},{1.1,0.4}}],Line[{{0.9,-0.4},{1.1,-0.4}}],Line
```

```
    [{{2,-0.5},{2,0.5}}],Line[{{1.9,0.5},{2.1,0.5}}],Line
    [{{1.9,-0.5},{2.1,-0.5}}],Line[{{3,-0.3},{3,0.3}}],Line
    [{{2.9,0.3},{3.1,0.3}}],Line[{{2.9,-0.3},{3.1,-0.3}}]}];

plotmrk1={{Errorbarplot,"OPE-ESC"},{Graphics[{Black,Line
    [{{0,0},{4,0}}]}], "Pole+Tran"}};


ShowLegend[Show[ErrorListPlot[Table[{data1[[i]],ErrorBar[σ[[i]]]},{i,
    Length[σ]}],Axes->{False,False}, PlotStyle->Red,PlotStyle->
    PointSize[.03]],Plot[{ym},{M,Mmin, Mmax},PlotStyle->{{Black,
    Thickness[0.002]}},Frame->True,Axes->{False,False}],FrameLabel->{"M
    ^-2 (GeV^-2)","LHS and RHS matching"}],makeLegend[plotmrk1
    ,0.6,0.3,{-0.8,0.25}]]


plotmrk2={{Errorbarplot,"OPE-ESC fitting"},{Graphics[{Blue,Point
    [{0,0}],Point[{1,0}],Point[{2,0}],Point[{3,0}],Point[{4,0}],Line
    [{{0,0},{4,0}}]}],"OPE-ESC"},{Graphics[{Purple,Line
    [{{0,0},{4,0}}]}], "Pole+Tran"}};

ShowLegend[Show[ErrorListPlot[Table[{data1[[i]],ErrorBar[σ[[i]]]},{i,
    Length[σ1]}],PlotStyle->Red,PlotStyle->PointSize[.005]],Plot[y4,{M,
    Mmin1, Mmax1}],ListPlot[Table[{data3[[i]]},{i,Length[σ3]}],
    PlotStyle->Blue,PlotStyle->PointSize[.005]],Plot[ym,{M,Mmin1, Mmax1
    }, PlotStyle->Purple],FrameLabel->{"M^-2 (GeV^-2)","LHS and RHS
    matching"}],makeLegend[plotmrk2,0.6,0.3,{-0.8,0.25}]]


(*log plot*)
If[tflag==0,yx=LAM0*Exp[-MN0^2*x];,yx=LAM0*MN0*Exp[-MN0^2*x];]

y4=F1[x^(-1/2),OMA0];

data1=Table[{(x1[[i]])^-2,Log[yf1[[i]]]},{i,1,Length[x1]}];
data33=Table[{(x3[[i]])^-2,Log[yf3[[i]]]},{i,1,Length[x1]}];

ShowLegend[Show[ErrorListPlot[Table[{data1[[i]],ErrorBar[σ[[i]]]},{i,
    Length[σ]}],Axes->{False,False}, PlotStyle->Red,PlotStyle->
    PointSize[.03]],Plot[{Log[yx]},{x,(Mmax)^-2, (Mmin)^-2},PlotStyle->{{
    Black,Thickness[0.002]}},Frame->True,Axes->{False,False}],
    FrameLabel->{"1/M^2 (GeV^-2)","Ln Π_s(M)"}],makeLegend[plotmrk1
    ,0.6,0.3,{0.4,0.25}]]

ShowLegend[Show[ErrorListPlot[Table[{data1[[i]],ErrorBar[σ[[i]]]},{i,
    Length[σ1]}],PlotStyle->Red,PlotStyle->PointSize[.005]],Plot[Log[y4
    ],{x,(Mmax1)^-2, (Mmin1)^-2}],ListPlot[Table[{data33[[i]]},{i,Length[σ
    3]}],PlotStyle->Blue,PlotStyle->PointSize[.005]],Plot[Log[yx],{x,(
    Mmax1)^-2, (Mmin1)^-2}, PlotStyle->Purple],FrameLabel->{"1/M^2 (GeV^-2)"
    ,"Ln Π_s(M)"}],makeLegend[plotmrk2,0.6,0.3,{0.35,0.25}]]
```

Term by term contributions

```
(* OPE side --- all dimensions *)
```

```
yf0=F0NEU[β0,OMA0,x];
yd1=F0d1NEU[β0,OMA0,x];
 yd2=F0d2NEU[β0,OMA0,x];
yd3=F0d3NEU[β0,OMA0,x];
yd4=F0d4NEU[β0,OMA0,x];

If[tflag==1,
ypol=LAM0*MN0*Exp[-MN0^2/x^2];

plotmrk4={{Graphics[{Blue,Line[{{0,0},{4,0}}]}], "Total"},{Graphics[{
    Dashed,Purple,Line[{{0,0},{4,0}}]}], "M^6"},{Graphics[{DotDashed,Red,
    Line[{{0,0},{4,0}}]}],"M^4"},{Graphics[{Dotted,Orange,Line
    [{{0,0},{4,0}}]}], "M^2"},{Graphics[{DotDashed,Brown,Line
    [{{0,0},{4,0}}]}], "M^0"}};

ShowLegend[Show[Plot[{yf0,yd1,yd2,yd3,yd4},{x,Mmin,Mmax},PlotStyle->{{
    Blue},{Dashed,Purple,Thickness[0.003]},{DotDashed,Red,Thickness
    [0.003]},{Dotted,Orange,Thickness[0.003]},{DotDashed,Brown,
    Thickness[0.003]}},FrameLabel->{"Borel Mass (GeV)","OPE Side"}]],
    makeLegend[plotmrk4, 0.3,0.2,{-0.7,0.35}]]
]

If[tflag==0,
ypol=LAM0*Exp[-MN0^2/x^2];

plotmrk5={{Graphics[{Blue,Line[{{0,0},{4,0}}]}], "Total"},{Graphics[{
    Dashed,Purple,Line[{{0,0},{4,0}}]}], "M^4"},{Graphics[{DotDashed,Red,
    Line[{{0,0},{4,0}}]}],"M^2"},{Graphics[{Dotted,Orange,Line
    [{{0,0},{4,0}}]}], "M^0"},{Graphics[{DotDashed,Brown,Line
    [{{0,0},{4,0}}]}], "M^-2"}};

ShowLegend[Show[Plot[{yf0,yd1,yd2,yd3,yd4},{x,Mmin,Mmax},PlotStyle->{{
    Blue},{Dashed,Purple,Thickness[0.003]},{DotDashed,Red,Thickness
    [0.003]},{Dotted,Orange,Thickness[0.003]},{DotDashed,Brown,
    Thickness[0.003]}},FrameLabel->{"Borel Mass (GeV)","OPE Side"}]],
    makeLegend[plotmrk5, 0.3,0.2,{-0.7,0.35}]]
]

(*Phen. Side --- pole, excited states, continuum*)
yope=F0NEUOPE[β0,OMA0,x];
yesc=F0NEUEsc[β0,OMA0,x];
yd40=F0d4NEU[0,OMA0,x];

plotmrk6={{Graphics[{Dashed,Black,Line[{{0,0},{4,0}}]}], "Pole"},{
    Graphics[{Dotted,Blue,Line[{{0,0},{4,0}}]}],"Excited"},{Graphics[{
    DotDashed,Red,Line[{{0,0},{4,0}}]}], "OPE"}};

ShowLegend[Show[Plot[{ypol,yesc,yope},{x,Mmin,Mmax},PlotStyle->{{Dashed
    ,Black,Thickness[0.003]},{Dotted,Blue,Thickness[0.003]},{DotDashed,
    Red,Thickness[0.003]}},FrameLabel->{"Borel Mass (GeV)","Phen. Side"
    }]],makeLegend[plotmrk6, 0.3,0.2,{-0.7,0.35}]]

plotmrk7={{Graphics[{Dashed,Black,Line[{{0,0},{4,0}}]}], "Excited"},{
    Graphics[{Dotted,Blue,Line[{{0,0},{4,0}}]}],"HDO"},{Graphics[{
```

```
    DotDashed,Red,Line[{{0,0},{4,0}}]}], "HDO at β=0"}};

ShowLegend[Show[Plot[{yesc/(ypol+yesc)*100,Abs[yd4]/(ypol+yesc)*100,Abs
    [yd40]/(ypol+yesc)*100 },{x,Mmin,Mmax},PlotStyle->{{Dashed,Black,
    Thickness[0.003]},{Dotted,Blue,Thickness[0.003]},{DotDashed,Red,
    Thickness[0.003]}},FrameLabel->{"Borel Mass (GeV)","Relative
    Contribution (%)"}]],makeLegend[plotmrk7, 0.5,0.2,{-0.7,0.35}]]
```

Historgram distribution

```
Print["Histograms of output parameters for all samples"]
Histogram[MNMN,Frame->True,FrameLabel->{"M_N","Counts"},HistogramRange
    ->{Mean[MNMN]-3*StandardDeviation[MNMN],Mean[MNMN]+3*
    StandardDeviation[MNMN]}]

Histogram[LAMLAM,Frame->True,FrameLabel->{"Λ","Counts"},HistogramRange
    ->{Mean[LAMLAM]-3*StandardDeviation[LAMLAM],Mean[LAMLAM]+3*
    StandardDeviation[LAMLAM]}]

Histogram[OMA,Frame->True,FrameLabel->{"w","Counts"},HistogramRange->{
    Mean[OMA]-0.5*StandardDeviation[OMA],Mean[OMA]+0.5*
    StandardDeviation[OMA]}]

Print["Histograms of output parameters for physical samples"]

Histogram[MNnew,Frame->True,FrameLabel->{"M_N","Counts"},HistogramRange
    ->{Mean[MNnew]-3*StandardDeviation[MNnew],Mean[MNnew]+3*
    StandardDeviation[MNnew]}]
Histogram[LAMnew,Frame->True,FrameLabel->{"Λ","Counts"},HistogramRange
    ->{Mean[LAMnew]-3*StandardDeviation[LAMnew],Mean[LAMnew]+3*
    StandardDeviation[LAMnew]}]

Histogram[OMAnew,Frame->True,FrameLabel->{"w","Counts"},HistogramRange
    ->{Mean[OMAnew]-3*StandardDeviation[OMAnew],Mean[OMAnew]+3*
    StandardDeviation[OMAnew]}]
```

Scatter plots

```
Print["Scatter plots of output parameters and the mass for all samples"
    ]
datL=LAMLAM; datM=MNMN;
lst1=Table[{datL[[i]],datM[[i]]},{i,Length[datL]}];
Lb1={"λ_0^2 ((2π)^-4 GeV^6)","M_N (GeV)"};
G1=ListPlot[lst1,PlotStyle->{Red},Frame->True,FrameLabel->Lb1, Axes->
    None](*PlotRange->{Mean[MNMN]-1*StandardDeviation[MNMN],Mean[MNMN
    ]+1*StandardDeviation[MNMN]}]*)

datO=OMA; datM=MNMN;
lst2=Table[{datO[[i]],datM[[i]]},{i,Length[datO]}];
Lb2={"w((2π)^-4 GeV^6)","M_N (GeV)"};
G2=ListPlot[lst2,PlotStyle->{Red},Frame->True,FrameLabel->Lb2, Axes->
    None]
```

```
Print["Scatter plots of output parameters and the mass for physical
    samples"]
datL=LAMnew;datM=MNnew;
lst1=Table[{datL[[i]],datM[[i]]},{i,Length[datL]}];
Lb1={"λ0^2 ((2π)^-4 GeV^6)","M_N (GeV)"};
G3=ListPlot[lst1,PlotStyle->{Red},Frame->True,FrameLabel->Lb1, Axes->
    None]

datO=OMAnew;datM=MNnew;
lst2=Table[{datO[[i]],datM[[i]]},{i,Length[datO]}];
Lb2={"w((2π)^-4 GeV^6)","M_N (GeV)"};
G4=ListPlot[lst2,PlotStyle->{Red},Frame->True,FrameLabel->Lb2, Axes->
    None]
Print["Scatter plots of the input parameters and the mass for physical
    samples"]

datO=Anew;
datM=MNnew;
lst2=Table[{datO[[i]],datM[[i]]},{i,Length[datO]}];
Lb2={"a (GeV^3)","M_N (GeV)"};
G5=ListPlot[lst2,PlotStyle->{Red},Frame->True,FrameLabel->Lb2, Axes->
    None];

datO=Bnew;
datM=MNnew;
lst2=Table[{datO[[i]],datM[[i]]},{i,Length[datO]}];
Lb2={"b (GeV^4)","M_N (GeV)"};
G6=ListPlot[lst2,PlotStyle->{Red},Frame->True,FrameLabel->Lb2, Axes->
    None];

datO=M0new;
datM=MNnew;
lst2=Table[{datO[[i]],datM[[i]]},{i,Length[datO]}];
Lb2={"m_0^2 (GeV^2)","M_N (GeV)"};
G7=ListPlot[lst2,PlotStyle->{Red},Frame->True,FrameLabel->Lb2, Axes->
    None];

datO=MSnew;
datM=MNnew;
lst2=Table[{datO[[i]],datM[[i]]},{i,Length[datO]}];
Lb2={"m_s (GeV)","M_N (GeV)"};
G8=ListPlot[lst2,PlotStyle->{Red},Frame->True,FrameLabel->Lb2, Axes->
    None];

datO=FSnew;
datM=MNnew;
lst2=Table[{datO[[i]],datM[[i]]},{i,Length[datO]}];
Lb2={"f_s ","M_N (GeV)"};
G9=ListPlot[lst2,PlotStyle->{Red},Frame->True,FrameLabel->Lb2, Axes->
    None];

If[sflag==0,GraphicsArray[{{G5},{G6},{G7}}], GraphicsArray[{{G5},{G6},{
    G7},{G8},{G9}}] ]
```